

MCDONNELL 40 KW GIROMILL WIND SYSTEM

Phase I-Design and Analysis
Volume II-Technical Report

August 1979

J.W. Anderson
R.V. Brulle
E.B. Birchfield
W.D. Duwe

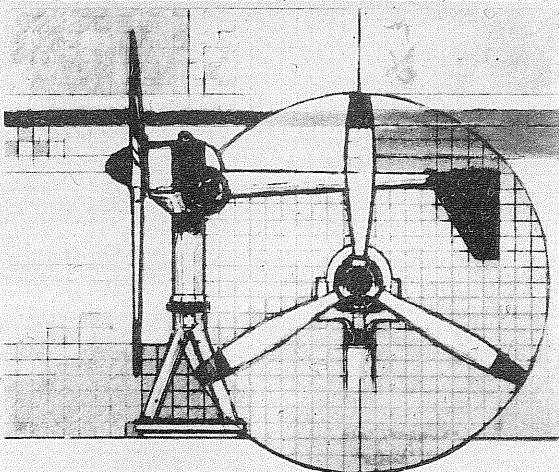
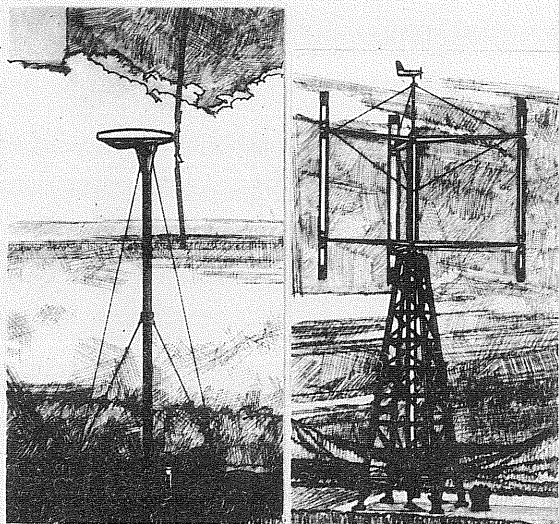
Prepared by
MCDONNELL AIRCRAFT COMPANY
P.O. Box 516
St. Louis, Missouri 63166

For
Rockwell International Corporation
Energy Systems Group
Rocky Flats Plant
Wind Systems Program
P.O. Box 464
Golden, Colorado 80402

Subcontract No. PF-64100

As Part of the
U.S. DEPARTMENT OF ENERGY
WIND ENERGY TECHNOLOGY DIVISION
FEDERAL WIND ENERGY PROGRAM

Contract No. DE-AC04-76DP03533



DISCLAIMER

This report was prepared as an account of work sponsored by the United States Government. Neither the United States nor the United States Department of Energy, nor any of their employees, makes any warranty, express or implied, or assumes any legal liability or responsibility for the accuracy, completeness, or usefulness of any information, apparatus, product, or process disclosed, or represents that its use would not infringe privately owned rights. Reference herein to any specific commercial product, process, or service by trade name, mark, manufacturer, or otherwise, does not necessarily constitute or imply its endorsement, recommendation, or favoring by the United States Government or any agency thereof. The views and opinions of authors expressed herein do not necessarily state or reflect those of the United States Government or any agency thereof.

Printed in the United States of America

Available from

National Technical Information Service
U.S. Department of Commerce
5285 Port Royal Road
Springfield, VA 22161

Printed Copy: \$13.00 Microfiche: \$3.50

MCDONNELL 40 KW
GIROMILL
WIND SYSTEM

Phase I - Design and Analysis

Volume II - Technical Report

August 1979

J.W. Anderson
R.V. Brulle
E.B. Birchfield
W.D. Duwe

Prepared by

McDonnell Aircraft Company
P.O. Box 516
St. Louis, Missouri 63166

For

Rockwell International Corporation
Energy Systems Group
Rocky Flats Plant
Wind Systems Program
P.O. Box 464
Golden, Colorado 80402

Subcontract No. PF-64100

As Part of the

U.S. DEPARTMENT OF ENERGY
WIND ENERGY TECHNOLOGY DIVISION
FEDERAL WIND ENERGY PROGRAM

Contract No. DE-AC04-76DP03533

ABSTRACT

The objective of Phase I of this contract was to determine a preferred configuration for the 40kW Giromill and to design that configuration. Phase I began on September 15, 1978 and was completed on June 15, 1979. Phase II, fabrication and testing, began on May 15, 1979, and results will be covered later.

The Giromill is a vertical axis windmill with a series of articulated vertical blades whose angles are controlled to maintain a constant RPM (when wind speed is sufficient). A microprocessor is used to process information on wind speed, wind direction, and RPM and establish blade position.

The Prototype Giromill, when connected to a utility grid, is designed to supply 40kW in a 20 MPH wind. By means of a kit, it can be converted to a stand-alone machine having a mechanical output. A 30-year life was a design objective. The Giromill is designed to withstand a peak gust of 125 MPH with a 1.5 safety factor.

Phase I was nine months in duration. It consisted first of a four-month period of trade studies during which a number of variations in the design were studied. Out of these studies evolved the configuration which became the basis for a six-month design period, which began during the last month of the trade-off period. Additional tasks performed during design were a Failure Mode and Effect Analysis, Preparation of a Test Plan, Definition of Test Instrumentation, and a Preliminary Production System Cost Analysis.

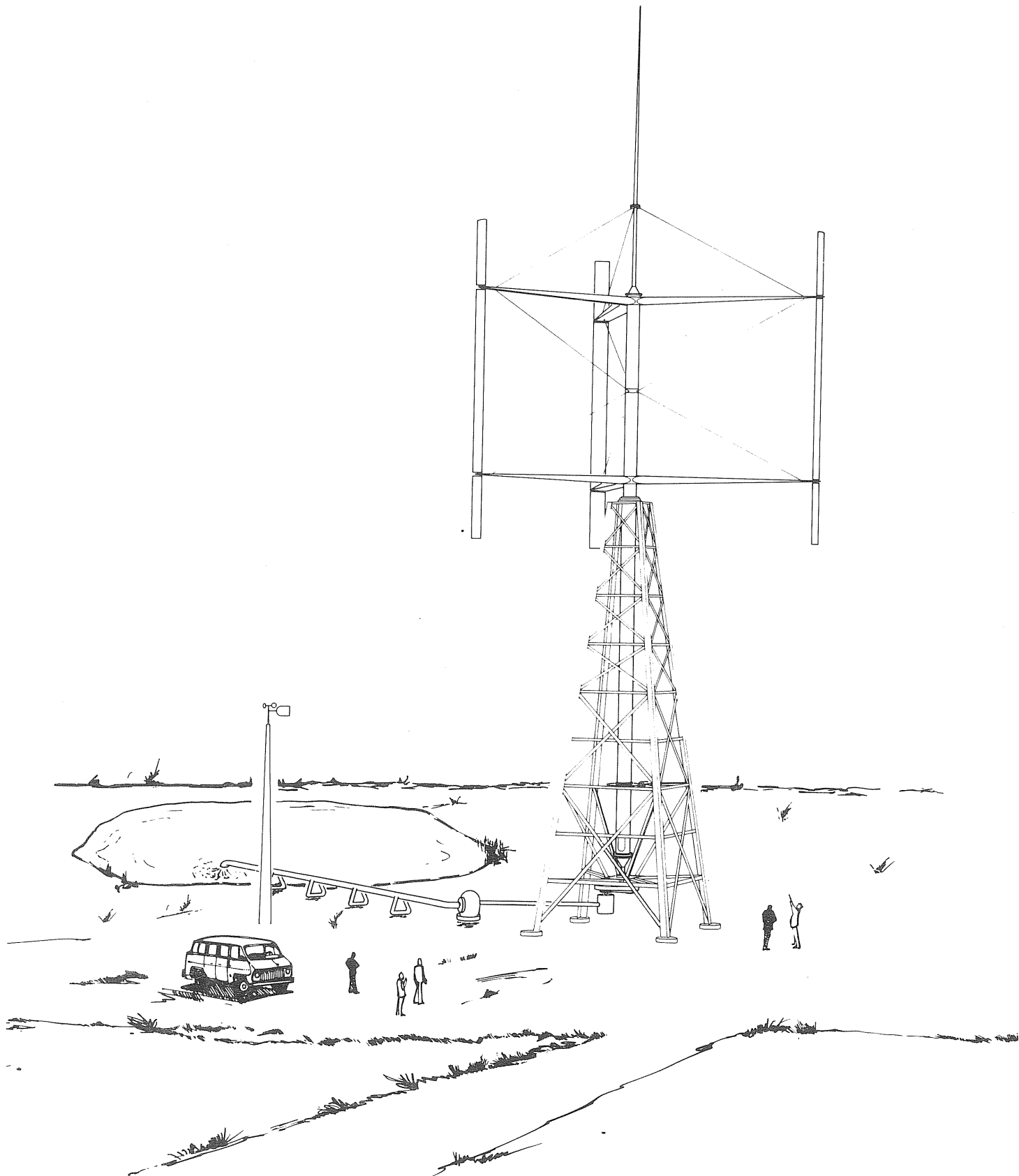
FOREWORD

This report summarizes the results of Phase I of a program to design and test a 40KW vertical axis windmill called a "Giromill". Phase I of this program covered trade studies, choice of a preferred configuration and detail design of that configuration. The 9-month program was conducted under contract PF64100F, awarded by the Rockwell International Energy Systems Group at Rocky Flats, Colorado, as part of the Department of Energy's (DOE) small windmill development program. Mr. Eugene Bange of Rockwell International was Contract Monitor.

McDonnell Aircraft Company (MCAIR) was prime contractor, with major assistance from Valley Industries through a subcontract and license agreement and from McDonnell Douglas Electronics Division (MDEC) through an intercompany work order. Valley Industries designed the fixed tower, the rotating tower, the support arms, and the mechanical and electrical output systems. Valley also designed the foundation. MDEC designed the control system and the blade actuators.

Mr. J. W. Anderson was Program Manager for MCAIR, Mr. William Duwe was Engineering Manager for Valley Industries, and Mr. Bert Lindsey was Engineering Manager for MDEC. The principal engineers for MCAIR were Messrs. Burt Birchfield, Bob Brulle, and Warren Strutman; for Valley Industries, Mr. Jim Herr; and for MDEC, Messrs. Tom Schmidt, Bob Udell, and Dick Grau.

This report is in two volumes. Volume I is an executive summary; Volume II contains a technical discussion of the entire program.



(THIS PAGE LEFT INTENTIONALLY BLANK)

TABLE OF CONTENTS

<u>Section</u>	<u>Page</u>
1. INTRODUCTION	1
1.1 BACKGROUND.	1
1.2 PROGRAM DESCRIPTION	1
2. DESIGN TRADE-OFF STUDIES	3
2.1 GEOMETRY.	4
2.2 DRIVE SYSTEM.	6
2.2.1 RPM Increase	6
2.2.2 Generator.	7
2.3 CONTROL SYSTEM.	8
2.3.1 Control Concept.	8
2.3.2 Blade Actuator Trade-Off Study	9
2.4 BLADE DESIGN.	10
2.4.1 Location of Blade Supports	10
2.4.2 Blade Offset Hinge	12
2.4.3 Steel Verses Aluminum Blade.	12
2.4.4 Blade Structural Arrangement	13
2.5 BLADE SUPPORT ARMS DESIGN	14
2.6 ROTATING TOWER.	14
2.7 FIXED TOWER	15
2.8 PREFERRED DESIGN SELECTED	16
3. DESIGN CRITERIA.	20
3.1 GENERAL	20
3.1.1 Hardware Cross Reference	20
3.1.2 Operating Specifications	20
3.1.3 Lifetime Goal.	20
3.1.4 Dependability.	20
3.1.5 Cost Goal.	21
3.1.6 Manufacturing Procedures	21
3.1.7 Structural Criteria.	22
3.2 ENVIRONMENTAL CONDITIONS.	22
3.2.1 Winds.	22
3.2.2 Temperature.	26
3.2.3 Rain, Snow, Hail and Ice	27

TABLE OF CONTENTS (Continued)

<u>Section</u>	<u>Page</u>
3.2.4 Corrosive Atmosphere	27
3.2.5 Lightning.	27
3.2.6 Dust	27
3.3 EMERGENCY	27
3.3.1 Emergency Stop	27
3.3.2 Rotor Locking.	27
3.4 ROTOR	27
3.4.1 Blades	27
3.4.2 Blade Support Arms	28
3.4.3 Rotating Tower	29
3.4.4 Disc Brake	30
3.5 FIXED TOWER	31
3.5.1 Tower.	31
3.5.2 Foundation	31
3.6 CONTROL SYSTEM.	32
3.6.1 Sensors.	34
3.6.2 Control Unit	34
3.6.3 Blade Actuators.	34
3.6.4 Power Distribution	36
3.6.5 Wiring	36
3.7 ELECTRICAL OUTPUT SYSTEM.	36
3.7.1 Speed Increaser.	36
3.7.2 Generator.	37
3.7.3 Electrical Equipment	37
3.8 MECHANICAL OUTPUT ADAPTER	37
3.9 TEST INSTRUMENTS.	37
4. AERODYNAMICS AND PERFORMANCE	38
4.1 AERODYNAMICS	38
4.1.1 Blade.	38
4.1.2 Blade Support Arms	42
4.1.3 Drag Breakdown	43
4.2 PERFORMANCE	43

TABLE OF CONTENTS (Continued)

<u>Section</u>	<u>Page</u>
5. EXTERNAL LOADS	48
5.1 CONDITION (MAXIMUM ULTIMATE OUTBOARD AND INBOARD RADIAL LOAD)	48
5.2 CONDITION 2 (MAXIMUM BLADE TANGENTIAL AND COMBINED RADIAL AND TANGENTIAL LOAD)	54
5.3 CONDITION 3A AND 3B, STORM LOADS, WITH AND WITHOUT ICE.	54
5.4 CONDITION 4 (OPERATING LOADS)	54
5.5 COMBINED LOADS.	54
6. ROTOR DESIGN	55
6.1 BLADES.	55
6.1.1 Structural Description	55
6.1.2 Static Stress Analysis	58
6.1.3 Blade Fatigue Analysis	61
6.2 SUPPORT TUBE FATIGUE.	63
6.2.1 Structural Description	63
6.2.2 Support Arms Stress Analysis	67
6.3 Rotating Tower.	67
6.3.1 Structural Description	67
6.3.2 Rotating Tower Stress Analysis	68
7. FIXED TOWER.	70
7.1 TOWER	70
7.1.1 Structural Description	70
7.2 FOUNDATION.	78
7.2.1 Structural Description	78
7.2.2 Stress Analysis.	78
8. WEIGHTS.	82
9. STRUCTURAL DYNAMICS.	83
9.1 VIBRATION ANALYSIS.	83
9.2 FLUTTER ANALYSIS.	83

TABLE OF CONTENTS (Continued)

<u>Section</u>	<u>Page</u>
10. CONTROL SYSTEM DESIGN.	89
10.1 CONTROL SYSTEM ANALYSES.	89
10.1.1 Linearized Steady State Control Analyses	89
10.1.2 Dynamic Analysis	93
10.1.3 Actuator Performance Analysis.	112
10.1.4 Actuator Simulator Analysis.	117
10.2 CONTROL UNIT	126
10.2.1 Processor.	126
10.2.2 Sensor Interface	129
10.2.3 Actuator Interface	133
10.2.4 Software	133
10.3 ACTUATOR	141
10.3.1 Motor.	141
10.3.2 Amplifier.	142
10.3.3 Gearbox	145
10.4 POWER DISTRIBUTION	146
10.4.1 Power System	146
10.4.2 Power Switching.	146
10.5 INTERCONNECT WIRING.	152
11. MECHANICAL AND ELECTRICAL OUTPUT POWER SYSTEM.	155
11.1 RPM INCREASER.	155
11.2 ELECTRICAL OUTPUT DESIGN 1	157
11.3 ELECTRICAL OUTPUT DESIGN 2	157
11.4 ELECTRICAL OUTPUT DESIGN 3	159
11.5 ELECTRICAL OUTPUT DESIGN 4	159
11.6 MECHANICAL OUTPUT KIT.	160
12. FAILURE MODE AND EFFECTS ANALYSIS.	163
13. TEST INSTRUMENTATION	167
14. TEST PLAN.	172
14.1 PRE-START UP CHECKOUT.	172
14.1.1 Visual Checkout.	172
14.1.2 Functional Checks.	172

TABLE OF CONTENTS (Concluded)

<u>Section</u>	<u>Page</u>
14.2 FIRST START UP CHECKS - ELECTRICAL CONFIGURATION	172
14.3 DYNAMICS TEST.	174
14.4 PERFORMANCE (LONG TERM) TESTING.	174
14.5 SPECIAL TESTS (INTENSIVE TESTING).	175
14.5.1 Emergency Simulations.	175
14.5.2 Development Tests.	175
14.5.3 System Improvement Tests	176
14.6 MECHANICAL SYSTEM TESTING.	176
14.7 MAINTENANCE PROCEDURES	176
15. PRELIMINARY BUDGETARY PRODUCTION COSTS	179
16. CONCLUSIONS AND RECOMMENDATIONS.	184
REFERENCES.	185
APPENDIX A - DETAILED STRENGTH ANALYSIS	A-1

LIST OF ILLUSTRATIONS

<u>Figure</u>		<u>Page</u>
1	Baseline Giromill Design Configuration.	3
2	Geometry Trade Study Matrix	4
3	Geometry Trade Study Comparison	5
4	Generator Cost Comparison for Operation with a Large Utility Grid.	8
5	Hydro/Mechanical Control System	9
6	Electrical vs Hydraulic Blade Actuation Cost.	10
7	Intermediate Supports Produces Lowest Bending Movement. . .	11
8	Blade Flexibility Must Be Considered in Sizing Actuator . .	12
9	Blade General Arrangement	13
10	Support Arm Trade Study Configurations.	14
11	Sensitivity to Power Output to Support Arm Fairing.	15
12	Cylindrical Steel Fixed Tower vs Truss Tower.	15
13	Baseline Giromill Design Configuration.	16
14	Selected Configuration.	17
15	Comparison of Configurations.	18
16	Summary of Changes.	18
17	Giromill Hardware Cross Reference	20
18	40 kW Wind Conversion System Specifications	21
19	Design Wind Profiles.	23
20	Wind Direction Variation Due to Gusts	24
21	Design Gust Velocity.	25
22	Peak Gust Magnitude - Frequency Relationship.	26
23	Rotor Parameters Definition	32

LIST OF ILLUSTRATIONS (Continued)

<u>Figure</u>		<u>Page</u>
24	Control System Design Criteria.	33
25	Control Function Variable Capability.	35
26	Control System Instrumentation Parameters	35
27	Rotor Blade Aerodynamic Characteristics	38
28	C_{lMAX} Comparison NACA Symmetrical Airfoils.	39
29	Minimum Drag Comparison NACA Symmetrical Airfoils	39
30	Effect of Tab Geometry on Blade Stability	40
31	Airfoil Comparison.	40
32	Blade Aerodynamic Characteristics	41
33	Rotor Aerodynamic Characteristics	41
34	Blade Aerodynamic Characteristics	42
35	Giromill Blade Aerodynamic Characteristics.	43
36	Drag Breakdown.	44
37	Giromill Estimated Performance.	44
38	Giromill Control Performance.	45
39	Power Output Breakdown.	46
40	Giromill Power Output	46
41	Annual Energy (Rotor Centerline at h = 75 ft)	47
42	Annual Energy (Rotor Centerline at h = 50 ft)	47
43	Summary of Critical Design Load Conditions.	48
44	Giromill Ultimate Design Load - (Condition 1).	49
45	Maximum Aerodynamic Radial Load - (Condition 1)	49
46	Design Gust Velocity.	50
47	Design Wind Profiles.	51

LIST OF ILLUSTRATIONS (Continued)

<u>Figure</u>		<u>Page</u>
48	Giromill Ultimate Design Load - (Condition 2)	52
49	Storm Loads - (Condition 3)	53
50	Blade Aerodynamic Normal Load	53
51	Design Criteria for Ice and Snow Conditions	54
52	Blade General Arrangement	56
53	Blade Cross - Section	56
54	Blade General Arrangement (View B).	57
55	Blade Assembly.	58
56	Blade Assembly - Freebody, Shear and Moment Diagrams - (Condition 1A).	59
57	Blade Skin Stress Analysis - (Condition 1A)	59
58	Blade Skin Stress Analysis - (Condition 1A)	60
59	Support Tube Stress Analysis - (Condition 1A)	60
60	Blade Fatigue Load Spectrum	61
61	Blade Fatigue Load Cycles	62
62	Blade Fatigue Life Estimate	62
63	Summary of Blade Skin Fatigue Analysis.	63
64	Support Tube Fatigue Life Estimate.	64
65	General Arrangement Support Arm	64
66	Arm/Tower Attachment.	65
67	View E-E.	65
68	Upper Arm Strut Connectors.	66
69	Top Strut Connection.	66
70	Intermediate Brace Connectors	67

LIST OF ILLUSTRATIONS (Continued)

<u>Figure</u>		<u>Page</u>
71	Rotating Tower.	68
72	Rotating Tower Loads at Upper Bearing Support	69
73	Fixed Tower	70
74	Fall Prevention Service	71
75	Upper Bearing	72
76	Upper Bearing Mounting.	72
77	Upper Bearing Mounting (Plan View).	73
78	Lower Bearing	74
79	Lower Bearing (Side View)	74
80	Lower Bearing Mounting (Plan View).	75
81	Caliper Brake	76
82	Plan View of Brake Support Assembly DWG D40386.	77
83	Side View of Brake Support Assembly	78
84	Foundation Pier	79
85	Anchor Rods	79
86	Fixed Tower Foundation Loads.	80
87	Fountain Pier Analysis Uplift	81
88	Maximum Soil Pressure (Ultimate Condition 3.4).	81
89	Giromill Weight Breakdown (Design 1).	82
90	Vibration Frequencies and Mode Shapes	84
91	Structural Frequencies vs Rotation (Fixed Coordinate System)	87
92	Typical Bending Pitch Blade Flutter Boundaries.	88
93	Blade Hinge Moment Stiffness	88

LIST OF ILLUSTRATIONS (Continued)

<u>Figure</u>		<u>Page</u>
94	Steady State Linearized Control System Representation (Induction Generator with Grid Tie-in)	90
95	Giromill Control (Steady State Linear System)	90
96	Steady State Linear System (Nomenclature)	91
97	Steady State Linearized Control Root Locus on K_R	91
98	Steady State Linearized Control Frequency Characteristics .	92
99	Steady State Linearized Control Time Responses.	92
100	Giromill Control System (SMP Simulation).	94
101	Giromill Control System CSMP Simulation - Actuator.	95
102	Giromill Control System CSMP Simulation - Blade Movement Components.	97
103	Blade Moment Equations.	98
104	Giromill Control System CSMP Simulation - Induced Flaw and Rotor Torque.	99
105	Induced Airflow and Rotor Torque Equations.	100
106	Giromill Control System CSMP Simulation - Rotor Dynamics. .	101
107	Giromill Control System CSMP Simulation - Generator	102
108	Giromill Control System CSMP Simulation - Controller.	103
109	Auxillary Equations Calculations.	105
110	20 MPH WInd Blade Airload	105
111	Blade Airloads.	106
112	Blade Force Relationship at Constant Power.	106
113	Blade Loads Due to Severe Gust.	107
114	Below Rated Power Wind Gust	108

LIST OF ILLUSTRATIONS (Continued)

<u>Figure</u>		<u>Page</u>
115	Blade 1 Normal Load and System Power.	108
116	Blade 1 Rock Angle and Rock Angle Error	109
117	Above Rated Power and Gust.	109
118	Blade 1 Angle-of-Attack and System Power.	110
119	Blade 1 Angle and Rock Angle Error.	111
120	Wind Gust Runs Comparison	111
121	Giromill Start-Up	112
122	Partial Power Performance	113
123	Partial Power Control Performance	114
124	Blade Actuator Torque Components.	115
125	Blade Actuator Requirements (20 MPH).	116
126	Blade Actuator Requirements (40 MPH).	116
127	Blade Actuator Maximum Rate and Acceleration.	117
128	Actuator Closed Loop Frequency Response	118
129	Actuator Closed Loop Frequency Response	118
130	Actuator Closed Loop Frequency Response	119
131	Actuator Math Model	121
132	Actuator Simiplied Model.	122
133	Rock Angle Servo System (List of Symbols)	123
134	Actuator Model Comparison (40 MPH).	124
135	Final Values Actuator Simulation Response	125
136	Envelope Drawing Giromill Control Unit.	127
137	Processor Functional Diagram.	128
138	Giromill Control System Diagram	130

LIST OF ILLUSTRATIONS (Continued)

<u>Figure</u>	<u>Page</u>
139	Wind Speed Sensing Flow Diagram 132
140	Programmed Rock Angle Profiles. 134
141	Memory Map of Look-Up Table PROM. 135
142	Giromill Control System - Processor Phase Sequence. 135
143	Processor Flow Diagram. 136
144	Software Symbol Definition. 140
145	Blade Actuator Assembly 142
146	Schematic Servo Amplifier Board 143
147	Schematic Servo Driver Board. 144
148	Gear Box Loads. 146
149	Control System Alternator Plan View 147
150	Control System Alternator (Side View) 148
151	Electrical Panel. 149
152	Envelope Drawing Giromill CSPSU 150
153	Giromill CSPSU Schematic Diagram. 151
154	Power Control Flow Diagram. 152
155	Slip Ring Assembly. 153
156	Wire Routing. 154
157	Speed Increaser 155
158	Electrical Drive System Assembly (Plan View). 156
159	Electrical Drive System Assembly (Side View). 157
160	Block Diagram of Giromill Electrical Output Power for Operation with a Large Utility Grid - Design 1. 158
161	Torque vs RPM 158

LIST OF ILLUSTRATIONS (Continued)

<u>Figure</u>		<u>Page</u>
162	Block Diagram of Giromill Electrical Output Power System for Operation as a Single Unit - Designs 2 and 3.	159
163	Block Diagram of Giromill Electrical Output Power System for Operation with Two or More Machines to Form an Independent Small Utility Grid - Design 4	160
164	Mechanical Drive System Assembly (Plan View).	161
165	Mechanical Drive System Assembly (Side View).	162
166	Failure Mode Effects Analysis	163
167	Giromill Schematic with Instrumentation Location.	168
168	Structural Instrumentation.	169
169	Additional Sensors or Controller Supplied Measurements. . .	170
170	Partial Instrumentation Approval.	171
171	Visual Inspection Checkout List	173
172	Functional Check of Selected Systems.	174
173	Emergency Simulation.	175
174	Recommended System Improvement Tests.	176
175	Giromill Estimated Performance.	177
176	Test Maintenance Proceeded.	178
177	Ground Rules for Costing 1000th Unit.	179
178	Giromill Budgetary Cost Estimate.	180
179	Fixed Tower Budgetary Cost Estimate	181
180	Rotating Tower Budgetary Cost Estimate.	181
181	Support Arm Budgetary Cost Estimate	181
182	Blade Budgetary Cost Estimate	182

LIST OF ILLUSTRATIONS (Concluded)

<u>Figure</u>		<u>Page</u>
183	Control System Budgetary Cost Estimate.	182
A-1	Support Arm Cross Section	A-1
A-2	Critical Loads on Root Attack Fitting	A-2
A-3	Upper Bearing Support Area.	A-4
A-4	Critical Leg Component Identification and Free-Body	A-7
A-5	Fixed Tower Column Cross-Section.	A-8

LIST OF SYMBOLS

The symbols defined herein are used generally throughout the text of the report. Symbols which are germane only to a particular section, usually associated with a computer program, are defined in the section where they are used.

A	Gust amplitude or area
a.c.	Aerodynamic center - % chord
AR _R	Rotor aspect ratio
b	Blade span - Ft
C	Blade chord - Ft
c	Distance to outer fiber from centroid - in.
c _d	Two dimensional drag coefficient
C _{dA}	Average support arm drag coefficient
C _{de}	Equivalent drag coefficient
C _{do}	Drag coefficient at zero angle of attack
CF	Centrifugal force - lb
c.g.	Center of gravity - % chord
c _l or C _l	Two dimensional lift coefficient
C _p	Power coefficient
D	Rotor diameter - ft
DLS	Design limit stress - psi
f	Stress - psi
f _b	Bending stress - psi
F _{TU}	Ultimate tensile stress - psi
g	Acceleration due to gravity - 32.2 ft/sec ²
G	Gust factor
h	Elevation - ft

H	Time - hours
h_o	Surface length - ft
h_r	Reference elevation - ft
I	Moment of inertia - slug ft ² or in ⁴
I_B	Blade inertia about pivot axis - slug ft ²
k	Factor for unsteady aerodynamics
K_T	Stress concentration factor
$K_{T_{nom}}$	Stress concentration for unloaded hole
$K_{T_{Total}}$	Maximum stress concentration
K_1-K_5	Controller command gains
LC	Learning curve
M	Bending moment - in.-lb
M.S.	Margin of safety
PA	Pivot axis
q	Dynamic pressure
R	Support arm length or radius - ft or in.
r_x	Truss length - ft
R_N	Reynolds number
S_A	Support arm reference area - ft ²
S_B	Blade reference area - ft ²
t	Blade thickness - ft or in.
t	Time - sec
T	Torque - ft-lb or in.-lb
\bar{V}	Mean wind - ft/sec
V_g	Longitudinal gust ~ ft/sec
V_h	Wind speed at elevation h - ft/sec

\bar{V}_h	Mean wind speed at elevation h - ft/sec
\bar{V}_r	Mean wind speed at referenced elevation - ft/sec
V_{ROTATION}	Velocity due to rotation - ft/sec
V_{TOTAL}	Total wind velocity - ft/sec
V_w	Wind speed - ft/sec
V_x, V_y, V_z	Load in x, y, and z directions - lb
W	Weight - lb
x, y, z	Axes
α_e	Effective angle of attack - Deg
α_i	Induced angle of attack - Deg
β	Flip axis angle - Deg
ψ	Blade phase angle - Deg
δ	Deflection - in.
λ	Blade speed ratio = $\frac{\omega R}{V_w}$
σ	Rotor solidity or stress - psi
θ_c	Commanded rock angle - Deg
θ_R	Blade rock angle - Deg
ω	Rotation rate - Rad/sec or RPM

1.0 INTRODUCTION

The objective of Phase I of the program was to determine the best configuration for a 40kW output vertical axis windmill and to complete its detail design.

1.1 BACKGROUND - Little effort has been spent toward development of vertical axis windmills. However, several studies and tests, including two performed by MCAIR for ERDA References 1 and 2, have indicated that the vertical axis Giromill has a higher wind energy conversion efficiency than a horizontal axis machine. For the same power output, a smaller projected area is required for the Giromill.

The solidity chosen for the Giromill, however is higher than that for a typical horizontal machine of the same power; and that, plus the requirement for blade support arms results in more rotating structure. On the other hand the blades and support arms can be manufactured at lower cost than the more complex blades of the very large horizontal axis machines.

Each machine has other complexities. The horizontal axis machine requires a yaw control system to keep its relatively heavy horizontal shaft and generator assembly turned into the wind. This also complicates the transfer of shaft power to ground level. For a vertical axis machine the rapid and continuous positioning of the blades may result in higher maintenance and replacement costs.

1.2 PROGRAM DESCRIPTION - Phase I of this program began during the first four months with design trade studies and development of design criteria. Near the end of these tasks, when the major elements of the selected configuration had been determined, detailed design began.

MCAIR designed the blades, which will be fabricated by MCAIR at St. Louis.

The other parts of the rotor, the support arms, and rotating tower were designed by Valley personnel. These parts will be fabricated at the Tallulah, Louisiana, plant of Valley Industries. Valley also designed the fixed tower and will fabricate it at Tallulah.

The foundation is similar to designs used frequently by Valley for fire lookout or windmill towers.

The control system was the primary responsibility of MDEC. The MDEC division in St. Charles, Missouri, designed the control unit and will build it. The MDEC division in Grand Rapids, Michigan, designed the actuator package consisting of electric motor, gear box, and amplifying unit. The basic electric motor will be procured from a vendor, but special windings will be installed by MDEC. MDEC designed the gear box and the amplifier and will build it in Grand Rapids.

The mechanical and electrical output systems were designed by Valley. Many of the components will be procured from vendors; the remaining parts will be fabricated at Tallulah.

2.0 DESIGN TRADE STUDIES

The proposal concept shown in Figure 1 was used as the starting point for the trade studies. The goal was to achieve minimum cost, consistent with performance goals and a system life of 30 years.

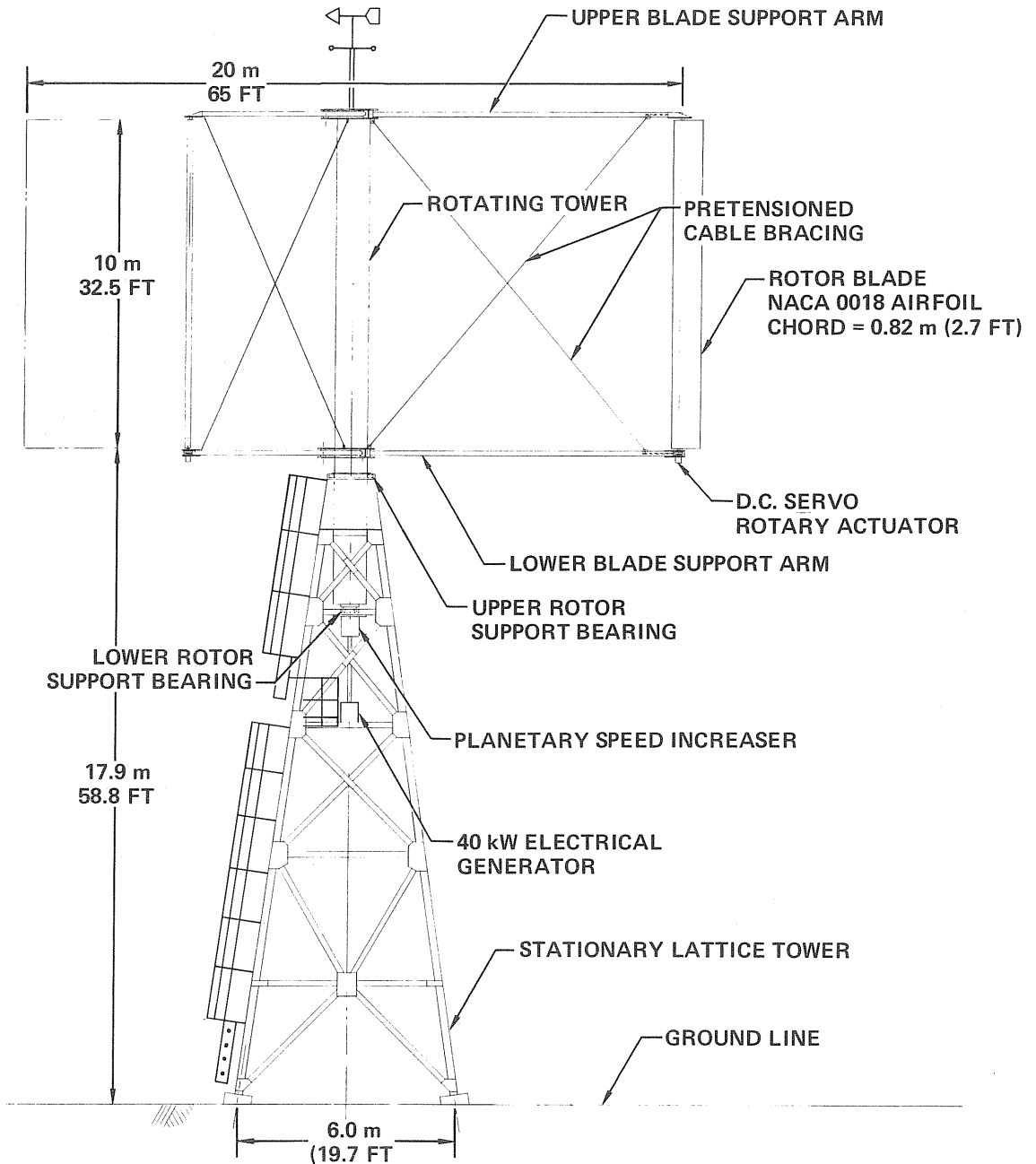


FIGURE 1
BASELINE GIROMILL DESIGN CONFIGURATION
Electrical System Configuration

GP79-0636-128

Seven major trade studies were conducted (Section 2.1 through 2.7) culminating in the preferred design (Section 2.8).

All trade studies were conducted concurrently, and the results of one were factored into the others as they became available. Also, other engineering analyses, such as structural dynamics, aerodynamics, and failure mode and effects, were integrated in the trades.

2.1 GEOMETRY - The geometry trade study between various configurations was accomplished by performing a structural sizing, determining the structural weight and rotor performance, and estimating a cost increment. The configurations investigated are shown in Figure 2. Configuration 1 is the baseline design that was initially proposed. The other configurations were derived from preliminary analyses and experience gained in previous studies (References 1 and 2).

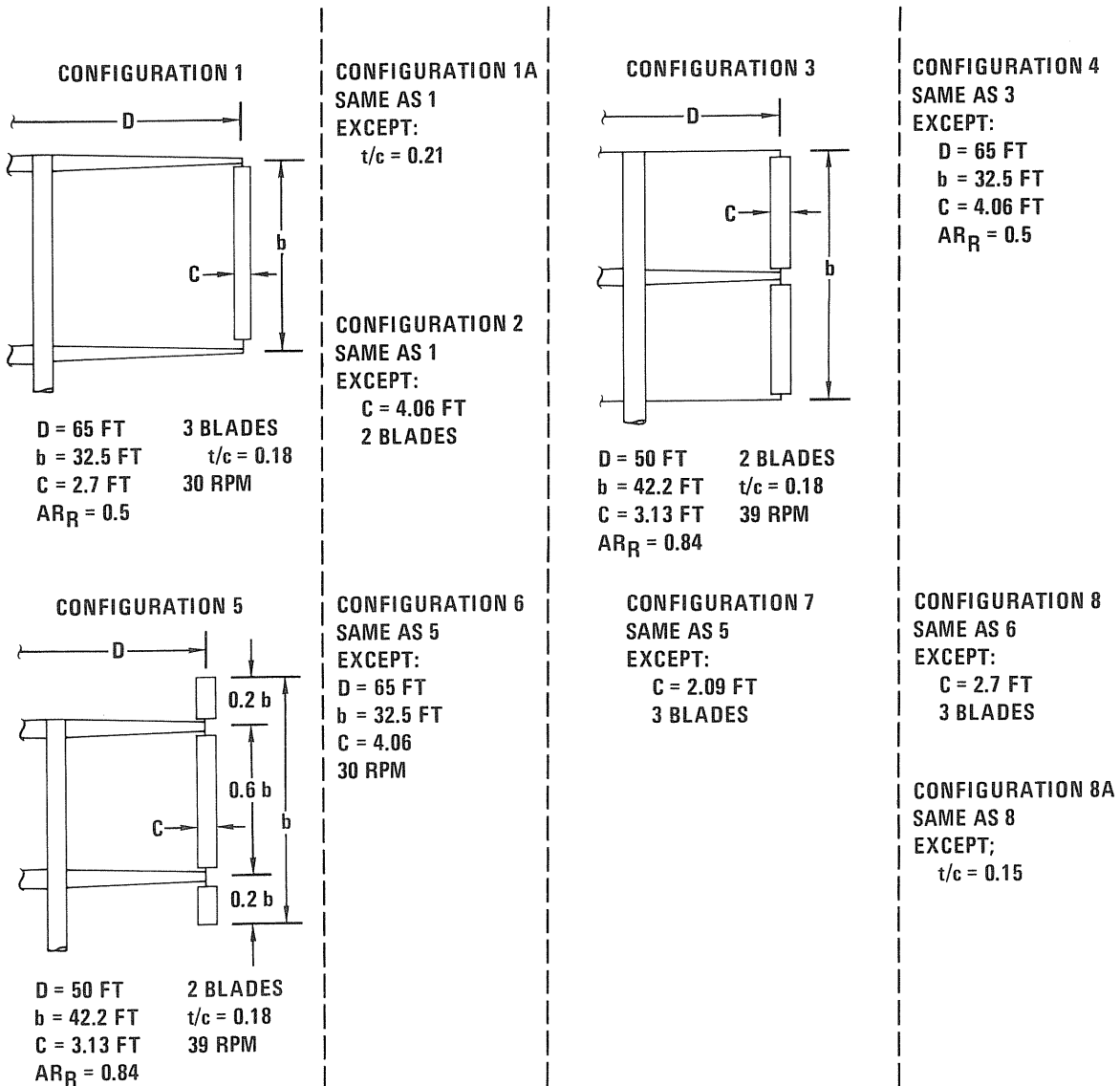


FIGURE 2
GEOMETRY TRADE STUDY MATRIX

All configurations had a solidity (σ) of 0.125. This value had been previously determined to be near optimum in terms of minimizing the performance loss due to aerodynamic damping while maintaining a reasonable RPM.

As previously mentioned, Configuration 1 was the proposal design. Configuration 2 was a two-bladed concept. Configuration 3 increased the rotor aspect ratio (AR_R) to 0.84, and incorporated a split blade with the primary support arm in the center. The end support arms reacted only the centrifugal load. Configuration 4 was a variation of 3. Configuration 5 incorporated a double split blade/support arm concept that minimized the blade bending moment. Configurations 6, 7, and 8 were variations of 5.

The results of this trade study are indicated in Figure 3. All values are put in terms of Configuration 1. A brief discussion follows.

CONFIGURATION	BLADES		SUPPORT ARMS		ROTATING TOWER		FIXED TOWER		CONTROL SYSTEM	TOTAL SYSTEM		
	(WT)	(COST)	(WT)	(COST)	(WT)	(COST)	(WT)	(COST)	(COST)	(WT)	(COST)	\$/kW
1 (PROPOSAL)	1.0	1.0	1.0	1.0	1.0	1.0	1.0	1.0	1.0	1.0	1.0	1.0
1A	0.70	0.83	0.94	1.01	1.0	1.0	1.0	1.0	1.0	0.97	0.94	0.98
2	0.66	0.75	0.67	0.68	1.0	1.0	1.0	1.0	0.78	0.91	0.86	0.86
3	0.64	0.83	0.36	0.32	1.26	1.19	0.94	0.94	0.80	0.87	0.84	0.81
4	0.48	0.74	0.46	0.42	1.0	1.0	1.0	1.0	0.80	0.85	0.86	0.85
5	0.55	0.89	0.48	0.53	0.82	0.87	1.04	1.04	0.85	0.84	0.83	0.80
6	0.48	0.85	0.65	0.70	0.68	0.76	1.08	1.08	0.85	0.86	0.87	0.87
7	0.48	0.93	0.67	0.75	0.82	0.87	1.04	1.04	1.10	0.88	0.92	0.89
8	0.49	0.93	0.84	0.99	0.68	0.76	1.08	1.08	1.10	0.91	0.98	0.98
8A	0.49	0.93	0.84	0.99	0.68	0.76	1.08	1.08	1.10	0.91	0.98	0.94

GP79-0636-3

**FIGURE 3
GEOMETRY TRADE STUDY COMPARISON**

Increasing the blade t/c is an effective way of reducing the weight of the blade. This is because the bending moment of inertia increases rapidly. This is seen by comparing Configurations 1 and 1A, where the blade weight was reduced 30% by increasing t/c from 0.18 to 0.21. The effect on cost per kWh, however, was small, since Giromill performance was decreased and the cost saving effect on other parts was small.

Comparing Configuration 2 with 1 (and also 5 and 7) shows the effect of two-bladed vs three-bladed rotors. Total blade area was kept the same. In both cases two blades cost less. With the blades fixed at the ends (Configurations 1 and 2), two blades also weigh less. With the blades supported to give minimum blade bending, three blades weigh less. This is because the thicker cross-section of the two-bladed configuration reduces

the load, thus decreasing the structure thickness to minimum gauge so that full advantage of the decreased stress level cannot be obtained (see Section 2.4). Both the weight and cost of the support arms are lower with two-bladed rotors.

The overall effect shows that two-bladed rotors would be more cost effective than three-bladed rotors if there were not other technical problem areas which must also be evaluated. For the Giromill two-bladed rotors, the torque output undergoes a large variation in each revolution. This torque ripple effect on the structure, speed increaser, and generator is not well understood. Most all the structural dynamic problems become more severe with a two-bladed rotor. The torque ripple coupled with the induction generator would have to be tested to be confident it would work. For this reason a three-bladed rotor was selected. As more is known about the Giromill operation, the problems with a two-bladed rotor should be more thoroughly investigated to determine if a system built to take advantage of the lower cost would be practical.

Configurations 1, 4, and 6 compare support arm concepts. Configurations 3 and 4 were thought to be attractive in that only one center arm would be needed, and the end ones could be simple since they would take only the blade outboard load. Also only two blade wipers would be needed to seal the blade/support arm interface, as opposed to four for Configuration 6. The overall cost trends verified the thought. Again, however, technical problems with a center support concept negated its cost advantage, the principal problem being the blade bending in a tangential direction. As configured, the end support arms offered no resistance in that direction. Making the end support arms capable of taking a load in the tangential direction essentially required three support arms per blade. This would have decreased the performance and increased the cost considerably.

Comparison of Configurations 8 and 8A show the effect of blade t/c with the minimum bending moment concept. In this case there was no effect on blade weight and cost because both blades were at minimum gauge. The lower dollars/kW is due to the higher performance with a thinner blade.

The effect of rotor aspect ratio (AR_R) can be ascertained by comparing Configurations 3 and 5 and 4 and 6. Both comparisons indicate that increasing AR_R from 0.5 to 0.84 is cost-effective.

The results of this trade study, along with others discussed later, lead to the selection of a three-bladed rotor having an AR_R of approximately 0.8. The blades are in three pieces and supported so they experience a near-minimum bending moment. The final design selected is described in Section 2.8.

2.2 DRIVE SYSTEM

2.2.1 RPM Increaser - The baseline RPM increaser was a planetary gear box having a 60-to-1 gear ratio with a direct coupling to the generator.

Investigation has not uncovered any planetary speed increasers that have the efficiency (over 90%) and low cost to be serious contenders. The large wheel drives used on large earth moving equipment, which use planetary sets as reducers, were initially thought of as likely candidates to be applied as windmill speed increasers. However, discussions with producers of these machines revealed unexpectedly low efficiency when back driven. As speed increasers, efficiency of less than 70% was quoted. One company offered to design a "special" that would be more efficient, but it would be costly and require additional time.

Parallel shaft helical gear increasers (or reducers) of the shaft mounted type are a stock item with several manufacturers of power transmission equipment. There seems to be no better developed class of gear boxes in standard routine production. The extensive service experience this class of gear set has seen is itself a very strong recommendation, for its reliability and competitive cost.

The shaft mounted gear set, as a reducer, is normally set up with the motor mounted directly on the case and the belt connected to the input shaft. In our application the power flow is reversed, but it is still convenient to mount the generator directly on the gear case and use a timing belt drive to couple the two.

To avoid the cost of a special gear set for the prototype Giromill, a standard ratio of 24.3 to 1 was selected, with the final ratio of 54.675 to 1 being achieved with a timing belt, with a ratio of 2.25 to 1, as the final stage.

2.2.2 Generator - The original baseline generator was a synchronous generator. However, studies indicate that to operate with an existing utility grid, three phase, 480 volt +5%, it would be preferable to use an induction generator for the following reasons:

(1) A cost of \$1,453 for induction generator and controls versus \$2,729 for the synchronous generator and controls (See Figure 4).

(2) Simplicity, requiring fewer components.

(3) No synchronizing controls required for connection to utility grid.

(4) Easier to disconnect in the event of utility grid failure. If there is no voltage on the utility grid the generator contactor will open, disconnecting the generator from the line. The contactor can reconnect the generator to the line when power input conditions are satisfactory.

(5) Better ability to absorb speed changes due to wind gusts. For example, if the speed has to increase 4% to get full load output, the speed could then increase another 4% before the induction generator would pull out of step with the line and at the same time it would generate approximately double the full load output.

(6) Simpler and more rugged rotating member.

	SYNCHRONOUS GENERATOR	INDUCTION GENERATOR
GENERATOR	\$1320.00	\$1100.00
VOLTAGE REGULATOR AND PARALLELING ACCESSORIES	396.00	—
LOAD SHARING CONTROL AND CURRENT TRANSFORMERS	292.00	—
AUTOMATIC SYNCHRONIZER	368.00	—
CIRCUIT BREAKER	130.00	130.00
MAGNETIC CONTACTOR	223.00	223.00
TOTAL	\$2729.00	\$1453.00

GP79-0636-21

FIGURE 4
GENERATOR COST COMPARISON FOR OPERATION WITH A LARGE UTILITY GRID
 480V Operation Approximate Costs (Lots of 1)

For the stand alone and small utility grid electrical systems designs the synchronous generator was selected because no field excitation is available for an induction generator and equipment would have to be added.

2.3 CONTROL SYSTEM - Trade studies on the control system proceeded along two directions: the overall control concept and the blade actuator concept.

2.3.1 Control Concept - Our proposal baseline assumed that a micro-processor controller would be required to meet the stand-alone capability. From a farmer or rancher's viewpoint, however, it was felt that the Giro-mill would be more attractive if the electronics could be eliminated.

Several ideas were looked at, the most promising being a hydro/mechanical system (Figure 5). A wind drag plate was used to activate high or low wind valves. The blades were modulated with a mechanical Stephenson linkage that mixed a high and low wind cam profile according to the rotor speed governor setting. This linkage drove a hydraulic valve to position the blade hydraulic actuator. A wind vane positioned the high and low cams for proper blade orientation with the wind.

A heavy ball in a shallow depression, sensitive to both vibration and rotor RPM, was used for emergency shutdown. The blade actuators were configured so that on shutdown, they would drive the blades to the positions shown on the lower right of Figure 5. This position would allow the entire rotor to weathervane into the wind.

This concept may indeed work. There were, however, many unknowns such as: how close can you maintain RPM, and what performance loss would you get due to non-optimum blade modulation? Also, the mechanical and

hydraulic arrangement would have to be developed and tested. Since we were confident we could make a microprocessor controller work and there was very little time for intensive development, this concept was not selected. Also, we wanted a versatile system that could easily be changed, which again pointed toward a reprogrammable microprocessor control unit.

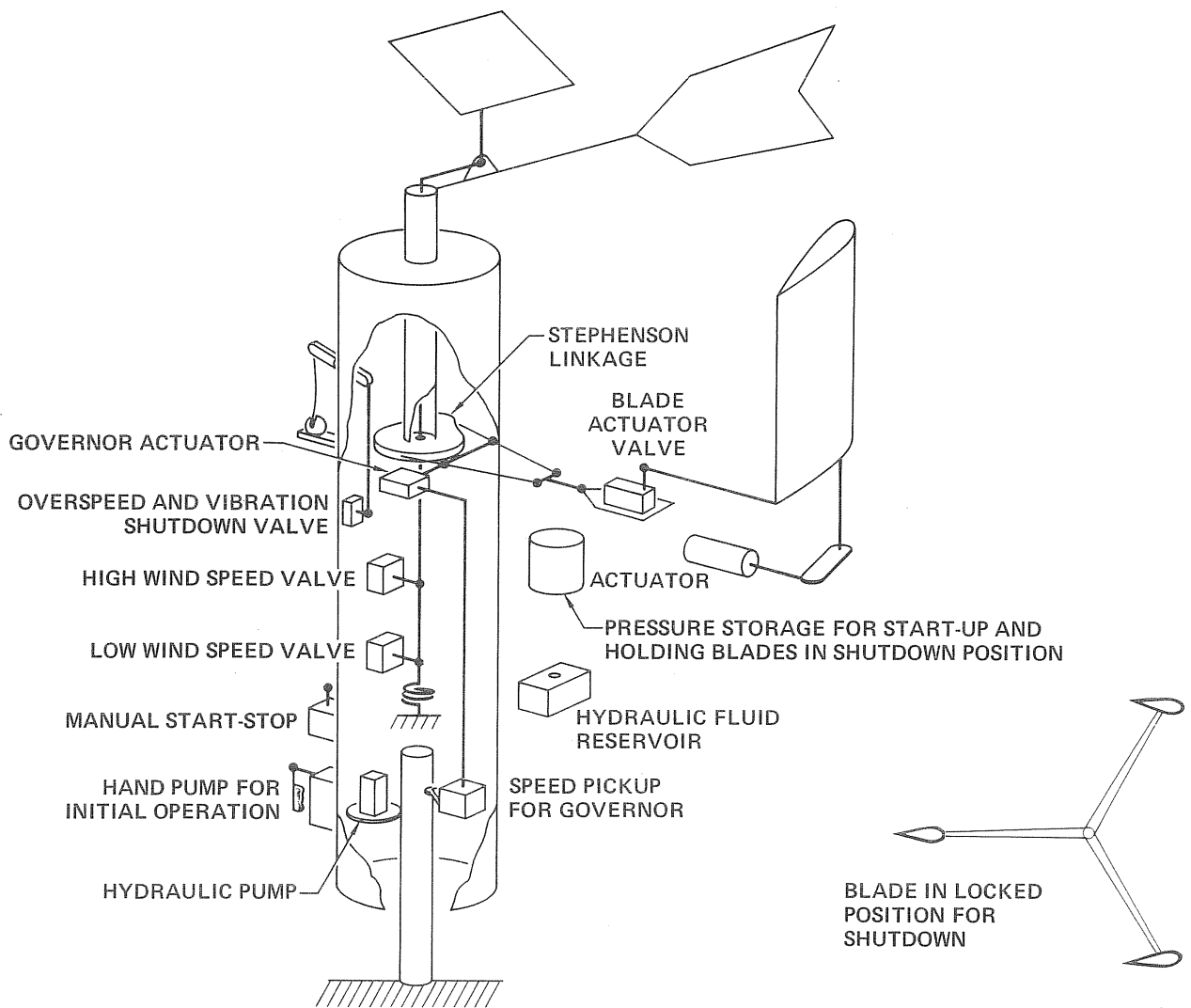


FIGURE 5
HYDRO/MECHANICAL CONTROL SYSTEM

2.3.2 Blade Actuator Trade Study - The proposal baseline assumed a rotary electrical actuator. A trade study against a hydraulic actuator was performed. Both linear and rotary hydraulic actuators were considered.

Linear actuators are restricted to a blade rock angle of $\pm 60^\circ$. This implied that blade weathervaning could not be implemented. However, analysis showed that without the weathervaning, the effects of storms on the other rotor components would be quite high. This precluded the use of linear actuators.

A more detailed trade study of rotary hydraulic versus electrical actuators was then undertaken. Concepts were sketched and the components defined and sized. The hydraulic system would cost over \$1,000 more than electrical, the hydraulic servo-valves being quite expensive. The component cost comparison is shown in Figure 6.

	ELECTRICAL	HYDRAULIC
ACTUATORS	1350	270
POWER SYSTEM	545	345
SERVO-VALVES	—	1713
PUMPS	—	133
VALVES	—	97
MISCELLANEOUS HYDRAULICS	—	459
CONTROLLER	2780	2780
WIRING	165	105
BLADE DRIVE BELT	150	150
SENSORS	440	674
TOTAL SYSTEM COST	\$5430	\$6726

GP79-0636-104

FIGURE 6
ELECTRICAL vs HYDRAULIC BLADE ACTUATION COST

In addition to higher costs hydraulics are susceptible to leakage, and require greater power, and rotary hydraulic actuators would have very limited life when subjected to the Giromill duty cycle.

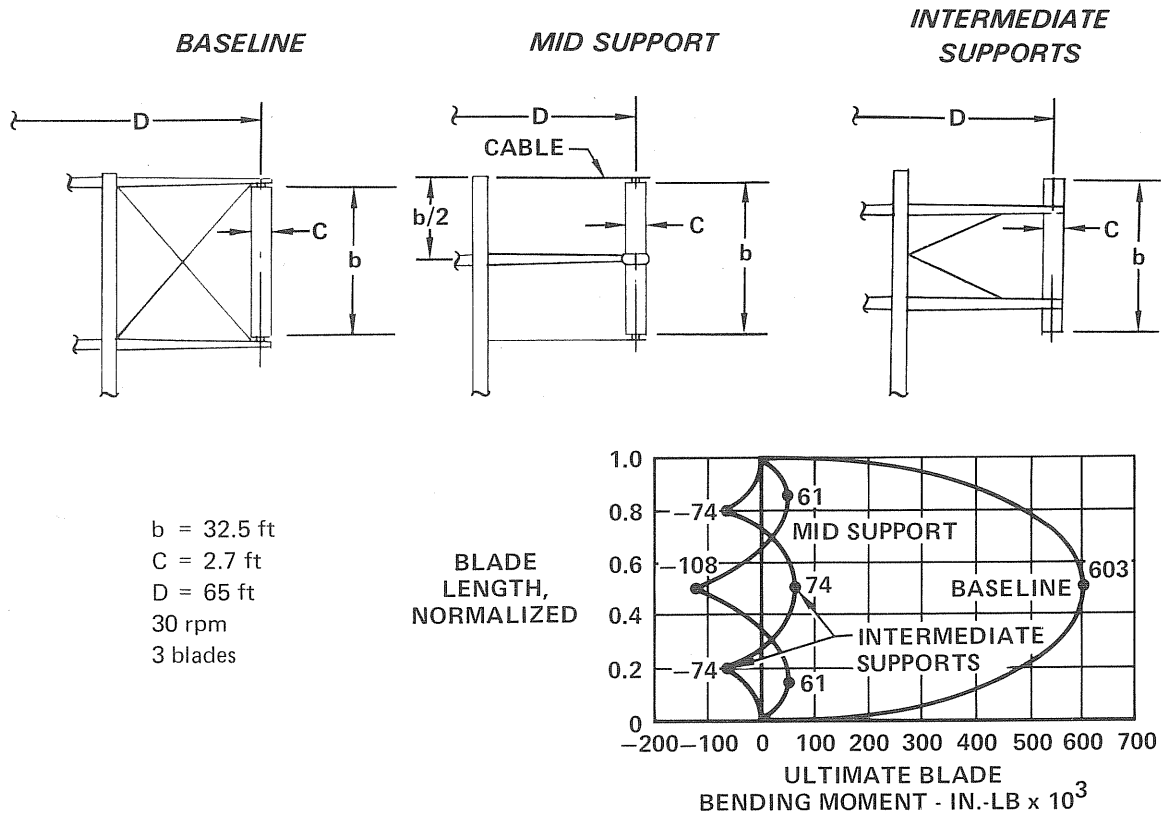
In view of this, electrical actuators were retained as the preferred system.

2.4 BLADE DESIGN - The proposal baseline blade consisted of a closed aluminum extruded leading edge torque box with a thin sheet metal trailing edge, stabilized by formed ribs. The blade was supported at the ends. To reduce costs and weight we evaluated (1) the location of the blade supports, (2) an offset hinge, (3) steel versus aluminum, and (4) several different structural configurations.

2.4.1 Location of Blade Supports - Parametric studies were conducted on methods of blade support to reduce the bending moment and blade deflection. These studies resulted in moving the blade supports closer together. Figure 7 shows the bending moment for three different blade support

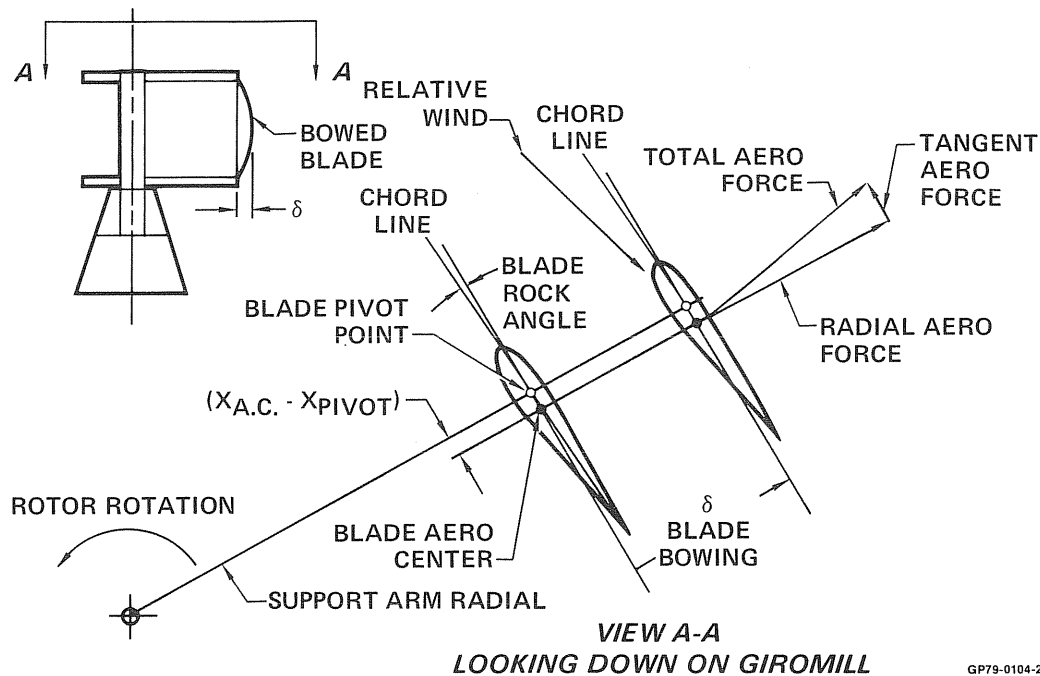
systems. The proposal baseline support system produces a bending moment of 603,000 in.-lb in the blade. The mid-support arm with cables at each end of the blade produces 108,000 in.-lb of bending moment. The intermediate supports reduce the bending moment to 74,000 in.-lb. The intermediate support system was selected because it produced the lowest bending moment and deflection in the blade. The smaller blade deflection reduces the actuator power requirements. (Figure 8).

For the intermediate support system the blades should be supported at approximately 20% and 80% of span to produce the lowest bending moment. The positions of the support arms were relocated slightly towards the center of the blade spans in order to obtain zero slope of the blade at the support arm and to obtain the optimum blade deflection. Bending moments at the support arms were increased slightly. However, torque requirements for the blade actuator were substantially reduced. Structural details are simplified by designing for zero slope at the support arms.



GP79-0226-4

FIGURE 7
INTERMEDIATE SUPPORTS PRODUCES LOWEST BENDING MOVEMENT



GP79-0104-27

FIGURE 8
BLADE FLEXIBILITY MUST BE CONSIDERED IN SIZING ACTUATOR
 Bowed Blade Hinge Moment Geometry

2.4.2 Blade Offset Hinge - The baseline blade design consisted of a centerline support with the axis of rotation about the blade centerline. This concept requires a discontinuity in the blade structure at the support arms where a steel tube is used to support the bearings and to carry the load from the end blades to the center blade. We looked at an offset hinge (Figures 9) so that the blade structure could be continuous. This concept looked very attractive, since the steel support tube could be eliminated. Smaller bearings could also be used, since the bearing is sized by the diameter of the support tube. This would mean a lighter and cheaper blade, since the blade structure would be continuous, the support tubes eliminated, and smaller support bearings could be used.

With this concept the blades could not be weathervaned in high winds; therefore the rotor had to be weathervaned. This caused large rotor loads. The actuator power requirements were also increased, since the moment arm to the applied loads was increased.

This concept was rejected since it caused large rotor loads in high winds and it required larger actuator power outputs.

2.4.3 Steel Versus Aluminum Blade - Steel was also evaluated as a blade material, to reduce cost. However, this resulted in a heavy blade and increased the actuator requirements. Plans were to use beaded aluminum in the trailing edge skins, which resulted in a galvanic corrosion area which would have to undergo special protection. The increased weight and potential corrosion problems eliminated steel as a blade material.

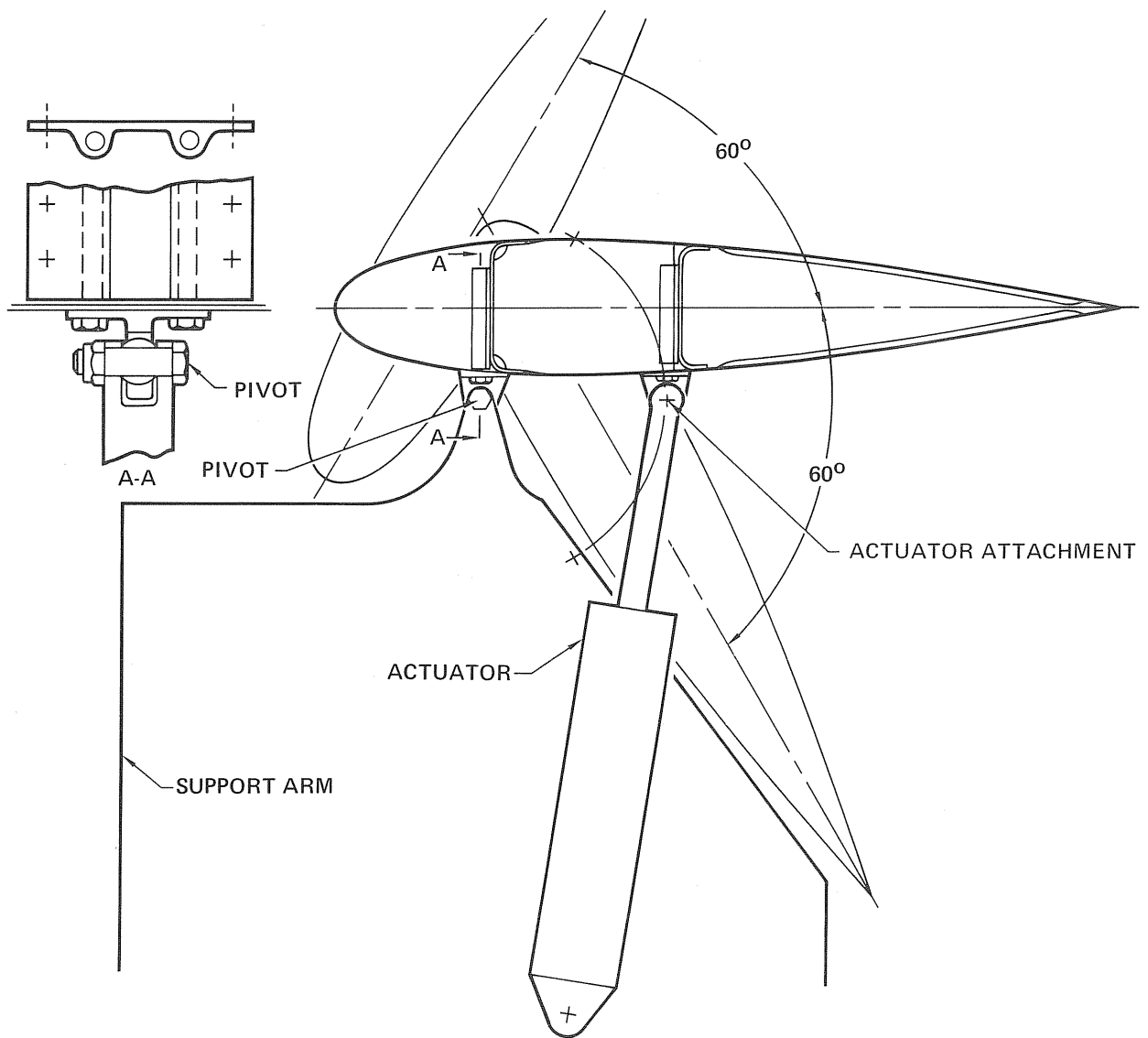


FIGURE 9
BLADE GENERAL ARRANGEMENT
 Offset Hinge

GP79-0636-32

2.4.4 Blade Structural Arrangement - The baseline blade consisted of a closed extruded leading edge torque box with a thin sheetmetal trailing edge, stabilized by formed ribs. To reduce cost an open extrusion and a formed leading edge, both with a sheetmetal spar, were investigated. It was found that the open extrusion or formed leading edge would be the cheapest to produce. For the prototype the formed leading edge would have the lowest cost. Also, a thin beaded trailing edge skin was selected to reduce the number of ribs. This lowered the cost of the ribs and also the assembly time.

Aluminum in the 6061-T6 condition was selected over steel for the blade material because of its higher structural efficiency in fatigue and

excellent resistance to weathering. A 4140 steel tube was selected to support the blades and interface with the support arms because of its high strength. The tube was cadmium plated for corrosion protection.

2.5 BLADE SUPPORT ARMS DESIGN - The proposal baseline support arms were made of two tubes covered with sheet metal, as shown in Figure 10. This configuration has a high drag coefficient, resulting in loss of a significant amount of rotor power. Also, the tubes are not as efficient in bending as in Configurations 2 and 3.

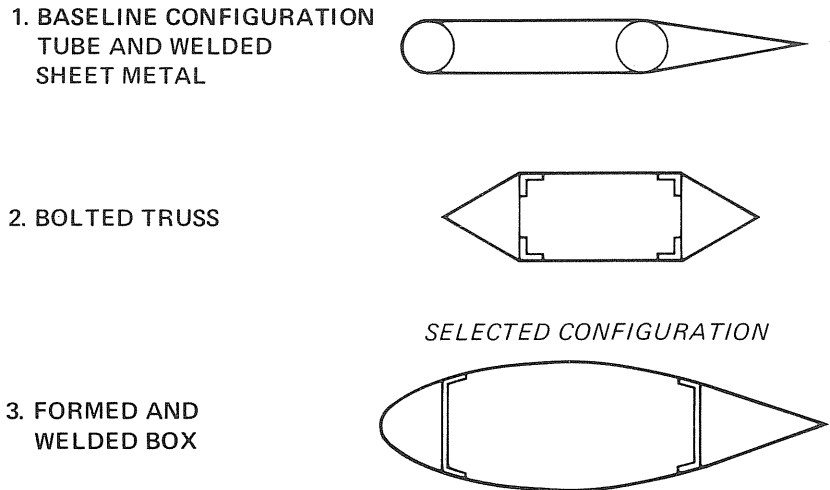


FIGURE 10
SUPPORT ARM TRADE STUDY CONFIGURATIONS

A study was made of the effect of streamlining the support arms, as shown in Figure 11. See Section 4.1.2 for additional discussion on support arm drag.

A bolted truss, covered with sheet metal, was the second configuration considered. It is efficient in bending strength but the loss in rotor power, due to support arm drag, is much greater than the baseline configuration.

The third configuration considered was a formed and welded box. This shape is efficient for carrying bending and combined loads. The drag coefficient is the lowest of the three configurations, resulting in the least loss of rotor power. For these reasons, Configuration 3 was selected.

2.6 ROTATING TOWER - The baseline rotating tower was a 0.125 in. thick steel tube 36 in. in diameter by 45 feet long. During the trade studies the wall thickness was increased to 0.187 in. for ease of fabrication. This reduced the diameter requirement to 24 in. In order to provide easy access to the speed increaser and generator for maintenance, it was also decided to extend the rotating tower to the base of the fixed tower

(moving the lower bearing, speed increaser and generator to the base of the fixed tower also). This requires a 95 ft tube. In production it is anticipated that the fixed tower will be shorter, reducing the length of the rotating tower. Extending the rotating tower reduces side loads on the rotor bearings.

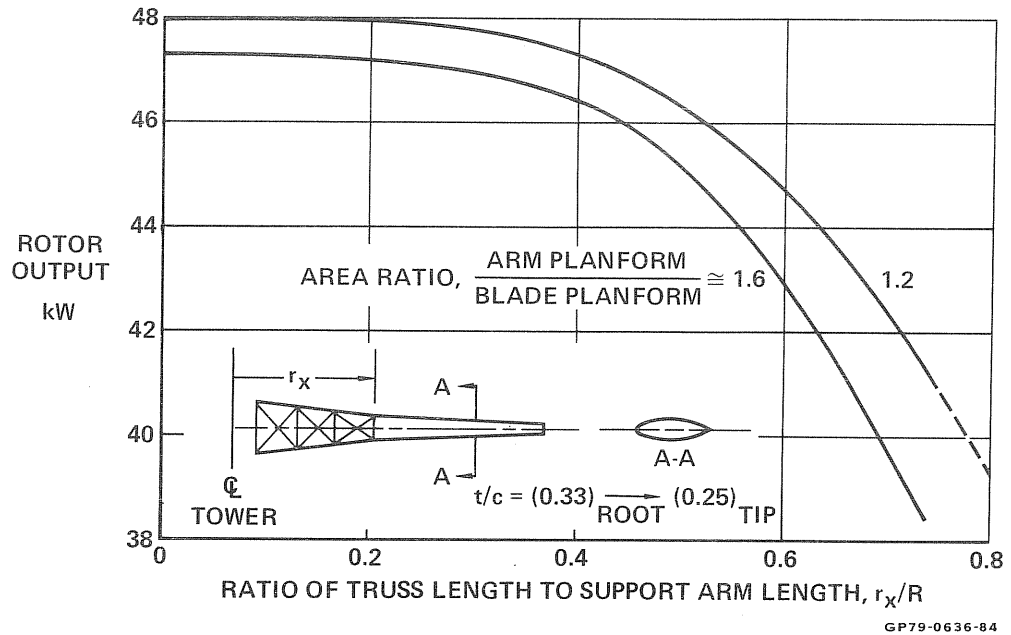


FIGURE 11
SENSITIVITY TO POWER OUTPUT TO SUPPORT ARM FAIRING
 Rotor Diameter = 54 Ft RPM = 36

2.7 FIXED TOWER - A trade study was made of a cylindrical steel tower versus the baseline truss type tower. The two towers were designed to be equivalent in stiffness. Since the base of a truss tower can be spread wider, a truss tower is more efficient than the cylindrical tower.

The cylindrical tower was estimated to weigh 50% more and cost 62% more than the truss tower. Therefore, the truss tower was selected for the final design. The results are summarized in Figure 12.

TOWER TYPE	SHELL DIAMETER	SHELL THICKNESS	TOTAL WEIGHT	RELATIVE COST OF 1000th UNIT
CYLINDRICAL	82.6 IN.	0.188 IN.	11,066 LB	1.62
TRUSS	-	-	7,365 LB	1.00

FIGURE 12
CYLINDRICAL STEEL FIXED TOWER vs TRUSS TOWER

2.8 PREFERRED DESIGN SELECTED - Figure 13 illustrates the configuration in the original proposal. It has three blades. The blades are supported at each end by the support arms. Crossed support struts are attached to the support arms. Two bearings in the top section of the fixed tower support the rotating tower. The fixed tower is a truss tower made of structural angles. The rotor is 65 feet in diameter by 32.5 feet tall.

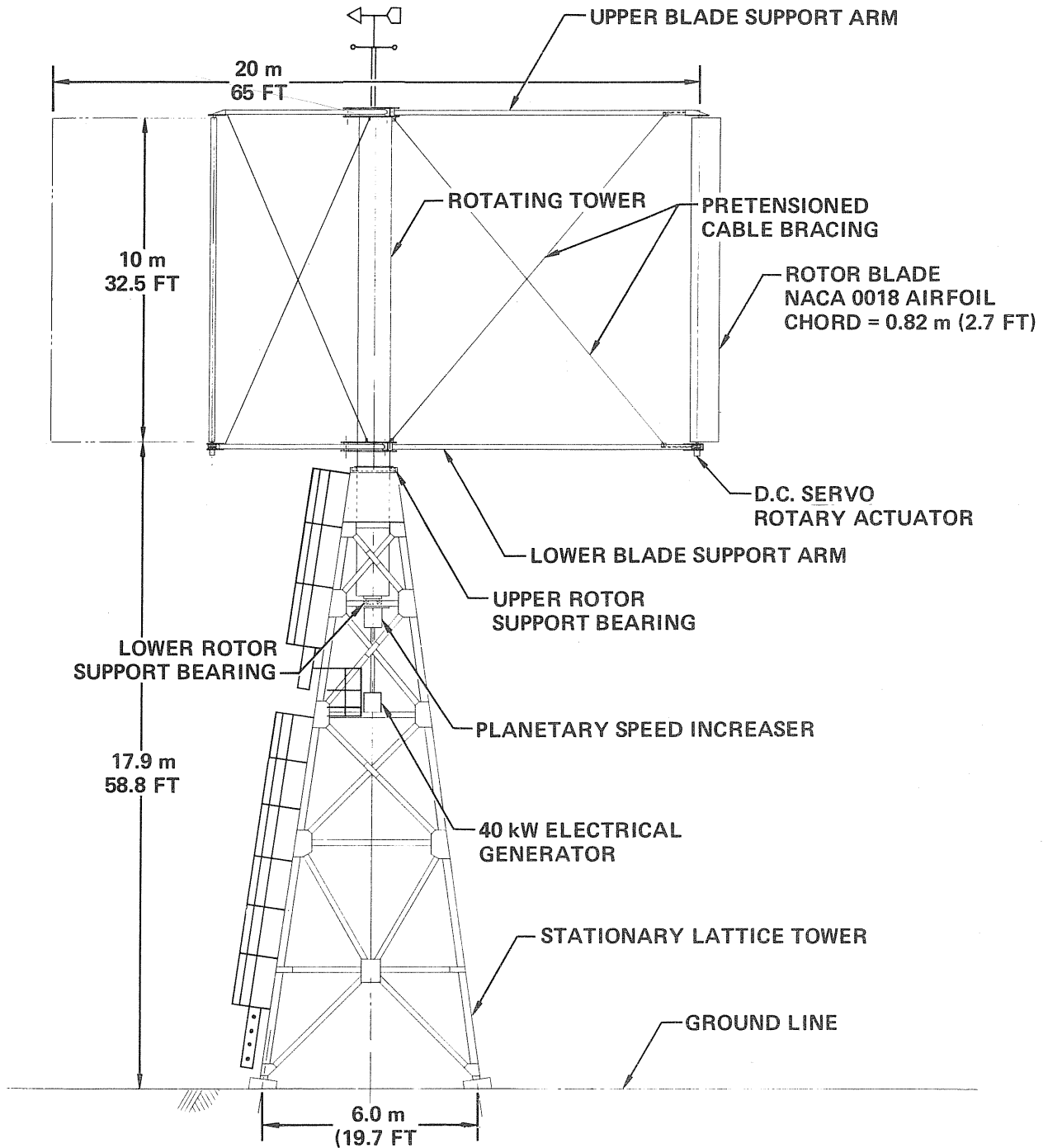


FIGURE 13
 BASELINE GIROMILL DESIGN CONFIGURATION
 Electrical System Configuration

The selected configuration is shown in Figure 14. The rotor has three blades and is 58 feet in diameter by 42 feet tall. The blade supports have been moved closer together. Two struts are attached to the upper support arms and one strut to the lower support arms. The rotating tower extends to the lower part of the tower. It is supported by bearings and the lower end of the fixed tower. The rotating tower was extended to the ground in order to reduce the bearing side loads and to locate the transmission and generator near the ground for easy maintenance. The fixed tower is a truss tower made of structural angles.

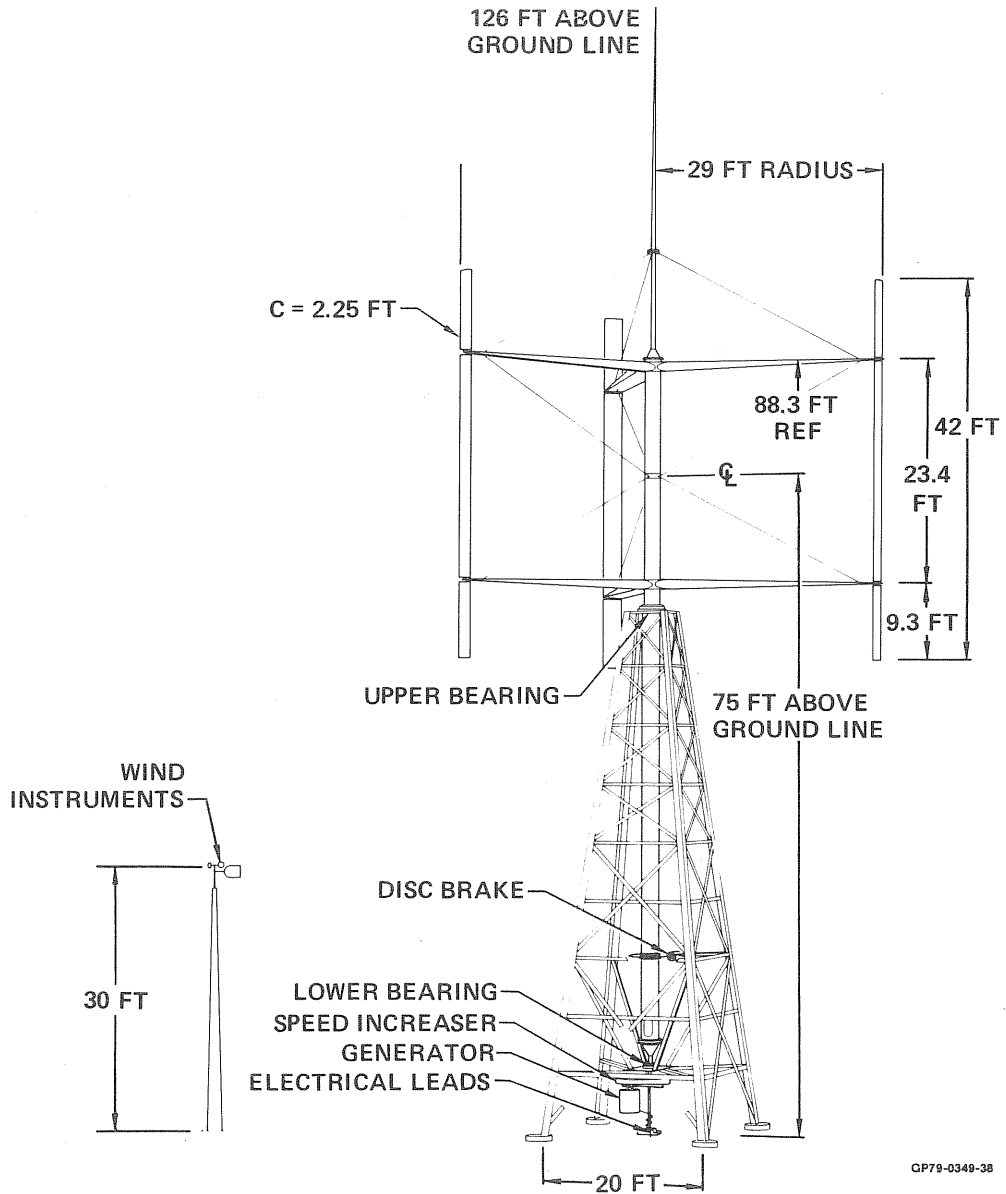


FIGURE 14
SELECTED CONFIGURATION

The configurations are compared in Figure 15. Figure 16 summarizes the changes from proposal configuration.

	PROPOSAL CONFIGURATION	CHOSEN CONFIGURATION
BLADES	ALUMINUM	ALUMINUM
● LENGTH (FT)	32.5	42
● CHORD (IN.)	31	27*
● AIRFOIL	NASA 0018	NASA 0018
SUPPORT ARMS	FAIRED STEEL TUBES	STREAMLINE STEEL SHELL
● RADIUS (FT)	32.5	29
● CHORD AT TIP (IN.)	24	18
ROTATING TOWER	STEEL CYLINDER	STEEL CYLINDER
● HEIGHT (FT)	45	95
● DIAMETER (IN.)	36	24
● RPM	30	33.5
FIXED TOWER	STEEL TRUSS	STEEL TRUSS
● HEIGHT (FT)	52	60
ACTUATORS	ELECTRIC	ELECTRIC
SPEED INCREASER RATIO	60:1	55:1
GENERATOR SPEED	1800	1800
CONTROL SYSTEM	ELECTRONIC	ELECTRONIC
ROTOR BRAKING	WEATHERVANING	WEATHERVANING AND DISC BRAKE

*Plus a 1.5 inch tab.

GP79-0636-43

**FIGURE 15
COMPARISON OF CONFIGURATIONS**

- MOVED BLADE SUPPORT POINTS
- INCREASED BLADE LENGTH
- DECREASED ROTOR DIAMETER
- IMPROVED STREAMLINING OF SUPPORT ARMS
- INCREASED HEIGHT OF FIXED TOWER
- CHANGED CONCEPT OF SUPPORT CABLES
- EXTENDED ROTATING TOWER TO GROUND LEVEL
- CHANGED CUT-OUT SPEED TO 40 MPH

GP79-0636-44

**FIGURE 16
SUMMARY OF CHANGES**

Another change from the proposal was the reducing of the cut-off wind speed from 60 MPH to 40 MPH. This reduced the available annual kWh by only 0.4 of one percent. This small loss in annual energy was more than offset by the reduction in the cost of the Giromill due to lower operating loads and lower blade actuator loads (see Section 10.1.3) in the 40 MPH wind.

The wind instruments were moved from the top of the rotating tower and placed on a 30 ft pole (Figure 14). The primary reason was the reported problems of others with maintenance on wind instruments. In this location they will much easier to service.

A lightning arresting pole was placed on top of the rotating tower. The tip was located so as to give a 45° angle between the Giromill axis of rotation and the line of sight between the upper tip of the blade and the tip of the lightning pole. This precludes the blades being hit by lightning and eliminates the need for brushes between the blades and support arms. Lightning current paths (brushes) are provided at the upper bearing and at the disc brake to take the current from the rotating tower to the fixed tower then to ground.

3.0 DESIGN CRITERIA

The design requirements specified herein refer to the prototype system being built. This system consists of a Giromill having an electrical power output and an adapter kit to convert the system to a mechanical power output.

3.1 GENERAL

3.1.1 Hardware Cross Reference - The subdivision of Giromill hardware defining the Giromill is presented in Figure 17.

GIROMILL SYSTEM	CONTROL SYSTEM	ELECTRICAL OUTPUT SYSTEM
ROTOR	CONTROL UNIT ASSEMBLY	ELECTRICAL DRIVE SYSTEM
● BLADES	● LOGIC ASSEMBLY	● RPM INCREASER
B LADE ASSEMBLY - CENTER	● DISCRETE COMPONENT ASSEMBLY	● GENERATOR
BLADE ASSEMBLY - ENDS	POWER SWITCHING UNIT	● ELECTRICAL EQUIPMENT
SUPPORT TUBE ASSEMBLY	● BATTERY MANUAL CIRCUIT BREAKER	MAGNETIC CONTACTOR
● BLADE SUPPORT ARMS	● ACTUATOR POWER CONTRACTOR	MANUAL CIRCUIT BREAKER
UPPER SUPPORT ARM	SENSORS	AUXILIARY CONTROL RELAY
LOWER SUPPORT ARM	● WIND	● MECHANICAL OUTPUT ADAPTER
UPPER BLADE SUPPORT SECTION	● RPM	● TEST INSTRUMENTS
LOWER BLADE SUPPORT SECTION	● VIBRATION	STRUCTURAL
STREAMLINE CABLES	● ROTOR POSITION	DYNAMICS
● ROTATING TOWER	SLIP RING ASSEMBLY	CONTROL
UPPER CABLE SUPPORT SECTION	● CONTROL FUNCTIONS	● WIND SENSOR MOUNTING POLE
ROTOR SUPPORT SECTION	● ACTUATOR POWER	
LOWER SECTION	POWER CIRCUIT	
LOWER BEARING AND TORQUE	● BATTERY SET	
OUTPUT SECTION	● ALTERNATOR	
LIGHTNING ARRESTING POLE	ACTUATOR ASSEMBLY	
FIXED TOWER	● MOTOR	
● TOWER	● ELECTRONICS	
TOWER STRUCTURE	● RPM SPEED REDUCER	
UPPER BEARING SUPPORT ASSEMBLY	● BLADE POSITION SENSOR	
LOWER BEARING SUPPORT ASSEMBLY		
DISC BRAKE STRUCTURAL		
MOUNTING ASSEMBLY		
● FOUNDATION		
● DISC BRAKE (PROTOTYPE ONLY)		

GP79-0636-134

FIGURE 17
GIROMILL HARDWARE CROSS REFERENCE

3.1.2 Operational Specifications - The system specifications are presented in Figure 18.

3.1.3 Lifetime Goal - The system shall have a minimum lifetime of 30 years, as a design objective. This relates to about 72,000 operating hours at maximum output power.

3.1.4 Dependability - The design goal shall be a system capable of operating with a maximum annual down time of 1% for causes other than insufficient wind.

	ELECTRICAL	MECHANICAL
OUTPUT POWER MODE OPTIONS	40 kW MIN. IN 9 m/s (20 MPH) AT SEA LEVEL DENSITY. 60 Hz, POWER FACTOR OF 0.8 OR HIGHER 1. MATCH WITH EXISTING UTILITY GRID: 3-PHASE, 480 VOLT ±5% 2. INDEPENDENT OF UTILITY GRID: SINGLE MACHINE, 3-PHASE, 480 VOLT ±5% 3. INDEPENDENT OF UTILITY GRID: SINGLE MACHINE, 240 VOLT ±5% 4. 3-PHASE 480 VOLT ±5%, FOR TIE-IN OF TWO OR MORE MACHINES	40kW MINIMUM IN 9 m/s WIND HORIZONTAL SHAFT AT CONSTANT SPEED OF EITHER 440, 880, OR 1760 RPM. SHAFT SPEED NOT TO VARY MORE THAN ±1% FOR WIND SPEED GREATER THAN 9 m/s
HEIGHT	CENTERLINE OF ROTOR SWEEPED AREA TO BE AT A HEIGHT OF 75 FT.	SAME
WIND RANGE CUT-IN	MINIMIZE WITH REGARDS TO ECONOMICS OF POWER PRODUCTION AND SYSTEM COST.	SAME
CUT-OUT*	27 m/s (60 MPH) MINIMUM. SELECTION OF A LOWER SPEED TO BETTER MEET PROGRAM OBJECTIVE OF LOW-COST POWER PRODUCTION MUST BE ADEQUATELY JUSTIFIED.	SAME
PEAK GUST PROTECTION	56 m/s (125 MPH) MINIMUM WITH A 1.5 SAFETY FACTOR	
CONTROLS START/STOP SHUTDOWN/CONTROL	AUTOMATIC AUTOMATIC FOR ROTOR OVERSPEED BACK-UP SHUTDOWN MECHANISM.	SAME
OPERATION	AUTOMATIC CUT-IN, AND CUT-OUT AUTOMATIC RE-ENGAGE AS WINDS DROP BELOW CUT-OUT SPEED	
OUTPUT	AS REQUIRED TO PROVIDE PROPER OUTPUT POWER MODE	

*A cut-out wind speed of 40 mph was selected for the prototype. (Section 10.1.3)

GP79-0636-133

FIGURE 18
40 KW WIND CONVERSION SYSTEM SPECIFICATIONS

3.1.5 Cost Goal - As a design goal, the cost of the final production system, including the tower but exclusive of the foundation and installation, should be \$500/kW (1977 \$). The power output shall be based on the output in a 20 MPH (9 m/s) wind at the centerline of the rotor. Cost shall include G&A and profit and be based on the 1000th unit to be manufactured.

3.1.6 Manufacturing Procedures - Standard manufacturing techniques and soft tooling are to be used. Present process specifications and quality control and material handling procedures will also be used.

3.1.7 Structural Criteria - For design all loading shall be multiplied by a factor of 1.5 to obtain ultimate loads. The minimum margin of safety shall be zero for these loads.

3.2 ENVIRONMENTAL CONDITIONS

3.2.1 Winds

A. Wind Profile - For determining yearly energy output, a wind speed at a height of 30 ft (9.1 m) will be used. The yearly wind profile is expressed as:

$$H = 8766 \text{ Exp} \left[\frac{-\pi}{4.06} \left(\frac{V_w}{\bar{V}_h} \right)^{2.27} \right]$$

where V_w = wind speed

\bar{V}_h = mean wind speed at elevation h

H = hours that the wind speed exceeds V_w .

The wind velocity will change as a function of height according to the 1/7 power law; or for the prototype Giromill having a swept area centroid at 75 ft (23 m).

$$\bar{V}_{h=75} = \left(\frac{75}{30} \right)^{1/7} \left(\bar{V}_{h=30} \right) = 1.14 \bar{V}_{h=30}$$

These two expressions result in the wind profile curve for the prototype Giromill of the type shown in Figure 19. For this typical 14 MPH mean wind profile, the prototype Giromill wind profile would have a mean wind of 15.95 MPH at 75 ft. A wind speed of 20 MPH or greater occurs 2392 hours per year.

B. Wind Speed Measurement - Wind speed sensors will be located remote from the Giromill on a 30 ft pole. For control system use the one minute averaged wind speed from the sensor must be related to the rotor centroid using the 1/7 power law, or

$$V_{h=75} = \left(\frac{75}{\text{Sensor height}} \right)^{1/7} \times V_{h=\text{sensor height}}$$

C. Wind Speed Operating Limits - The Giromill rated wind speed is 20 MPH (9.0 m/s) at the swept area centroid of $h = 75$ ft (23 m). Operating wind range is between 10 and 40 MPH ($h = 75$ ft). These are average values computed over a one minute period.

D. Operating Life - From the wind profile curve shown in Figure 19 the Giromill will operate at full power 2400 hours per year. For 30 years this results in an operating life of 72,000 hours. In addition it could operate at reduced power another 3600 hrs per year.

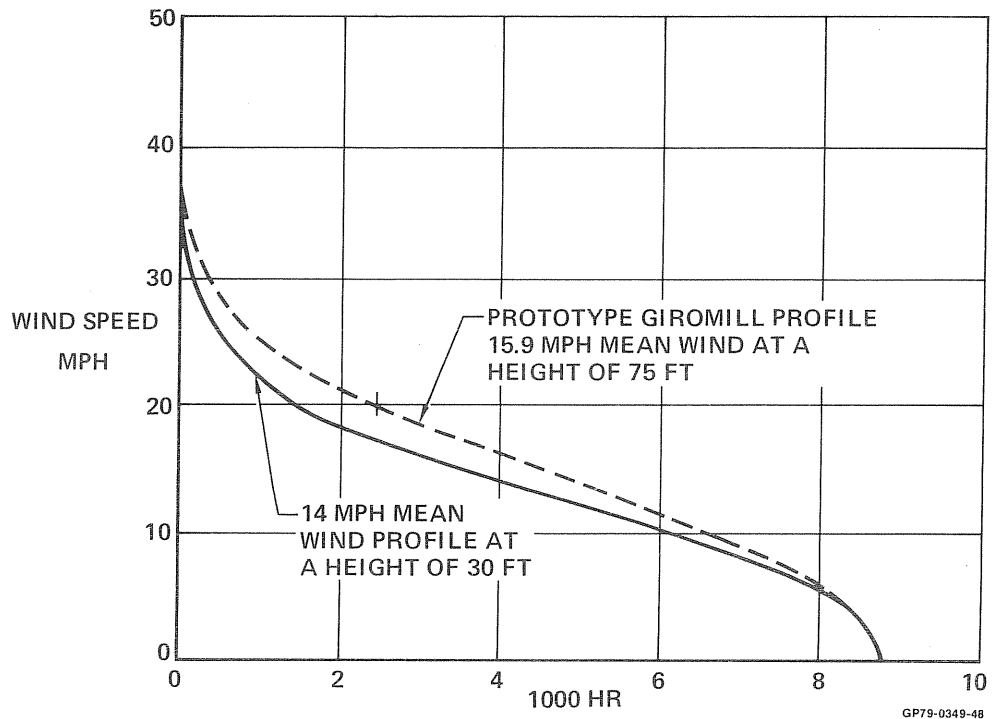


FIGURE 19
TYPICAL DESIGN WIND PROFILES

E. Longitudinal Wind Gusts - Longitudinal wind gusts are gusts acting in the direction of the average wind. They are specified as a gust factor multiplier to give the gusts that are expected with the average wind. Loads computed will include the effects of gusts superimposed on the average wind and be considered in the operating life of Paragraph D. The gusts are for use in establishing the structural design fatigue criteria.

Gusts are given as a gust factor

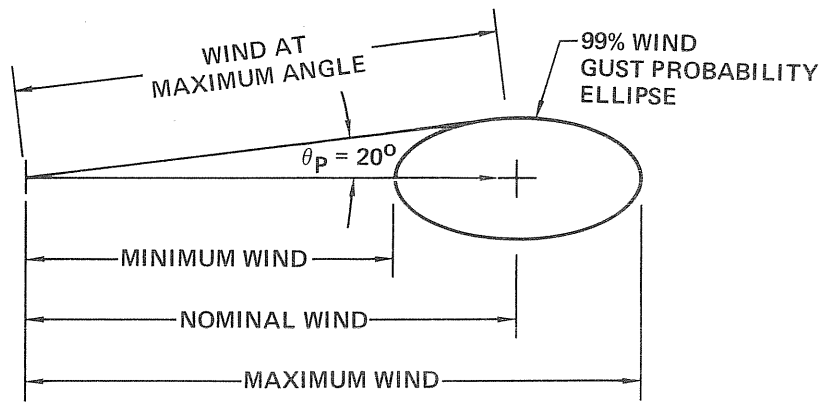
$$G = \frac{V}{\bar{V}}$$

where V is the maximum wind

\bar{V} is the one minute average wind.

G was computed using the equations given in Reference 3, Pages 840-843. For the Giromill operating wind range, $12 \leq V_w \leq 40$ MPH, $G = 1.3$.

F. Lateral Gusts - An angular or lateral gust variation can also occur. The distribution of this variation is an ellipse as shown in Figure 20. This figure and the angular wind fluctuation of $\pm 20^\circ$ was extracted from Reference 4. The value of $\theta_p = \pm 20^\circ$ contains 99% of the expected wind fluctuations. For design purposes we will use the greater loads as computed from Paragraph E or F.



GP79-0636-2

FIGURE 20
WIND DIRECTION VARIATION DUE TO GUSTS

G. Vertical Gusts - For the Giromill, vertical gusts have little effect. Hence they will not be considered.

H. High Wind Operating Criteria - The maximum operating wind is 40 MPH. A maximum expected gust velocity should also be imposed. This will give the maximum operating loads on the system.

The maximum gust velocity should be determined as per Reference 5. The gust velocity spectrum to be used is reproduced in Figure 21.

I. Discrete Gust Environment - Discrete gusts are used to assess the structural and control dynamics. The technique used is extracted from requests for proposals on DOE wind turbine projects. (For example see Reference 6.) Because of the Giromill's vertical axis the only gust of importance is the longitudinal one. This is because a longitudinal gust changes both dynamic pressure and blade angle of attack more than a lateral gust. The discrete longitudinal gust equation is given in Reference 6 as:

$$V_g = \frac{1}{2} A \left[1 - \cos \frac{\pi t}{T} \right]$$

where V_g is the longitudinal gust to be added to the mean wind,

t is the time,

T is the gust half period, and

A is the gust amplitude, defined as

$$A = 3.0 \frac{\bar{v}_r}{\ln\left(\frac{h_r}{h_o}\right)} \left[1 - \text{EXP} \left(\frac{-\bar{v}_r T}{1.48h} \right) \right]^{1/2}$$

where \bar{v}_r is the mean wind speed at a referenced elevation above ground level,

h_r is the reference elevation,

h_o is the surface length, and

\bar{v}_h is the mean wind at elevation h , given as

$$\bar{v}_h = \bar{v}_r \left[\frac{\ln(h/h_o)}{\ln(h_r/h_o)} \right]$$

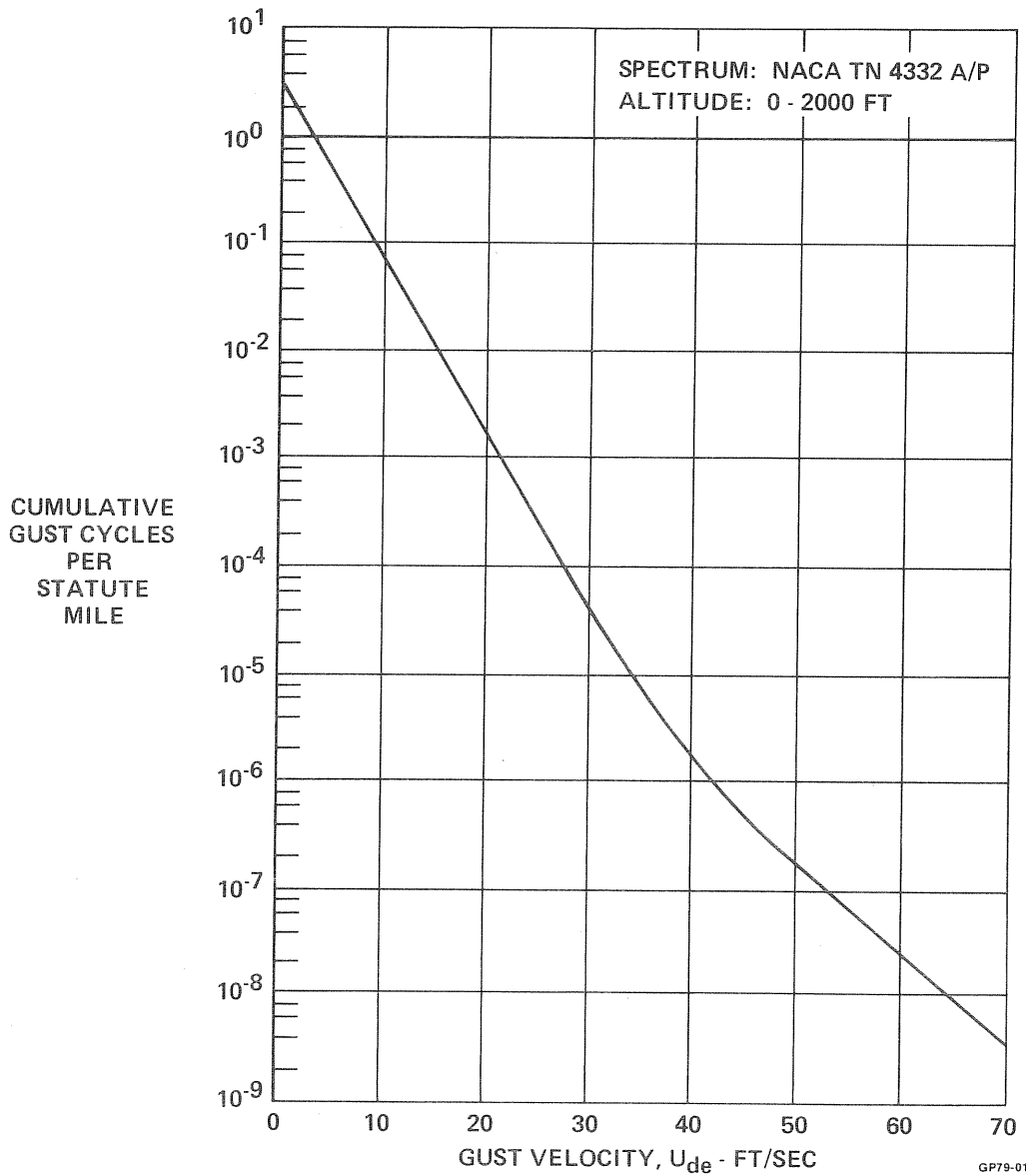


FIGURE 21
DESIGN GUST VELOCITY

The longitudinal discrete gust environment is obtained by vector addition of the gust with the mean wind at elevation h . To assess the dynamics and control, the Giromill should be completely immersed in the gust and the gust gradients across the swept area be neglected. The gust magnitude is evaluated at the centerline of the swept area. The gust half period, T , should be selected over a range of values which encompasses the significant periods of response of the Giromill. One complete gust cycle should be applied. The dynamics and control characteristics should then be assessed for a sufficient number of values of T to guarantee that all frequencies of concern are taken into account.

J. High Wind Non-Operating Environment - The Giromill will be designed for a storm wind of 125 MPH occurring at a height of 75 ft. This peak can be a steady state wind or a gust.

The discrete gust equations discussed in paragraph I were used to establish the mean wind, gust amplitude, and gust period to get 125 MPH. The relationships are plotted in Figure 22.

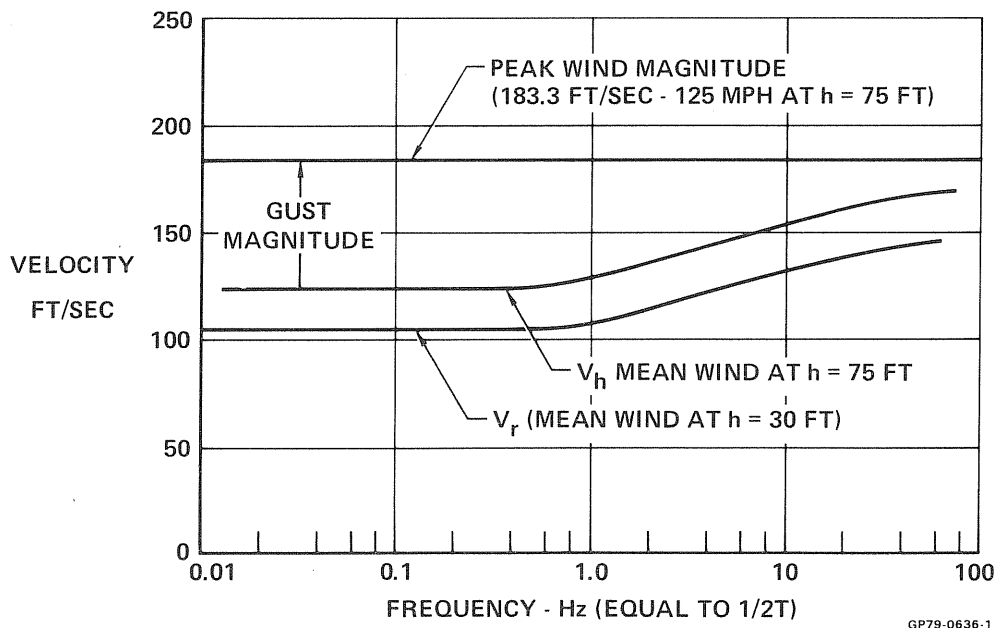


FIGURE 22
PEAK GUST MAGNITUDE - FREQUENCY RELATIONSHIP

K. Wind Gradients - The effects of wind gradients, both horizontal and vertical, will not be considered in the present design.

3.2.2 Temperatures - The design temperature range is from -40°C (-40°F) to $+60^{\circ}\text{C}$ (140°F). The Giromill must be able to operate in that temperature range. However, the system life and reliability can be degraded when operating at temperatures below -20°C (-4°F) and above $+40^{\circ}\text{C}$ (104°F).

3.2.3 Rain, Snow, Hail and Ice - Heavy rain at a rate of 1.5 in. per hour while operating.

Heavy snow which can accumulate on a horizontal surface at a slope no greater than 45°. Specific gravity of snow is 0.2 (Reference 7).

Hail stones up to 1 in. diameter while operating.

Heavy icing which can accumulate to 3 in. on surfaces facing into the wind or normal to the wind, whichever is critical. Specific gravity of ice is 0.9.

3.2.4 Corrosive Atmosphere - The humidity, temperature, and salt content for a coastal region should be considered.

3.2.5 Lightning - The Giromill system will be designed to provide for safely transmitting lightning strikes on the system to the ground.

3.2.6 Dust - The system should be capable of sustained operation under dusty conditions prevalent in the farm areas of the U.S.

3.3 EMERGENCY - The system shall be designed so that failure will not compromise the safety of the system. Safety critical systems shall be designed so that they are fail safe.

3.3.1 Emergency Stop - The rotor will be stopped by feathering the blades and, under emergency conditions, then engaging the brake. Provisions for emergency stopping of the rotor must be provided for the following:

- o Excessive Vibration
- o Rotor Overspeed
- o Inability of the rotor to start
- o Inability of the rotor to maintain RPM
- o Blade rock angles do not track commanded values

A manual stop should also be provided in the control system.

3.3.2 Rotor Locking - Some means of locking the rotor must be provided for maintenance purposes.

3.4 ROTOR - The nominal dimensions of the rotor are diameter = 58 ft and blade span = 42 ft, giving a capture area of 2436 sq ft. The total blade chord is 2.375 ft. The nominal rotor RPM is 33.5 giving an operating blade speed ratio $\lambda = 3.47$ in a 20 MPH wind.

3.4.1 Blades

A. Blade Shape - The blade will consist of a symmetrical NACA 0018 airfoil having a chord of 2.25 ft plus a 1.5 inch fixed full span tab to assure the aerodynamic center is at 25% chord. The chord and thickness will be constant over the entire blade span.

B. Blade Pivot - The blade pivot will be at 22% C.

C. Blade Center of Gravity - The blade CG will be at 23.25% C, or $0.3375 \pm .067$ inches measured from the blade pivot point.

D. Blade/Support Arm Interface - The juncture between the blades and support arms shall be aerodynamically tight. This should be maintained through a blade rock angle of at least ± 10 degrees.

E. Blade Actuator Interface - Provisions must be made to accommodate the blade actuator drive.

F. Blade/Instrumentation Interface - One blade will be instrumented and provisions must be made to bring out the instrumentation signals through slip rings.

G. Blade Pivot Inertia - Blade pivot (22% C) inertia should be kept to a minimum to minimize blade actuator torque requirements.

H. Air Loads - The Greatest operating air loads on the blades occur in a 20 MPH wind. The design operating air loads to use for analysis are the nominal loads in a 20 MPH wind with a longitudinal gust factor, $G = 1.3$ superimposed. Note, lateral gusts (Section 3.2.1F) do not cause as large a load as a longitudinal gust. In addition, an ultimate operating air load will be considered. This will consist of operating in a 40 MPH wind with a superimposed gust determined as per Section 3.2.1H. This ultimate operating load should be applied in a normal and chordwise direction.

When the Giromill is shut down, power will be released to the blade acutators allowing the blades to weathervane into the wind. This will minimize the blade normal load and essentially give only a drag load. The drag load with an ice coating on the blade (Section 3.4.1I) should be considered up to 125 MPH winds.

I. Icing - The Giromill should be operable in a 20 MPH wind with the blades having a 1/2 inch thickness of ice on the leading edge tapering, to 0 at 75% chord. This condition is expected no more than one percent of the operating time.

Non-Operating - The blades should withstand an ice storm which would deposit 3" of ice over 1/2 the blade area or 1.5" over the entire blade. This icing condition could occur simultaneously with the 125 MPH wind gusts.

J. Snow - Since the blades are vertical no appreciable snow accumulation can occur.

K. Flutter Speed Boundary - The blade shall not experience flutter under any operating or non-operating condition.

3.4.2 Blade Support Arms

A. Blade Support Arm Shape - The support arms should be aerodynamically streamlined to reduce drag. This is especially true for the outboard 50%.

B. Support Arm/Blade Interface - The interface with the blades must provide for a flat wiper area that will aerodynamically seal the blade covering a blade rock angle of at least ± 10 deg.

C. Support Arm/Blade Actuator Interface - The blade actuators will be mounted on the lower support arms. The preferred mounting is to stay within the support arm moldline. If this is not possible, a streamlined fairing must be provided. Also the actuator motor and power amplifier must be cooled with a forward facing air scoop.

The back structure on which the actuator is mounted should provide a stiffness of at least 240,000 inch-pound/rad. measured at the blade pivot.

D. Support Arm/Rotating Tower Interface - The support arms will be attached to the rotating tower using pinned joints. The upper support arm will have upper and lower streamlined wire bracing. The lower support arm will have an upper wire bracing.

E. Support Arm/Instrumentation Interface - One set (lower and upper) of support arms can be instrumented.

F. Air Loads - The operating air loads on the support arms are negligible in comparison with the blade loads they have to carry.

The high Wind (125 MPH) with a 3 inch thick ice layer should be used as the non-operating criteria.

G. Icing - The Giromill shall be able to operate in a wind of 20 MPH with 0.5 inch of ice on the top surface of each support arm.

An ice accumulation of 3 inches on the top surface could occur. The effects of this ice load on non-operating condition should be computed in conjunction with the storm wind loads caused by 125 MPH wind.

H. Snow - Snow can accumulate on the top surface of the support arm at a slope of 45° when not operating. Snow is not expected to accumulate to interrupt operation.

3.4.3 Rotating Tower

A. Tower Shape - The rotating tower should consist of a minimum size round tube, the diameter balanced against weight and cost. It should, however, have a diameter no greater than 1/20 of the rotor diameter. Between the support arms, the tube shall have a narrow double spiral, 2 inch high, to ensure that no vortex street can form off the tube. External access steps and conduit for wire bundles may be mounted on the surface of the tube if desired.

B. Rotating Tower/Support Arm Interface - The support arms will be attached to the rotating tower by welding structural rings and support gussets to the tower and bolting the support arm to that structure. This structure must be aligned so that: (a) the upper and lower support arm blade pivot centers are within ± 2.0 in. from each other, (b) the upper arms are perpendicular to the rotating tower within ± 0.5 deg., and (c) the center lines of the upper arms (defined by a line through the

center of the rotating tower and the blade pivot point) are $120^\circ \pm 2.0$ deg. from each other.

C. Rotating Tower/Fixed Tower Interface - The rotating tower interfaces with the fixed tower through two bearings and disc brake. The upper bearing fits around the rotating tower and is connected to the fixed tower through a structure that takes only radial (horizontal) loads. The lower main bearing holds the entire weight of the rotor in addition to its share of the total horizontal load.

D. Rotating Tower/Disc Brake Interface - The disc brake is mounted on a flange attached to the rotating tower and turns between "C" clamp brake shoes mounted on the fixed tower.

E. Rotating Tower/Speed Increaser Interface - The speed increaser gear box is mounted directly on the smaller adapter section of the rotating tower immediately below the lower main bearing.

F. Rotating Tower/Control System Interface - A rotor angle position sensor that will relate blade 1 with the wind direction sensor will be mounted on the rotating tower shaft that extends through the speed increaser. Various wire bundles will be mounted inside the rotating tower.

A series of slip rings will also be provided on the rotating tower shaft below the speed increaser to provide an electrical access for both control and instrumentation functions.

G. Rotating Tower/Instrumentation Interface - The rotating tower will be strain gaged to verify the computed loads during the test. This instrumentation wiring, along with control wires and other component instrumentation wires, must be routed down the rotating tower to the slip rings.

H. Air Loads - The operating air loads on the rotating tower are negligible in comparison with the loads induced by the support arms.

The high wind (125 MPH gusts) with ice accumulation is used to calculate the non-operating loads.

I. Icing - The Giromill should be able to operate with 0.5 inches of ice over one-half of the perimeter of the rotating tower or 0.25 inches over the entire perimeter

The ice to consider under non-operating condition, in conjunction with the high wind gusts (Section 3.2.3) is 3 inches over half of the perimeter normal to the wind directions, or 1.5 in. over the entire perimeter.

J. Snow - Since the rotating tower is vertical no snow can accumulate.

3.4.4 Disc Brake - A disc brake is installed to provide an extra safety margin. It will be engaged only for emergency stopping. Normally,

the rotor will be braked with the blades in the feathered condition so that no aerodynamic torque is generated. The disc brake should be sized, however, considering one stop in a 40 MPH wind with aerodynamic torque being generated. After this stop, the brake pads can be replaced if necessary.

The braking system should be fail-safe so that a loss of battery or control power will engage it.

3.5 FIXED TOWER - The fixed tower is a square steel truss. The base is 20 ft, height 59.53 ft, and the top 5 ft square. The upper main bearing transmits only radial loads. The lower main bearing, which is supported by tension members connected to the corner posts in the lower truss bay, carries the rotor weight. The corner posts are anchored to a pier foundation.

3.5.1 Tower

A. Tower Structure - The truss tower will consist of structural steel angles bolted together. A ladder with an OSHA-approved safety bar will be mounted on one side.

B. Fixed Tower/Rotating Tower Interface - The fixed tower interfaces with the rotating tower through two bearings and by a disk brake. The upper bearing is mounted (bolted) on plates that form the top surface of the fixed tower. These plates can flex vertically, which will minimize vertical (thrust) loads in the bearings. The lower bearing supports the tower (rotor) weight. This bearing is mounted on a platform that has four tension members tied to the corner posts. The disc brake calipers are held by a truss structure also fastened to the corner posts.

C. Fixed Tower/Control Interface - Four control boxes will be mounted at the base of the fixed tower.

The Control Unit contains the microprocessor and associated control system circuitry. The power switching unit contains power switching relays manual switches, fuses and terminals for connecting power wiring.

The line switch box contains the magnetic contactors that connects the generator on line, a manual circuit breaker, and an auxiliary relay actuated by the control system.

The instrumentation box is used for terminating the instrumentation wiring.

D. Tower Alignment - Tower tolerances will be controlled so that when erected on the foundation, the vertical alignment will be within 1.0 degrees.

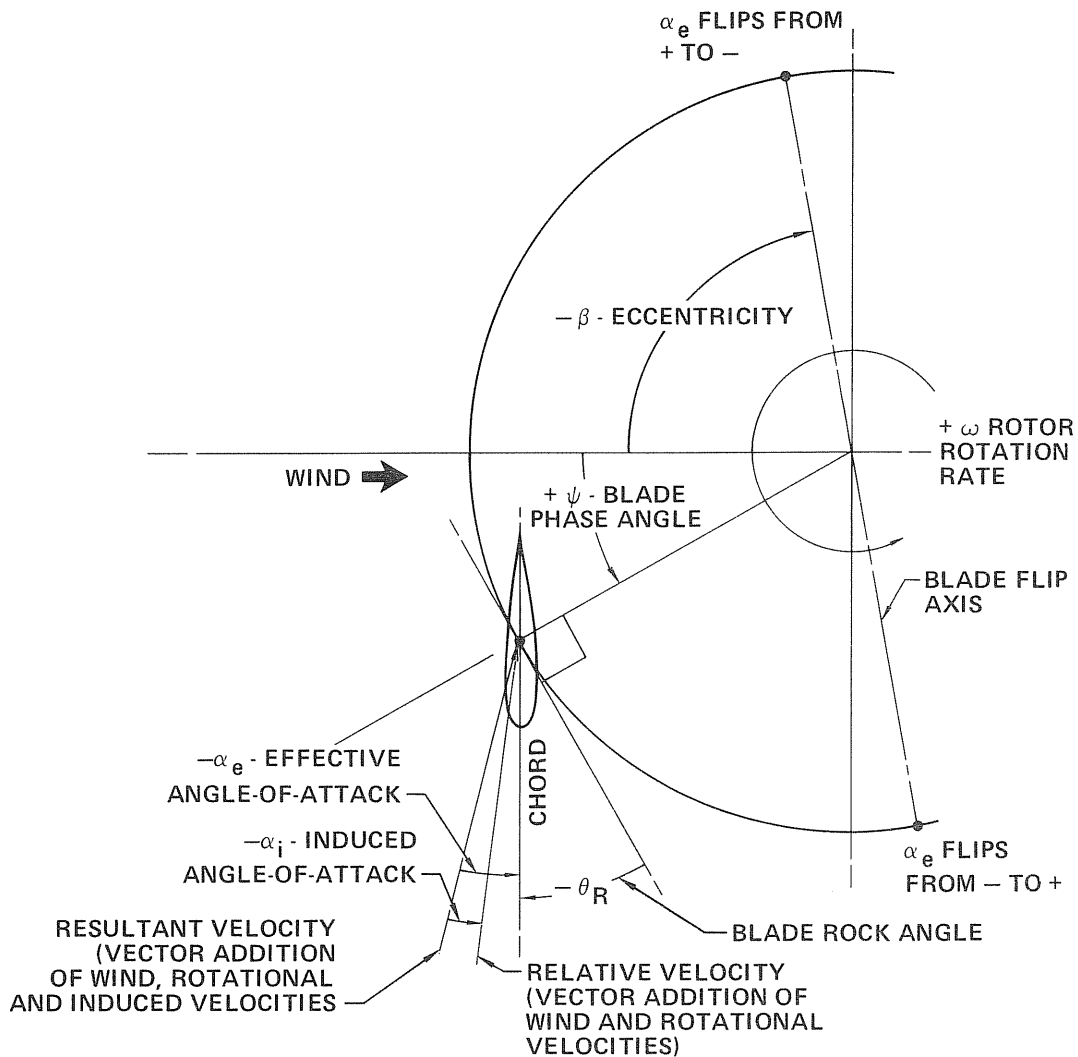
E. Storm Wind Drag Loads - The tower must withstand the storm wind loads on the entire Giromill.

3.5.2 Foundation - A steel reinforced concrete foundation will support the Giromill. It will consist of four piers that anchor the tower

corner posts in the ground. Foundation alignment of the piers will be considered in the tower vertical alignment.

3.6 CONTROL SYSTEM - The control system consists of electrical blade actuators that modulate the blades. Blade modulation controls the angle of attack as the blade rotates, which in turn controls the RPM of the rotor. A microprocessor controller provides the operation logic and control functions. A wind speed sensor provides inputs to start or stop the Giromill, and a wind direction sensor is used to keep the blade flip region at 90° and 270° to the wind. A battery and charger system provides the power.

The parameters commonly referred to in the control system are shown in Figure 23.



Note: Some angles shown negatives to be consistent with normal Giromill operating conditions.

GP79-0636-16

FIGURE 23
ROTOR PARAMETERS DEFINITION

The rotor rotates counter clockwise (looking down on it). The blades are at $-\alpha_e$ over the upwind portion of the rotor rotation, and at $+\alpha_e$ on the downwind or aft portion. The flip axis, where the blades flip from $+\alpha_e$ to $-\alpha_e$ is defined as β ; for the Giromill $\beta = -90^\circ$. The blade flipping occurs over 30° of rotor travel, $\pm 15^\circ$ from the flip axis. The blade actuators control the blades rock angles, θ_R , according to the schedules programmed in the microprocessor.

The rotor is stopped by releasing the power to the blade actuators. Since the blade pivot point is forward of the aerodynamic center, the blades are then free to weathervane into the wind, letting the rotor coast down. The system is then in a standby mode, ready to start when the wind is within limits. A normal stopping of the rotor does not activate the disc brake and the rotor is free. An emergency stop sequence also applies the disc brake and makes the system inert.

The control system will maintain constant rotor RPM when the wind is between 20 and 40 MPH for both the mechanical and electrical configurations. For winds below 20 MPH, the rotor RPM will depend on the load and how it varies with RPM. However, the mechanical configuration must be capable of constant RPM operation if the load varies with wind speed as used in a wind-assist pumping mode. Other control system design criteria are given in Figure 24.

COMPLETE STAND-ALONE CAPABILITY. IDENTICAL SYSTEM FOR:

- ELECTRICAL WITH UTILITY GRID TIE-IN
- MECHANICAL
- ELECTRICAL STAND-ALONE

PROVISIONS INCORPORATED FOR ELECTRICAL TIE-IN WITH MINI-GRID WITH MINIMUM MODIFICATION.

START AUTOMATICALLY WHEN WIND (V_w) IS IN RANGE

- V_w NOT LESS THAN 10 MPH AND GREATER THAN 13 MPH FOR ONE MINUTE
- V_w NOT MORE THAN 40 MPH AND LESS THAN 37 MPH FOR ONE MINUTE

RUN AS LONG AS: $10 \leq V_w \leq 40$ MPH AVERAGED OVER ONE MINUTE

REVERT TO STANDBY MODE WHEN: $V_w < 10$ OR $V_w > 40$ MPH

REVERT TO SHUTDOWN (BRAKE ON) MODE WHEN:

- ROTOR LOCKED AND CANNOT TURN
- ROTOR CANNOT MAINTAIN RPM (5 TRIES)
- EXCESSIVE VIBRATION
- ROCK ANGLE DOES NOT TRACK (COARSE CHECK)
- MANUAL (MAINTENANCE) SHUTDOWN

CONTROL RPM WITH $\pm 1\%$ FOR $20 \leq V_w \leq 40$ MPH

FAIL SAFE DESIGN SO ANY CONTROL FAILURE WILL CAUSE SHUTDOWN

GP79-0636-132

**FIGURE 24
CONTROL SYSTEM DESIGN CRITERIA**

3.6.1 SENSORS

A. Wind Direction - A wind direction sensor is required to monitor location of blade flip axis (Angle β in Figure 23). A time constant of 0.5 sec is sufficient for the response of the wind direction sensor.

B. Wind Speed - The wind speed sensor is monitored during the standby mode allowing the controller to determine when sufficient wind is available. The wind speed sensor also shuts down the rotor when the wind exceeds the boundary values, limits the low wind speed cam profile, and modifies the rock angle commands. This sensor can be remotely mounted, up to 50 ft away. The wind speed measured at the sensor height should be related by the 1/7 power law to the expected wind speed at the centroid height of the rotor (75 ft). A response time constant of 0.25 sec should be sufficient for the wind speed.

C. RPM - This sensor provides feedback to the controller for RPM control. The resolution should be at least 0.002 rad/sec when related to rotor rate.

D. Vibration - A vibration sensor, mounted at the top of the fixed tower, is used to shut down the Giromill in event of excessive vibrations or "g" loads in a horizontal direction. The response of the sensor should be flat from about 0.25 Hz to 10.0 Hz. The shutdown threshold should be variable so that various values can be tested. Initially the vibration level for shutdown should be set at 0.25 g's. Remote resetting should be available. Easy access should be provided for varying the shutdown threshold.

E. Rotor Position - A rotor position sensor (referenced to Blade 1) is required. This sensor works in conjunction with the wind direction sensor for calculating and updating the blade phase angle

3.6.2 Control Unit - The control unit consists of the microprocessor, integrated circuits, circuit boards, and associated components. It provides the logic for performing the basic control functions. The unit will be constructed using non-mass-production techniques. It must have reprogrammable memory devices and the capability to vary the parameters and functions listed in Figure 25. Also, the various parameters used in the controller must be available for recording during the test. These parameters are shown in Figure 26. Preferably, a simple device is desired which is able to recall any parameter used in the controller and record it.

The unit must be protected in an enclosure mounted on the control panel at the base of the fixed tower. The enclosure and connecting wiring must be weatherproof, requiring no additional shelter.

3.6.3 Blade Actuators - Each of the blades will be modulated by a separate electromechanical blade actuator. The actuator will be coupled to the blade by a timing belt installation. The unit will use direct current and respond to an analog position command. Position feedback element, signal and power electronics, the motor, and other components will be packaged as a single unit.

1. IN RANGE WIND SPEED COUNTER RATE
2. START UP WIND SPEED, BOTH HIGH AND LOW
3. SHUT DOWN WIND SPEED, BOTH HIGH AND LOW
4. WIND SPEED LOW PASS FILTER TIME
5. CONTROLLER COMMAND GAINS - K_1 THROUGH K_5
6. REFERENCE RPM
7. OVERSPEED RPM
8. ON-OFF CAPABILITY FOR COARSE θ_R COMPARISON FAILURE DETECTION
9. CAM LIMIT FLAG VALUES AS $f(V_w)$
10. ROCK ANGLE PROFILES AS $f(\psi)$
11. NUMBER OF ROCK ANGLE PROFILES

GP79-0636-131

**FIGURE 25
CONTROL FUNCTION VARIABLE CAPABILITY**

1. COMMANDED BLADE ROCK ANGLE FOR ALL THREE ACTUATORS
2. ACTUAL BLADE ROCK ANGLES FROM ALL THREE ACTUATORS
3. ROTOR POSITION OF BLADE 1
4. WIND VELOCITY
5. WIND DIRECTION
6. ROTOR RPM
7. COMMANDED CAM ROCK ANGLE

GP79-0636-130

**FIGURE 26
CONTROL SYSTEM INSTRUMENTATION PARAMETERS**

The actuator shall not fail structurally when a torque of 3767 in.-lb is applied at the output pulley. It will have sufficient strength to modulate the blades to the required rock angles with a factor of 1.25 applied to the torque.

The motor will drive a timing belt pulley through a gearbox. This pulley will be connected to a blade modulation pulley with a timing belt. The ratio between the motor rpm and blade rpm will be optimized to give the least power drawn in a 20 MPH wind.

The gearbox must operate under 11g horizontal acceleration added to the normal vertical 1.0g. It should be able to operate continuously in this environment for 336 hours. Following this time period, a one hour period can be assumed where the blades are weathervaned by the wind to redistribute the grease.

A potentiometer located within the actuator package will feed back the blade rock angle. this potentiometer should have a linear range of ± 60 and should be able to provide rock angle control over $\pm 180^\circ$. The pot will be aligned with the blade position when the blades and actuators are assembled on the rotor. A means of providing this alignment must be provided.

Static stiffness at the output shaft should be a minimum of 29,333 in.-lb/rad. with power on and a fixed position command voltage. A means of changing the actuator gain to vary this stiffness requirement should be provided.

3.6.4 Power Distribution - The power distribution system includes the power system (batteries and charging alternator) and the power switching unit.

Power System - The power system consists of a 48 volt battery set and charging system. The batteries must be arranged so that a neutral and ± 24 volts can be used. The battery set should have sufficient capacity to cold soak at -20°C for 5 days in a standby mode and be able to perform 5 false starts of one minute duration. At -40°C the battery set should be able to provide for one start. Start up can be assumed to take 600 watts.

The battery charging alternator should be large enough to accommodate the total Giromill electrical load, and still have sufficient capacity to charge the batteries at a rate of one hour per start attempt.

The Giromill power system will be protected by circuit breakers or fuses to cut off power in event of a short.

Power Switching Unit - The power switching unit contains the start and stop/reset buttons that provide operator control. It also contains the battery power circuits that are controlled by the controller unit.

These components are mounted in a box fixed to the control panel at the base of the Giromill. The box and associated wiring must be weatherproof. The unit should be mounted near the batteries and alternator to minimize the length of the power wires.

3.6.5 Wiring - All control system wiring must be weatherproof. It must be shielded, and the signal and return be twisted pairs. It must also be protected against lightning by surge suppressors.

Power wiring must be large enough to keep the voltage drop between the battery and actuator to less than 2 volts.

3.7 ELECTRICAL OUTPUT SYSTEM - This system consists of the speed increaser, generator, and associated electrical equipment to tie in to a utility grid.

3.7.1 Speed Increaser - The speed increaser must be rated to absorb 50 kW of power with a continuous cyclic variation of $\pm 60\%$. The frequency of this cyclic variation can be assumed to vary from 0.25 to 1.0 Hz. In addition it should be able to withstand a peak power cycle of $\pm 80\%$ about

50 times per year, and be able to absorb an ultimate load corresponding to 5 times the rated power, without failure.

3.7.2 Generator - The generator will be an induction type rated at 40 kW, 480 volts, 60 Hz, three phase, and a 0.8 power factor or higher at 1830 RPM. It must operate with satisfactory temperature rise with ambient temperature range from -40°C to $+60^{\circ}\text{C}$. It must be able to operate with the shaft up, and be belt driven. Efficiency must be 91% or greater at full load.

The generator should be rated for 40 kW with a continuous cyclic variation of $\pm 60\%$. The frequency of this cyclic variation can be assumed to vary from 0.25 to 1.0 Hz. In addition it should be capable of absorbing a peak power cycle of $\pm 80\%$ about 50 times per year.

3.7.3 Electrical Equipment - The electrical equipment consists of a combination magnetic starter and circuit breaker and a control relay, all mounted in an enclosure on the control panel. All of these components are standard.

3.8 MECHANICAL OUTPUT ADAPTER - A right angle gear box will be mounted in place of the generator when the Giromill is converted to a mechanical output. No other modifications should be required. The output shaft should be horizontal at a height between 2 and 5 feet. The rotational speed shall be fixed at either 440, 880, or 1760 RPM.

3.9 TEST INSTRUMENTS - Sufficient instrumentation will be installed to determine the loads, structural frequencies, and mode shapes, actuator temperatures, and selected control system parameters. The instrumentation interface with Rocky Flats Test Center will be a junction box mounted on the control panel. Control parameters instrumentation can have its interface junction as a terminal connector on the controller box.

4.0 AERODYNAMICS AND PERFORMANCE

The aerodynamic characteristics of the various parts were estimated, and the performance of the Giromill computed.

4.1 AERODYNAMICS

4.1.1 Blade - A study was conducted to pick the best airfoil for the blade. Features desired were:

- a) A symmetrical airfoil (required)
- b) A high c_l/c_d
- c) Aerodynamic center at 0.25 C or greater
- d) No abrupt stall characteristic

Airfoil sections investigated included the NACA 4-digit and 6-series airfoils. In most cases a thickness ratio of 0.18 was used for evaluation. Data were extracted from Reference 8.

Figure 27 shows the two-dimensional lift-to-drag characteristics of the blade. This plot included a representative equivalent value of drag for the support arms, $C_{de} = 0.0043$, and was related to an average Reynolds number (R_N) of 1.8×10^6 . This figure shows that the NACA-0018 and 63A018 airfoils had a comparable c_l/c_d value of about 45.

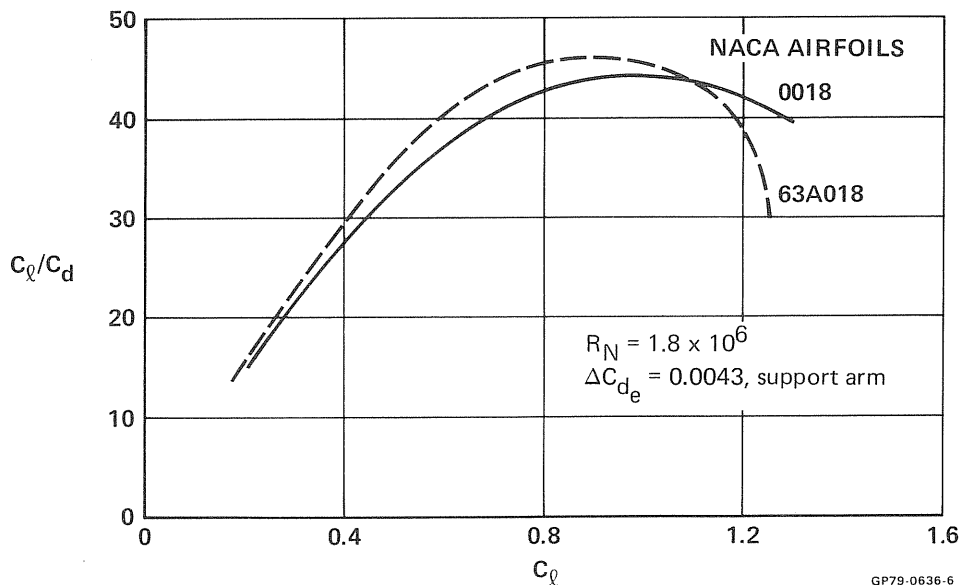
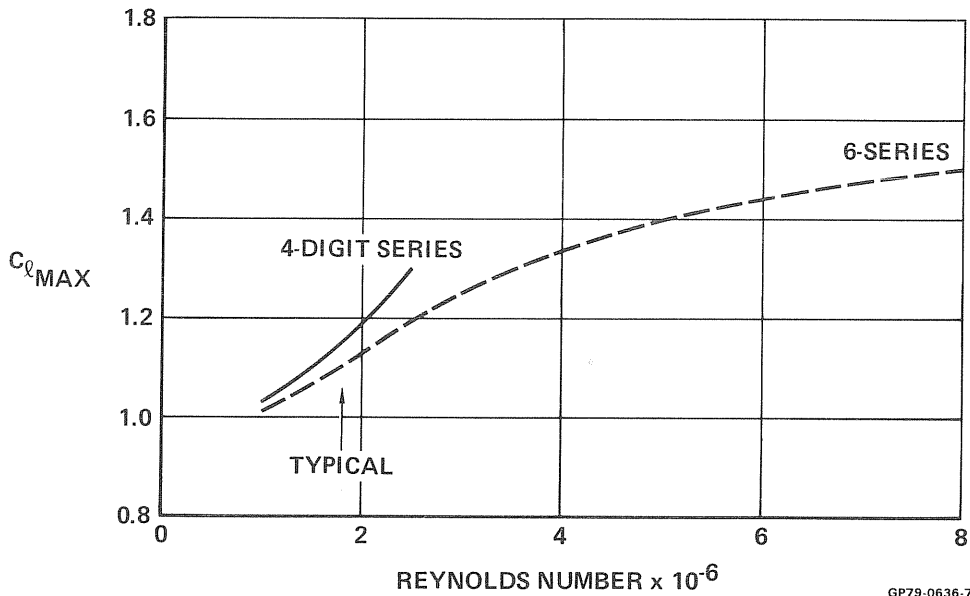


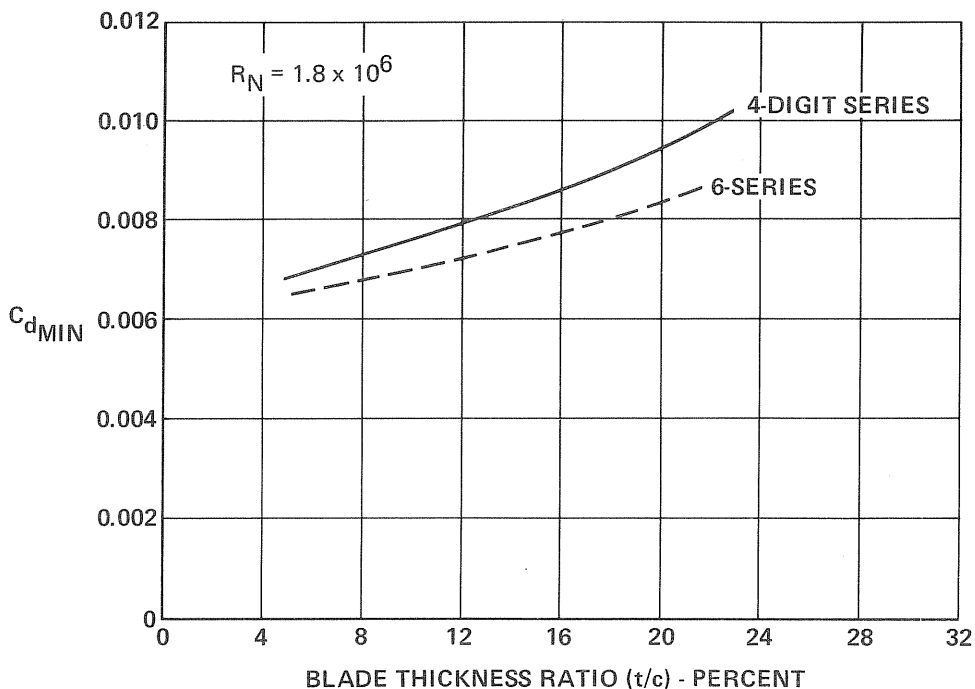
FIGURE 27
ROTOR BLADE AERODYNAMIC CHARACTERISTICS

Figure 28 indicates that the 4-digit airfoils have a slightly higher $C_{l_{max}}$ at the typical operating R_N , but Figure 29 indicates the 6-series has a definitely lower drag.



GP79-0636-7

FIGURE 28
 $C_{l_{MAX}}$ COMPARISON NACA SYMMETRICAL AIRFOILS



GP79-0636-8

FIGURE 29
MINIMUM DRAG COMPARISON NACA SYMMETRICAL AIRFOILS

Another aerodynamic characteristic examined was the aerodynamic center (a.c.). Figure 30 indicates that the basic 63A018 airfoil has a further aft a.c., and would require no blade tab to assure the blade a.c. is at 25%C. A 0018 airfoil would require a full span tab a little larger than 5% chord.

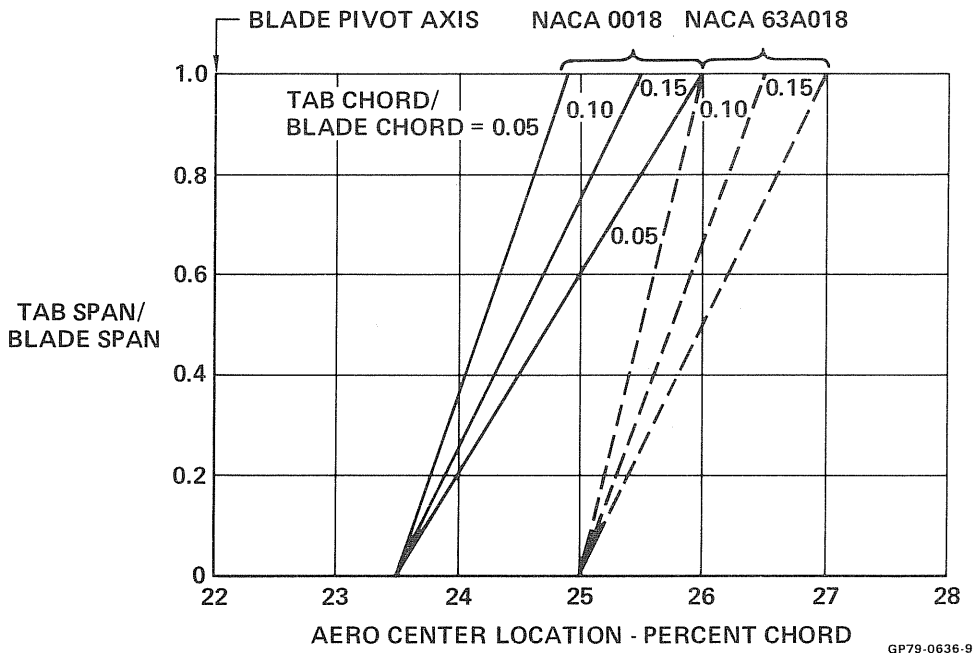


FIGURE 30
EFFECT OF TAB GEOMETRY ON BLADE STABILITY

From these analysis it appeared that the 6-series airfoil would be slightly better than the 4-digit type. However, from a structural point the 6-series was not at all attractive, since the maximum thickness region is less, as seen in Figure 31. This figure compares the NACA 0018 airfoil shape with the 63₃018 (cusped trailing edge) and 63A018 (modified with a straight trailing edge). The leading edge of the 0018, which reacts the bending moment, has a greater depth. This was of paramount importance and was the overriding reason for selecting the NACA 4-digit airfoil for the Giromill.

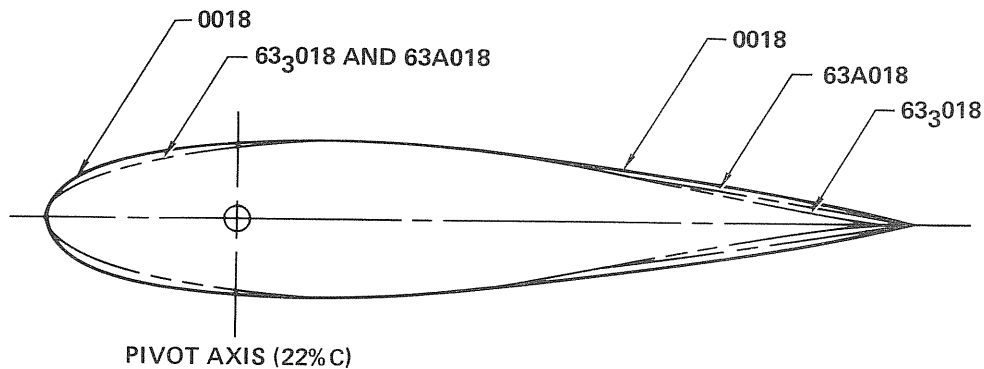
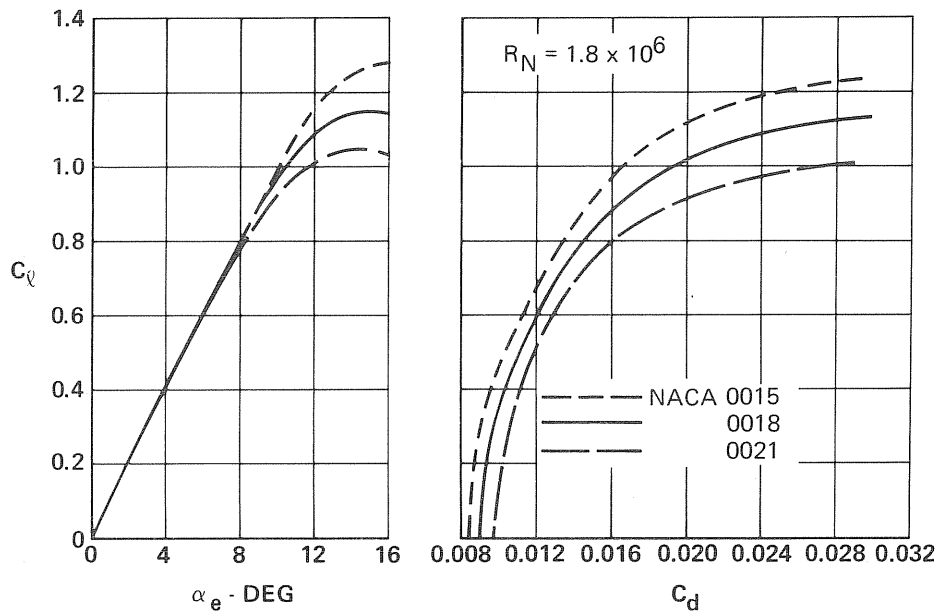


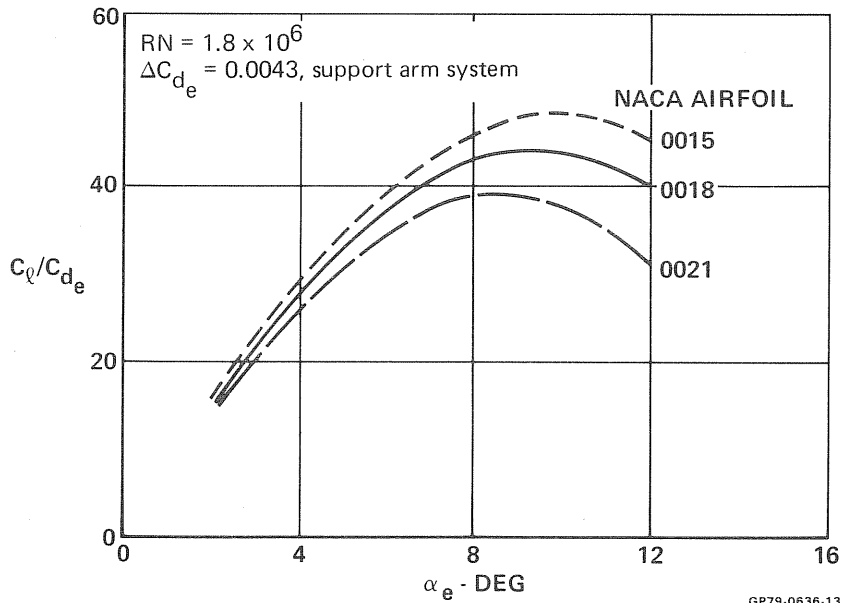
FIGURE 31
AIRFOIL COMPARISON

Figures 32 and 33 plot the aerodynamic characteristics of the NACA 4-digit airfoil sections used in the trade studies. Performance calculations showed that rotor performance changed approximately $-0.52 \text{ kW}/\% \text{ t/c}$ change.



GP79-0636-11

**FIGURE 32
BLADE AERODYNAMIC CHARACTERISTICS**



GP79-0636-13

**FIGURE 33
ROTOR AERODYNAMIC CHARACTERISTICS**

The airfoil selected for the 40kW prototype Giromill is a NACA 0018 with 5.5% full span tab. The blade chord is 27 inches (28.5 inches with the tab). The estimated aerodynamics of this airfoil are given in Figure 34 for the low α_e region, and shown in Figure 35 over $180^\circ \alpha_e$. These characteristics were used in the performance estimates.

4.1.2 Blade Support Arms - A study was performed to determine the performance effect of support arm drag. Reference 2 formulated a procedure for estimating this drag by referencing it to an equivalent drag coefficient acting at the blade, or:

$$C_{d_e} = 0.25 C_{d_A} \frac{S_A}{S_B}$$

Where: C_{d_e} is a drag coefficient acting at the blade which produces the same rotor torque as the integrated drag of the support arms.

C_{d_A} is an average support arm drag coefficient

S_A is the support arm reference area

S_B is the blade reference area

Using this relationship, it was determined that the Giromill would lose 1.0 kW per .0026 C_{d_e} increase. Streamlining of the support arms is a necessity.

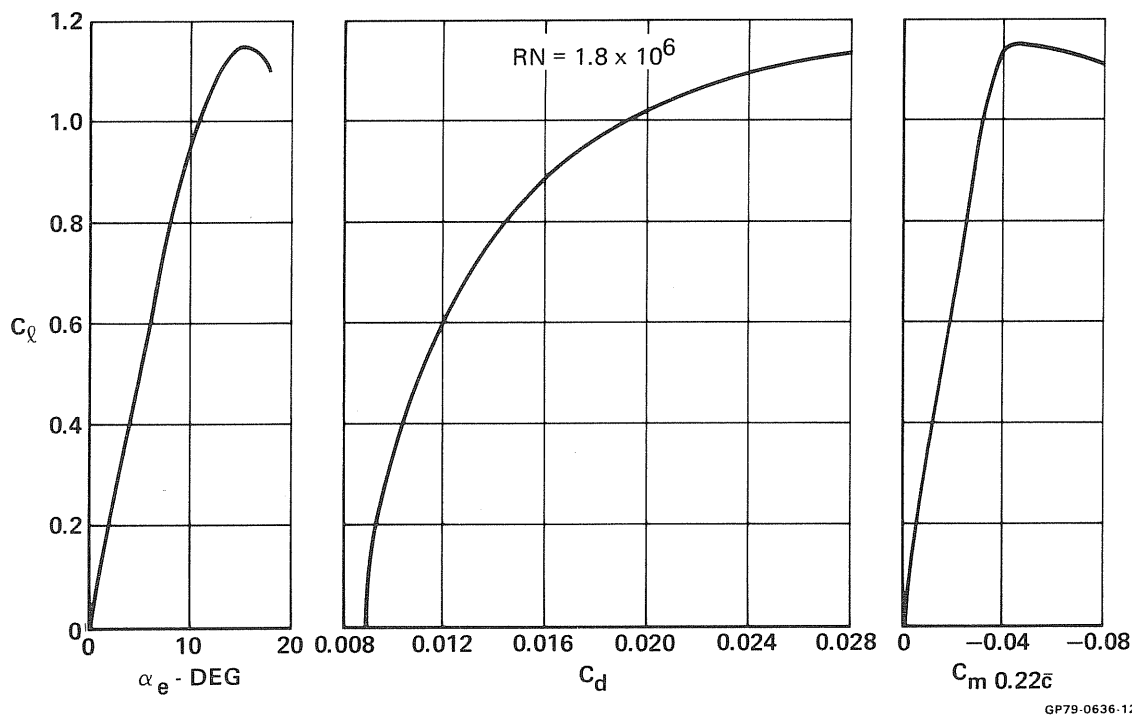


FIGURE 34
BLADE AERODYNAMIC CHARACTERISTICS
NACA 0018 With Trailing Edge Modification

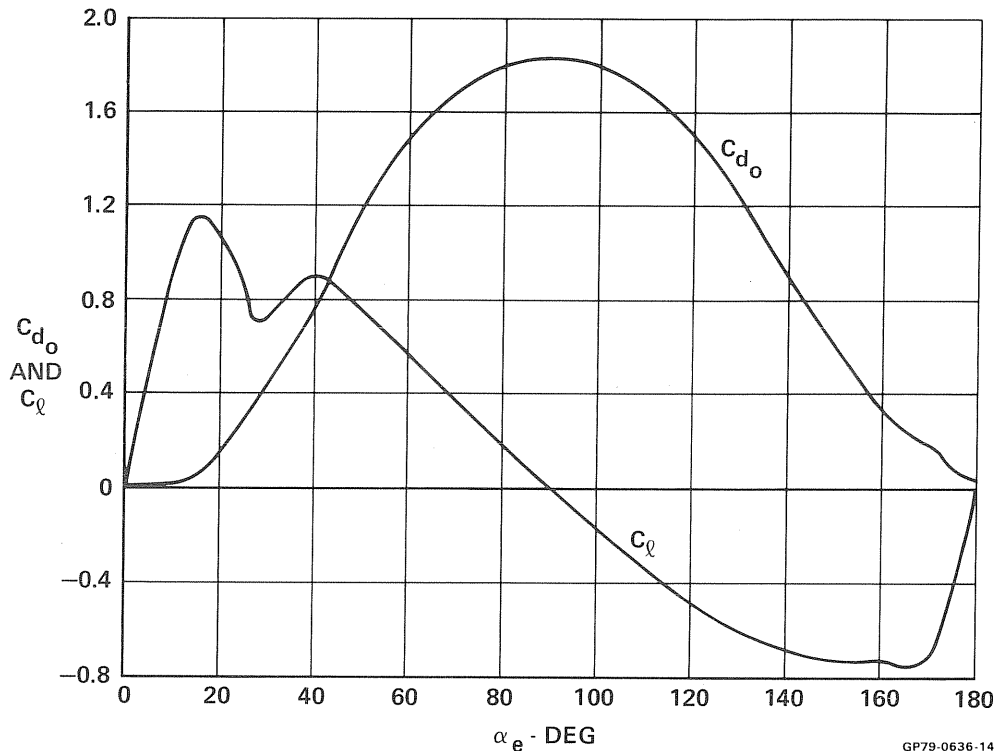


FIGURE 35
GIROMILL BLADE AERODYNAMIC CHARACTERISTICS

4.1.3 Drag Breakdown - A drag breakdown of the rotor is shown in Figure 36. This estimate was used in the performance calculations discussed in the next section.

4.2 PERFORMANCE - Performance calculations were made employing the Larsen Cyclogiro Performance Computer Program. The theory behind this program is explained in Reference 9. The estimated performance of the Giromill is shown in Figure 37. This performance plot accounts for the drag of all rotor components, but does not account for the power lost due to blade aerodynamic damping.

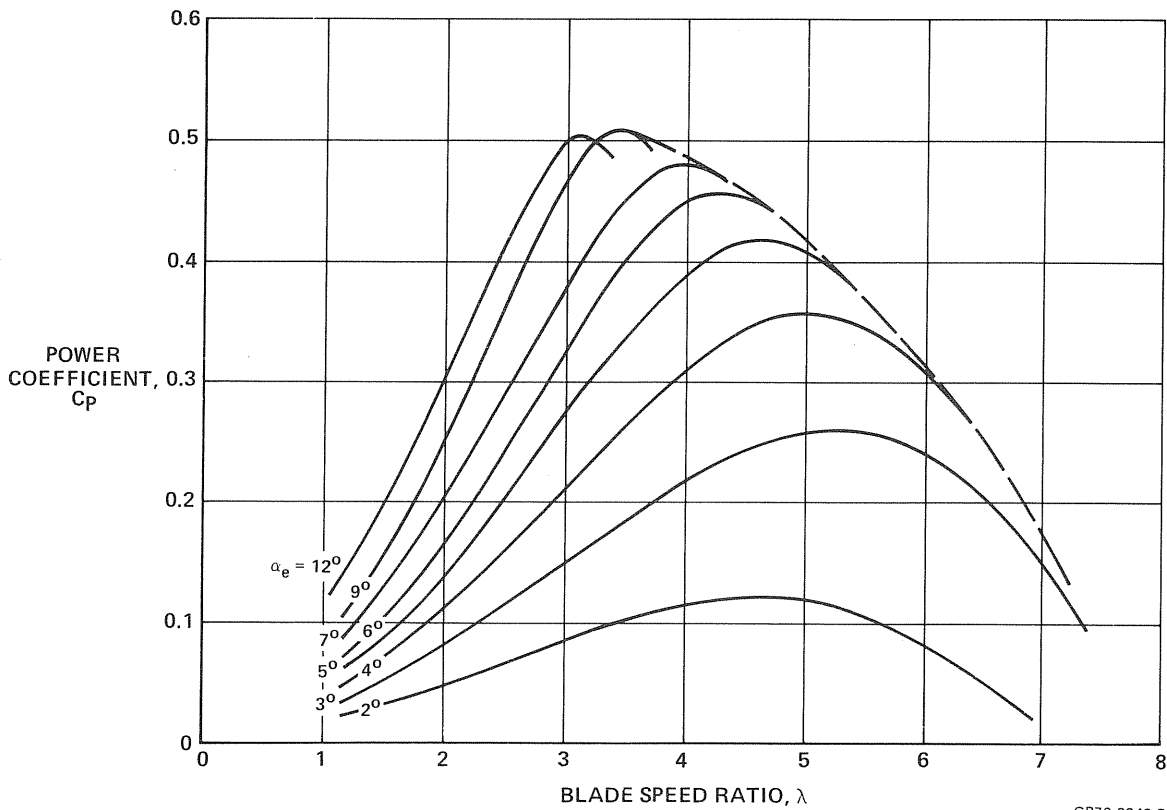
The aerodynamic damping loss is shown in Figure 38. This figure also shows lines of constant rotor power (from 10 kW to 50 kW). Also shown is the power coefficient variation for discrete wind rock angle cams from 12 to 40 MPH (circled points). The double dashed lines emanating downward from these discrete wind points show how the power coefficient would vary maintaining a constant blade rock angle profile.

To achieve an output of about 40 kW from an electrical generator requires the rotor to have an output of about 50 kW. The 50 kW constant power line therefore shows the rock angle variation needed for constant power above a wind speed of 20 MPH.

COMPONENT	ΔC_{de}	NO. PER BLADE	C_{de}
BLADE	0.009000	1	0.00900
SUPPORT ARM	0.002350	2	0.00470
STREAMLINE WIRE	0.000383	3	0.00115
BLADE FAIRING	0.000200	2	0.00040
ACTUATOR FAIRING	0.000130	1	0.00013
COOLING HOLES	0.000225	2	0.00045
WIRE FITTING	0.000030	3	0.00009
EQUIVALENT C_{de} PER BLADE			0.01592

GP79-0636-15

**FIGURE 36
DRAG BREAKDOWN**



GP79-0349-5

**FIGURE 37
GIROMILL ESTIMATED PERFORMANCE**

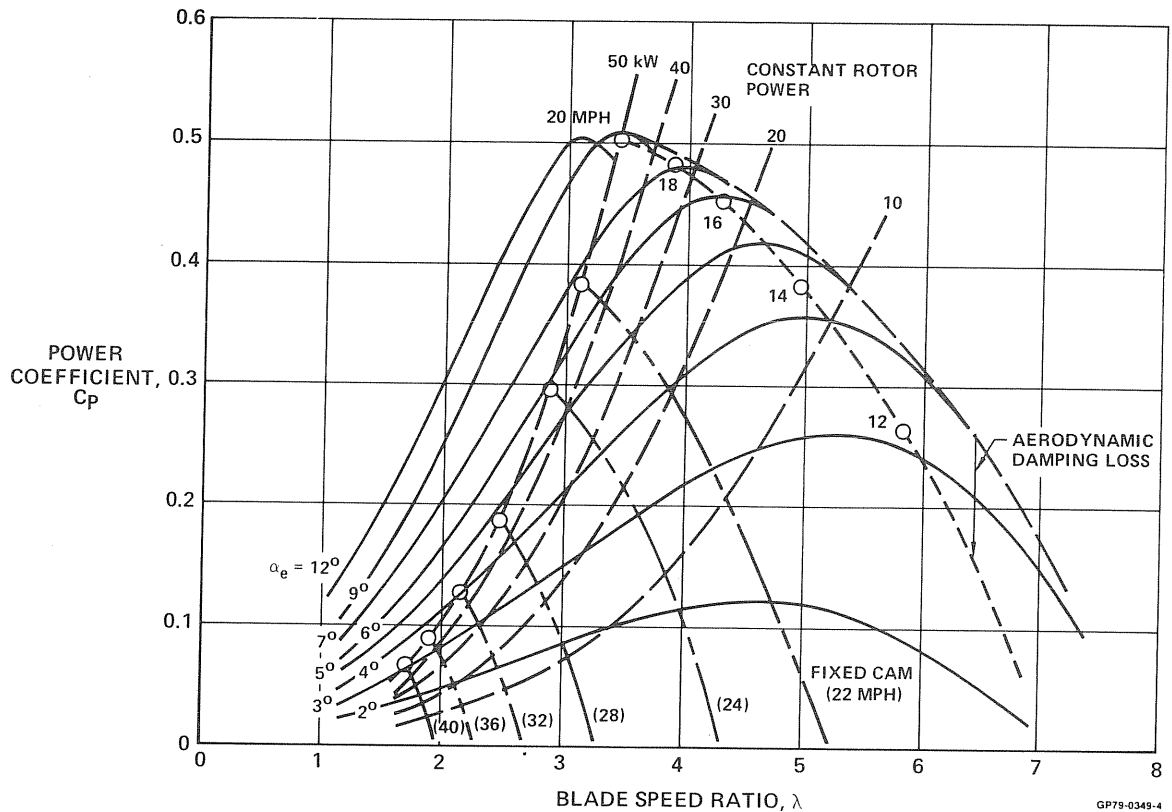
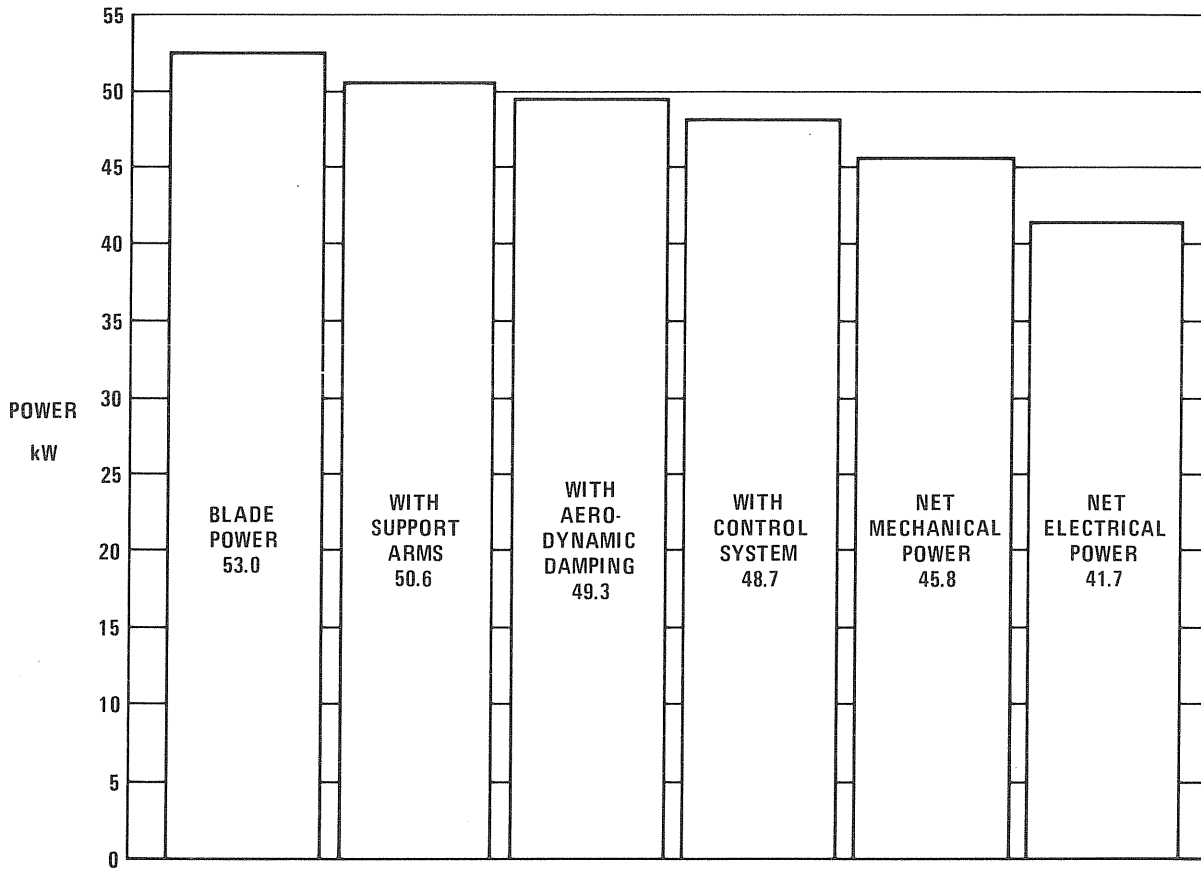


FIGURE 38
GIROMILL CONTROL PERFORMANCE

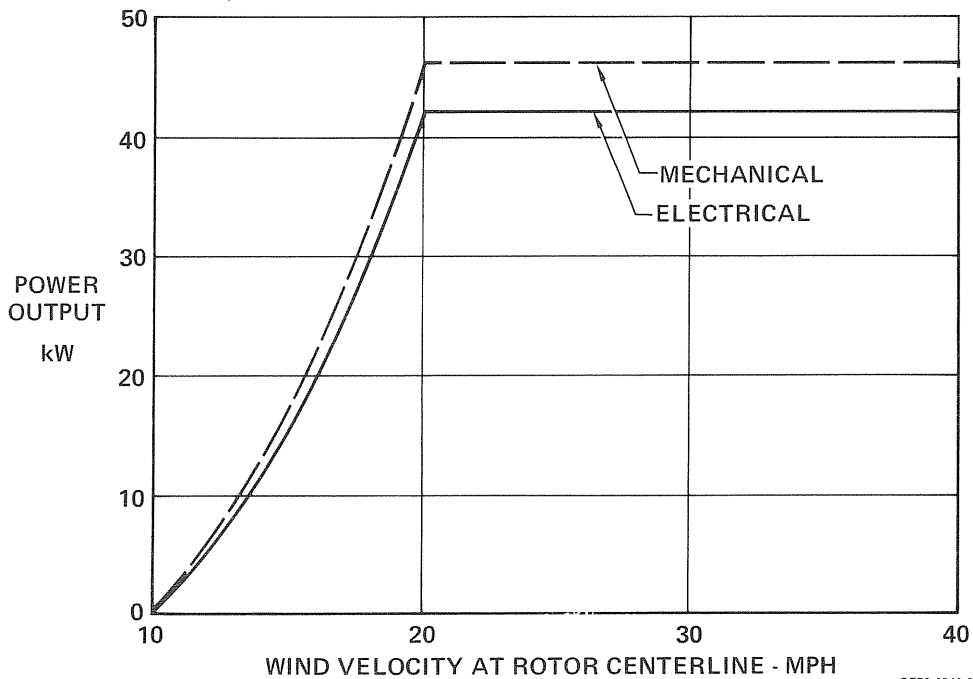
A power output breakdown is shown in Figure 39 for a wind of 20 MPH. The blade power of the prototype Giromill (no support arm drag) could provide 53 kW. Adding blade support arms reduces the power to 50.6 kW, and subtracting the power lost due to aerodynamic damping cuts that down to 49.3 kW. The control system is estimated to take about 200 watts per actuator, on the average. Therefore 0.6 kW is allocated for control purposes. The mechanical efficiency is estimated at 94%, and the generator efficiency 91%, giving the net mechanical and electrical power values shown.

The preceding performance estimates were used to calculate the annual energy. Figure 40 shows the power output as a function of wind velocity. This power output was then integrated with wind profile curves, using the relationships established in Section 3.2.1. The resulting annual energy expected from the Giromill as a function of the mean wind speed site is shown in Figures 41 and 42 for two rotor centerline heights: 75 ft. for a prototype Giromill and 50 ft., which is planned for production units. These charts can be used for calculating energy costs.



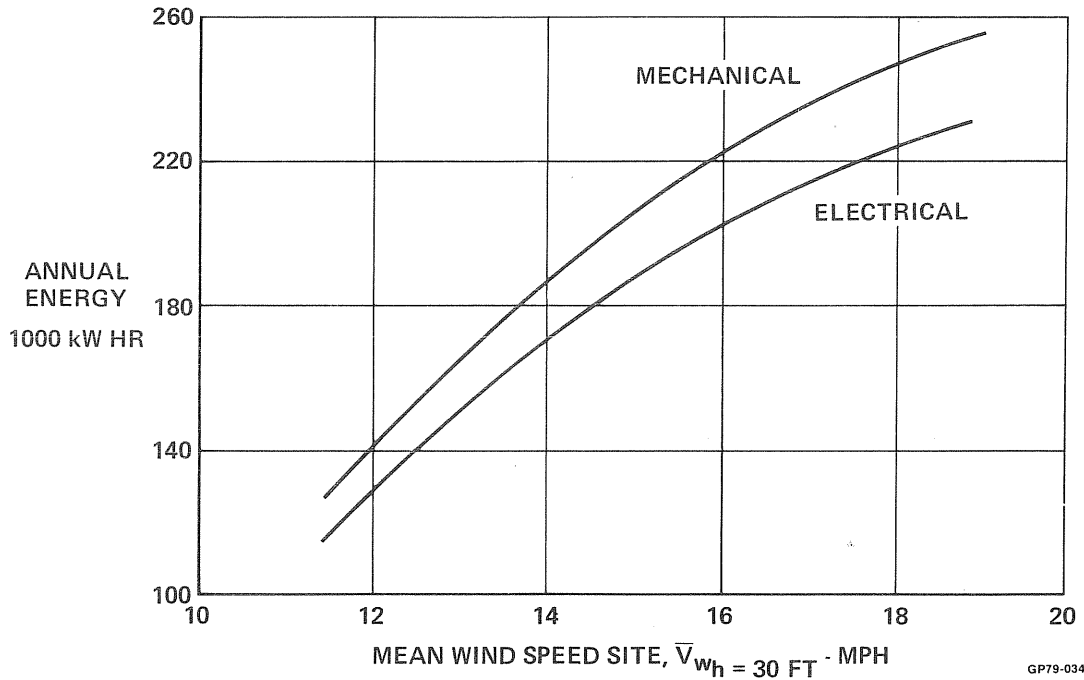
GP79-0636-5

FIGURE 39
POWER OUTPUT BREAKDOWN
 20 MPH Wind



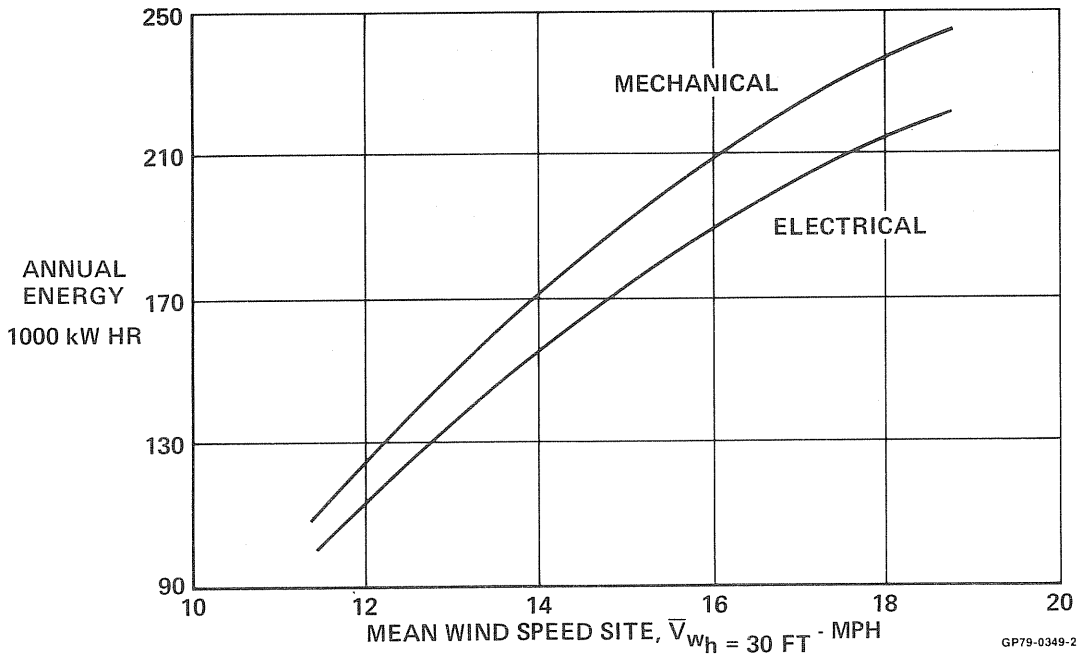
GP79-0349-3

FIGURE 40
GIROMILL POWER OUTPUT



GP79-0349-1

FIGURE 41
ANNUAL ENERGY
 Rotor Centerline at h = 75 Ft
 High Wind Cutoff 40 MPH
 Low Wind Cutoff 10 MPH



GP79-0349-2

FIGURE 42
ANNUAL ENERGY
 Rotor Centerline at h = 50 Ft
 High Wind Cutoff 40 MPH
 Low Wind Cutoff 10 MPH

5.0 EXTERNAL LOADS

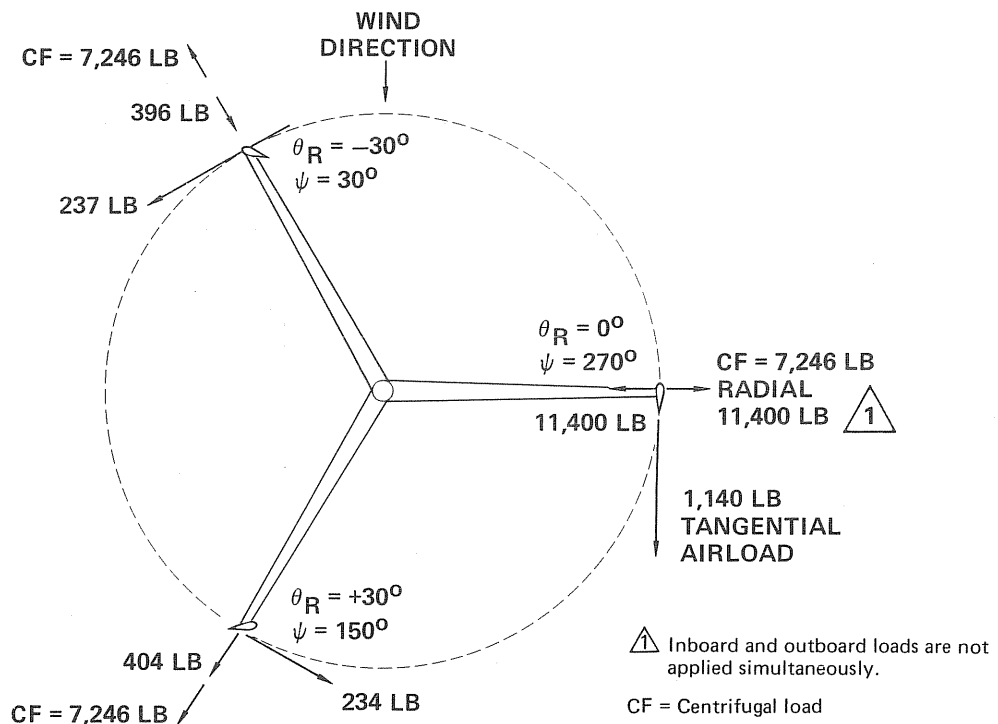
The external loads applied to the Giromill are aerodynamic and inertia loads. The inertia loads are comprised of centrifugal (radial) loadings, weight loadings and snow and ice loadings. The critical design load conditions are given in Figure 43. The calculation of those loads 1A and 1B is given below.

	CONDITION	DESCRIPTION	BLADES	SUPPORT ARMS	ROTATING TOWER	FIXED TOWER
ULTIMATE LOADS	1A	MAXIMUM OUTBOARD BLADE RADIAL LOAD	✓		✓	✓
	1B	MAXIMUM INBOARD BLADE RADIAL LOAD		✓	✓	✓
	2	MAXIMUM BLADE TANGENTIAL AND COMBINED RADIAL AND TANGENTIAL LOAD		✓	✓	
	3A	STORM LOADS WITH ICE		✓		✓
	3B	STORM LOADS WITHOUT ICE				✓
	4	OPERATING LOADS FOR FATIGUE DESIGN	✓	✓	✓	✓

GP79-0573-21

**FIGURE 43
SUMMARY OF CRITICAL DESIGN LOAD CONDITIONS**

5.1 CONDITION (MAXIMUM ULTIMATE OUTBOARD AND INBOARD RADIAL LOAD) - The loads for this condition are shown in Figure 44. The ultimate radial and tangential air loads shown are developed by a dynamic stall condition where a gust hits the blade at 270 degrees from the wind. At this position the velocity vectors for the wind, rotation, and gust add directly to give the highest possible velocity. A sample calculation is shown in Figure 45. The k factor for unsteady aerodynamics is taken from Ref. 10. The 50 ft/sec. gust velocity used in the calculation was taken from a gust spectrum (Figure 46) developed in Ref. 5. This spectrum is given in terms of gust cycles per static mile versus gust velocity. To use this spectrum we need to establish the number of miles of air flowing by the Giromill in 30 years.



GP79-0573-22

FIGURE 44
GIROMILL ULTIMATE DESIGN LOAD
(Condition 1)

$$\psi = 270^\circ$$

$$\theta_R = 0^\circ$$

$$V_{\text{WIND}} = 40 \text{ MPH} = 59 \text{ FT/SEC}$$

$$V_{\text{ROTATION}} = 69 \text{ MPH} = 102 \text{ FT/SEC}$$

$$V_{\text{GUST}} = 50 \text{ FT/SEC}$$

$$V_{\text{TOTAL}} = 211 \text{ FT/SEC}$$

$$\text{ULTIMATE RADIAL LOAD} \equiv 1.5k C_{N\alpha(\text{MAX})} q S$$

$$= 1.5 (1.25) (1.16) (62.4) (99.75)$$

$$= 11,400 \text{ LB}$$

WHERE:

$k \equiv 1.25$ FACTOR FOR UNSTEADY AERODYNAMICS;

$C_{N\alpha(\text{MAX})} \equiv$ MAXIMUM STEADY-STATE AERODYNAMIC LIFT COEFFICIENT

$q \equiv$ DYNAMIC PRESSURE

$S \equiv$ BLADE SURFACE AREA

GP79-0349-45

FIGURE 45
MAXIMUM AERODYNAMIC RADIAL LOAD
(Condition 1)

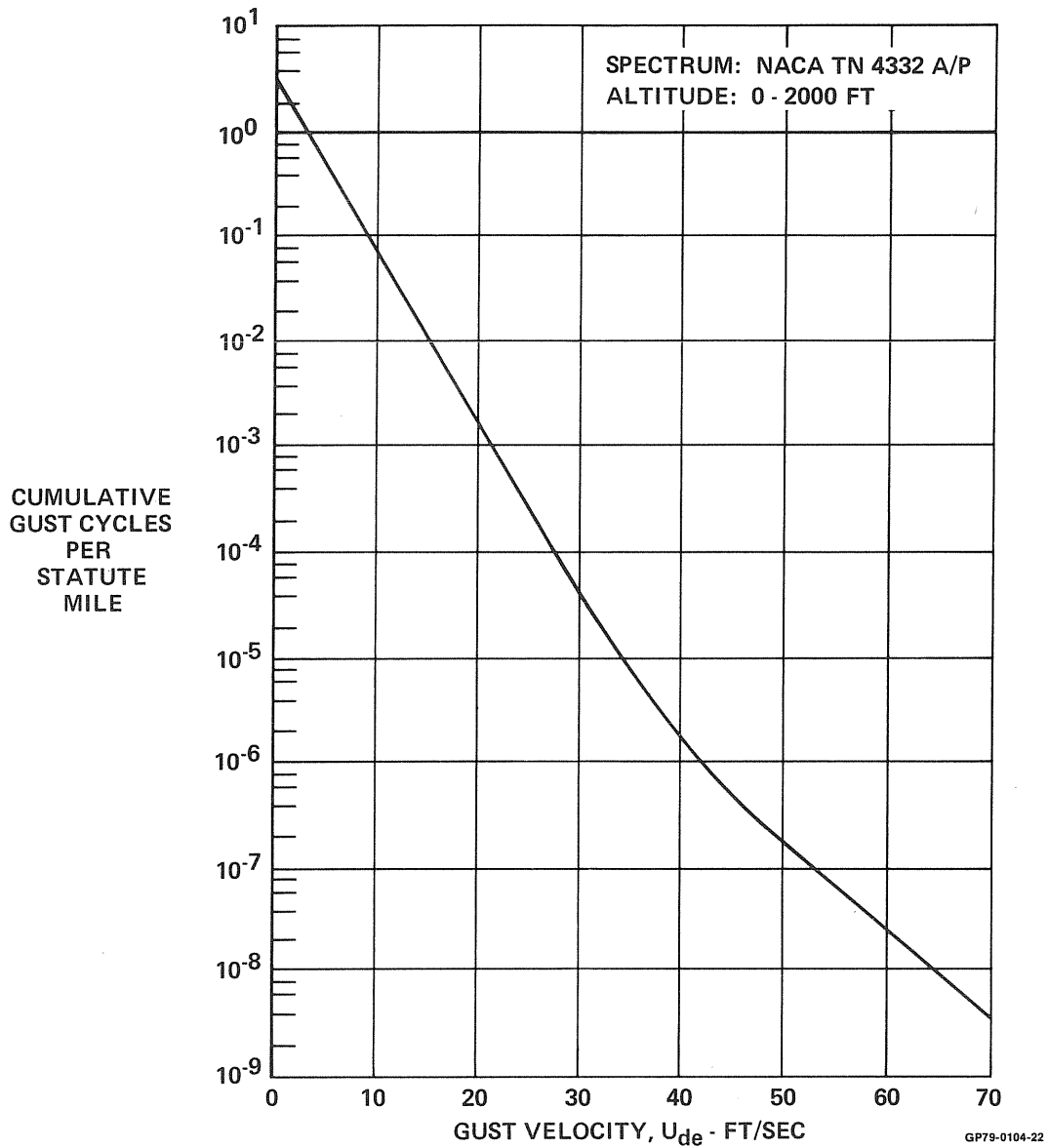


FIGURE 46
DESIGN GUST VELOCITY

$$\text{TOTAL MILES} = 15.9 * (24) (365) (30)$$

$$= 4.2 \times 10^6 \text{ MILES}$$

$$\frac{\text{CUMULATIVE GUST CYCLES}}{\text{STATUS MILE}} = \frac{1}{4.2 \times 10^6} = 2.38 \times 10^{-7}$$

$$\text{FROM FIGURE 46 } V_{\text{GUST}} = 50 \text{ FT/SEC}$$

The centrifugal load shown in Figure 44 is calculated as follows

$$CF = 1.5 \frac{WR}{g} \omega^2$$

$$\omega = \text{Rotational velocity} = 33.5 \frac{\text{rev}}{\text{min}} = 3.506 \frac{\text{rad}}{\text{sec}}$$

$$R = \text{Giromill radius} = 29 \text{ ft}$$

$$W = \text{Blade weight} = 436.4 \text{ lb}$$

$$g = \text{Acceleration of gravity} = 32.2 \text{ ft/sec}^2$$

$$CF = 1.5 \frac{W}{g} R \omega^2 = \frac{(1.5) (436.4) (29) (3.506)^2}{32.2} = 7246 \text{ pounds}$$

* Mean wind determined from Figure 47.

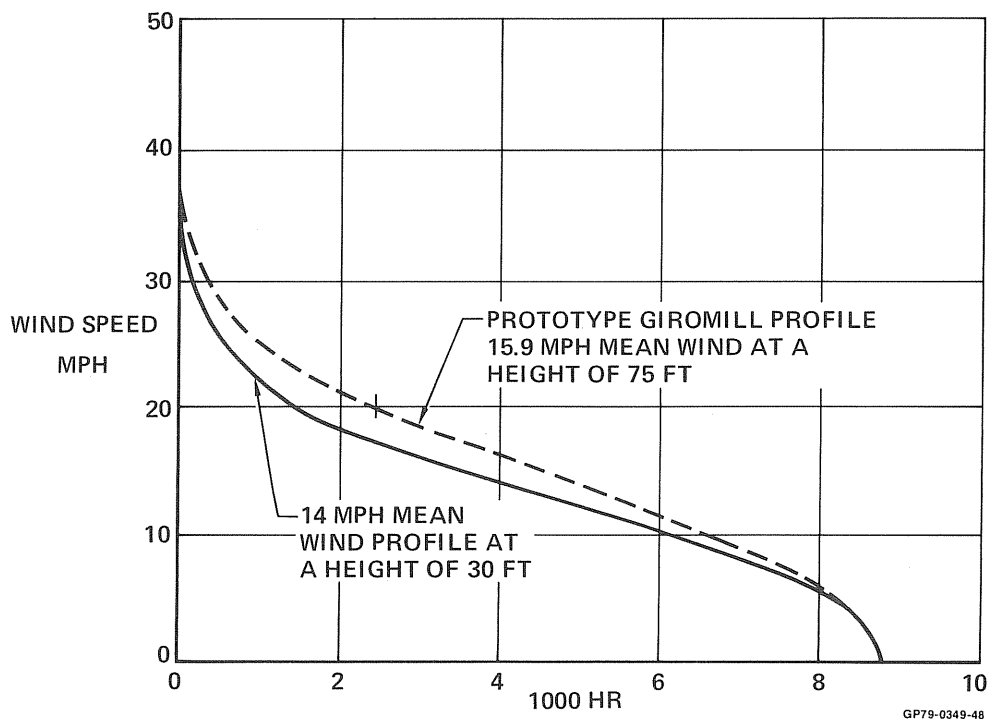


FIGURE 47
DESIGN WIND PROFILES

5.2 CONDITION 2 (MAXIMUM BLADE TANGENTIAL AND COMBINED RADIAL AND TANGENTIAL LOAD) - The loads for this condition are shown in Figure 48. The blade position at which this condition occurs ($\psi = 195^\circ$) was determined by using the Larsen Cyclogiro Performance Computer Program (Ref. 9). The loads were calculated based on the blade going through a dynamic stall as for Condition 1. The centrifugal load is the same for those two conditions since the rotational velocity is constant at 33.5 RPM.

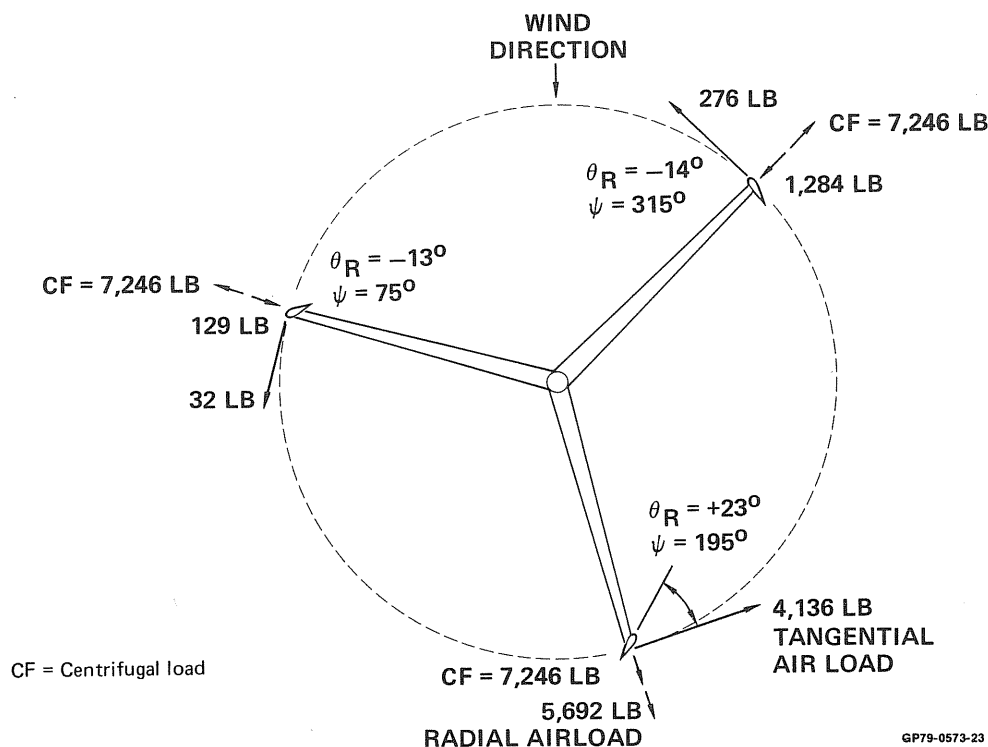


FIGURE 48
GIROMILL ULTIMATE DESIGN LOAD
(Condition 2)

5.3 CONDITION 3A AND 3B, STORM LOADS, WITH AND WITHOUT ICE - Storm wind loads were calculated at a 125 MPH wind, both with no ice and for a 3 inch ice accumulation. Loads are given for wind direction normal to one side of the tower. Wind loads for direction 45° to normal are assumed equal to the normal load direction. The maximum wind loads occur at a wind direction approximately 30° from the normal and are 10% above the loads given in Figure 49 for the fixed tower. These loads were multiplied by a 1.5 factor for ultimate design.

5.4 CONDITION 4 - (OPERATING LOADS) - The greatest air loads on the blades occur in a 20 MPH wind. For fatigue design we used the normal air loads in a 20 MPH wind, plus loads in a 20 MPH wind with a longitudinal gust factor of 1.3 superimposed. These loads (Figure 50) were calculated using the Larsen Cyclogiro Computer Program. Some of the high gust loads discussed in Section 5.1 were included in the fatigue spectrum (Section 6.1.2).

FIXED TOWER				
TRUSS SECTION (NUMBER OF TOWER BAYS FROM BASE)	NO ICE		3-INCH ICE	
	PROJECTED FRONTAL AREA (FT ²)	DRAG (LB)	PROJECTED FRONTAL AREA (FT ²)	DRAG (LB)
1	43.2	5,264	77.7	8,484
2	25.4	2,784	49.1	4,960
3	11.6	1,176	23.8	2,216
4	11.7	1,144	24.4	2,160
5	9.2	860	18.5	1,548
6	9.8	876	19.6	1,572
TOTAL		12,104		20,940

GIROMILL COMPONENTS		
ITEM	DRAG NO ICE (LB)	DRAG 3-IN. ICE (LB)
BLADES	102	219
SUPPORT ARMS	256	344
STRUT WIRE AND FITTINGS	43	174
ROTATING TOWER: ABOVE FIXED TOWER	896	1,077
INSIDE FIXED TOWER	1,696	1,980
TOTAL	2,993	3,794

FIGURE 49
STORM LOADS
(Condition 3)

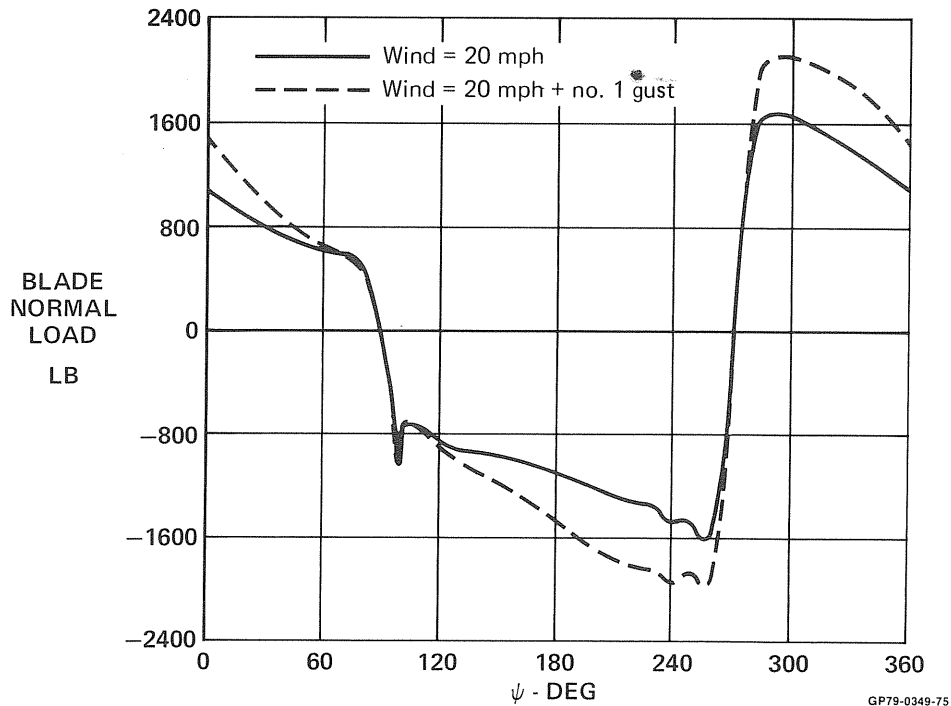


FIGURE 50
BLADE AERODYNAMIC NORMAL LOAD

5.5 COMBINED LOADS - The aerodynamic and centrifugal loadings discussed in the previous section were combined with the Giromill weight and the ice and snow loadings. These external loads were input into the NASTRAN computer program Reference to obtain internal loads for the complete Giromill. The internal loads are given in the form of free-bodies and bending moment diagrams in the stress analysis section (see Section 6 and 7). The criteria used for calculating the ice and snow loads are given in Figure 51.

STRUCTURE	NON-OPERATING REF: MIL-STD-210B	OPERATING
BLADES	3 INCHES NORMAL TO WIND OVER ONE-HALF OF SURFACE AREA, OR 1.5 INCHES OVER ENTIRE SURFACE MAY OCCUR SIMULTANEOUSLY WITH 125 MPH WIND	0.5 INCH MAXIMUM AT LEADING EDGE, TO 0 INCH AT 75% CHORD, OR 0.25 INCH OVER ENTIRE SURFACE MAY OCCUR SIMULTANEOUSLY WITH WINDS UP TO 20 MPH
SUPPORT ARMS	3 INCHES ON TOP SURFACE MAY OCCUR SIMULTANEOUSLY WITH 125 MPH WIND	0.5 INCH ON TOP SURFACE MAY OCCUR SIMULTANEOUSLY WITH WINDS UP TO 20 MPH
ROTATING TOWER	3 INCHES NORMAL TO WIND OVER ONE-HALF OF PERIMETER, OR 1.5 INCHES OVER ENTIRE PERIMETER MAY OCCUR SIMULTANEOUSLY WITH 125 MPH WIND	0.5 INCH OVER ONE-HALF OF PERIMETER, OR 0.25 INCH OVER ENTIRE PERIMETER MAY OCCUR SIMULTANEOUSLY WITH WINDS UP TO 20 MPH
FIXED TOWER	3 INCHES ON TOP AND WINDWARD SURFACES MAY OCCUR SIMULTANEOUSLY WITH 125 MPH WIND	0.5 INCH ON TOP AND WINDWARD SURFACES MAY OCCUR SIMULTANEOUSLY WITH WINDS UP TO 20 MPH

Snow Conditions:

- Snow is assumed to accumulate on the support arms only, at a slope no greater than 45° to horizontal.
- Giromill is assumed to operate with ice but without snow.

FIGURE 51
DESIGN CRITERIA FOR ICE AND SNOW CONDITIONS

GP79-0636-18

6.0 ROTOR DESIGN

The rotor consists of a central steel tube rotating tower with three aluminum blades supported by six steel support arms (two support arms for each blade). The support arms are pinned at the rotating tower and supported by a streamlined steel rod that runs from the tip of the support arms to the rotating tower. A bearing at the top of the fixed tower and a bearing at the lower end of the fixed tower support the rotating tower. The rotating tower extends to the ground to reduce the bearing loads and to locate the transmission and generator for easy maintenance.

6.1 BLADES

6.1.1 Structural Description - Each Giromill blade is a two-cell sheet metal airfoil consisting of a 0.16 thick leading edge skin, a 0.125 thick channel spar, and a 0.020 thick beaded trailing edge skin. These three parts are 6061-T6 aluminum. The blades are composed of three sections as shown in Figure 52; a 24.6-foot center section and an 8.7 foot section attached to each end. A cross-section of the blade is shown in Figure 53. Blade bending, shear, and torsion are carried by the leading edge and spar. The beaded trailing edge structure acts as a truss member to transfer local air loads to the leading edge torque box, thus eliminating the need for intermediate ribs. A 1.5 inch full span tab was added to the chord to insure that the aerodynamic center was far enough aft to obtain weathervaning.

Each blade is supported by two rotor arms. Attachment of the blade to the rotor arm is accomplished through a 4140 steel tube fitting inserted into the end of each blade section (Figure 54). Blade bending is transferred to the tube by a couple between two machined aluminum ribs. Torsion in the blade is reacted through bolts attaching the root rib to a flange on the support tube fitting. Blade modulation during operation is accomplished through a tooth-drive belt which is attached to the actuator in the support arm and to a sprocket attached to the support tube.

Fixed ballast is placed in the leading edge of the blades in order to place the c.g. at 23.25 percent of chord. An adjustable ballast is attached to the root rib for fine tuning the c.g. location during testing.

The steps used in fabricating the blade are shown in Figure 55. First the leading edge ribs are riveted to the leading edge with the steel support tubes used as a jig to position the ribs. Then the leading edge, channel spars, and trailing edge are positioned. These are riveted at the channel spar with the trailing edge open as shown in Figure 55. In production, an automatic riveting machine will be used to reduce cost; however, this requires a special set up of expensive tooling which could not be justified for one prototype. Therefore, the prototype will be assembled with hand bucked rivets on one side of the spar and blind rivets on the other. The trailing edge rivets are then installed. The final step is to rivet the end closure sheet metal ribs in place.

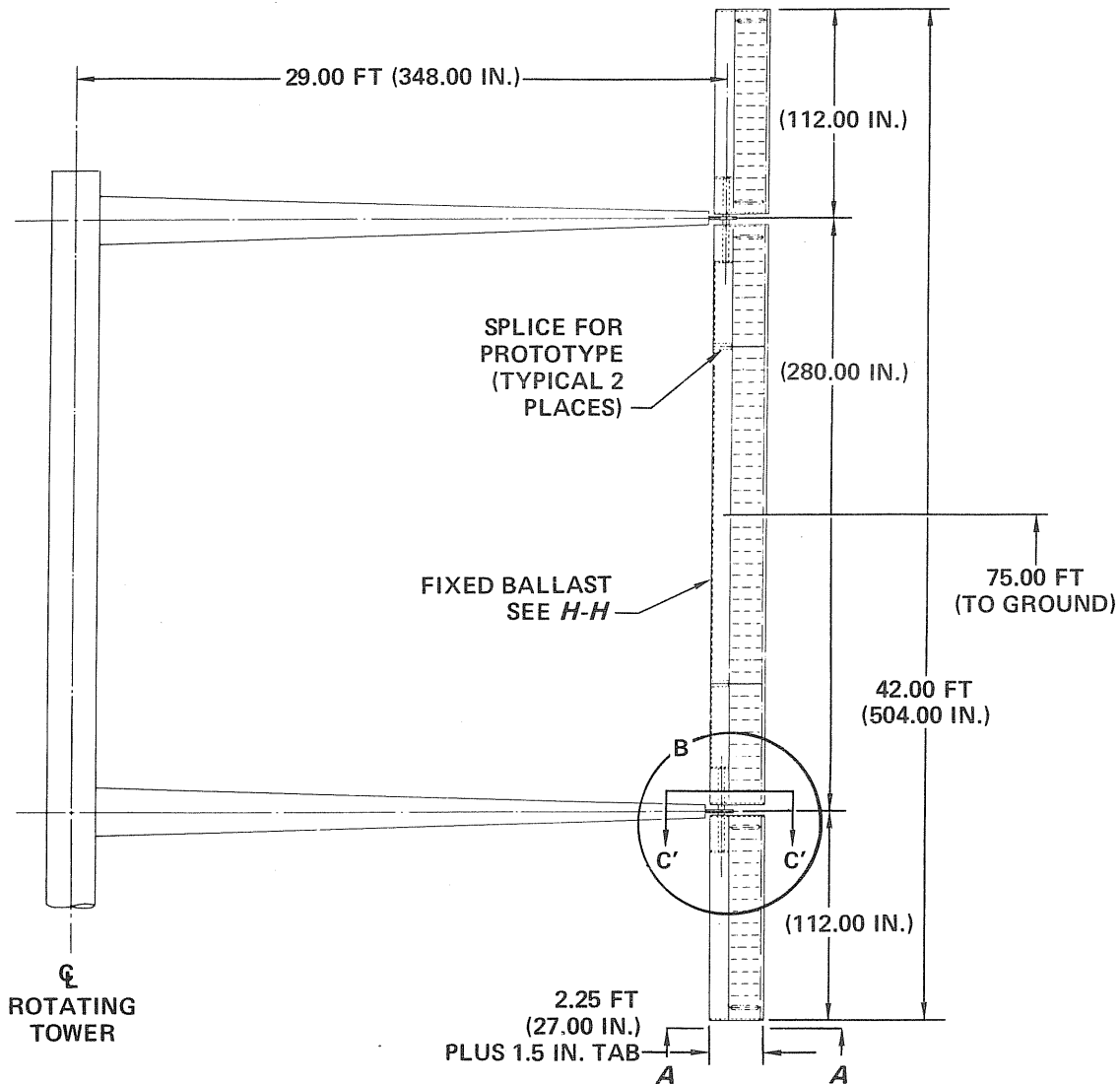


**FIGURE 52
BLADE GENERAL ARRANGEMENT**

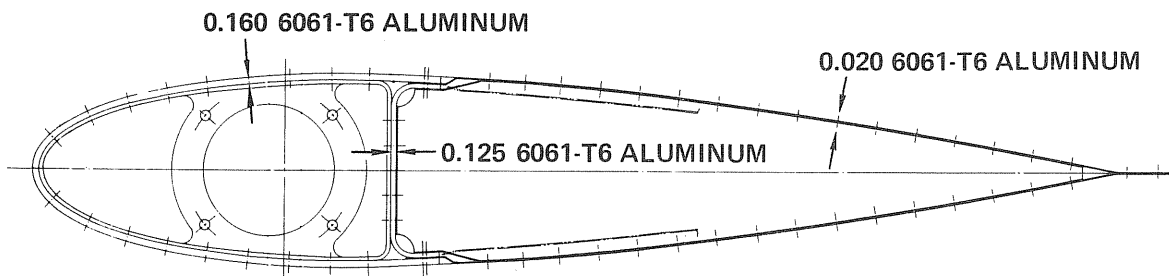


**FIGURE 53
BLADE CROSS SECTION**

GP79-0636-107

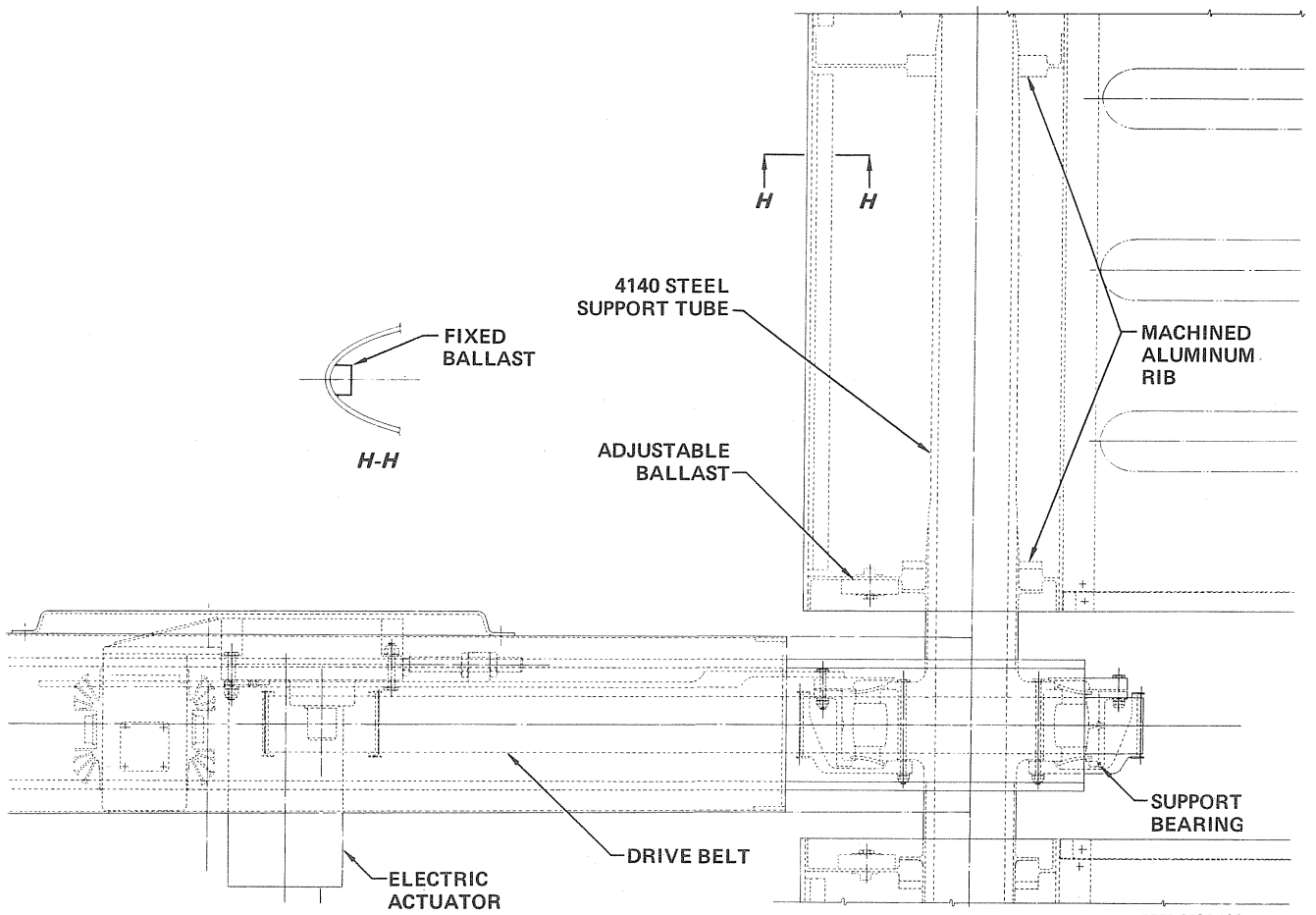
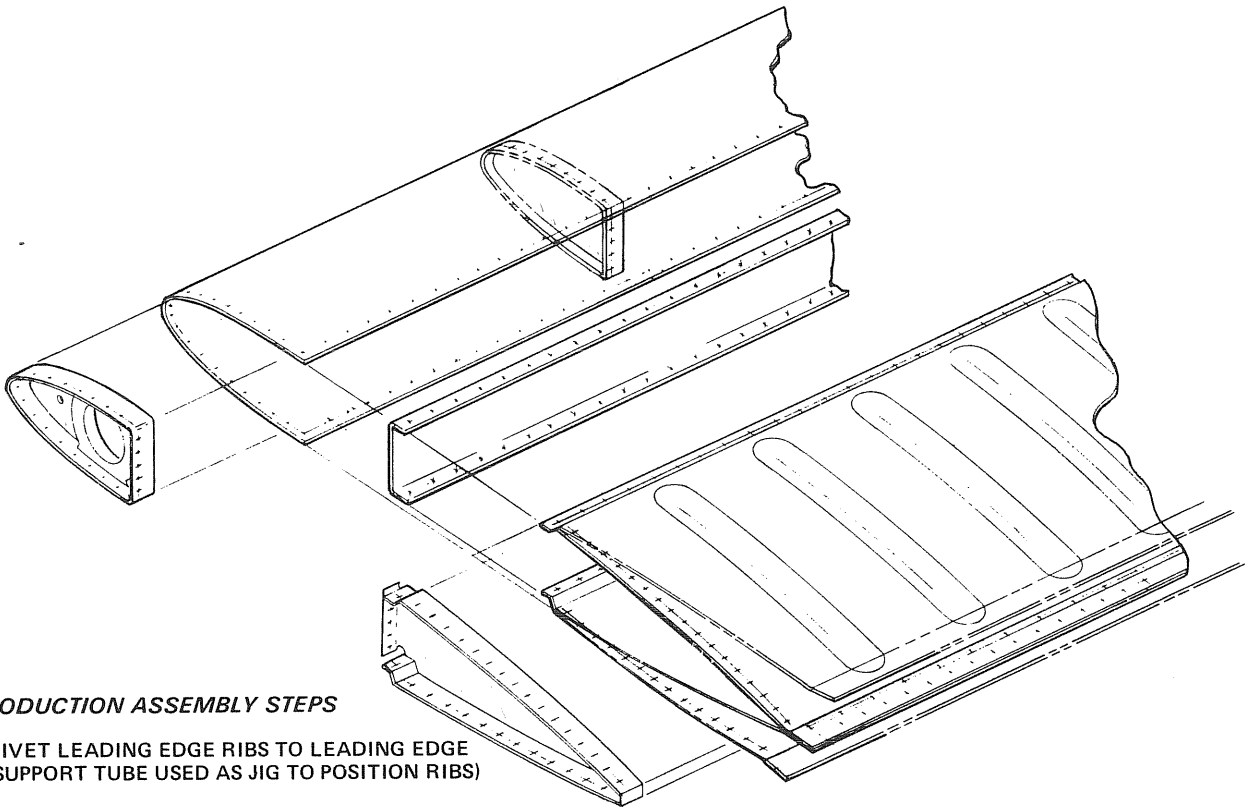


FIGURE 54
BLADE GENERAL ARRANGEMENT
 (View B)



PRODUCTION ASSEMBLY STEPS

1. RIVET LEADING EDGE RIBS TO LEADING EDGE
(SUPPORT TUBE USED AS JIG TO POSITION RIBS)
2. POSITION LEADING EDGE, CHANNEL SPARS AND TRAILING EDGE IN PLACE
3. RIVET WITH TRAILING EDGE OPEN AS SHOWN*
4. RIVET TRAILING EDGE
5. RIVET END CLOSURE SHEET METAL RIBS IN PLACE

*Prototype is assembled with blind rivets on one side

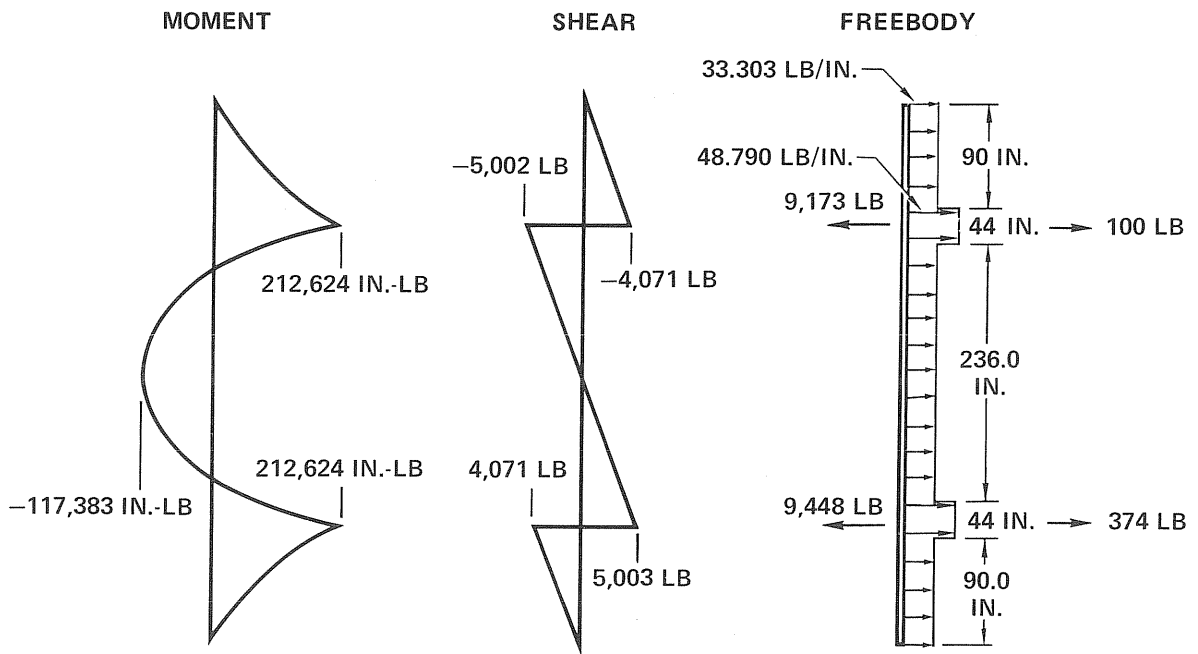
GP79-0573-25

**FIGURE 55
BLADE ASSEMBLY**

6.1.2 Static Stress Analysis - The highest stresses in the blade occur during Condition IA (see Section 5.1). The shear and moment diagrams and overall blade free body for this condition are shown in Figure 56. The highest bending moment in the blade, 212,624 in.-lb, occurs in the steel support tube area.

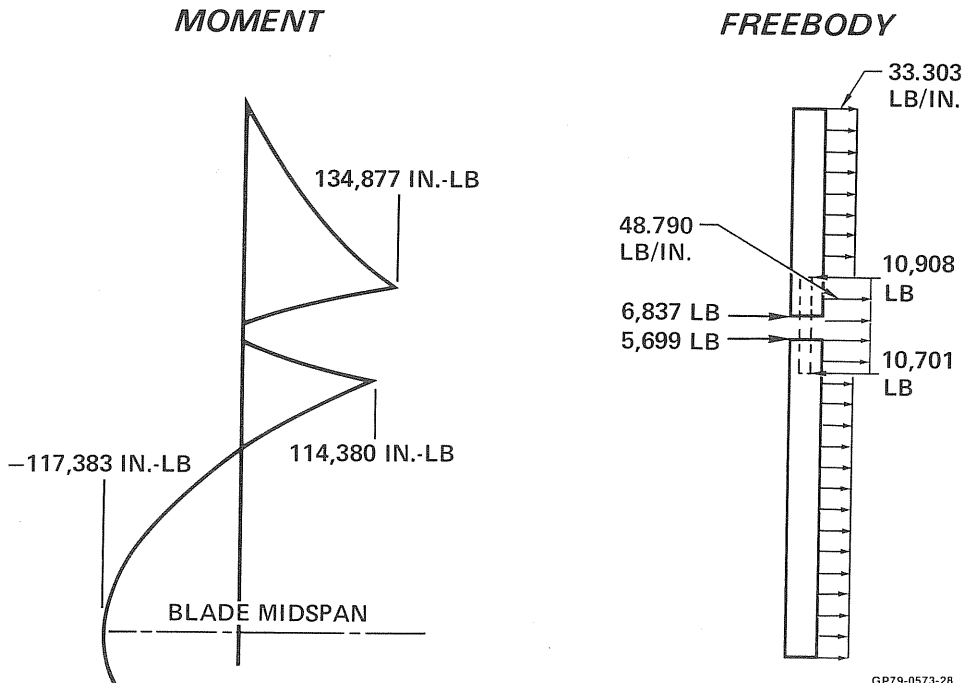
Figure 57 shows a bending moment and free-body diagram for the bending moment in the blade skin which includes the effect of the support tube reactions. The maximum moment at the inboard rib is 134,877 in.-lb and produces a margin of safety of 0.89 as shown in Figure 58. The high margin of safety is due to the fact that the blade was sized by fatigue requirements and not static strength.

The highest stresses in the steel support tube occur at Section A-A (Figure 59), where the support tube wall thickness is 0.25 inch. At this location, the bending moment is 196,344 in.-lb. The maximum bending moment of 212,624 in.-lb occurs at a location where the support tube wall is thicker and, thus, produces lower stresses.



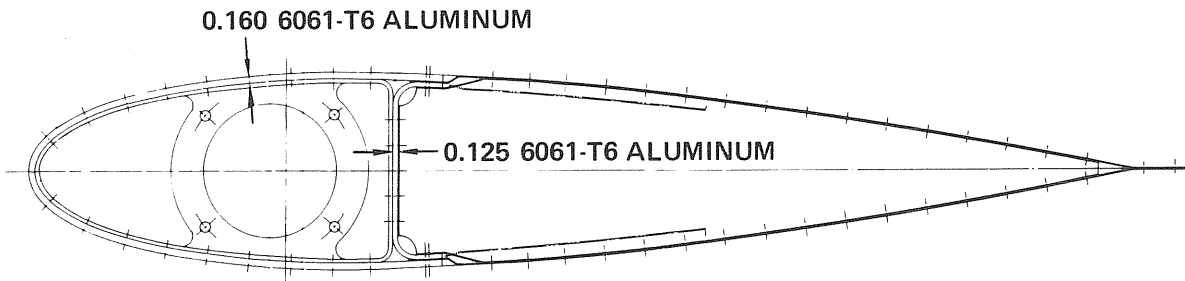
GP79-0573-27

FIGURE 56
BLADE ASSEMBLY -FREEBODY, SHEAR AND MOMENT DIAGRAMS
 (Condition 1A)



GP79-0573-28

FIGURE 57
BLADE SKIN STRESS ANALYSIS
 (Condition 1A)



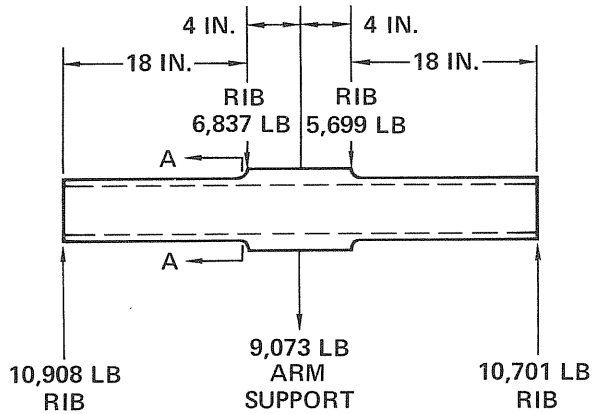
$$I_X = 14.77 \text{ IN.}^4$$

MAXIMUM MOMENT = 134,877 IN.-LB

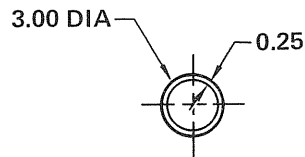
$$f_b = \frac{Mc}{I} = \frac{134,877 (2.43)}{14.77} = 22,190 \text{ PSI}$$

$$\text{M.S.} = \frac{42,000}{22,190} - 1 = +0.89$$

FIGURE 58
BLADE SKIN STRESS ANALYSIS
 (Condition 1A)



SECTION A-A



MATERIAL: 180 KSI STEEL

$$I = 2.059 \text{ IN.}^4$$

$$f = \frac{Mc}{I} = \frac{(196,344) (1.5)}{2.059}$$

$$f = 143,038 \text{ PSI}$$

$$\text{M.S.} = \frac{180,000}{143,038} - 1 = +0.26$$

GP79-0573-30

FIGURE 59
SUPPORT TUBE STRESS ANALYSIS
 (Condition 1A)

6.1.3 Blade Fatigue Analysis - The blade fatigue life analysis was based on Miner's Cumulative Damage Theory. The total number of load cycles used in the analysis was based on operating the Giromill for 6000 hours per year for 30 years at 33.5 RPM and a utilization factor of 0.99. The total number of load occurrences and the corresponding blade loads are shown in Figure 60.

NO. OF OCCURRENCES	MAXIMUM LIMIT AIR LOAD	MAXIMUM LIMIT INERTIA LOAD	MAXIMUM LIMIT ICE LOAD	MAXIMUM LIMIT STRESS	MINIMUM LIMIT STRESS	STRESS RATIO	FATIGUE LOAD CYCLES
1	±7,600	+4,831	0	+14,794	-5,302	-0.36	0.5
52	±6,000		0	+12,678	-3,186	-0.25	26
6,634	±4,000		0	+10,034	-542	+0.05	3,317
0.954×10^6	±2,000		0	+7,390	+2,102	+0.28	0.477×10^6
0.9×10^6	±2,000		+2,028	+10,071	+4,783	+0.47	0.45×10^6
0.9×10^6	±1,600		+2,028	+9,543	+5,312	+0.56	0.45×10^6
177.6×10^6	±2,000		0	+7,390	+2,102	+0.28	177.6×10^6
177.6×10^6	±1,600		0	+6,861	+2,631	+0.38	177.6×10^6

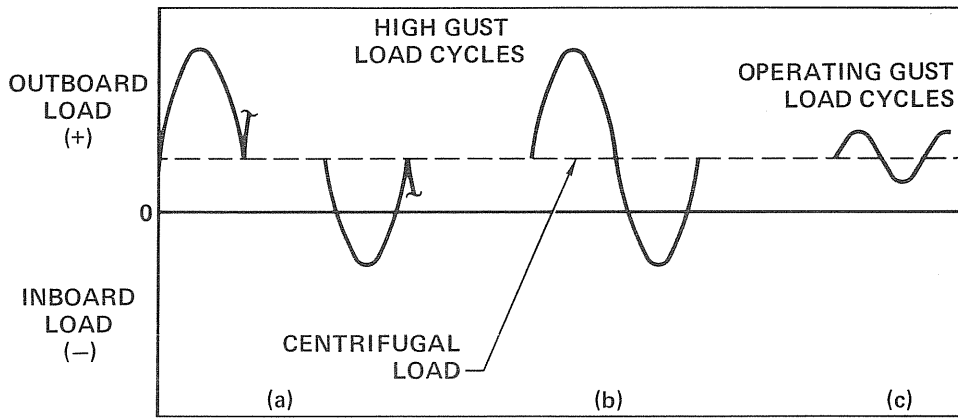
Total occurrences = $33.5 \times 6,000 \times 60 \times 30 \times 0.99 = 358 \times 10^6$ cycles

GP79-0636-71

**FIGURE 60
BLADE FATIGUE LOAD SPECTRUM**

A standard NACA curve of cumulative gust cycles versus gust velocity (Reference 5) was used to calculate the number of discrete gust load cycles at specific gust loads whose magnitudes were greater than those experienced during normal operation. Gust velocities at these higher blade loads were assumed to be proportional to the maximum design gust load (Condition 1), as described in Section 5.0. All other load cycles were assumed to occur in conjunction with normal operating loads. To account for low-level gust loads, which occur during normal operation, one-half of the normal operating loads were assumed to occur in conjunction with small gust loads which produced blade air loads up to 1.3 times the normal operating loads. To account for possible ice loadings on the blades before automatic shutdown, 1 percent of the normal operating cycles were assumed to occur with icing.

As shown in Figure 61, the high gust load cycles (a), may coincide with either maximum positive or maximum negative air loads. For fatigue analysis it was conservatively assumed that only one-half of the total calculated high gust cycles occur but that all occur at maximum excursion, i.e., from maximum positive to maximum negative (cycle (b) in Figure 61). Under operating air load conditions the total number of calculated occurrences were used and all were assumed to coincide with maximum excursions (cycle (c) in Figure 61). The load cycles used in the fatigue analysis are tabulated in Figure 60.



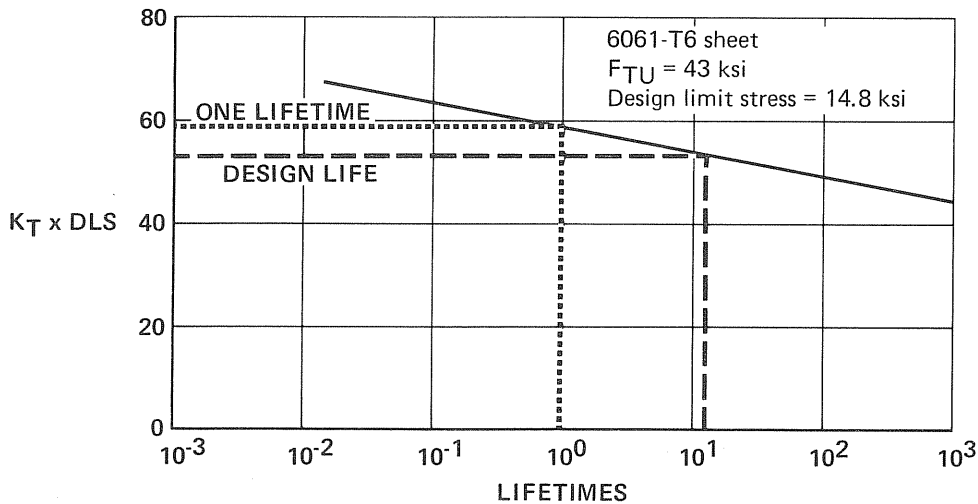
GP79-0636-72

**FIGURE 61
BLADE FATIGUE LOAD CYCLES**

Constant life (Goodman) diagrams, published in Reference 11 for wrought products of 6061-T6 aluminum alloy and K_T values of 1, 2, 3, and 4, were used to construct a curve of stress concentration (K_T) times design limit stress (DLS) versus life for the previously described fatigue load spectrum. Using the curve (Figure 62), the fatigue life of several locations along the blade was determined. Maximum values of stress concentration were determined from the formula:

$$K_{T_{Total}} = (K_{T_{nom}} + \frac{\sigma_{brg}}{\sigma_{nom}})$$

where $K_{T_{nom}}$ is the stress concentration for an unloaded hole, σ_{brg} is the bearing stress in the hole, and σ_{nom} is the nominal tensile stress in the blade skin.



GP79-0636-74

**FIGURE 62
BLADE FATIGUE LIFE ESTIMATE**

A summary of the fatigue critical areas is shown in Figure 63.

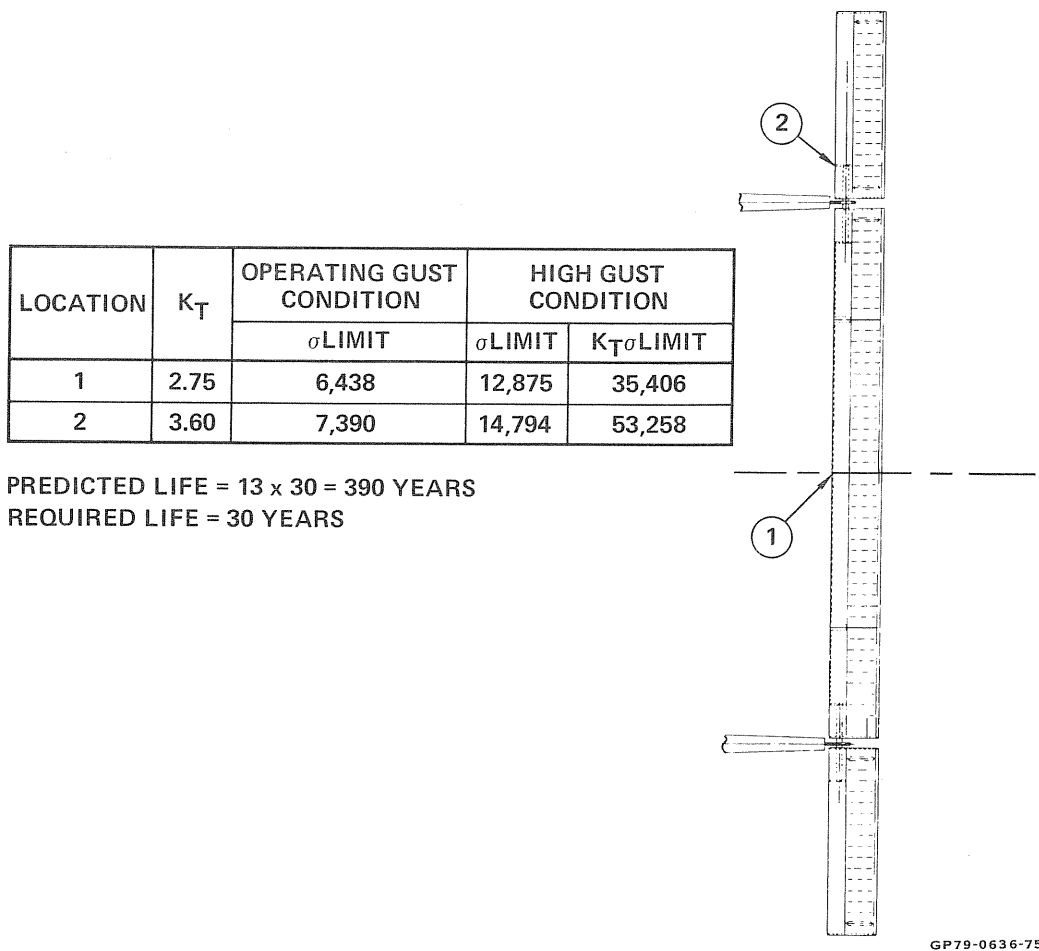


**FIGURE 63
 SUMMARY OF BLADE SKIN FATIGUE ANALYSIS**

Support Tube Fatigue Analysis - The fatigue life of the blade support tube was analyzed in the same manner as the blade, using the same fatigue load spectrum shown in Figure 60. Constant life diagrams published in Reference 11 for 4140 steel, heat-treated to 160 ksi, were used to construct a curve (Figure 64) of K_T (DLS) vs life. The fatigue-critical area is located at the inboard blade support. At this point, $K_T = 1.7$, due to a flange, and the maximum limit stress is 95.4 ksi. Based on Figure 64 for K_T (DLS) = 162.2 ksi more than adequate fatigue life is estimated for the component.

6.2 SUPPORT ARMS

6.2.1 Structural Description - Each support arm is a welded steel box. Two channels formed of 0.105 A36 steel are covered with a 0.060 A36 steel skin. The arms are tapered and streamlined to minimize aerodynamic drag with the outboard half smaller and more streamlined. The outline of

the support arms is shown in Figure 65. The support arms are painted with a zinc-rich primer followed by an epoxy intermediate coat and a top coat of polyurethane.

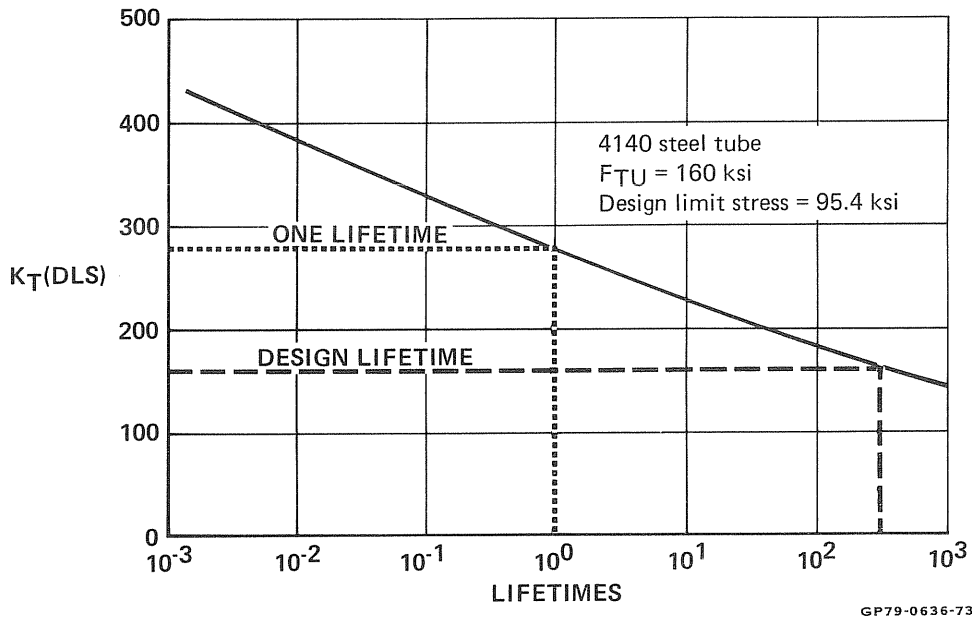


FIGURE 64
SUPPORT TUBE FATIGUE LIFE ESTIMATE

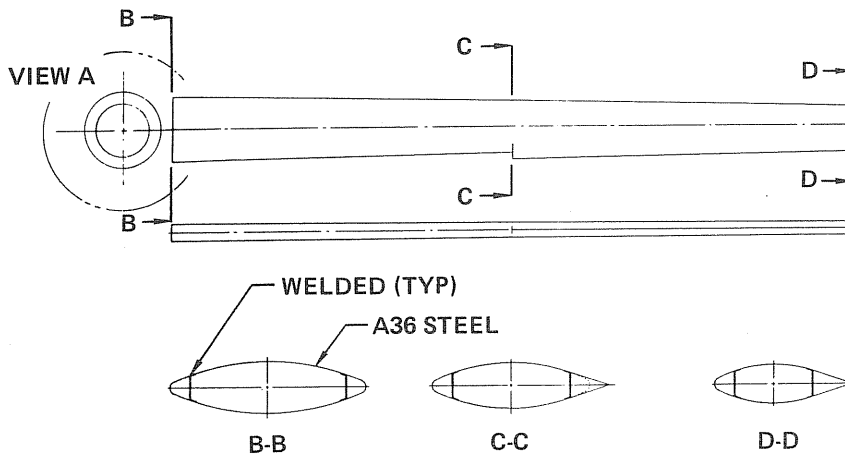


FIGURE 65
GENERAL ARRANGEMENT SUPPORT ARM

Attachment of the support arms to the rotating tower is shown in Figures 66 and 67. The tangential loads are taken by Bolt "B". Vertical and radial loads are taken by Bolt "C".

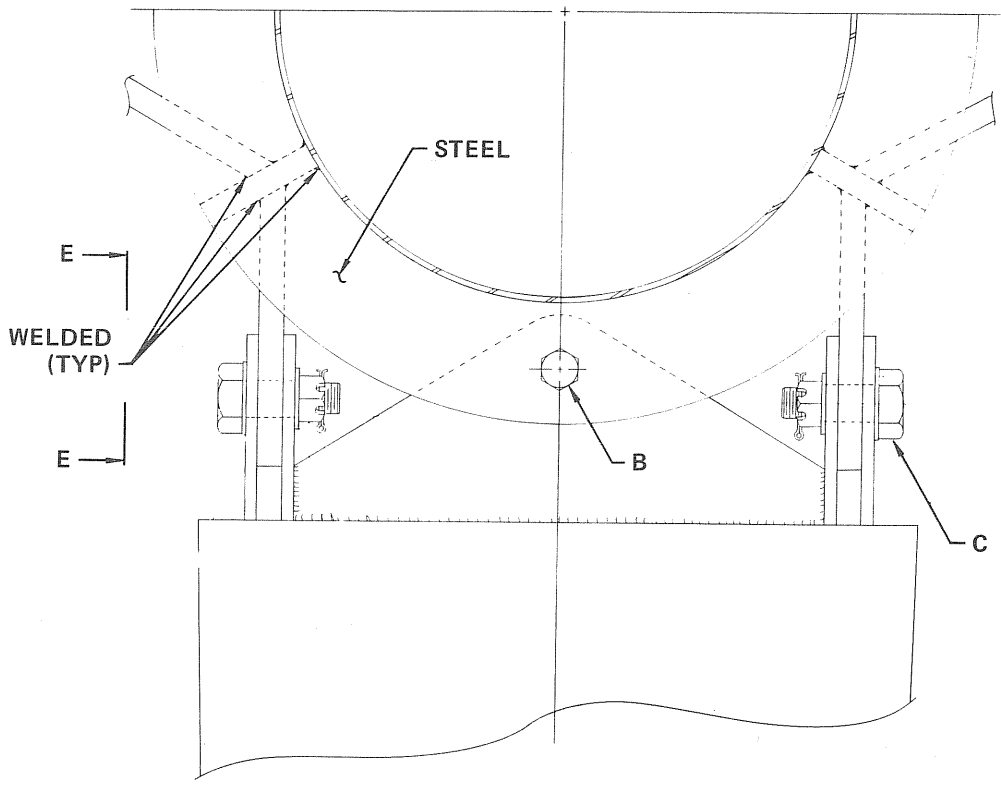
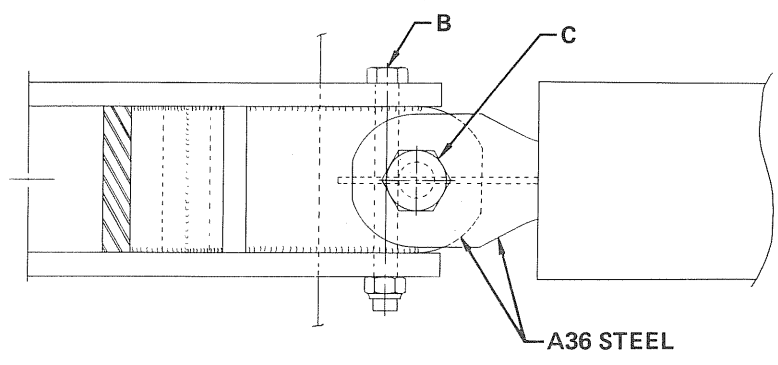


FIGURE 66
ARM /TOWER ATTACHMENT

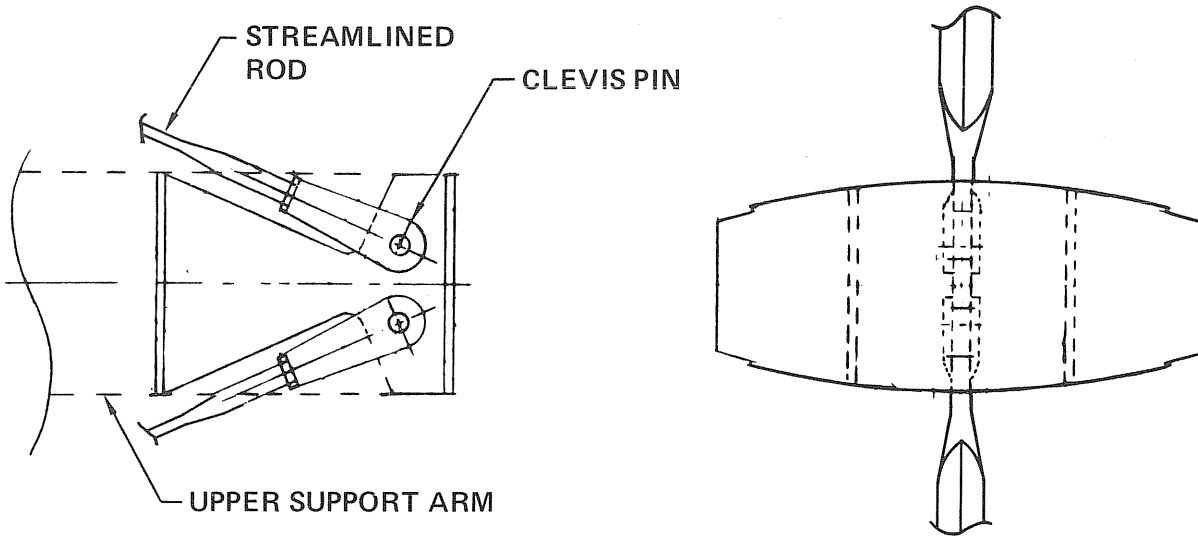
GP79-0636-28



GP79-0636-29

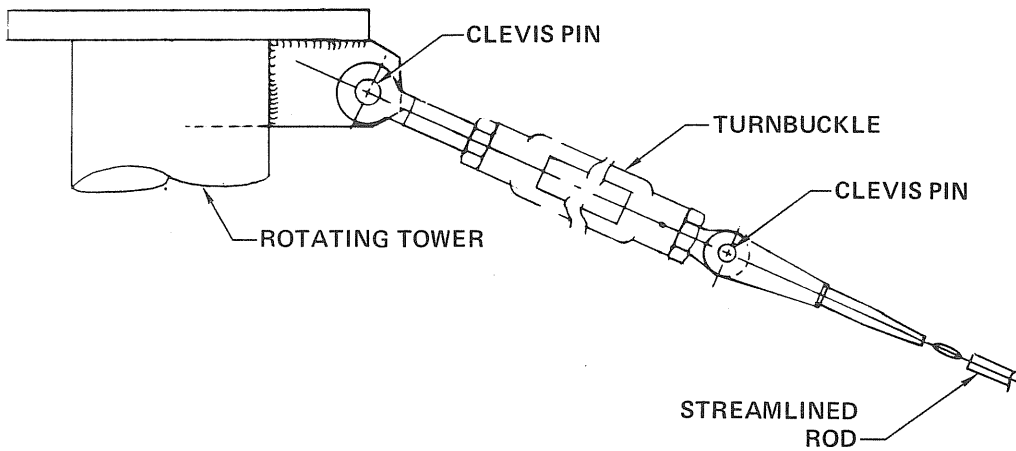
FIGURE 67
VIEW E-E

The struts for the support arms are streamlined and are formed from 0.625 in. diameter stainless steel rod. They are attached to the support arms with clevis pins as illustrated in Figure 68. The inboard ends of the struts are attached to the rotating tower with clevis pins and turnbuckles, as shown in Figures 69 and 70. The turnbuckles are used for rigging adjustments.



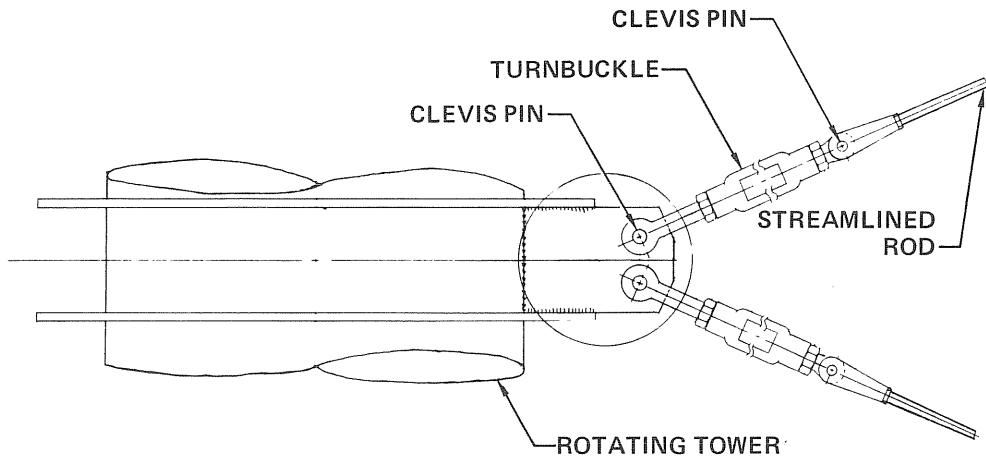
GP79-0636-27

FIGURE 68
UPPER ARM STRUT CONNECTORS



GP79-0636-25

FIGURE 69
TOP STRUT CONNECTION



GP78-0636-24

**FIGURE 70
INTERMEDIATE BRACE CONNECTORS**

6.2.2 Support Arms Stress Analysis - The support arms were designed primarily by tangential loads at the blade attach (Cond 2) and by icing conditions on the outer surface (Cond 3A). These loading conditions are described in Section 5.0. Icing conditions produced maximum bending stresses in the cover skins and maximum tensile loads in the support struts. Tangential loads on the arms produced maximum loads in the lugs attaching the arm to the rotating tower. Detailed stress analysis of the cover skin, root attach lugs, and support struts are presented in Appendix A.

6.3 ROTATING TOWER

6.3.1 Structural Description - The rotating tower is basically a 24 inch diameter, 3/16 inch thick A36 steel pipe with a section of 6 inch diameter steel pipe attached to each end. The tower is supported by an upper and a lower bearing attached to the fixed tower. The upper bearing reacts only side loads while the lower bearing reacts all vertical as well as side loads. The 6 inch diameter pipe at the bottom is bolted to the 24 inch diameter pipe through standard flanges and transmits torque to the speed increaser. The 6 inch diameter pipe at the top is also bolted to the 24 inch diameter pipe through standard flanges and provides support structure for the support arm struts and the 30 ft. tall lightning arrestor pole. The structural arrangement of the rotating tower is shown in Figure 71.

Large steel rings, welded to the pipe, redistribute concentrated loads from the support arm attach fittings.

The rotating tower was sized to meet stiffness as well as strength and fatigue requirements. Tower torsional frequencies were important from a control standpoint as discussed in Section 10.2 and for structural dynamic consideration as discussed in Section 9.1.

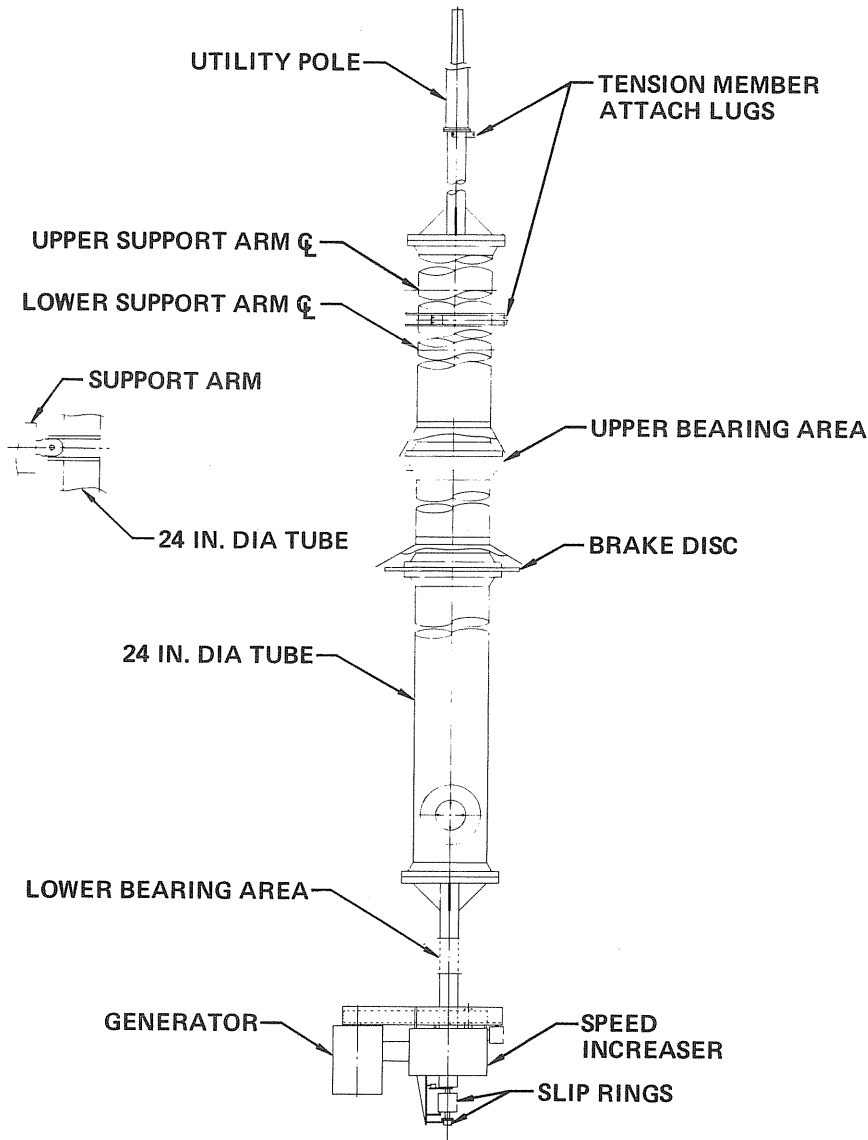


**FIGURE 71
ROTATING TOWER**

Corrosion protection is provided by a coating of zinc-rich primer followed by an intermediate epoxy coat and a top coat, of polyurethane paint.

6.3.2 Rotating Tower Stress Analysis - Maximum bending moments and shear loads on the tower occur at the upper bearing support. Torsion loads reach a maximum at the upper bearing support and remain constant throughout the lower section. Maximum shear, axial, and bending loads at this location are summarized in Figure 72. All loads tabulated are ultimate with the exception of those in Condition 4 which are "limit" operating loads.

CONDITION	V _x (LB)	V _y (LB)	V _z (LB)	M (IN. LB)	T (IN. LB)
1A	11,304	2,020	13,333	2.49 x 10 ⁶	0.232 x 10 ⁶
1B	11,538	2,020	13,333	2.029 x 10 ⁶	0.232 x 10 ⁶
2	12,863	174	13,333	1.27 x 10 ⁶	1.547 x 10 ⁶
3A	1,963	0	39,326	0.533 x 10 ⁶	0.022 x 10 ⁶
3B	1,515	0	13,333	0.431 x 10 ⁶	0.019 x 10 ⁶
4*	292	2,811	8,889	0.491 x 10 ⁶	0.249 x 10 ⁶

*Limit operating

GP79-0636-92

FIGURE 72
ROTATING TOWER LOADS AT UPPER BEARING SUPPORT

The tube was analyzed for combined torsion, bending and compression loads according to methods outlined in Reference 16. The minimum margin of safety for combined stresses occurs under Condition 1B, the maximum bending condition. Maximum torsional stresses occur during Condition 2, but the combined stresses produce a higher margin of safety due to reduced bending stresses. Detailed stress analyses are presented in Appendix A.

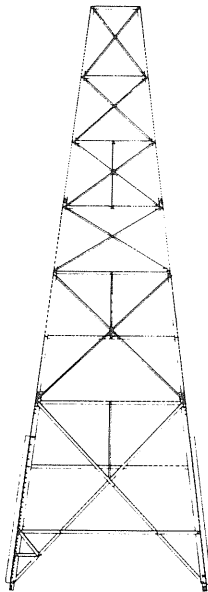
7.0 FIXED TOWER

7.1 TOWER

7.1.1 Structural Description - The fixed tower (Figure 73) is a truss made of ASTM A36 structural steel angles with bolted joints. Hot dip galvanizing is applied for corrosion resistance. A ladder with a fall prevention device (Figure 74) is supplied on one side.

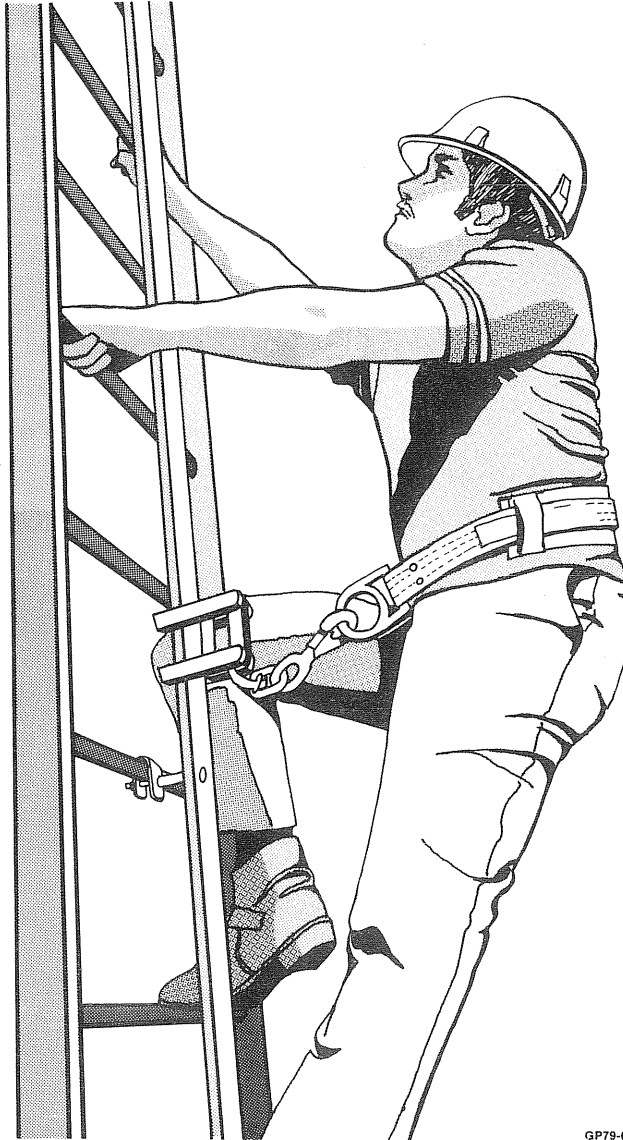
The upper bearing for the rotor is a sealed ball bearing, manufactured by Kaydon Bearing Division of Keene Corporation shown in Figure 75. Four grease fittings are provided for relubrication. The bearing seals are replaceable without disassembling the structure. A conical cover is installed over the bearing to protect it from rain and sunlight.

The inner bearing race is bolted to a flange on the rotating tower as shown in Figure 76. The outer race is bolted to a steel ring for reinforcement. To provide a flexible mounting, the bearing assembly is attached to the fixed tower with four thin sheets of steel, as shown in Figure 77. This mounting is designed to allow the upper bearing to take side loads without imposing thrust or bending moment loads. The thrust load is taken by the lower bearing.



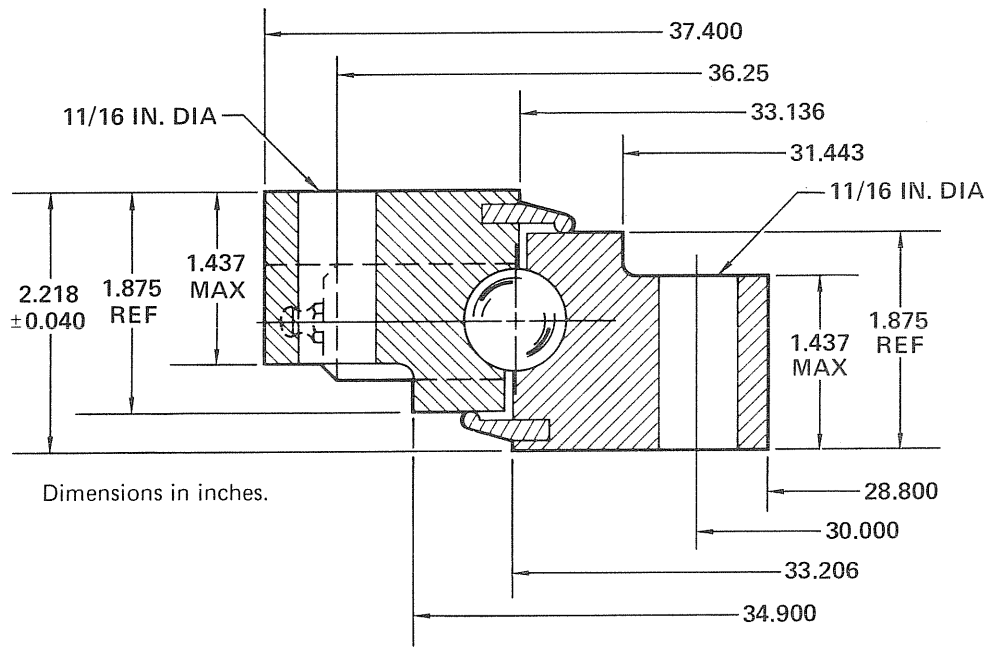
GP79-0636-51

**FIGURE 73
FIXED TOWER**



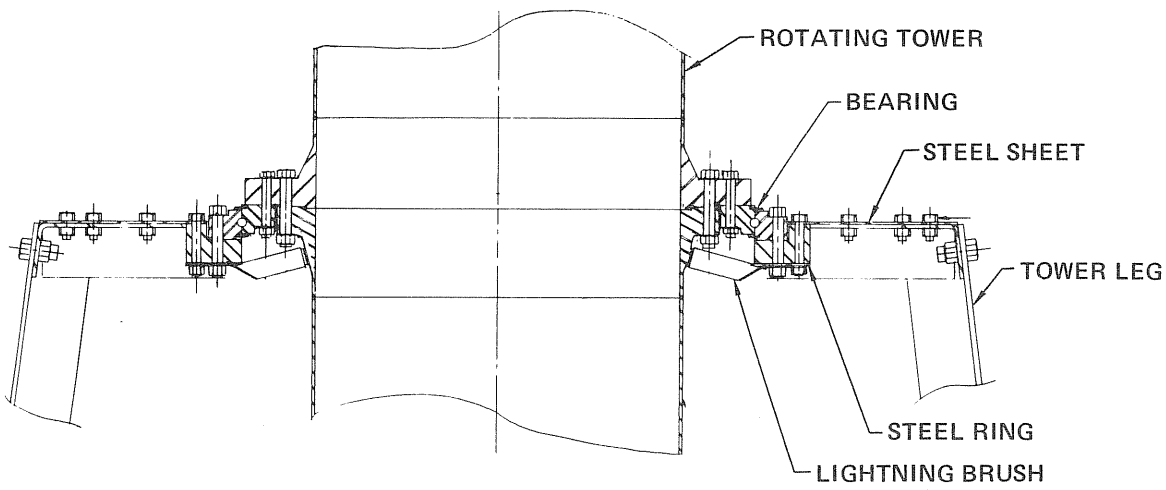
GP79-0349-95

FIGURE 74
FALL PREVENTION SERVICE



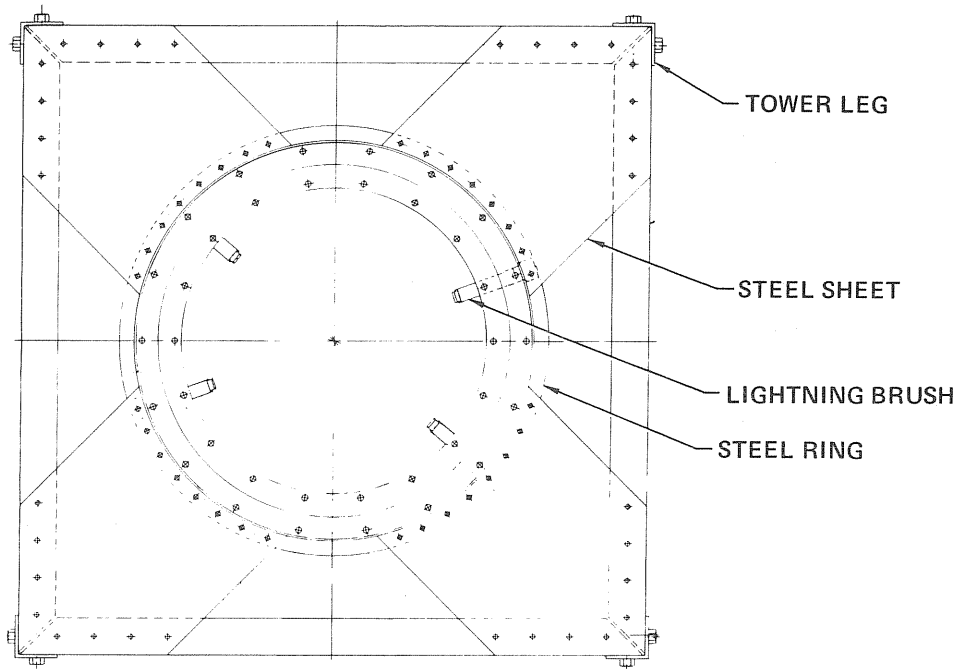
GP79-0349-82

FIGURE 75
UPPER BEARING



GP79-0636-50

FIGURE 76
UPPER BEARING MOUNTING
Side View



GP79-636-49

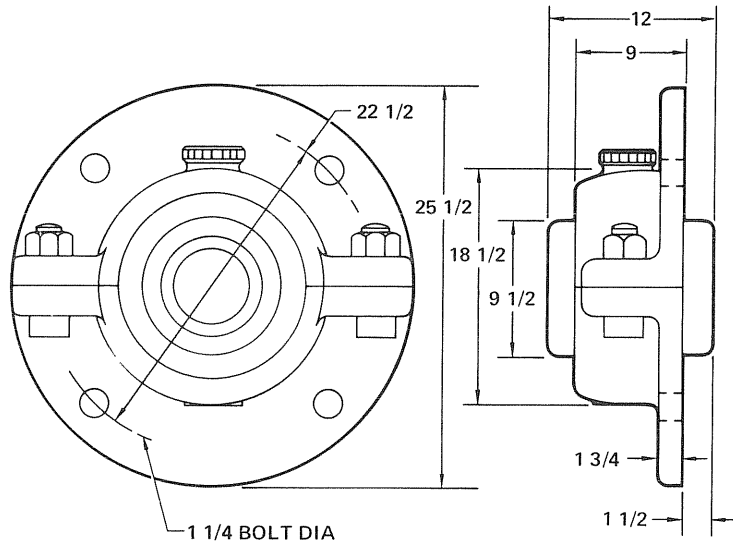
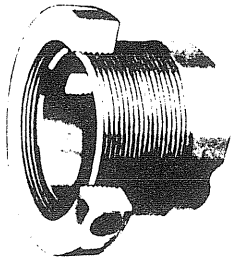
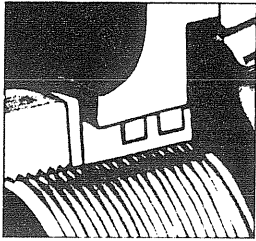
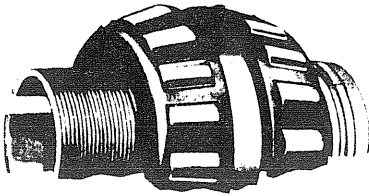
FIGURE 77
UPPER BEARING MOUNTING
 Plan View

A tapered roller bearing, manufactured by Reliance Electric Company, is used for the lower bearing (Figure 78). This bearing can also be relubricated and is bolted to a plate that is suspended from the four tower legs by four tension members. Turnbuckles are used to adjust the length of the tension members for proper location of the bearing. Four horizontal members take the side load on the bearing. See Figures 79 and 80.

An emergency disc brake system is designed into the prototype. The disc is bolted between two flanges of the rotating tower. The caliper brake is attached to one side of the fixed tower with a truss (See Figures 81 and 82). The caliper, manufactured by Goodyear Aerospace Corporation, is actuated by internal springs and released by hydraulic pressure.

Figure 83 illustrates the caliper brake. In all normal operating and standby modes the caliper is in the released position. A hydraulic system powered by the 48 Vdc control system provides the hydraulic pressure.

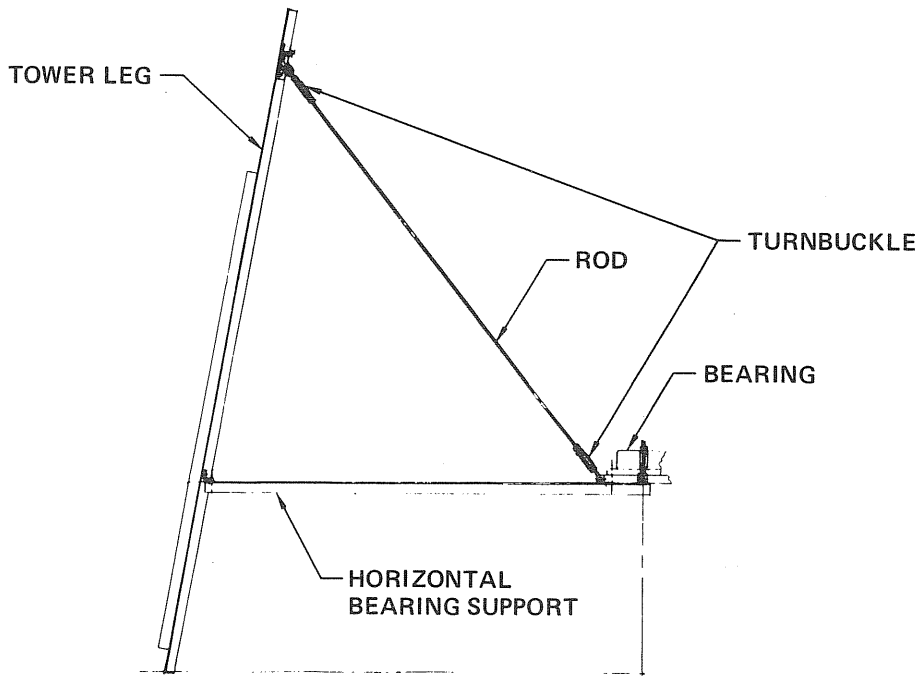
For lightning protection, four brushes, each one inch square, provide a parallel path around the upper bearing. Four one-inch brushes also run on the brake disc to provide a parallel path around the lower bearing. These brushes also keep the brake disc burnished assuring good brake pad contact with the disc. A one inch diameter grounding rod is attached to each leg of the fixed tower.



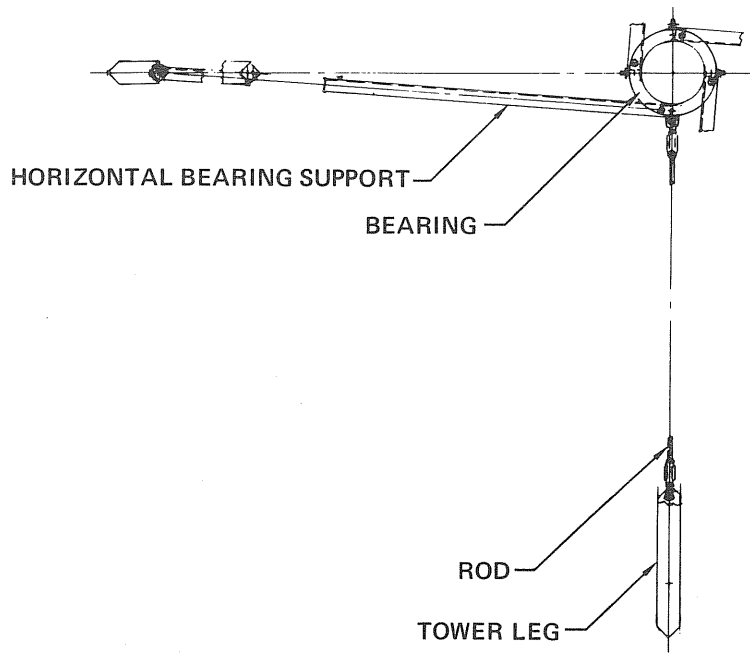
Dimensions in inches.

**FIGURE 78
LOWER BEARING**

GP79-0349-76

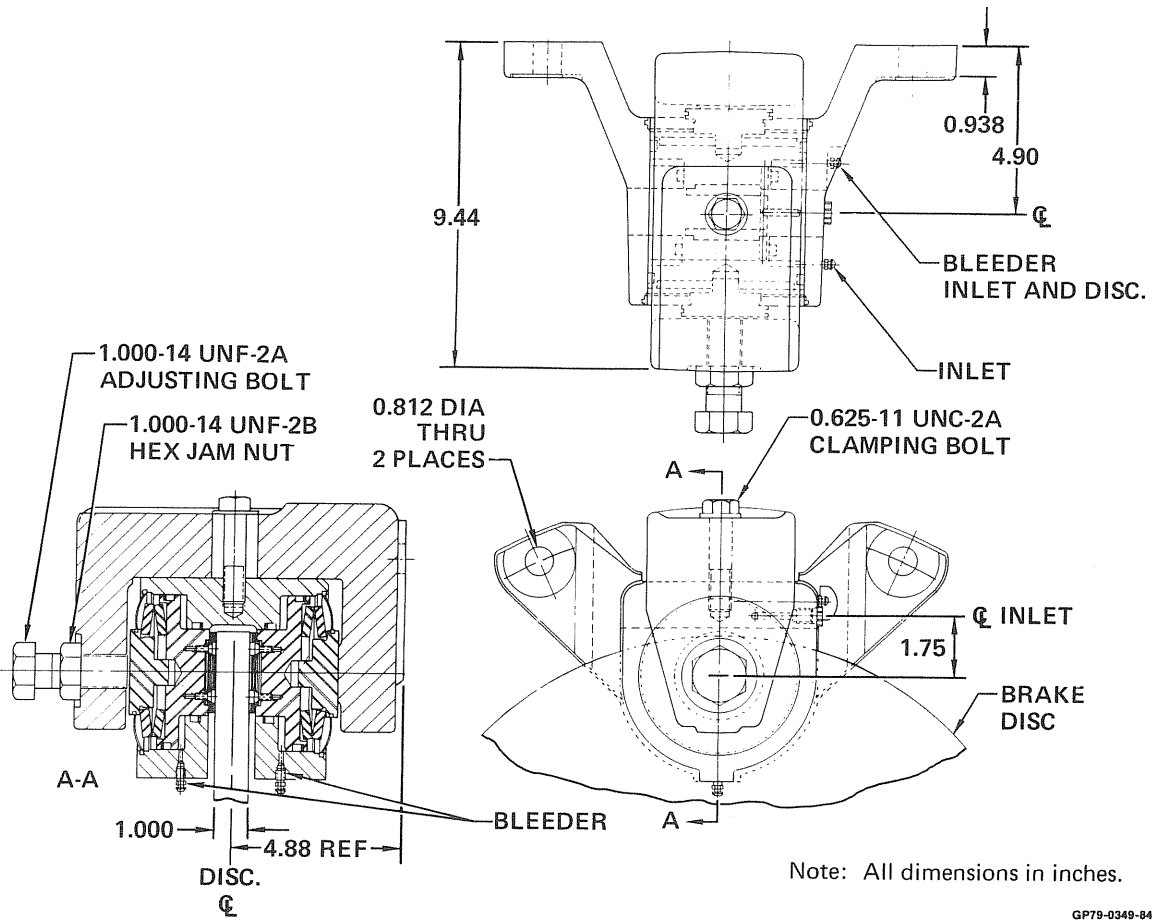


**FIGURE 79
LOWER BEARING
Side View**



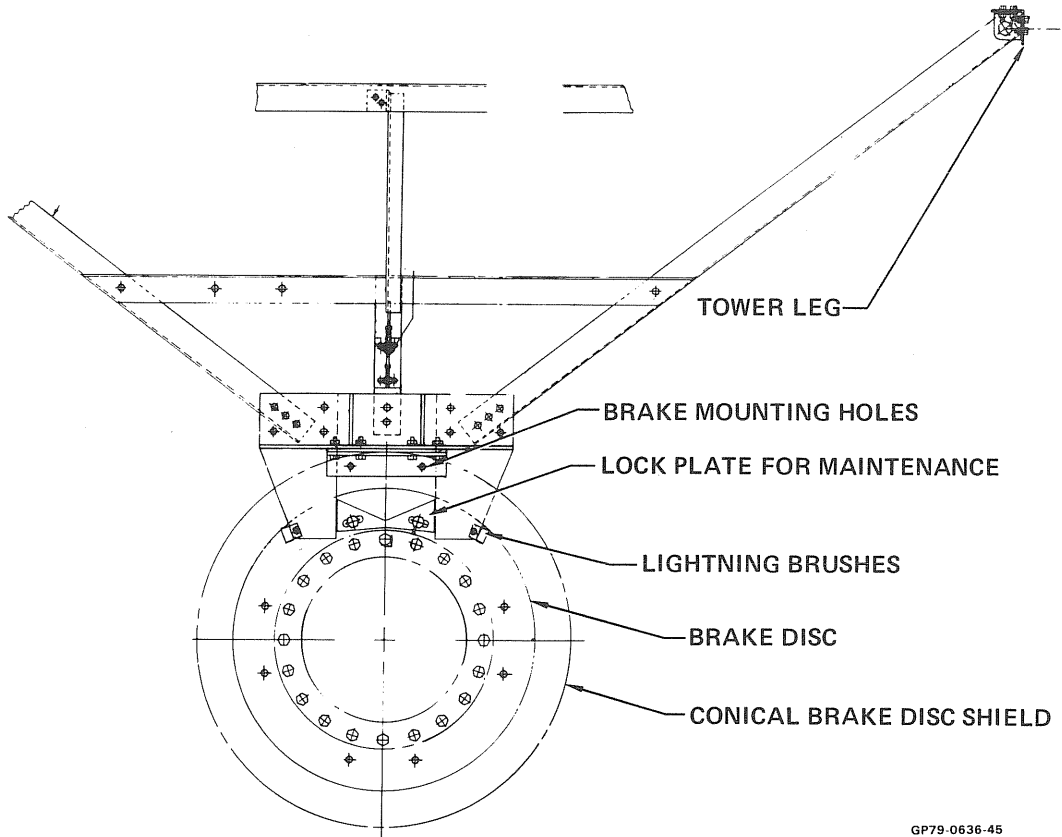
GP79-0636-47

FIGURE 80
LOWER BEARING MOUNTING
Plan View



GP79-0349-84

**FIGURE 81
CALIPER BRAKE**



GP79-0636-45

FIGURE 82
PLAN VIEW OF BRAKE SUPPORT ASSEMBLY DWG D40386

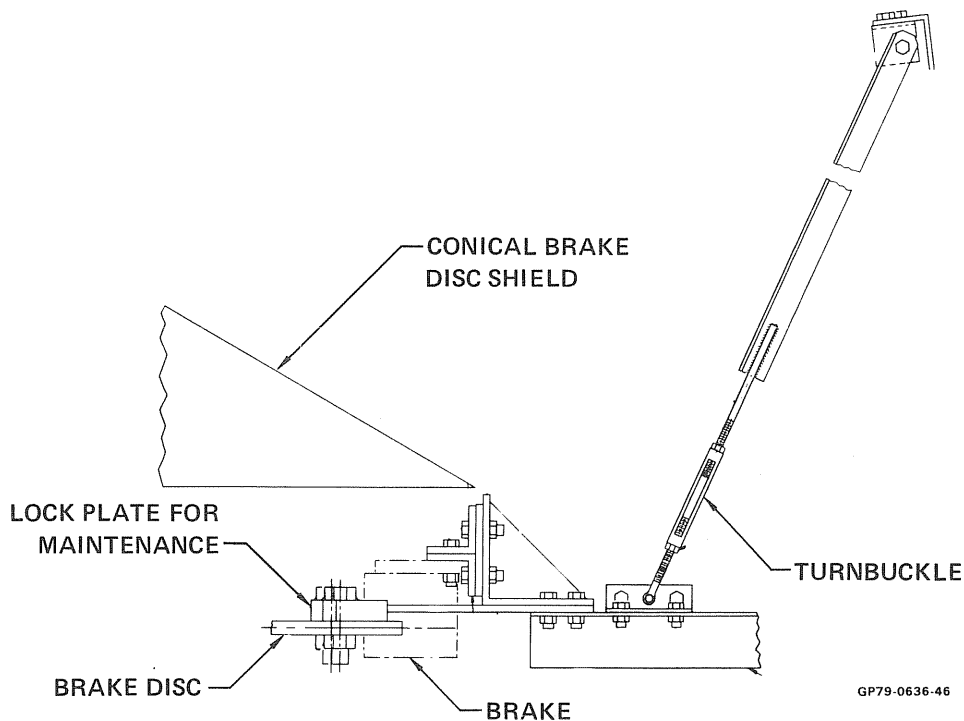


**FIGURE 83
SIDE VIEW OF BRAKE SUPPORT ASSEMBLY**

7.1.2 Fixed Tower Stress Analysis - A NASTRAN (Ref. 15) finite element model of the fixed tower structure was developed as an aid in structural dynamic and strength evaluations. Using this model, the loads on each individual member of the tower (girt, leg, or angle brace) were computed for all loading conditions. In this manner, the most critically loaded components were selected for more in-depth strength analyses.

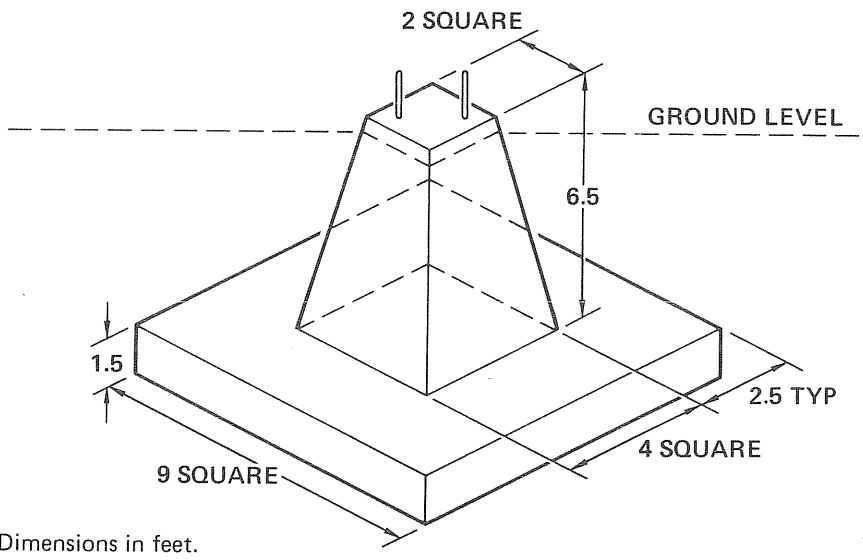
The tower leg to which the rotor torque link is attached is the most critically loaded member. This is because it must react the torque load transmitted through the speed increaser in addition to normal tower loadings. Detailed stress analyses are presented in Appendix A.

7.2 FOUNDATION

7.2.1 Structural Description - The foundation for the fixed tower is a spread foundation made up of four concrete piers reinforced with steel. The base of each pier is 9 feet square by 1.5 feet thick and is 7.5 feet below ground level. A column tapered from 4 feet square at the base to 2 feet square at the top of the pier extends 6 inches above ground level.

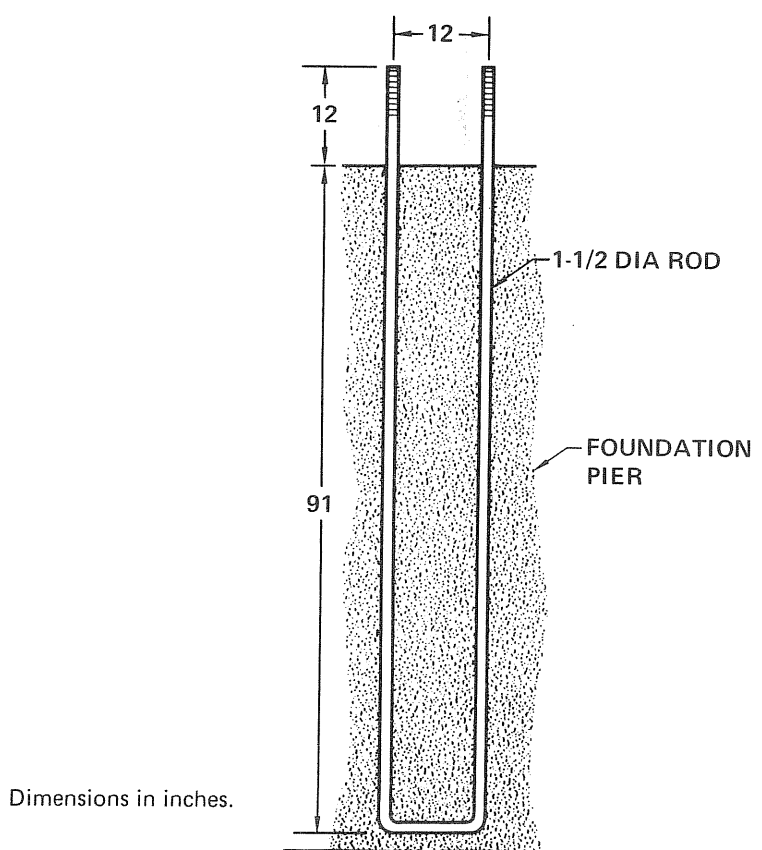
Figure 84 illustrates a typical pier. Two 1.5 inch anchor rods extend 12 inches out of the top of each pier as shown in Figure 85.

7.2.2 Stress Analysis - The foundation was designed for the soil conditions at the Rocky Flats test site. The soil analysis report of Reference 18 was the basis for this analysis.



GP79-0349-134

**FIGURE 84
FOUNDATION PIER**



GP79-0636-108

**FIGURE 85
ANCHOR RODS**

Figure 86 summarizes the loads at the base of the fixed tower that must be reacted by the foundation. Loading condition 1B gives the maximum ultimate uplift load of 29,200 lb. For this condition the margin of safety is 3.0 as shown in Figure 87.

Ultimate condition 3A results in the maximum soil pressure under the pier. The 57.2 kip vertical reaction, combined with the horizontal reactions of -11.3 kips and -15.8 kips, results in a maximum soil pressure of 3.866 kips per square foot. The allowable ultimate soil pressure for the Rocky Flats test site is 15 kips per square foot. Therefore the margin of safety is 2.9 for this condition. This analysis is summarized in Figure 88.

CONDITION	REACTION NO.	REACTION LOADS (KIPS)		
		x	y	z
ULTIMATE CONDITION 1A (MAXIMUM BLADE RADIAL OUTBOARD)	1	8.6	6.7	40.4
	12	-7.3	4.7	5.0
	23	4.8	3.1	-29.1
	34	-3.5	1.0	7.6
ULTIMATE CONDITION 1B (MAXIMUM BLADE RADIAL INBOARD)	1	-3.8	-1.3	7.6
	12	5.1	-3.4	-29.2
	23	-7.5	-5.0	5.0
	34	8.9	-7.0	35.2
ULTIMATE CONDITION 2 (MAXIMUM COMBINED RADIAL AND TANGENTIAL)	1	-5.2	-2.7	5.0
	12	5.1	-2.7	-27.4
	23	-8.9	-6.4	7.6
	34	8.8	-6.4	40.4
ULTIMATE CONDITION 3A (125 MPH STORM WIND AND 3 INCHES OF ICE)	1	-3.5	-10.0	-20.0
	12	-3.9	3.9	18.6
	23	-11.3	-15.8	57.2
	34	3.9	-3.9	18.6
ULTIMATE CONDITION 3B (125 MPH STORM WIND AND NO ICE)	1	-3.3	-7.3	-17.8
	12	-1.3	1.3	6.3
	23	-6.0	-8.6	30.4
	34	1.3	-1.3	6.3
LIMIT OPERATING CONDITION 4 (FOR FATIGUE)	1	0.2	4.7	-3.2
	12	-2.2	7.8	7.6
	23	-2.3	2.2	8.6
	34	0.3	5.3	-7.6

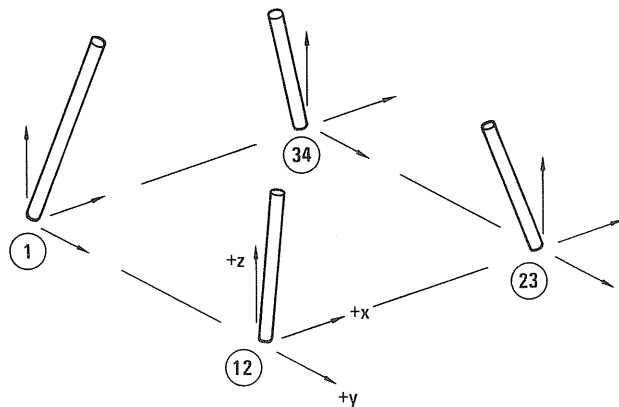
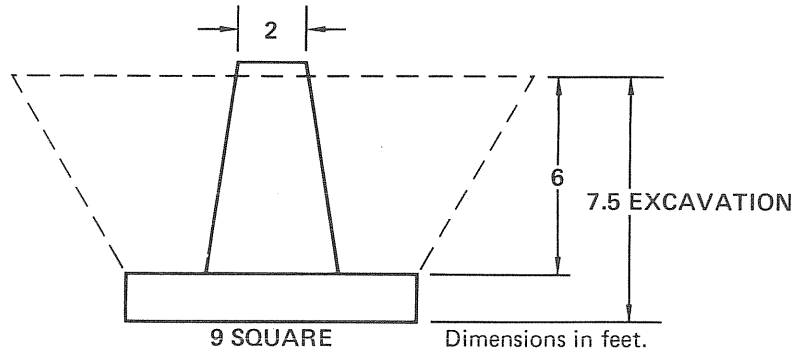


FIGURE 86
FIXED TOWER FOUNDATION LOADS

GP79-0349-144



$$\text{Weight}_{\text{conc}} = 150 \text{ lb/ft}^3$$

$$\text{Weight}_{\text{earth}} = 100 \text{ lb/ft}^3$$

$$\text{Weight}_{\text{conc}} = 27,325 \text{ lb}$$

$$\text{Weight}_{\text{fill}} = 89,750 \text{ lb}$$

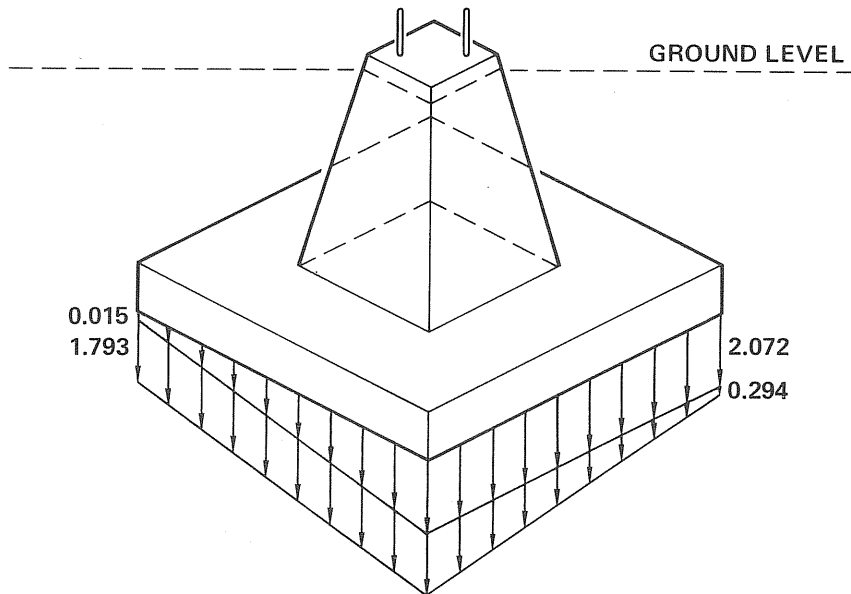
$$\text{Total weight} = 27,325 \text{ lb} + 89,759 \text{ lb} = 117,084 \text{ lb}$$

$$\text{Ultimate uplift (condition 1B)} = 29,200 \text{ lb}$$

$$\text{M.S.} = \frac{117,084}{29,200} - 1 = 3.0$$

GP79-0349-135

FIGURE 87
FOUNTAIN PIER ANALYSIS UPLIFT



$$\text{Maximum soil pressure} = 2.073 + 1.793 = 3.866 \text{ kips per sq ft}$$

$$\text{Allowable ultimate pressure} = 15 \text{ kips per sq ft}$$

$$\text{M.S.} = \frac{15}{3.866} - 1 = 2.9$$

GP79-0349-145

FIGURE 88
MAXIMUM SOIL PRESSURE
Ultimate Condition 3A
Reaction No. 23

8.0 WEIGHTS

Giromill weights were estimated for both the prototype and production units. The production unit has a shorter tower giving a blade ground clearance of 30 ft. Production unit weights were used for cost estimation shown in Section 15. The component weights are shown in Figure 89.

Also estimated were the prototype Giromill mass moments of inertia of the rotor and blades which were required for control system analyses. The rotor inertia included all rotating mass except for the speed increaser and generator. The calculated rotor inertia was 75,350 slug-ft.

The blade mass moment of inertia about its pivot axis (0.22C) was calculated as 2.99 slug-ft². This includes all rotating parts of the blade, i.e., blade structure, belt sprocket, and inner bearing races.

	PRODUCTION UNIT WEIGHT (LB)	PROTOTYPE WEIGHT (LB)
ROTOR		
BLADES	1,308	1,308
BLADE FAIRINGS	90	90
SUPPORT ARMS	4,430	4,430
ROTATING TOWER	8,350	11,000
FIXED TOWER		
STRUCTURAL	9,280	13,465
UPPER BEARING	190	190
LOWER BEARING	560	560
CONTROL SYSTEM	400	400
ELECTRICAL OUTPUT SYSTEM		
GEARBOX	850	850
GENERATOR	480	480
BELT STAGE AND ELECTRICAL EQUIPMENT	210	210
	26,148	32,983

GP79-0636-135

FIGURE 89
GIROMILL WEIGHT BREAKDOWN
Design 1

9.0 STRUCTURAL DYNAMICS

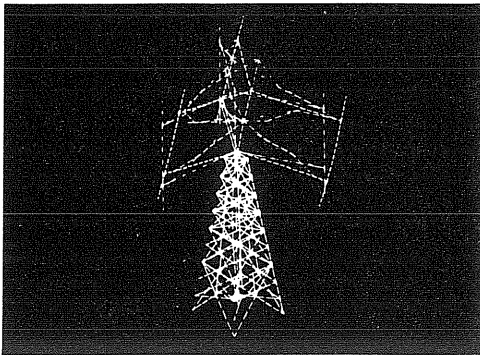
Structural dynamics studies were used to ensure that design adequacy existed in the areas of vibration, flutter, and structural response. For the final design configuration vibration frequencies were determined for the individual blades, arms, support rods, rotating and fixed tower, both as individual elements and coupled together. Flutter and divergence were assessed for the blades, arms, and support rods. Potential mechanical instability and large resonance responses due to matching the vibratory and rotary frequencies were checked. Elastic transfer functions were derived and blade feathering studies were analyzed. Gust response and general or steady vibratory response were also evaluated. System plunging mode frequencies were determined. All results indicated that adequate design was achieved to account for these conditions.

9.1 VIBRATION ANALYSIS - Figure 90 shows current NASTRAN vibration results for the final design configuration, as displayed by CRT. These are the principal modes of interest, and generally show good agreement with the earlier hand calculation or component analysis.

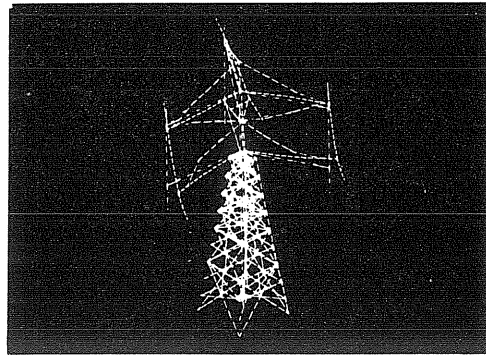
Figure 91 is a frequency diagram comparing the vibration modes of interest and their possible excitation due to rotational forcing functions. Note that the advancing and retreating branches of rotating tower bending intersect the 1P and 3P excitation lines above the operating frequency. This same behavior is shown for the support-arm lag-lead bending mode. This suggests smooth startup and shut-down with minimum vibration.

9.2 FLUTTER ANALYSIS - Figure 92 shows flutter boundaries for the blade, considering blade pitch and blade bending degrees of freedom. Six pivot axis locations are plotted. The prototype location is 22% of chord (PA/C = 0.220). The center of gravity for the prototype is 23.5% of chord (c.g./C = 0.235). The aerodynamic center (a.c./C) location of 25% was used.

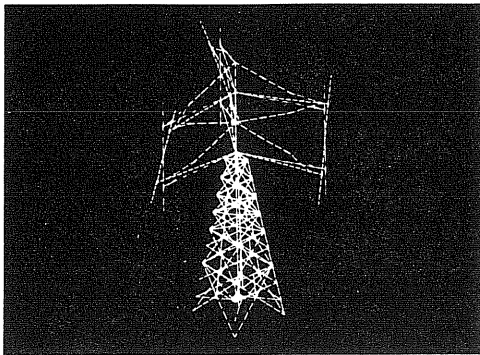
Figure 93 shows stiffness data from the blade actuation system through backup structure. These springs add in series of the form $1/K_T = 1/K_1 + 1/K_2$ etc. or $K_T = 129,000$ in.-lb/rad. The blade inertia, I_B , about the pivot axis is 2.99 slug-ft². Using these values of K_T and I_B produces a natural operating pitch frequency of 9.5 Hz. For this frequency the prototype blade flutter speed is well above the required value of 1.2 V_{max} .



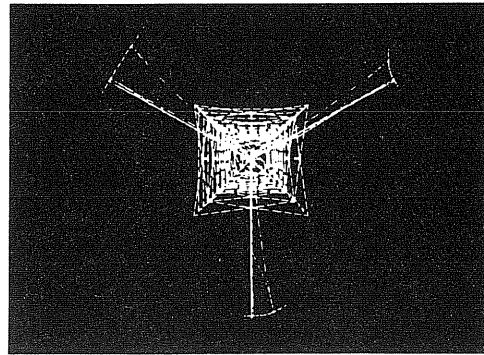
1.36 Hz
 PINNED-PINNED BENDING OF THE
 ROTATING TOWER ABOUT THE
 UPPER AND LOWER BEARINGS



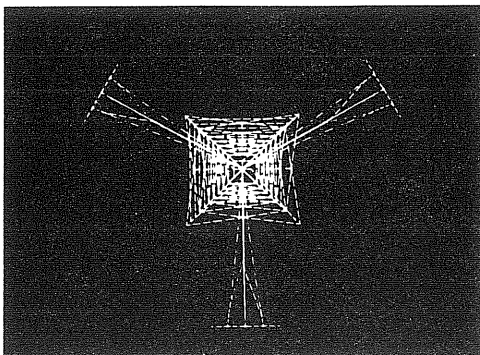
4.26 Hz
 FIXED TOWER BENDING



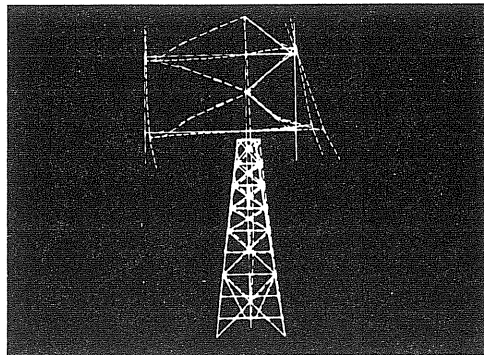
2.81 Hz
 ROTATING TOWER TORSION WITH
 A NODE ABOUT MID-SPAN OF THE
 UPPER AND LOWER SUPPORT ARMS



4.26 Hz
 PLAN VIEW



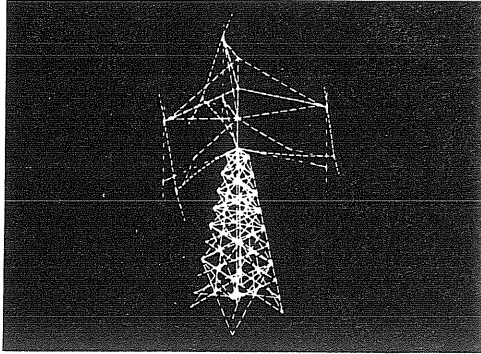
2.81 Hz
 PLAN VIEW



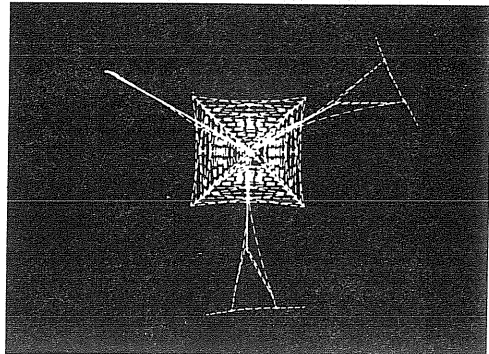
4.26 Hz
 SIDE VIEW

GP79-0636-39

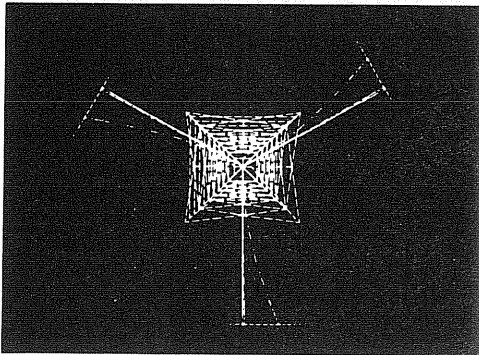
FIGURE 90
 VIBRATION FREQUENCIES AND MODE SHAPES



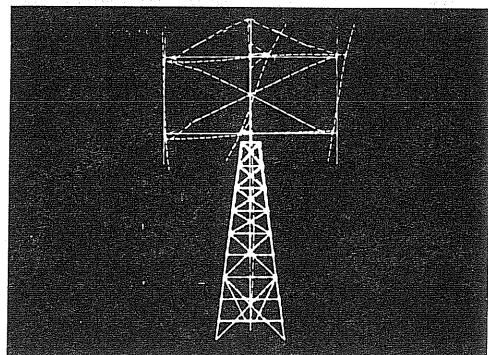
4.77 Hz
 ROTATING TOWER TORSION
 COUPLED WITH LOWER SUPPORT
 ARMS IN-PLANE BENDING



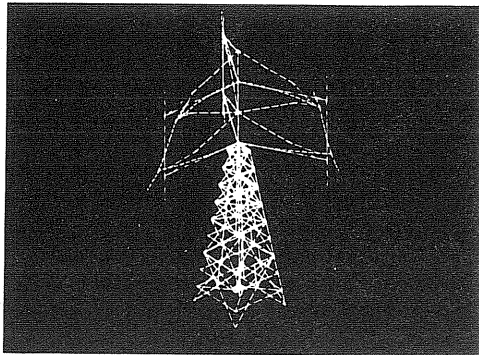
5.03 Hz
 PLAN VIEW



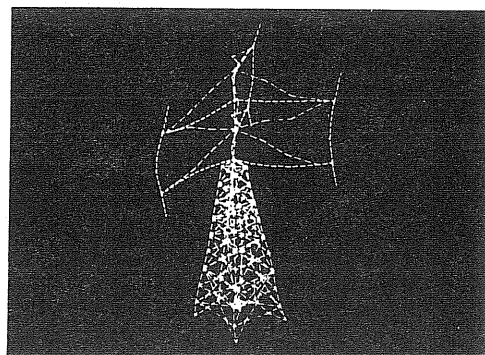
4.77 Hz
 PLAN VIEW



5.03 Hz
 FRONT VIEW



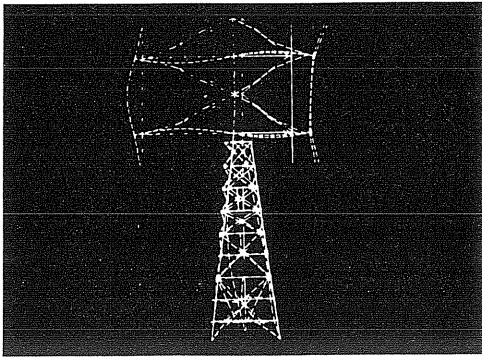
5.03 Hz
 SUPPORT ARMS
 IN-PLANE BENDING



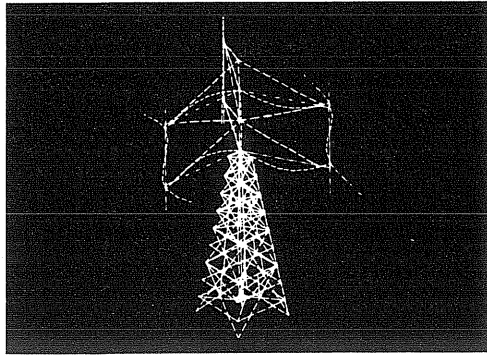
5.71 Hz
 FIXED TOWER BENDING COUPLED
 WITH ROTATING TOWER SUPPORT
 ARMS, AND BLADE BENDING

GP79-0636-40

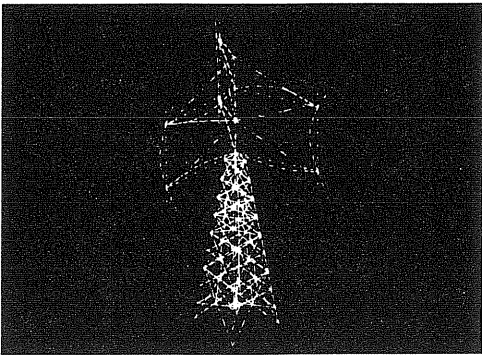
FIGURE 90 (Continued)
 VIBRATION FREQUENCIES AND MODE SHAPES



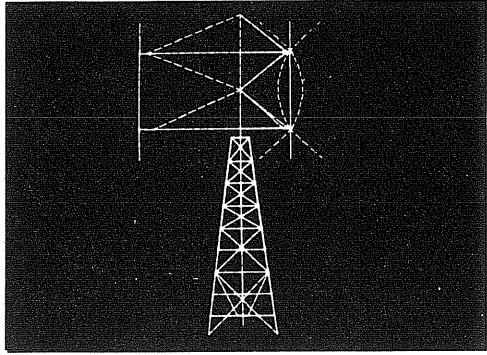
5.71 Hz
SIDE VIEW



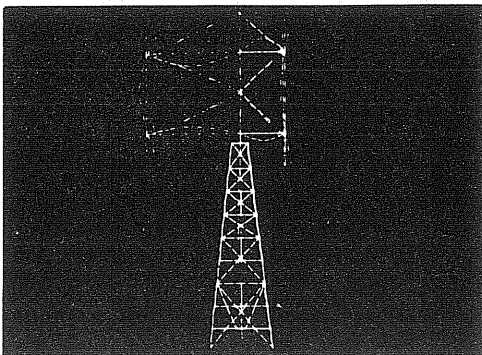
7.35 Hz
UPPER AND LOWER SUPPORT
ARMS ANTI-SYMMETRIC
FLAT-WISE BENDING



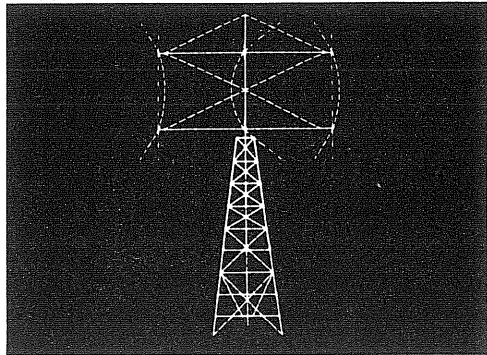
6.1 Hz
UPPER AND LOWER SUPPORT ARMS
SYMMETRIC FLAT-WISE BENDING
COUPLED WITH BLADE FLAP BENDING



11 Hz
BLADE CHORD-WISE BENDING



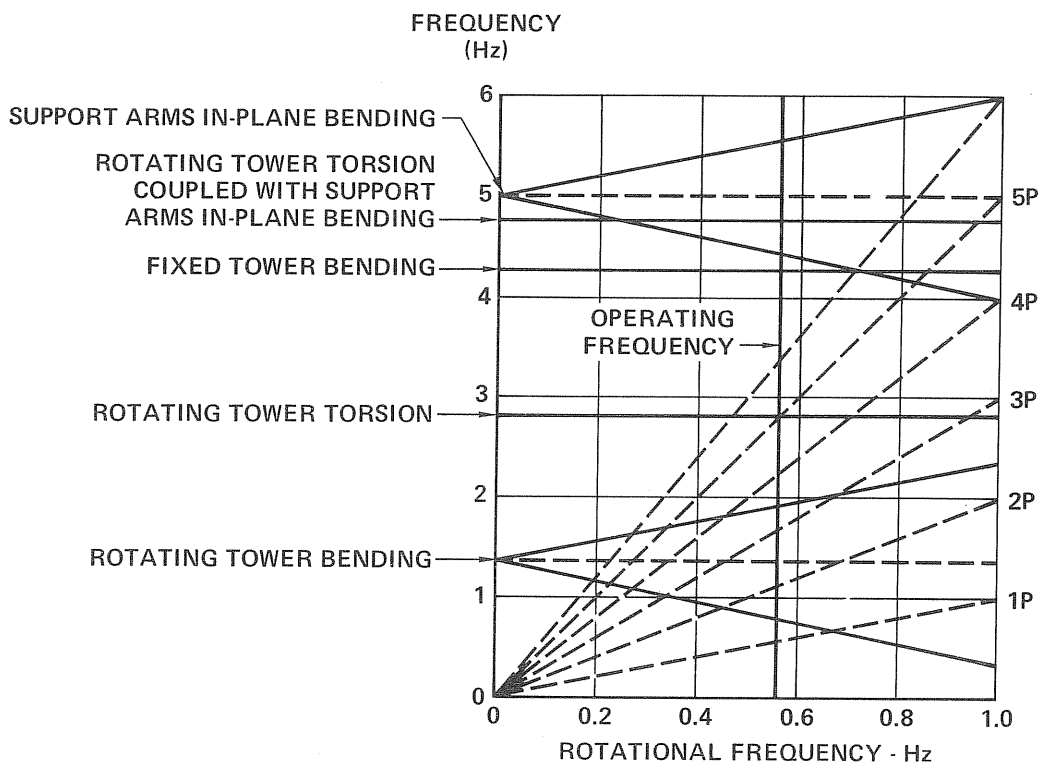
6.1 Hz
SIDE VIEW



11 Hz
FRONT VIEW

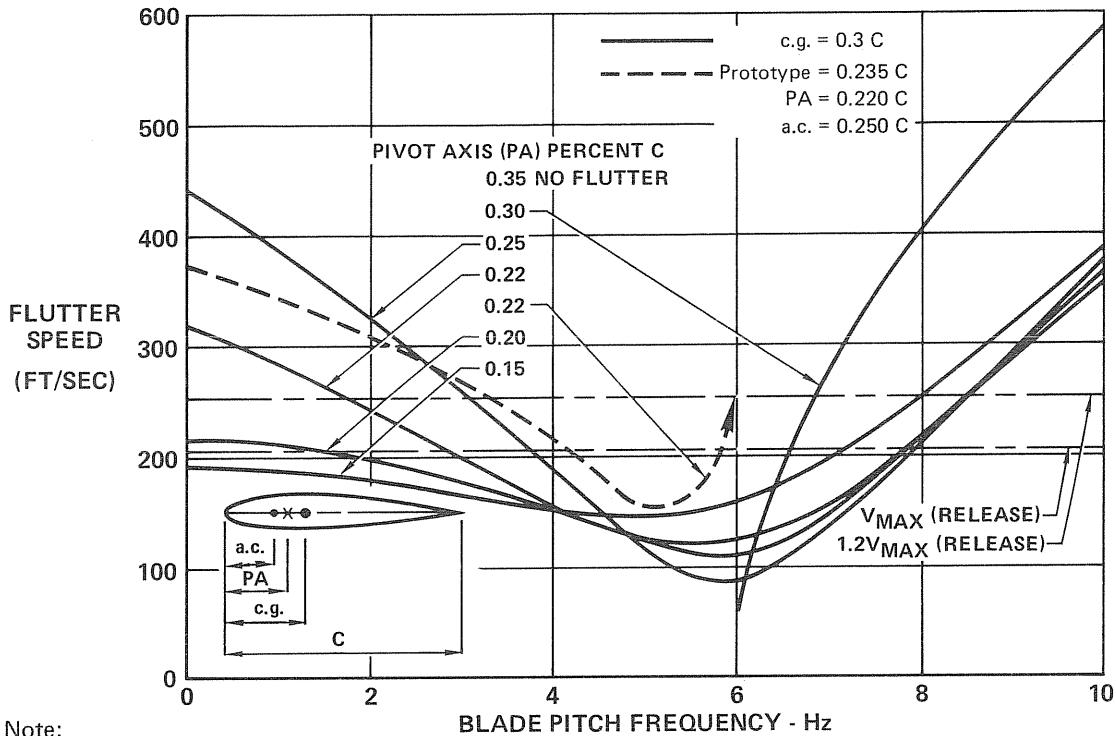
GP79-0636-41

FIGURE 90 (Continued)
VIBRATION FREQUENCIES AND MODE SHAPES



GP79-0636-31

FIGURE 91
STRUCTURAL FREQUENCIES vs ROTATION
 Fixed Coordinate System



Note:
For second bending-pitch and second bending-twist
no flutter in the operating speed range.

GP79-0636-136

FIGURE 92
TYPICAL BENDING PITCH BLADE FLUTTER BOUNDARIES

ITEM	HINGE MOMENT STIFFNESS (IN.-LB/RAD)	DEFLECTION (RAD/IN.-LB)
DRIVE BELT	300,000	3.33×10^{-6}
SPROCKETS	5,000,000	0.20×10^{-6}
ACTUATOR	264,000	3.79×10^{-6}
BACKUP STRUCTURE	2,350,000	0.426×10^{-6}
TOTAL K_T	129,000	7.75×10^{-6}

$$\omega = \sqrt{\frac{K_T}{I_B}} = \sqrt{\frac{129,000}{2.99 (12)}} = 59.96 \frac{\text{RAD}}{\text{SEC}} = 9.5 \text{ Hz}$$

GP79-0636-137

FIGURE 93
BLADE HINGE MOMENT STIFFNESS

10. CONTROL SYSTEM DESIGN

The control system design must provide for (1) start up when favorable wind conditions exist, (2) proper blade modulation to maintain operating RPM and power output within allowable tolerances, (3) shutdown in high wind, and (4) shutdown when abnormal operating conditions occur. The microprocessor controller gives a complete stand alone capability.

The control system is identical for 3 of the 4 electrical output designs (See Figure 18 Designs 1, 2, & 3) and the mechanical output system. It requires only minor additions to adapt for the mini-grid system (Design 4) and provisions have been incorporated in the design.

A proportional-plus-integral feedback on generator RPM, summed with a measured blade speed command, is used for RPM control in the gusty wind conditions expected. The rock angle commands generated by the controller are transmitted to individual electrical blade actuators, which set the blade angles. Each actuator consists of an electrical motor, power amplifier, and gear box.

10.1 CONTROL SYSTEM ANALYSES - Two major analysis efforts were undertaken. One studied the closed loop response of the entire Giromill system (controller, actuators, rotor, and generator). The other concentrated on defining the actuator response characteristics. Both of these studies started with a simplified analysis and gradually increased in sophistication as knowledge was acquired on the system operation.

10.1.1 Linearized Steady State Control Analyses - This first study was undertaken to get an early evaluation of the control response characteristics that would be required. It consisted of a simplified steady state analysis of the blade and actuator, the rotor system, control unit, and generator. A simplified representation of the system was studied as shown in Figure 94, and a mathematical block diagram is shown in Figure 95. The symbol nomenclature is defined in Figure 96.

The analysis assumed that a phase angle of 240° was representative of the average rotor conditions. This established K_α , $K_{T\alpha}$, and K_{BD} in terms of the aerodynamic characteristics at that point. Root locus, frequency, and time responses to variations of the parameters shown in Figure 95 were used to evaluate the system. Typical results from this linear analysis are shown in Figures 97 through 99.

Figure 97 shows a root locus plot (low frequency) on the controller gain $K_{\theta R}$. For this case, only a proportional feedback control being employed, i.e., $K_I=0$. The system exhibits a typical root locus, showing that as the gain is increased the system will damp oscillations caused by the rotating tower.

The square symbols indicate the gain value used in the frequency and time plots shown in Figures 98 and 99. This high gain effectively damped the rotating tower oscillations.

ACTUATOR

- K_A - MOTOR GAIN
- L_a - MOTOR INDUCTANCE
- R_o - MOTOR RESISTANCE
- K_b - MOTOR BACK EMF GAIN
- J - LOAD PLUS MOTOR INERTIA
- f - MOTOR FRICTION
- N_A - ACTUATOR GEAR RATIO
- G_{ev} - ACTUATOR GAIN
- T_c - COMPENSATION TIME CONSTANT

BLADE

- $K_{T\alpha}$ - ROCK ANGLE TO BLADE LOAD CONVERSION CONSTANT
- K_{BD} - BLADE DAMPING CONSTANT

ROTOR

- K_α - BLADE LOAD TO ROTOR TORQUE CONVERSION CONSTANT
- I_R - ROTOR INERTIA
- K_{RD} - ROTATING TOWER DAMPING CONSTANT
- K_{RS} - ROTATING TOWER SPRING CONSTANT
- N - ROTOR GEAR RATIO

CONTROL UNIT

- $K_{\theta R}$ - CONTROLLER GAIN
- K_I - CONTROLLER INTEGRAL GAIN
- τ_c - CONTROLLER TIME DELAY

GENERATOR

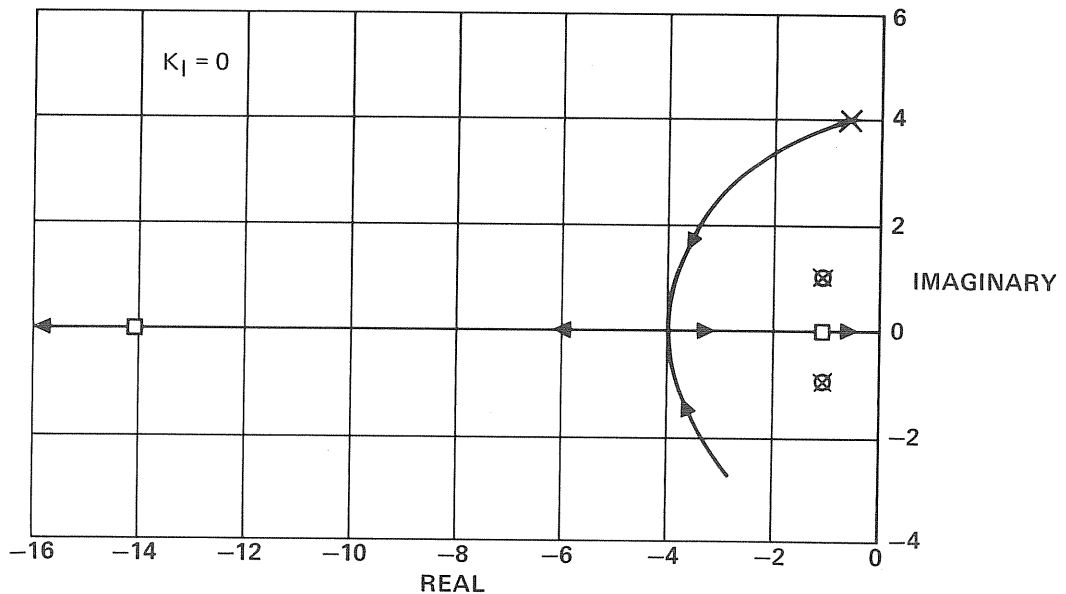
- I_g - GENERATOR GEAR BOX INERTIA
- K_g - GENERATOR OUTPUT GAIN
- ω_g - NOMINAL GENERATOR RATE

GENERAL

- θ_c - COMMANDED ROCK ANGLE
- θ_R - ACTUAL ROCK ANGLE
- θ_e - ROCK ANGLE ERROR
- θ_m - MOTOR ANGLE
- $\dot{\psi}$ - ROTOR ANGLE RATE
- $\dot{\psi}_g$ - GENERATOR RATE
- S - LaPLACE OPERATOR

GP79-0636-34

FIGURE 96
STEADY STATE LINEAR SYSTEM
Nomenclature



GP79-0636-36

FIGURE 97
STEADY STATE LINEARIZED CONTROL ROOT LOCUS ON $K_{\theta R}$

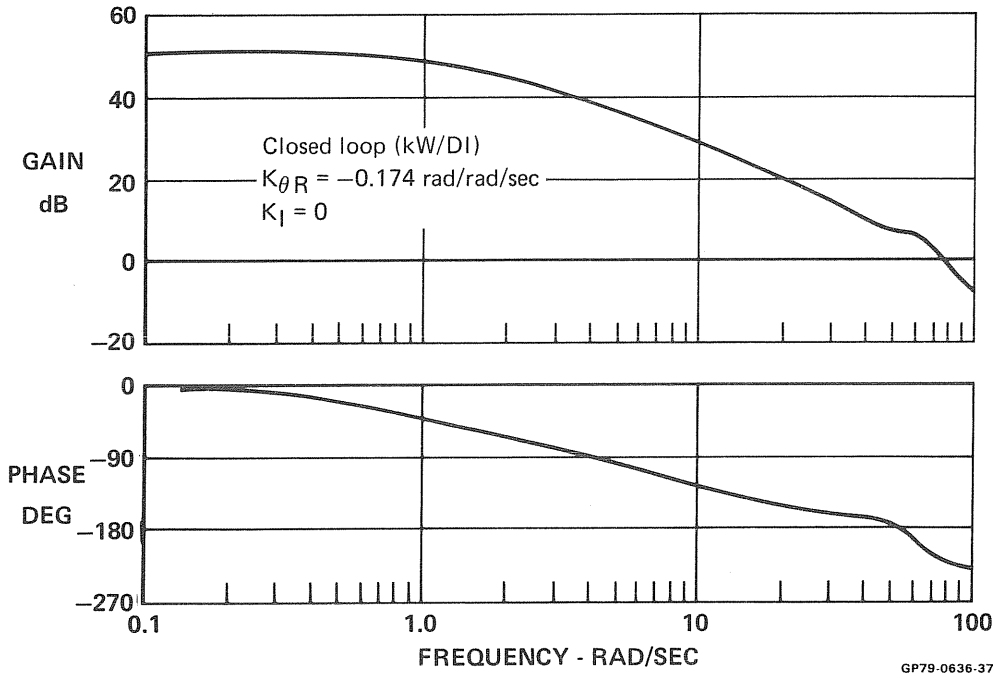


FIGURE 98
STEADY STATE LINEARIZED CONTROL FREQUENCY CHARACTERISTICS

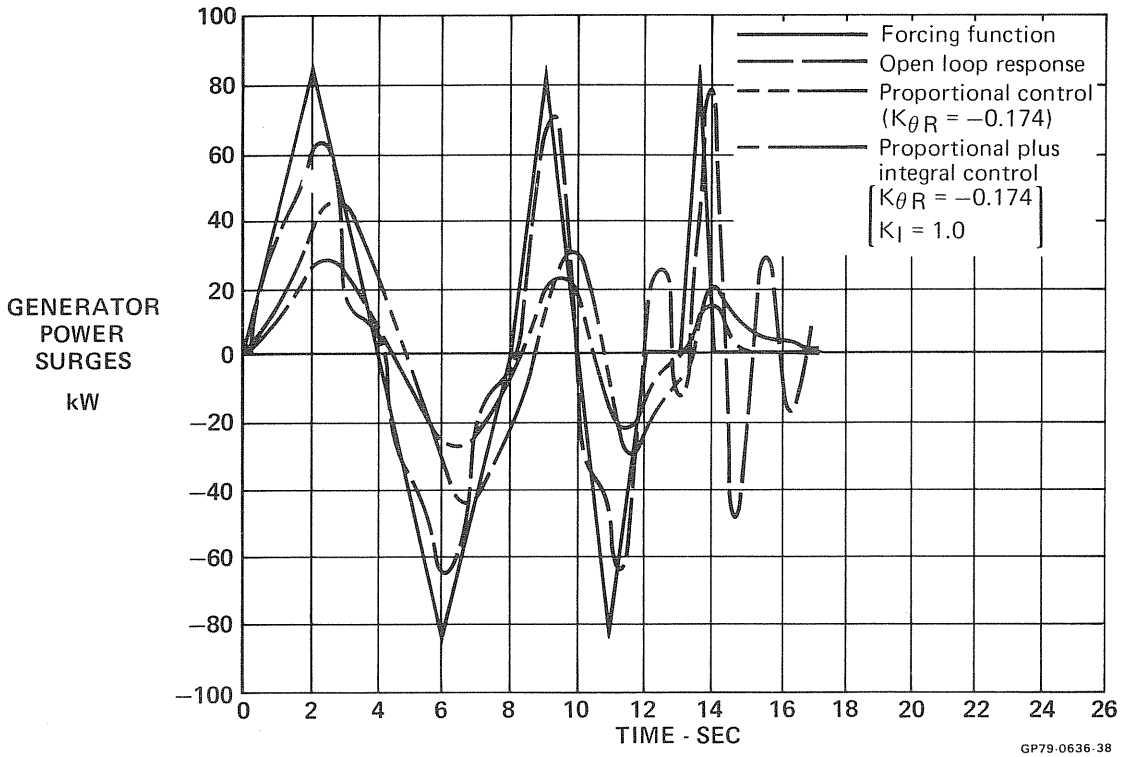


FIGURE 99
STEADY STATE LINEARIZED CONTROL TIME RESPONSES

There was another root locus loop (not shown) having a frequency in the neighborhood of 65 radians per second, which represented the actuator motor characteristics.

Figure 98 shows the closed loop frequency response of the system with the gain value $K_{\theta R}$ represented by the square symbols in Figure 97. The response is power output to disturbance angle of attack (k^W/DI). Again, a typical system frequency response is evident.

Figure 99 shows the time response to an arbitrary saw-tooth type of forcing function. The amplitude of the forcing function was such that it could cause power surges over twice the nominal operating power. Three frequencies were simulated: 1/8, 1/4, and 1/2 cycles per second.

Three responses are plotted: (1) the open loop response, (2) proportional control only, and (3) proportional plus integral control. The open loop response shows that power surges can occur which are almost equal to the amplitude of the forcing function. It also shows that the rotating tower torsional frequency, estimated at that time at 0.6 Hz, was excited and caused several cycles of ringing. Closing the loop through a proportional controller reduced the power surges considerably and prevented the ringing. Adding an integral feedback loop further reduced the power surges, to a manageable level.

Studies using this system representation were done to gain an insight of the system characteristics, support various trade studies, and establish boundaries of various parameters to be looked at using the more complex CSMP simulation covered in the next section. This study, as simple as it was, served its purpose very well. It gave an overall view of the entire system, and being linear, was adaptable to standard analysis techniques.

10.1.2 Dynamic Analysis - It was felt that an accurate simulation of the entire operating Giromill system was required. This is a new system, embodying an innovative control scheme, and confidence was needed that it would work. The Continuous System Modeling Program (CSMP) was employed (Reference 12).

Figure 100 shows a block diagram of the simulation. For explanation purposes the simulation has been divided into six sections. The explanation is for one blade. In the actual simulation three blades were used.

The actuator section is shown outlined in Figure 101. This is a simplified representation that checked well against a full non-linear simulation completed by MDEC-GR (See Section 10.1.4). The rock angle profiles commanded by the controller are discrete values, commanded every 12.8 ms. This creates a step profile which is difficult for the actuator to follow. The profile is therefore filtered (smooth) by a lag circuit $\frac{1}{\tau_{e3}s+1}$. This lag circuit requires that the rock angle commands in the controller be offset an angular amount corresponding to the time constant τ_{e3} . The smooth rock angles (θ_{RC}) are compared to the actual

θ_R , and then rock angle error (θ_e) turns the motor through the gain G_{ev} and the stabilizing network $\frac{\tau_{e1} S+1}{\tau_{e2} S+1}$.

The limiting values, designated SP31 and SP41, simulate the current limiting function of the power amplifier. The motor is represented by an inductance, resistance, and gain along with the back EMF. The limits SP1 and SP2 represent motor torque limits. The switch which cuts off the motor torque simulates the blades being released to weathervane.

The motor windage and friction, along with the blade moment components, are then summed with the motor torque. The resultant torque then acts on the motor and load inertial $JM + \frac{JL}{NA^2}$ to get the motor acceleration, which is integrated to get motor rate. Integrating again gives motor position, and by relating through the actuator gear ratio (NA), the blade rock angle is obtained.

The blade moment components are outlined in Figure 102, and the equations are given in Figure 103. The C_l and C_d values were presented in Figures 34 and 35 as a function of α_e . The section that simulates the airflow induced effects and calculates the rotor torque is outlined in Figure 104. The governing equations are shown in Figure 105. The induced effects equations (α_i) are empirically derived relations.

The rotor dynamics section is outlined in Figure 106. This is a standard representation of a torsional spring/inertia system that has a spring constant K_{RS} , and damping constant K_{RD} .

The generator section is outlined in Figure 107. This also includes the RPM sensor simulation. The resulting rotor torque, as calculated from the tower dynamics section, is subtracted from the generator output torque and acts on the speed increaser and generator inertia. The resulting acceleration is integrated and multiplied by the speed increaser gear ratio to give generator rate. The generator rate is related to the generator output by the gain, K_g . Note that the generator is not connected until the rotor reaches 32.92 RPM, which is 1800 RPM at the generator.

Rotor rate is also related to the RPM sensor output period by counting 128 teeth of a 162 tooth gear connected to the high speed side of the speed increaser. This period, which is 58.2 ms at the nominal rotor rate, is used as the input time to the controller. This means that the controller updates the RPM period approximately every 58.2 ms. The CSMP simulated this by quantizing this period similar to the quantizing of the rock angle profiles.

The control system provides for a constant RPM under varying load and wind conditions. The control unit simulation section is outlined in Figure 108. The RPM period, T , is the primary feedback loop. The controller computes a change in the value of λ_f that will correct for any

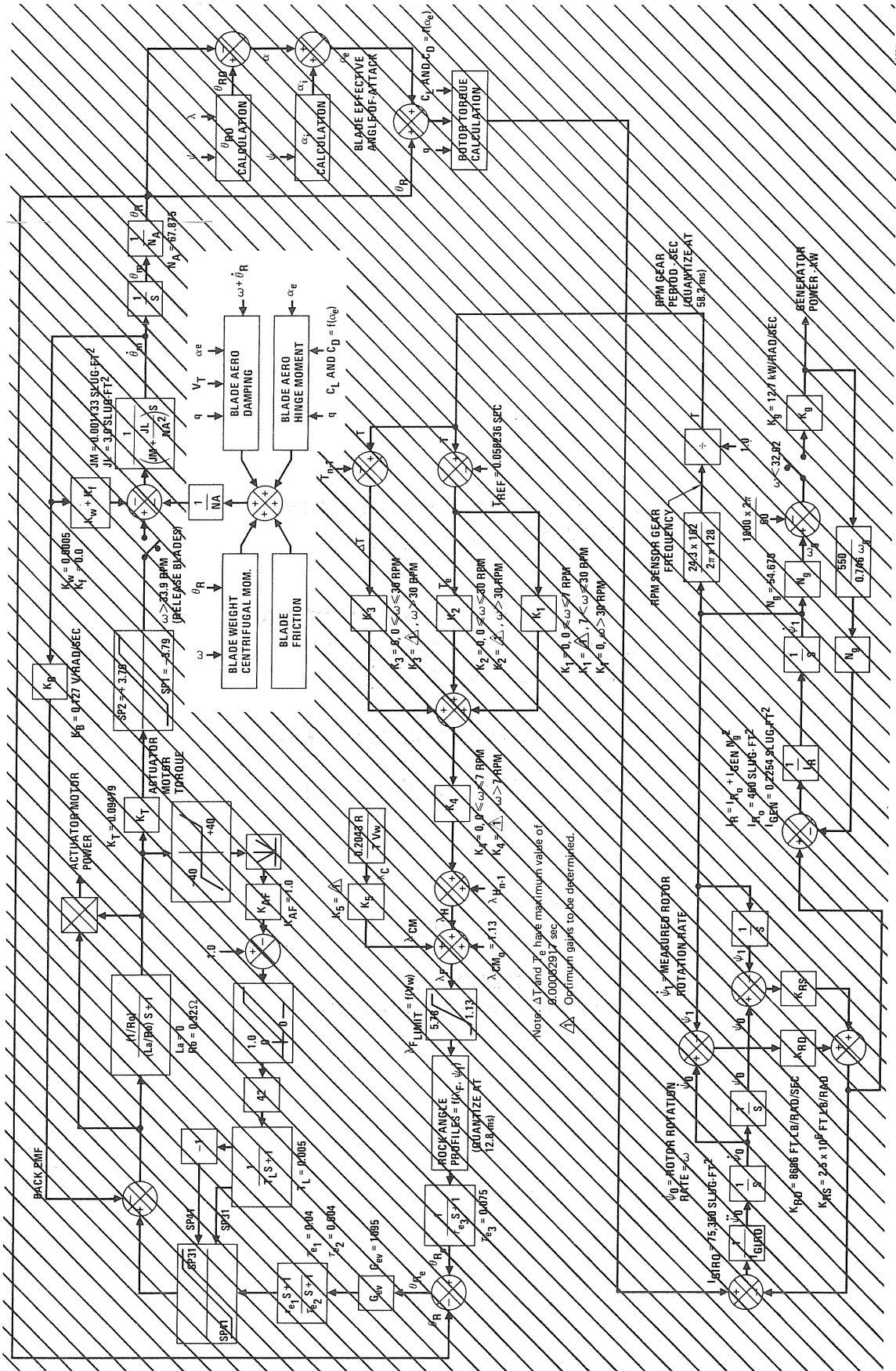


FIGURE 102 GIROMILL CONTROL SYSTEM CSMP SIMULATION - BLADE MOMENT COMPONENTS

1. BLADE WEIGHT CENTRIFUGAL MOMENT

$$= - \frac{\text{BLADE WT}}{g} \times \omega^2 R \times X_{cg} \cos \theta_R$$

2. BLADE AERODYNAMIC DAMPING MOMENT

$$= \frac{qS\bar{c}^2}{2V_T} \left[-C_{mq} + C_{Lq} \left(\frac{X_{cp}}{\bar{c}} \cos \alpha_e \right) \right]$$

3. BLADE AERODYNAMIC HINGE MOMENT

$$= qS\bar{c} \left[-\frac{X_{cp}}{\bar{c}} \left(C_D \sin \alpha_e + C_L \cos \alpha_e \right) \right]$$

4. BLADE FRICTION

$$= \text{FRICTION FORCE} \left(\frac{\dot{\theta}_R}{|\dot{\theta}_R|} \right)$$

GP79-0636-52

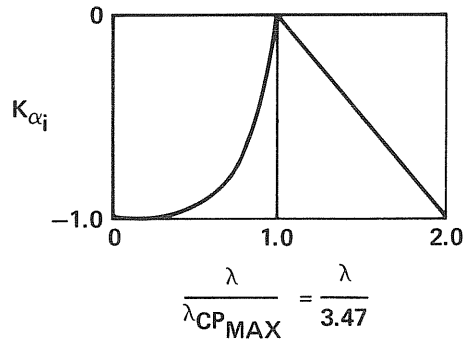
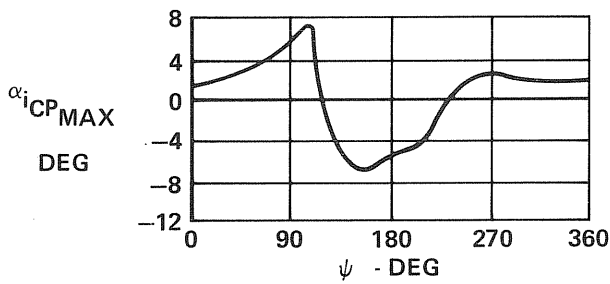
**FIGURE 103
BLADE MOMENT EQUATIONS**

1. BLADE ROCK ANGLE FOR ZERO ANGLE-OF-ATTACK,

$$\theta_{R_0} = -\text{TAN}^{-1}\left(\frac{\text{COS } \psi}{\lambda - \text{SIN } \psi}\right)$$

2. INDUCED ANGLE-OF-ATTACK

$$\alpha_i = \alpha_{i\text{CPMAX}} [1 + K_{\alpha_i}]$$



3. ROTOR TORQUE

$$= qSR [C_l \text{ SIN } (\theta_R + \alpha_e) - C_d \text{ COS } (\theta_R + \alpha_e)]$$

SUM ALL THREE BLADES

GP79-0636-54

FIGURE 105
INDUCED AIRFLOW AND ROTOR TORQUE EQUATIONS

RPM error. λ_F is the specific rock angle profile (sometimes referred to as cam λ_F) that is command by the controller. The rock angle profiles stored in the microprocessor are shown in Figure 140 in Section 10.2. The controller interpolates between the values stored in the microprocessor to define the blade rock angle as a function of blade phase angle, ψ .

Five controller gains, K_1 through K_5 , are employed. Gain K_1 is used only for start up. It is an integral gain constant that slowly brings the Giromill up to a speed of 30 RPM. Note, that up to 7 RPM, only cam $\lambda_F = 1.13$ is used, K_1 starting to integrate to higher λ_F cams after that point.

Gains K_2 and K_3 are the integral and proportional gains normally controlling the Giromill. They take over from the start up gain K_1 when 30 RPM is reached. Gain K_4 is a general gain that multilplies K_1 , K_2 and K_3 .

Gain K_5 relates the measured blade speed ratio command value to be summed with the RPM feedback value. This feature was added to provide versatility to the controller and it appeared to provide for a faster response due to a wind gust.

The actual values for the gains is still being determined. The implementation of the gain values in the controller is such that they can be easily changed during the test.

Figure 109 provides other auxiliary equations.

Figure 110 shows how well the CSMP was simulating the normal blade load. The more rounded blade load produced by the CSMP simulation is due to the smoothing of the blade rock angles from that used in the performance program. This smoothing was done to reduce actuator reversing cycles. The CSMP yielded a good representation of the loads, which gave confidence to the entire simulation.

One of the features investigated was the maximum blade loads expected with wind gusts. A windmill is a dynamic system that responds to wind gusts. Design of the blades should be based on the dynamic loads. Since dynamic loads were not available when we started this program, we assumed that blade loads would be based on a static gust factor of 1.3 (see Section 3.2.1 and 5.4). This assumption was checked using CSMP.

Figure 111 shows the blade normal force for various steady state winds. Note that as the wind velocity is increased, the blade normal force is decreased. The reason is that the Giromill has a constant power output for winds over 20 MPH. Therefore, the tangential blade component is constant. Since the rock angles are greater as the wind increases, the blade normal force decreases. This is shown in Figure 112. Maximum blade loads occur in a 20 MPH wind.

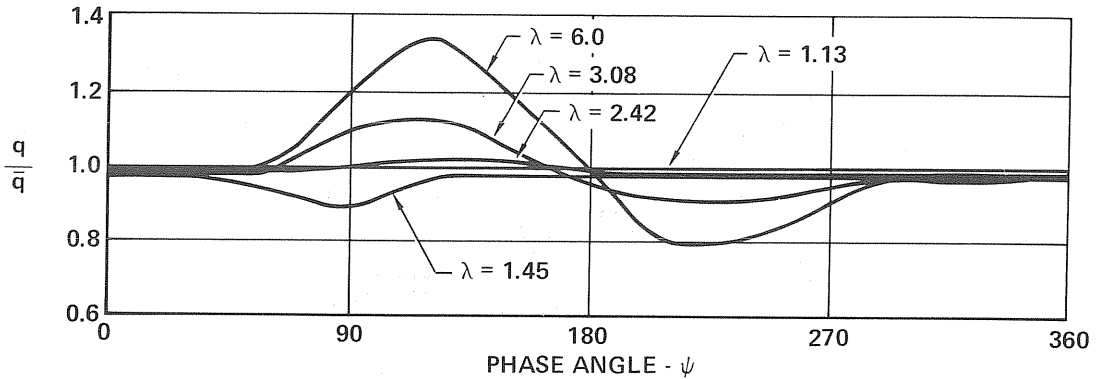
To get an estimate of expected blade loads in a severe gust, the gust rise time criteria of Reference 13 was used. In a 30 MPH wind, a gust of

1. BLADE DYNAMIC PRESSURE (q)

$$\bar{q} = \frac{\rho}{2} [(R\omega - V_w \sin \psi)^2 + (V_w \cos \psi)^2]$$

THEN

$$\bar{q} = \frac{q}{\bar{q}} \bar{q} \text{ WHERE } \frac{q}{\bar{q}} = f(\lambda, \psi)$$



2. BLADE VELOCITY (V_T)

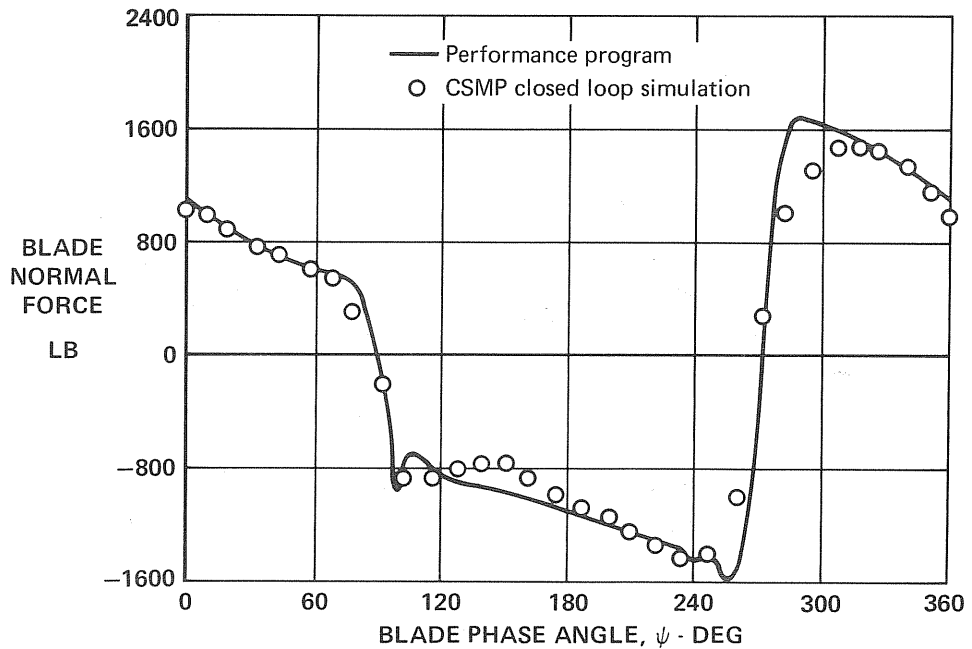
$$V_T = \sqrt{\frac{2\bar{q}}{\rho}}$$

3. BLADE SPEED RATIO (λ)

$$\lambda = \frac{\omega R}{V_w}$$

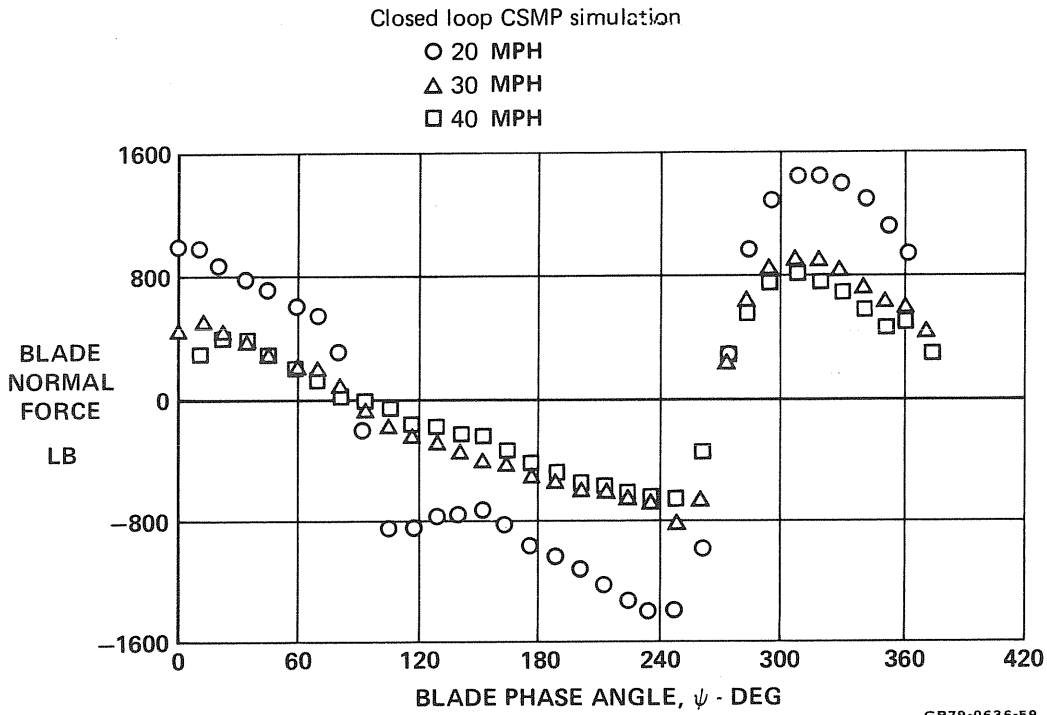
GP79-0636-53

FIGURE 109
AUXILLARY EQUATIONS CALCULATIONS



GP79-0636-60

FIGURE 110
20 MPH WIND BLADE AIRLOAD



**FIGURE 111
BLADE AIRLOADS**

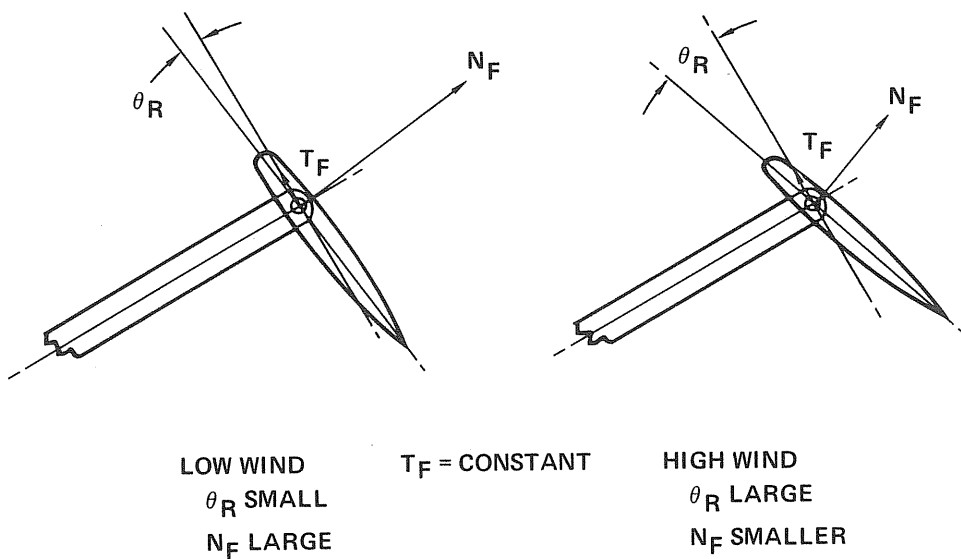


**FIGURE 112
BLADE FORCE RELATIONSHIP AT CONSTANT POWER**

14.5 MPH with 1/2 second rise time has less than 0.005 probability of occurrence. This gust value results in the blade loads shown in Figure 113.

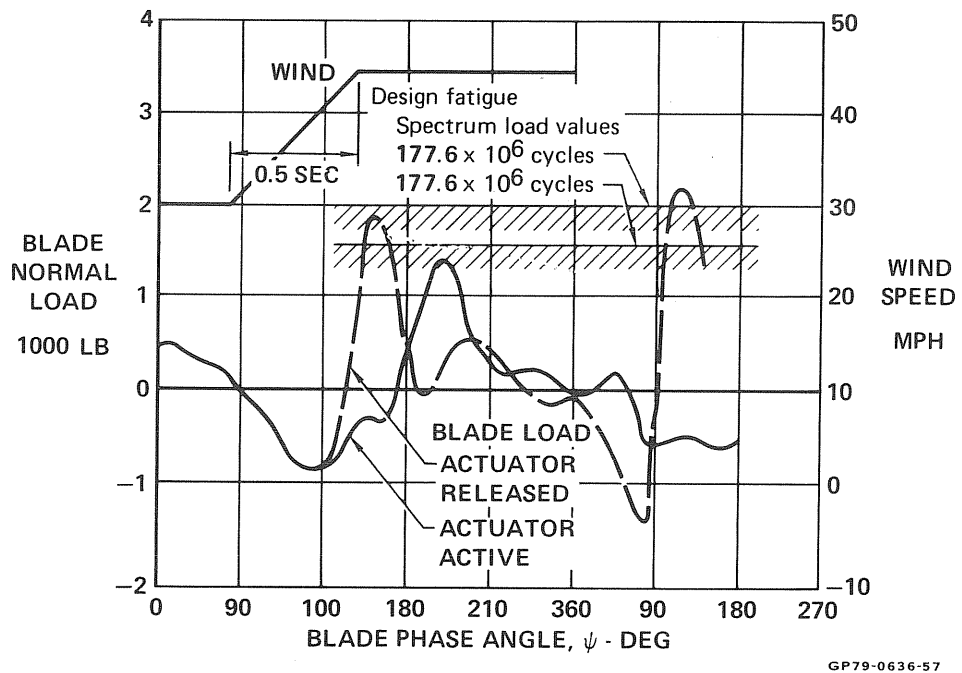


FIGURE 113
BLADE LOADS DUE TO SEVERE GUST

The solid line shows the blade loads with the actuator active through the gust. The maximum load does not reach the lowest fatigue spectrum load value taken from Figure 60. However, a wind gust of this magnitude causes a generator power surge to 75 kW. Assuming that this is higher than desired the controller would command the blades to be released into a weathervane mode.

The dashed line shows the blade loads due to releasing the actuator. There is a significant overshoot in blade angle of attack. However, the airloads are only slightly greater than the second fatigue spectrum load. With the blades weathervaning the rotor RPM decreases rapidly, being less than 30 at the end of the plotted values in Figure 113.

Many of the analyses used a wind gust profile for evaluating the system. Two profiles used are shown in Figures 114 and 117, both followed by some plotted analysis results. A below rated power wind gust (Figure 114) refers to a wind gust that does not exceed the maximum cut-off wind speed, for our case 40 MPH (58.7 ft/sec). The above rated power wind gust exceeds this value. These gusts were extracted from Reference 14.

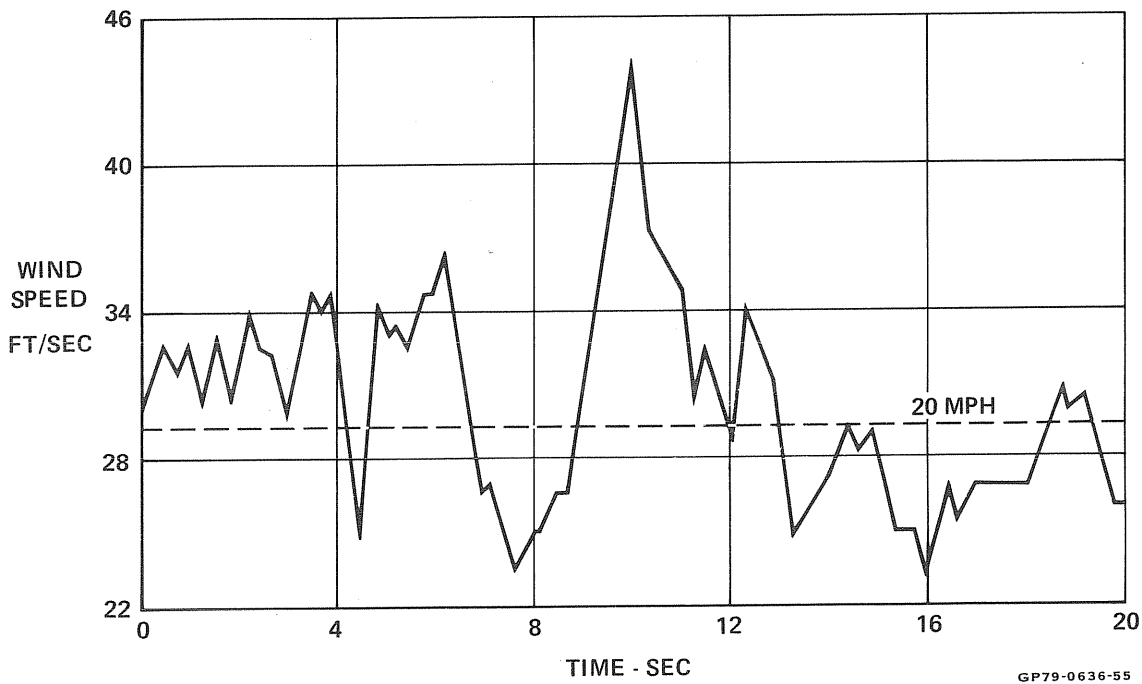


FIGURE 114
BELOW RATED POWER WIND GUST

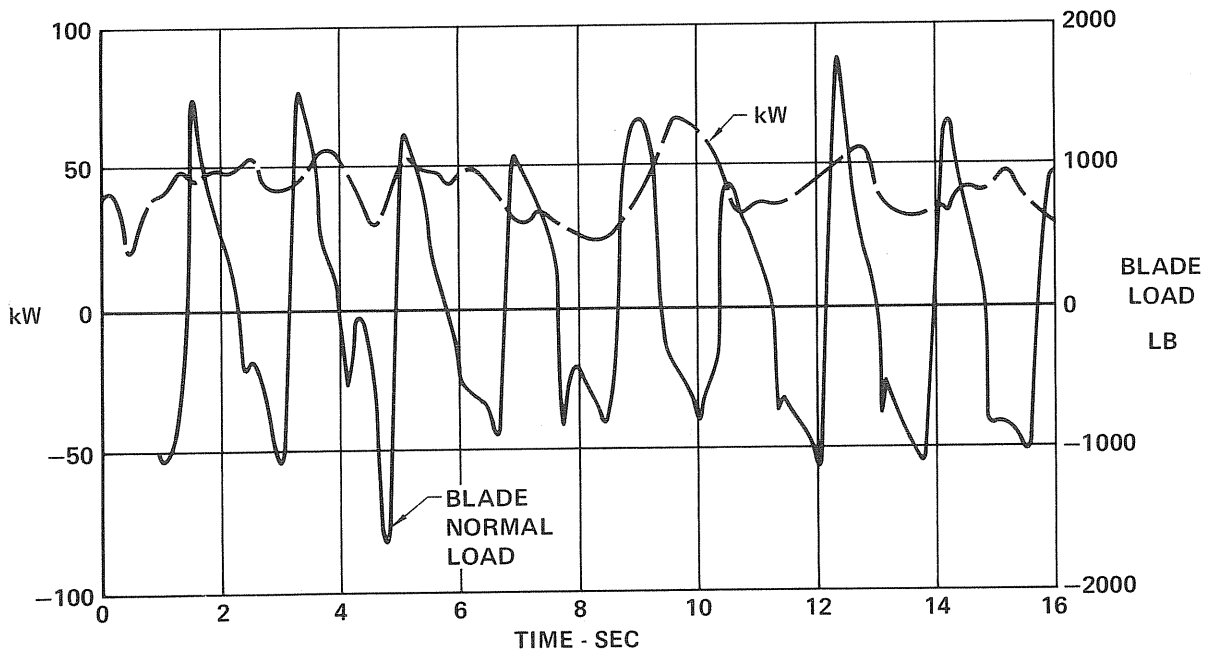
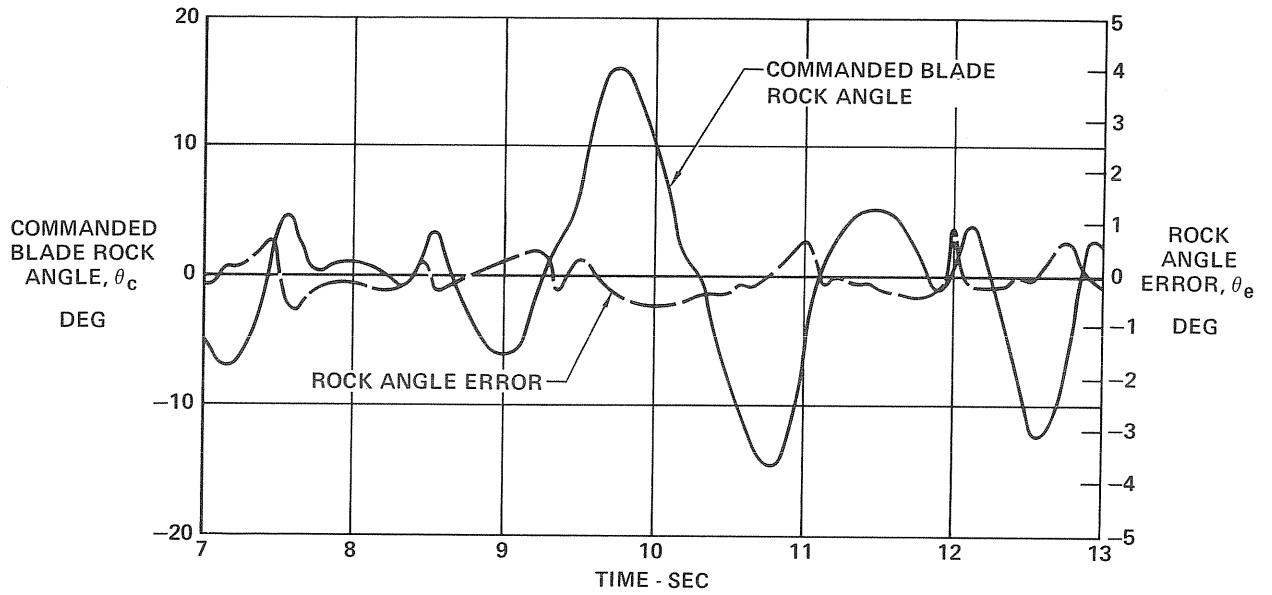
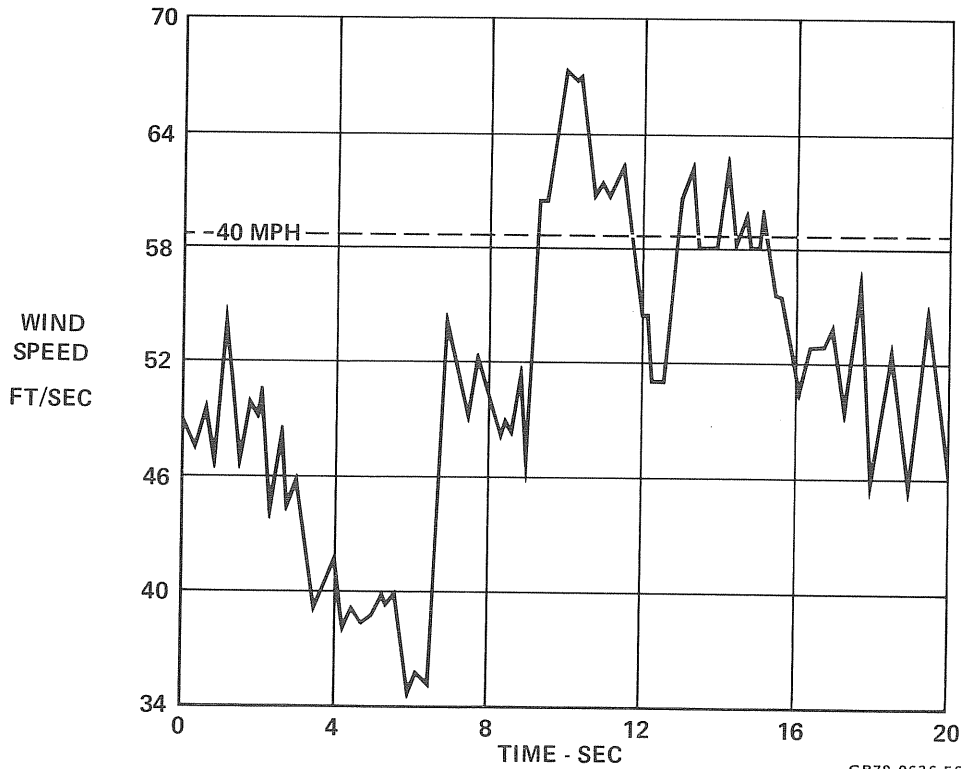


FIGURE 115
BLADE 1 NORMAL LOAD AND SYSTEM POWER
Below Rated Power Wind Gust



GP79-0636-62

FIGURE 116
BLADE 1 ROCK ANGLE AND ROCK ANGLE ERROR
 Below Rated Power Wind Gust



GP79-0636-56

FIGURE 117
ABOVE RATED POWER WIND GUST

Figure 115 shows the power variation and blade 1 normal load. Note that the maximum power output corresponds to the high wind gust (approximately at 10 sec), but the maximum blade load does not. Blade load and gust magnitude are not highly correlated. The same can be said of blade angle of attack, as shown in Figure 118. The largest α_e does not necessarily occur at the time of maximum gust.

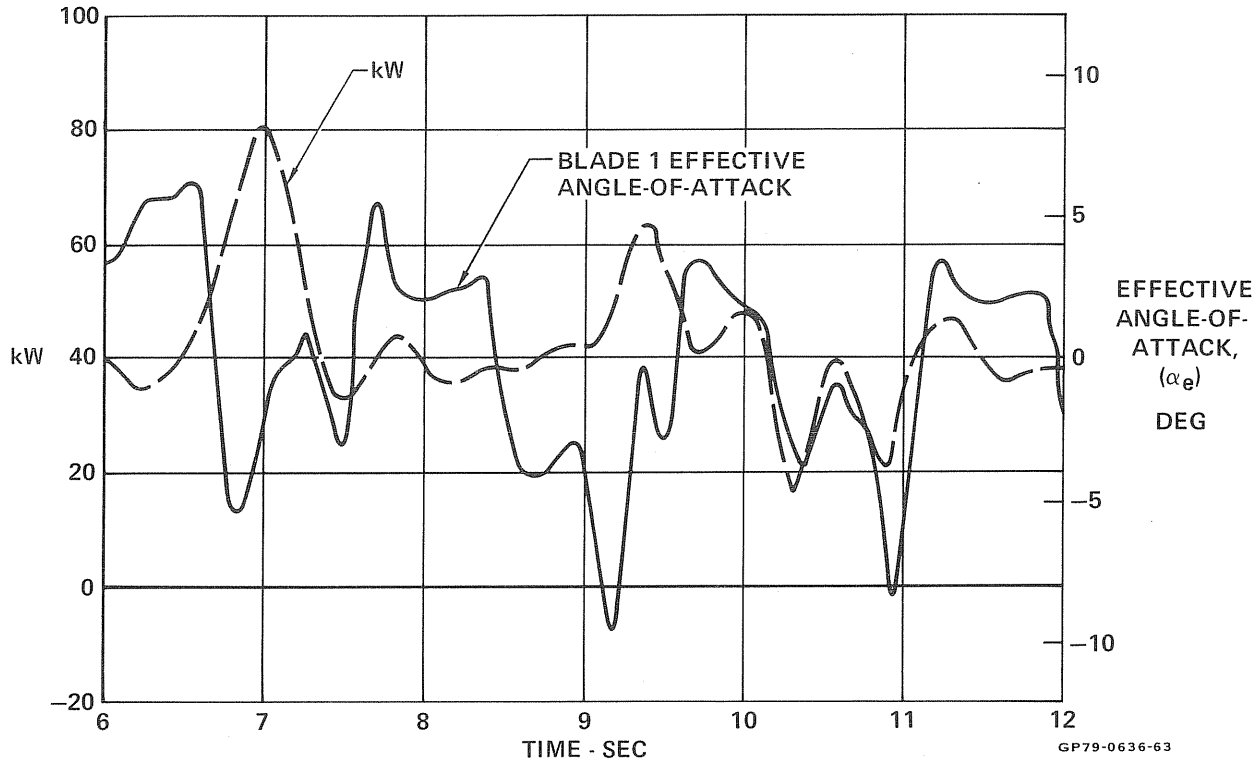


FIGURE 118
BLADE 1 ANGLE-OF-ATTACK AND SYSTEM POWER
 Above Rated Wind Gust

Figures 116 and 119 show the rock angle profiles and rock angle error (difference between commanded and actual) for the two wind gusts. The error is small for the low wind speed but increases at higher winds. This is because the rock angle increases as the wind increases, and the actuator has more difficulty in following the profile. Figure 120 compares several other parameters of these two cases.

Start-up simulations were also completed. The RPM build up and commanded cam λ_F values are plotted in Figure 121 for a 12 and 20 MPH wind. Start-up is done by commanding cam $\lambda_F = 1.13$ until 7 RPM is reached. At this time an integral gain (K_I in Figure 100) is activated, which slowly integrates up the commanded λ_F values. At 30 RPM, control is switched to the normal operating system. This causes a slight discontinuity in the commanded λ_F values, as shown in the plots. No difficulty in starting was indicated.

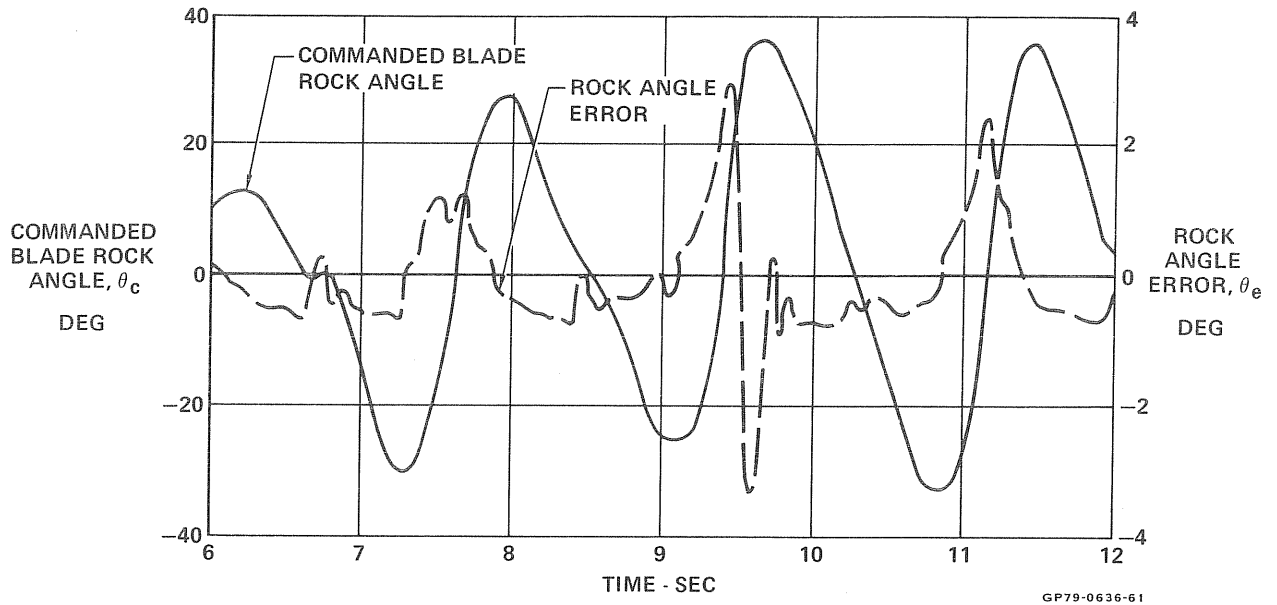
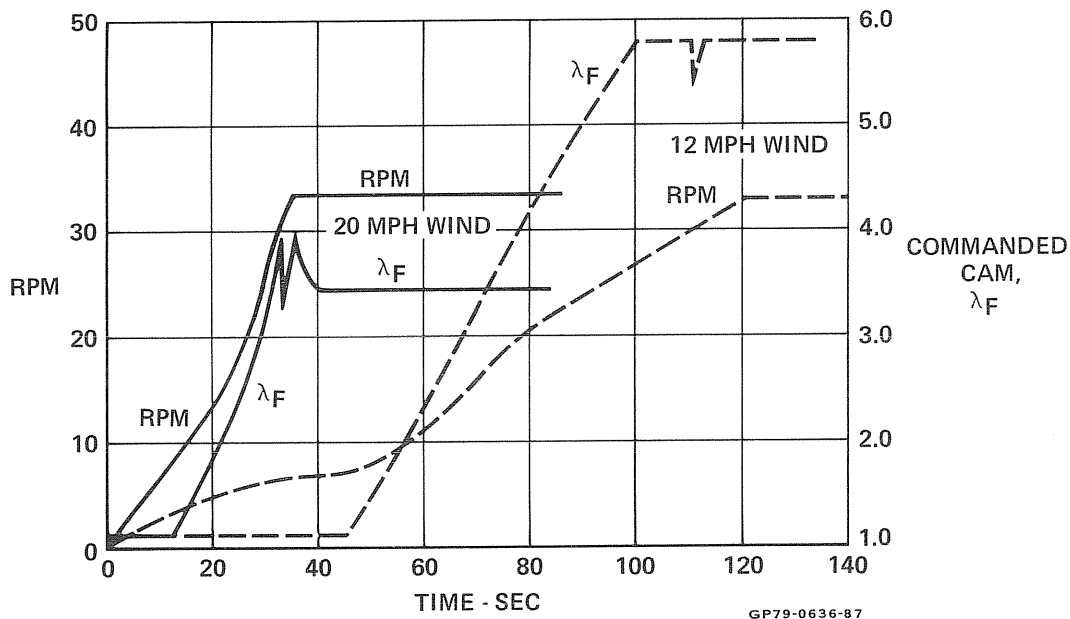


FIGURE 119
BLADE 1 ANGLE AND ROCK ANGLE ERROR
 Above Rated Power Wind Gust

		ABOVE RATED WIND GUST	BELOW RATED WIND GUST
MAX BLADE LOAD	(LB)	1333	1718
MAX KW OUTPUT		79	67
MAX BLADE ROCK ANGLE ERROR	(DEG)	3.3	1.0
AVERAGE ACTUATOR MOTOR POWER OVER 18 SEC	(WATTS)	90	74
MAX ROTOR ACCELERATION	(RAD/SEC ²)	0.356	0.139
MAX BLADE ANGLE-OF-ATTACK	(DEG)	11.8	14.3

GP79-0636-76

FIGURE 120
WIND GUST RUNS COMPARISON

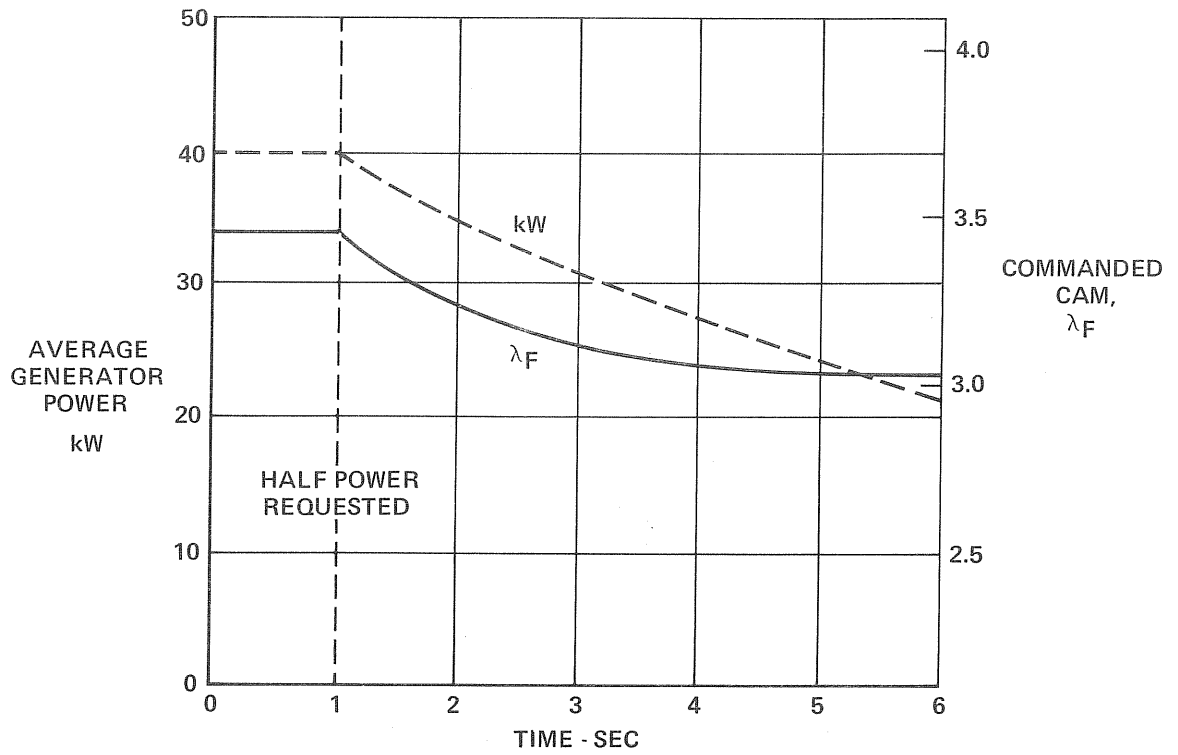


**FIGURE 121
GIROMILL START-UP**

A partial power simulation was also investigated. This was done by changing the reference RPM to give a 20 kW output at the generator, or dropping the generator RPM from 1830 to 1815 (See Section 11.2). The results are plotted in Figures 122 and 123. Figure 122 shows how power output and commanded cam λ_F values varied with time. Within five seconds after half power was requested, λ_F and kW were almost at equilibrium.

Another way of showing this is presented in Figure 123. This figure is similar to Figure 38 except that cam values are given in terms of λ_F rather than wind MPH. The initial point was at $\lambda_F = 3.47$ (20 MPH) cam. Rotor power output is approximately 50 kW, but because of mechanical and electrical efficiency, generator power is 40 kW. The arrows show how λ_F was driven down by the controller towards a new equilibrium C_p of about 0.25. This shows that the controller unit can control the Giromill over the complete power envelope.

10.1.3 Actuator Performance Analysis - In order to size the actuator, power, maximum torque, maximum acceleration, and maximum rate all required definition. A performance computer study was then performed, using a simplified quasi-steady-state representation of the actuator. The CSMP analysis, reported in Section 10.1.2, and the detailed simulation analysis of Section 10.1.4 were then used to establish the gains and time constants for proper actuator operation.



GP79-0636-86

FIGURE 122
PARTIAL POWER PERFORMANCE
 20 MPH Wind

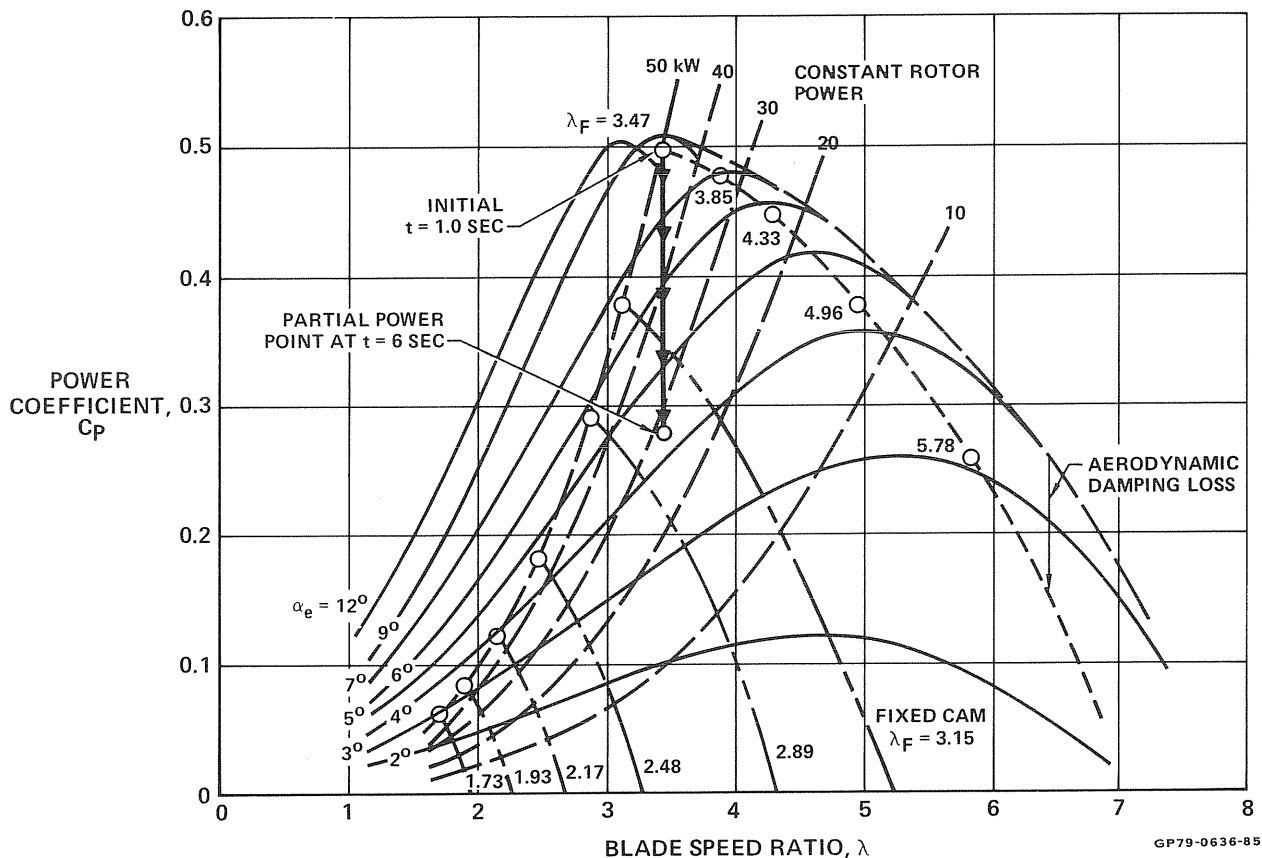
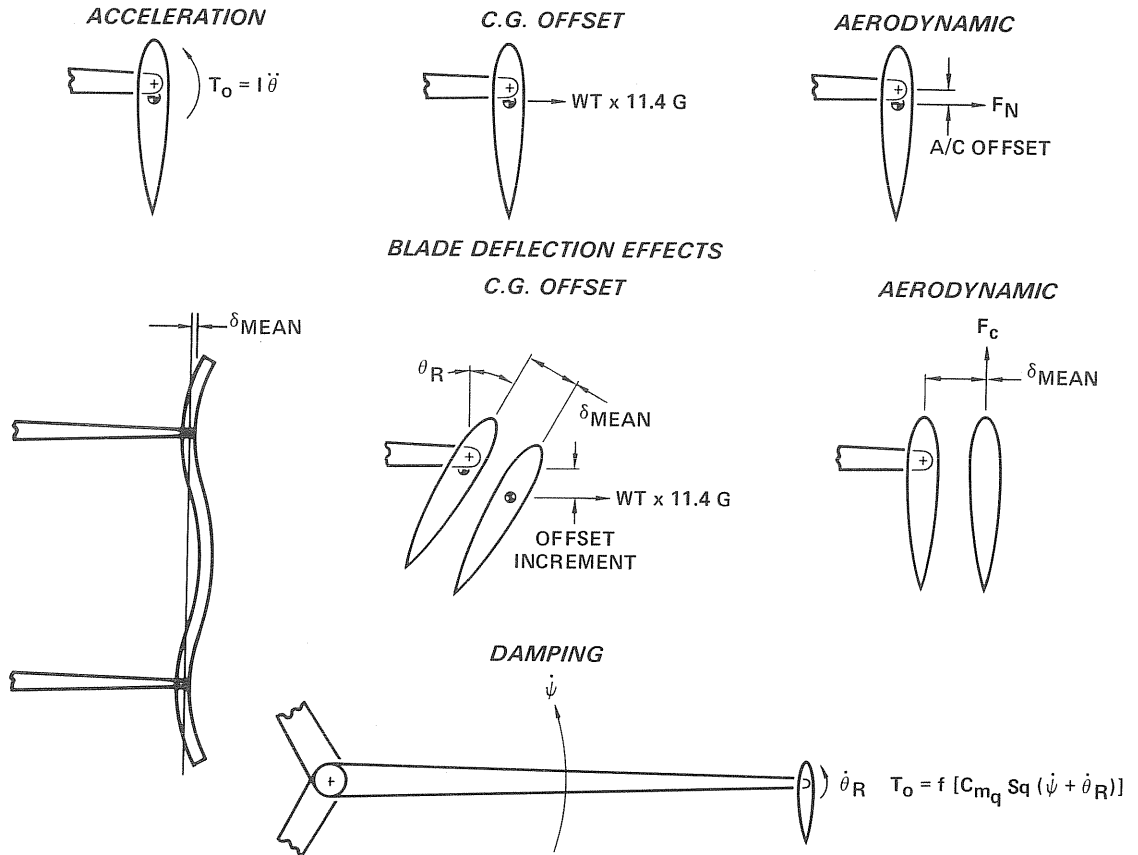


**FIGURE 123
PARTIAL POWER CONTROL PERFORMANCE**

The torque components that the actuator would have to react against are summarized in Figure 124. Five external torques must be considered:

- 1) Acceleration, which is the inertia of the blade times the angular acceleration.
- 2) The torque due to the c.g. not being on the pivot axis.
- 3) The aerodynamic airload because the a.c. is not on the pivot axis.
- 4) The blade deflection effects, which adds a component due to the c.g./pivot axis offset and another component that accounts for the chord-wise airload.
- 5) The blade aerodynamic damping component.

These torques must be reacted by the magnetic torque of the motor. Motor and gearbox inertia must also be considered.



GP79-0636-109

**FIGURE 124
BLADE ACTUATOR TORQUE COMPONENTS**

A computer program was written that computed the torque, acceleration, and rate requirements for the various conditions expected. A simplified blade rock angle profile was employed, using a Fourier series representation.

Figures 125 and 126 show the requirements calculated. These are values expressed at the output shaft of the actuator (motor plus gearbox but not including actuator to blade pulley ratio). The oscillatory nature of the curves is due in part to the Fourier series representation of the blade rock angles.

Figure 127 shows how the actuator rate and acceleration vary with wind speed. This exponential increase was the primary reason for lowering the cut-off wind speed from 60 to 40 MPH. Designing an actuator for a wind of 60 MPH, which occurs only a small percentage of the time, was not cost-effective.

Methods of reducing the rates and accelerations were explored. However, it was felt that the time and resources were not adequate to arrive at an acceptable solution that could be implemented at this time.

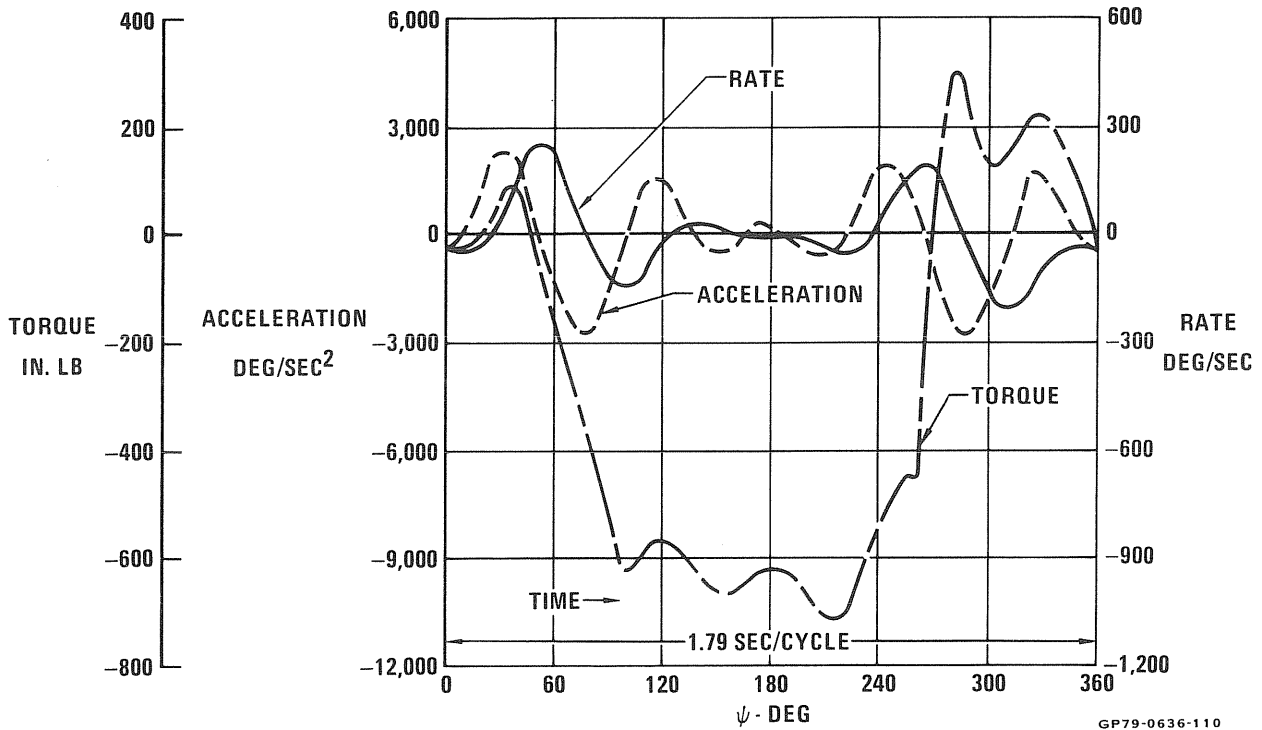


FIGURE 125
BLADE ACTUATOR REQUIREMENTS
20 MPH

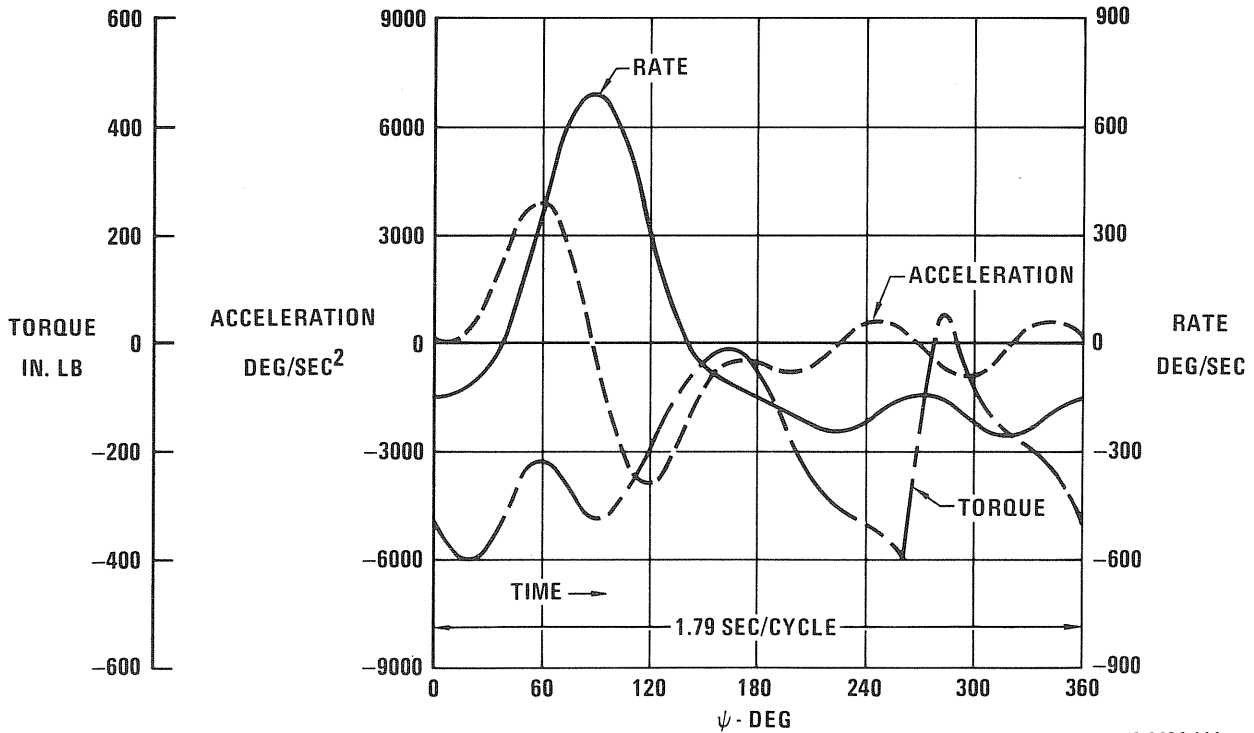
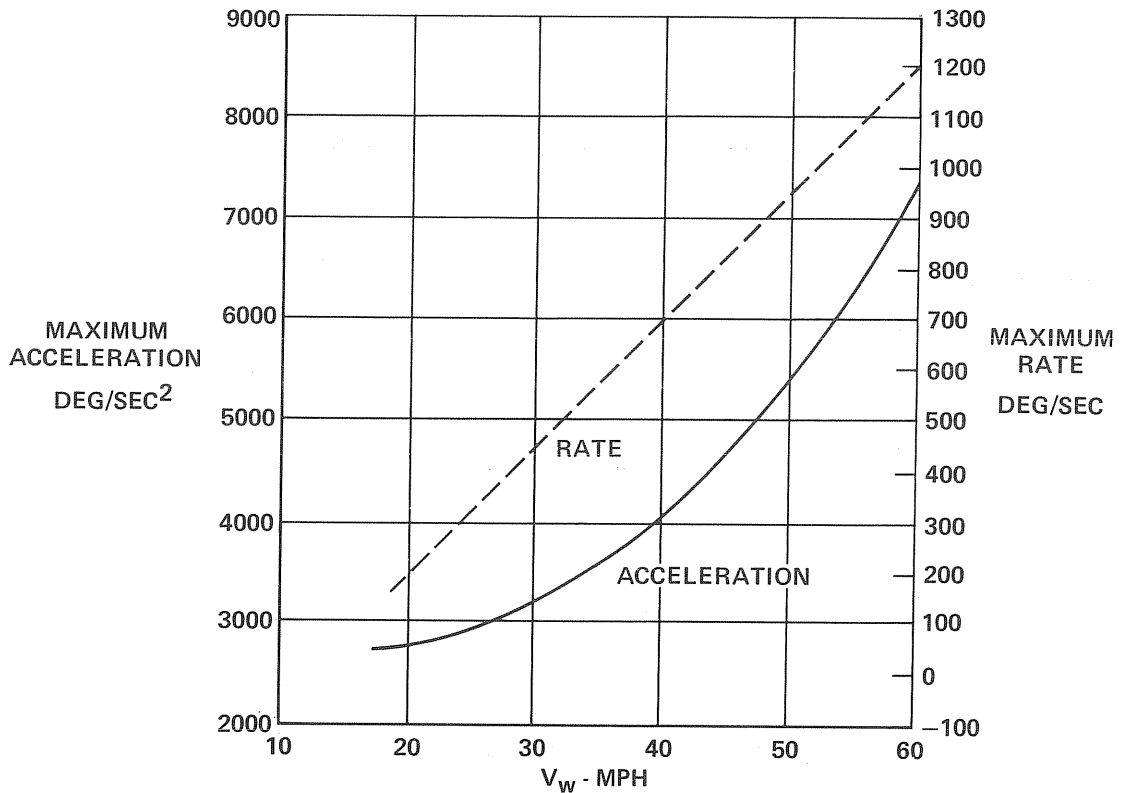


FIGURE 126
BLADE ACTUATOR REQUIREMENTS
40 MPH



GP79-0636-112

FIGURE 127
BLADE ACTUATOR MAXIMUM RATE AND ACCELERATION

10.1.4 Actuator Simulation Analysis - The actuator requirements were implemented in analyses using the CSMP simulation set up and with a more detailed simulation conducted at MDEC-GR, the actuator designer. The CSMP results were discussed in Section 10.1.2.

The frequency response characteristics of the linearized dynamic model of the actuator (Figure 101) are shown in Figures 128, and 129. The figures present the expected blade position that will be obtained for: a direct blade angle input command (θ_R/θ_C) and a prefiltered angle input command (θ_R/θ_{CF}), and the actuator load torques seen at the actuator (θ_R/T_O).

The fundamental frequency of the actuator command input will be 3.5 radians/sec (33.5 RPM). Other components of the command signal will be less than the fifth harmonic of the fundamental (17.5 radian/sec). The frequency resonance with a prefilter (Figure 128) shows that the amplitude of the output blade angle will match the blade angle command signal out to ten times the fundamental (35 radians/second).

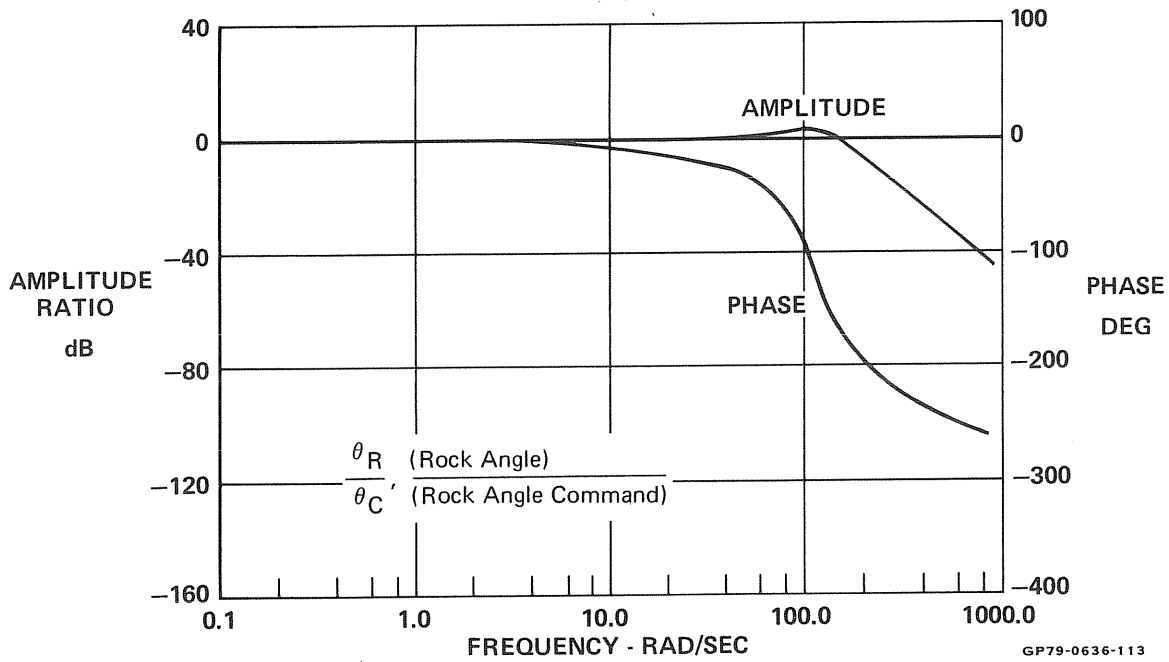


FIGURE 128
ACTUATOR CLOSED LOOP FREQUENCY RESPONSE

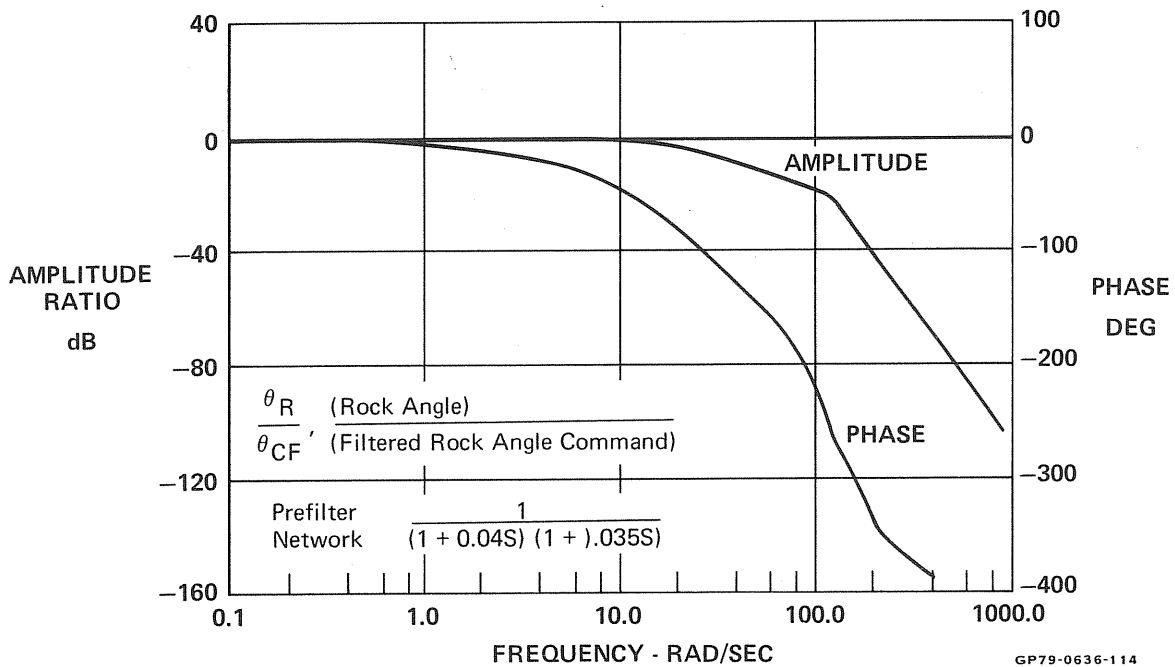


FIGURE 129
ACTUATOR CLOSED LOOP FREQUENCY RESPONSE

Since the current of the actuator motor is proportional to the acceleration of the input command signal, and the command signal from the controller is a series of discrete steps, it was necessary to add a prefilter to the actuator control loop, smoothing the input signal by reducing the high frequency signal component. The frequency response of the actuator control loop with the prefilter is shown in Figure 129. The amplitude response shows the blade angular position will track the command input within 3 db for frequencies less than 0.5 radians/second. The prefilter does cause the blade angle to lag the command input by 15 degrees at the fundamental input frequency (3.5 radians/second). This lag was compensated for by shifting the input rock angle profile schedule forward by 15 degrees.

The effect of the load torques on the actuator control loop is shown in Figure 130. The load torques keep the blade from following the desired command input signals. The figure shows that over the frequency range of concern (less than 35 radians/sec) that the blade position will be offset by 0.16 degrees (-16 db) for each ft-lb. of torque seen at the actuator motor. The load torque acting on the Giromill blade when reduced by the actuator gear ratio is usually well below 1.5 ft-lb at the actuator motor. Thus the load torques will introduce less than 0.25 degree of error in blade position during one rotation.

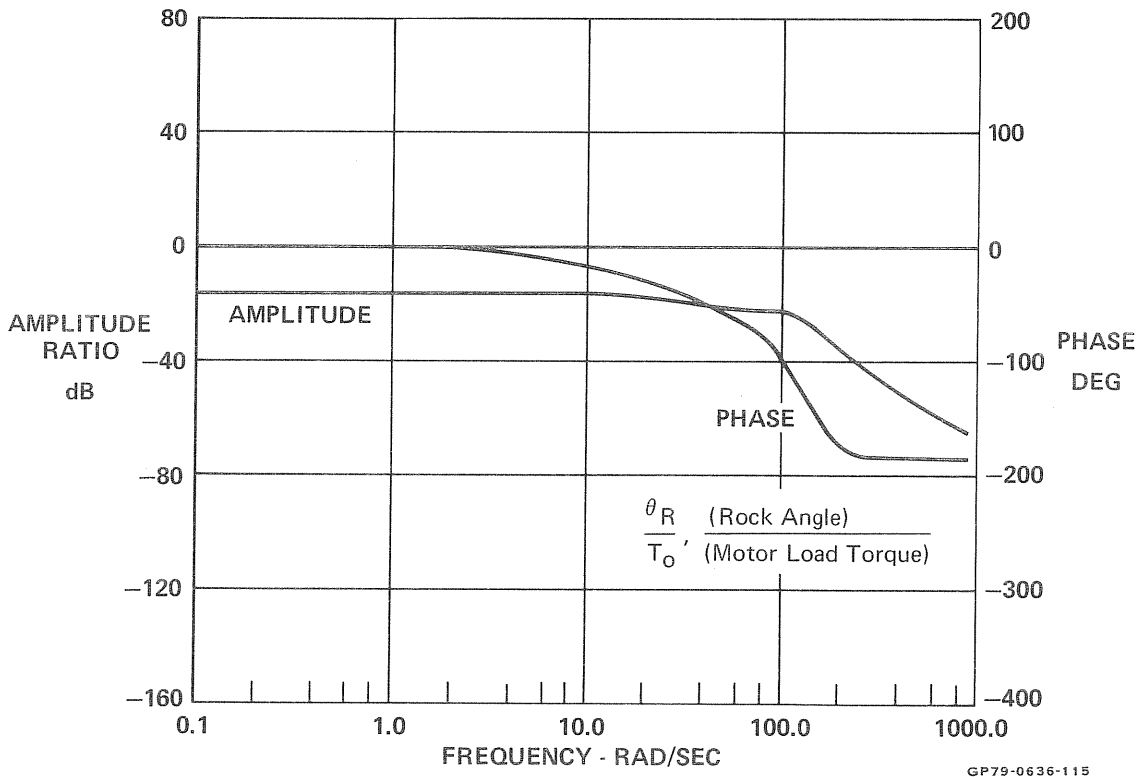


FIGURE 130
ACTUATOR CLOSED LOOP FREQUENCY RESPONSE

A non-linear simulation model of the actuator was developed and run by MDEC-GR engineers to:

- 1) Determine if the actuator loop is stable with the required loop gain.
- 2) Determine the actuator loop dynamic error.
- 3) Determine if the simplified actuator model used by MCAIR (CSMP Section 10.1.2) adequately represents the actuator loop.
- 4) Determine the maximum operating temperature of the motor and power transistors.
- 5) Determine the effect of some parameter variations.

Figure 131 shows the complete non-linear block diagram simulation. This represents an accurate simulation of the actuator motor, amplifier circuits, and gearing. Figure 132 is a simplified model block diagram which can be directly related to the model used in the CSMP simulation.

The combined constants used in the simplified model are obtained from the individual component gains of Figure 131, using the equations shown on Figure 132. These equations are analytic except for eq. 4, where the normal definition is divided by the factor "2", to make the simplified model response conform to the non-linear model. The basis for this factor lies in the switching duty cycle of the amplifier; during the "off" time, the motor is open circuited and no damping exists consequently, the apparent damping (average) is reduced. The value 2 is an estimate which gives acceptable results.

Figure 133 is a list of alphanumeric symbols and definitions for both block diagrams. This is a computer printout of all symbols used, and some of them may not be used in the final version.

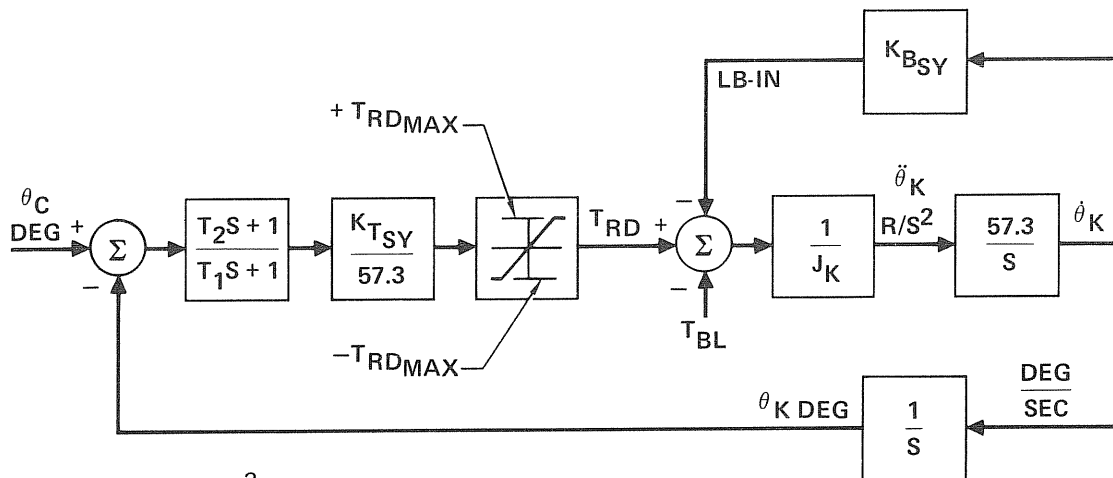
System errors simulated do not include transducer linearity or alignment errors nor, electronic scaling or drift errors.

Sample results are shown in Figures 134 and 135.

Good stability was achieved using a system stiffness up to 322,068 lb-in./rad (at the blade) and compensation time constants of $T_1 = 0.004$; $T_2 = 0.04$. The response to the rock angle commands (including a step input at $t = 0$) for two Giromill rotations is shown in Figure 134.

Both, the full non-linear simulation and the simplified simulation, give similar responses. The full simulation response is not as smooth as the simple model. And has an error 0.5 deg. larger. This is logical, because the full simulation includes effects of backlash and friction.

This difference can probably be neglected. The simplified model should adequately represent the servo in MCAIR Giromill simulations.



1. $J_K = (N_{AM}N_{AR})^2 J_M + 12J_B$
2. $\dot{\theta}_{KMAX} = ((E_S - E_{TD}) / (K_E N_{AM}N_{AR})) 6000$
3. $T_{RDMAX} = (I_{ML} K_T N_{AM}N_{AR} EFF) / 16$
4. $K_{BSY} = ((T_{RDMAX}) / (\dot{\theta}_{KMAX})) / 2$
5. $K_{TSY} = K_{FT} K_{SH} K_{EC} (1/E_{LC}) K_{MD} (1/R_A) (K_T / 16) N_{AM}N_{AR} EFF 57.3$

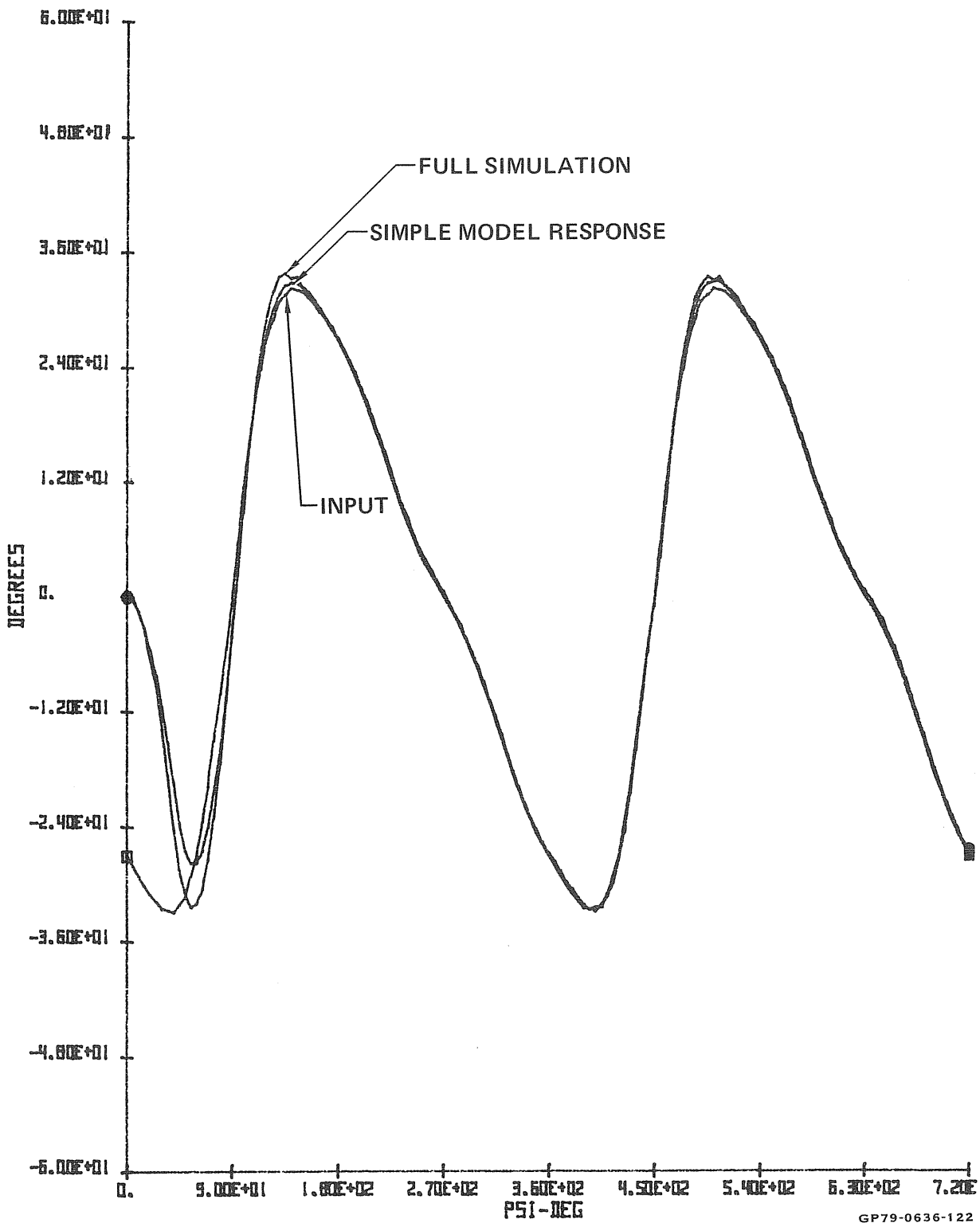
GP79-0636-120

**FIGURE 132
ACTUATOR SIMIPLIED MODEL**

SYMBOL	DESCRIPTION	UNITS	SYMBOL	DESCRIPTION	UNITS
A	A CONSTANT	-	KS	GEARING STIFFNESS CONSTANT	LB-IN/DEG
B	A LOGIC CONSTANT	---	KSH	FEEDBACK CHANNEL GAIN	VOLT/VOLT
CLAMP1	FRICTION ALGORITHM VARIABLE(1)	---	KT	MOTOR TORQUE GAIN	OZ-IN/AMP
CLAMP2	FRICTION ALGORITHM VARIABLE(2)	---	KTSY	SYSTEM TORQUE CONSTANT	LB-IN/RAD
CVTEST1	FRICTION ALGORITHM VARIABLE(1)	---	NAM	GEAR RATIO, MOTOR/ACTUATOR	DEG/DEG
CVTEST2	FRICTION ALGORITHM VARIABLE	---	NAR	GEAR RATIO, ACTUATOR/BLADE	DEG/DEG
DDTHETAM	MOTOR ACCELERATION	RAD/SEC	NPSI	NO. OF REVOLUTIONS OF TOWER	REV
DDTHETAR	BLADE ACCELERATION	RAD/SEC	NTA	GEAR RATIO, TRANSDUCER/ACTUATOR	---
DELTHS	HEAT SINK TEMP RISE	DEG-C	PMD	POWER DISSIPATED THRU MOTOR	WATTS
DELTTJ	TRANSISTOR TEMP RISE	DEG-C	PMDAVG	" " " " (AVG)	WATTS
DIFF	THETAR-THETAK	DEG	PMW	POWER INPUT TO MOTOR	WATTS
DPSI	TOWER ROTATION VELOCITY	RPM	PSI	TOWER ROTATION	DEG
DT	TIME INCREMENT	SEC	PSIC	" " (FROM REF)	DEG
DTHETAK	BLADE VELOCITY(SIMPLE MODEL)	DEG/SEC	PT	POWER DISSIPATED THRU TRANSISTOR	WATTS
DTHETAM	MOTOR VELOCITY	DEG/SEC	PTAVG	" " " " (AVG)	WATTS
DTHETAMAX	MOTOR VELOCITY,MAX	DEG/SEC	PUSED	TOTAL POWER USED	WATTS
DTHETAMO	" " (AT ACTUATOR OUTPUT)	DEG/SEC	RA	MOTOR ARMATURE RESISTANCE	OHMS
DTHETAMS	MOTOR VELOCITY AT T=0.	DEG/SEC	RB	BRUSH RESISTANCE	OHMS
DTHETAR	BLADE VELOCITY	DEG/SEC	REVERSE1	FRICTION ALGORITHM VARIABLE	---
DTHETARS	BLADE VELOCITY AT T=0.	DEG/SEC	REVERSE2	FRICTION ALGORITHM VARIABLE	---
DTHKMAX	BLADE VELOCITY MAX	DEG/SEC	RHS	HEAT SINK THERMAL RESISTANCE	DEG-C/WATT
DTMAX	TIME INCREMENT, MAX	SEC	RTM	ARMATURE THERMAL RESISTANCE	DEG-C/WATT
DTMIN	TIME INCREMENT, MIN	SEC	RTT	TRANSISTOR THERMAL RESISTANCE	DEG-C/WATT
EB	BACK EMF VOLTAGE	VOLTS	RW	WINDING RESISTANCE	OHMS
EBD	DUTY CYCLED BACK EMF VOLTAGE	VOLTS	SM	MOTOR SPEED	RPM
EC	COMMAND SIGNAL	VOLTS	STEPSIZE	INTEGRATION STEPSIZE	SEC
ECL	" " (LIMITED)	---	STILL1	FRICTION ALGORITHM VARIABLE(1)	---
ED	DUTY CYCLE RATIO	D.C.--	STILL2	FRICTION ALGORITHM VARIABLE(2)	---
EDL	LIMITED DUTY CYCL	---	STOP	TIME AT END OF SIMULATION	SEC
EE	ERROR VOLTAGE	VOLTS	T	TIME	SEC
EEC	" " (AMPLIFIED)	VOLTS	TAD	ACTUATOR DEVELOPED TORQUE	LB-IN
EEL	" " (COMPENSATED)	VOLTS	TAMB	AMBIENT TEMPERATURE	DEG-C
EEZ	" " "	VOLTS	TARM	ARMATURE TEMPERATURE	DEG-C
EF	FEEDBACK VOLTAGE	VOLTS	TBD	BLADE DEVELOPED TORQUE	LB-IN
EFF	GEARING EFFICIENCY RATIO	---	TBF	BLADE FRICTION TORQUE	LB-IN
EI	CURRENT FEEDBACK SIGNAL	VOLTS	TBL	BLADE LOAD TORQUE	DEG
EIB	" " " (LIMITED)	VOLTS	TD	PREFILTER TIME CONSTANT	SEC
ELC	COMPENSATED ERROR SIGNAL LIMIT	VOLTS	THETAA	BLADE SIDE OF BACKLASH	DEG
EM	MOTOR VOLTAGE	VOLTS	THETAB	ACTUATOR BACKLASH	DEG
ERROR	SYSTEM ERROR	DEG	THETAC	COMMANDED ROCK ANGLE	DEG
ERRORS	SYSTEM ERROR(SIMPLE MODEL)	DEG	THETAK	ROCK ANGLE OF BLADE(SIMPLE MODEL)	DEG
ES	SUPPLY VOLTAGE	VOLTS	THETAMB	OUTPUT SIDE OF BACKLASH	DEG
ET	TRANSDUCER OUTPUT VOLTAGE	VOLTS	THETAMO	MOTOR DISPLACEMENT(AT ACT.OUTPUT)	DEG
ETD	TRANSISTOR VOLTAGE DROP	VOLTS	THETAR	ROCK ANGLE OF BLADE	DEG
ETU	DUTY CYCLED TRANSISTOR VOLTAGE	VOLTS	THETAS	INPUT SIDE OF GEAR STIFFNESS	DEG
FRICTN1	MOTOR FRICTION TORQUE	LB-IN	THETAT	TRANSDUCER DISPLACEMENT	DEG
FRICTN2	BLADE FRICTION	LB-IN	TM	MOTOR TORQUE	LB-IN
IM	MOTOR CURRENT	AMPS	TMA	MOTOR TORQUE APPLIED	LB-IN
IHL	MOTOR CURRENT LIMIT	AMPS	TMD	MOTOR DAMPING TORQUE	LB-IN
JB	BLADE INERTIA	SLUG-FT(SQ)	TME	MOTOR ELECTRICAL TIME CONSTANT	SEC
JK	SYSTEM INERTIA	LB-IN-SEC(SQ)	TMF	MOTOR FRICTION TORQUE,MAX.	OZ-IN
JM	MOTOR INERTIA	LB-IN-SEC(SQ)	TML	MOTOR LOAD TORQUE	LB-IN
KAF	CURRENT FEEDBACK GAIN	VOLTS/AMP	TMM	MOTOR TORQUE	OZ-IN
KBSY	SYSTEM MOTOR DAMPING	LB-IN/DEG/SEC	TNETH	NET MOTOR TORQUE	LB-IN
KCC	INPUT SIGNAL SCALING GAIN	VOLTS/DEG	TNETR	NET BLADE TORQUE	LB-IN
KE	MOTOR DAMPING CONSTANT	OZ-IN/DEG/SEC	TRD	BLADE TORQUE(SIMPLE MODEL)	LB-IN
KE	MOTOR BACK EMF CONSTANT	VOLTS/KRPM	TRDMAX	MAX DEVELOPED BLADE TORQUE	LB-IN
KEC	AMPLIFIER GAIN	VOLT/VOLT	TTJ	TRANSISTOR JUNCTION TEMPERATURE	DEG-C
KFT	FEEDBACK TRANSDUCER GAIN	VOLTS/DEG	T1	LAG TIME CONSTANT,ERROR	SEC
KIB	CURRENT FEEDBACK GAIN	VOLTS/AMP	T2	LEAD TIME CONSTANT,ERROR	SEC
KMD	MOTOR AMPLIFIER GAIN	VOLTS/D.C.	VW	WIND SPEED	MPH
KFAC	PREAMP GAIN, INPUT	VOLT/VOLT	#BYE		
KPAR	PREAMP GAIN, FEEDBACK	VOLT/VOLT			

GP79-0636-123

FIGURE 133
ROCK ANGLE SERVO SYSTEM
List of Symbols



GP79-0636-122

FIGURE 134
 ACTUATOR MODEL COMPARISON
 40 MPH

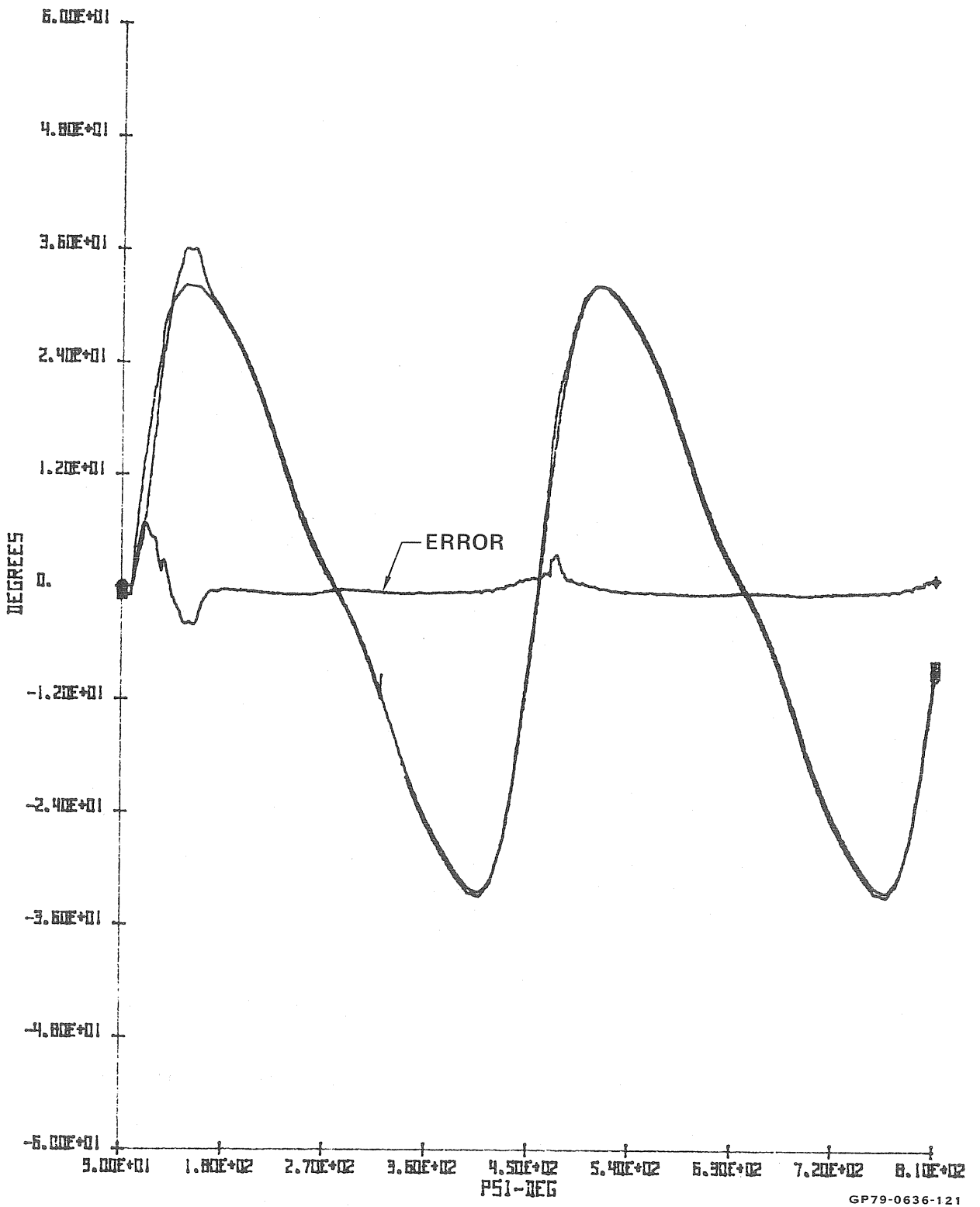


FIGURE 135
FINAL VALUES ACTUATOR SIMULATION RESPONSE

The signal for the rock angle servo is generated in the micro-processor as a digital value and converted to an analog signal thru a first order hold device (D/A). Thus, the signal is discrete in both amplitude and time. The signal being applied to the servo is actually a series of small steps (in increments of 0.5°) at intervals of 0.0128 sec. This effect was simulated by adding a first order hold to the input signal. No attempt was made to discretize the amplitude. Simulation results showed a large increase in motor power dissipated (from 120 to 320 watts) and a response delay of 2.6° approximately.

To improve this performance, a filter with a time constant equal to T_2 (0.04 sec) was added and a time shift of T_2 (lead) was added to the input signal. This lowered the motor power to 133 watts and reduced the system error to an acceptable value. The final simulation response is shown in Figure 135. The large initial error is a starting transient.

Several parameter variations were investigated including:

a) Compensation time constants - These have a major effect upon system damping. Many runs were made with T_2 ranging between 0.02 and 0.06 with T_1 approximately 10 times smaller. The best position response was obtained with $T_2 = 0.06$ but a high frequency limit cycle appeared (this resulted in increase motor power dissipation).

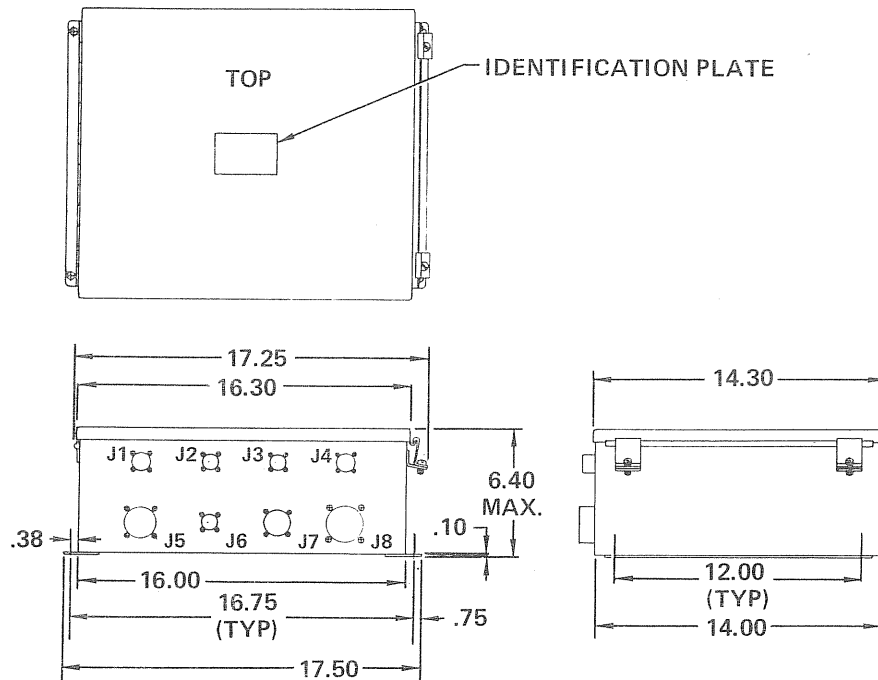
b) Gain - Can affect both, damping and accuracy. The simulation was run with both, the nominal stiffness (264,000 lb-in./rad at the blade) and gain 20% higher. No significant change was observed.

c) Backlash - Can affect stability and accuracy. The simulation was run with both 0° and 0.16° backlash. No significant change was observed.

10.2 CONTROL UNIT - The control unit is enclosed in a 14 in. x 16 in. x 6 in. JIC type box which is electrically interfaced via MS connectors to sensors, actuators, and power. The envelope drawing of the control unit is shown in Figure 136. The hinged cover provides full access to the control unit electronics. Switches, potentiometers, jumpers and digital readout are provided in the prototype unit to enable efficient installation checkout and variation of control parameters.

Low power standby circuitry, which operates independent of the control unit processor, monitors wind speed and determines if power should be applied to the remaining control unit circuits.

10.2.1 Processor - The control unit utilizes an 8-bit CMOS micro-processor (RCA CDP1802) in conjunction with input/output interface circuits to perform the controller function for the entire control system. The microprocessor program is resident in Programmable Read Only Memories (PROMS). Provisions are made for 6144 words of PROM memory resident in three $2K \times 8$ PROMS (Intel 2716). Scratchpad memory is provided as 256 words of Random Access Memory Storage (RAM).



GP79-0573-40

FIGURE 136
ENVELOPE DRAWING GIROMILL CONTROL UNIT

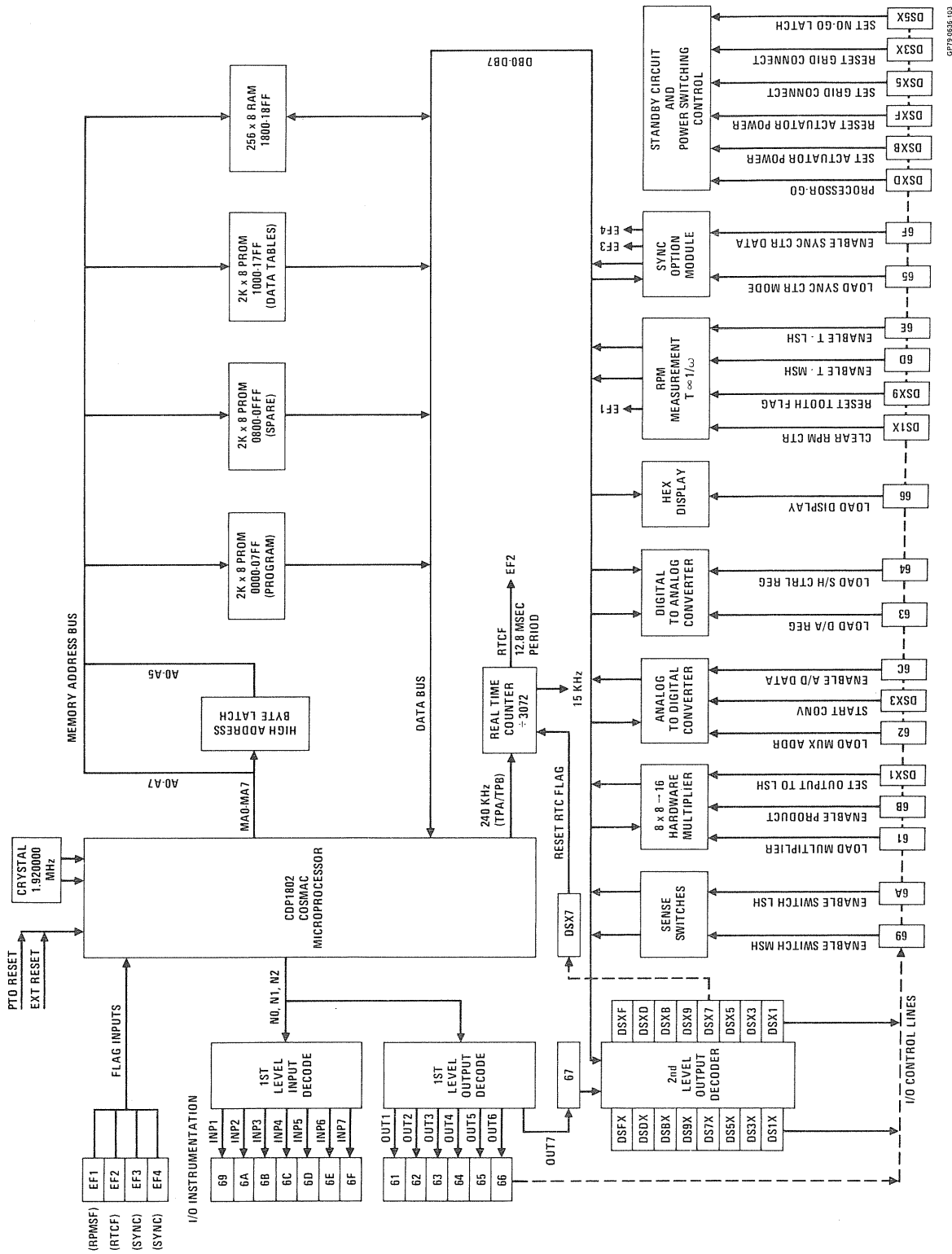
A processor functional diagram, Figure 137, shows the method of connecting the functional input/output modules to the microprocessor's data bus. I/O control lines are activated by processor commands. Control lines labeled "DSXY" generate discrete strobes such as set and reset commands.

Sixteen sense switches implemented as two 8-element DIP assemblies provide for manual inputs. The most significant half of these switches controls the operating mode. The least significant half of these switches selects which RAM variable is transmitted to the Hex display and instrumentation analog output.

Multiplication is performed by a Large Scale Integration (LSI) multiplier circuit connected via the microprocessor data bus, thus eliminating time consuming software multiplication.

Analog to digital conversion is implemented by a programmable front end multiplexer plus an 8-bit A/D converter. The multiplexer is configured for three differential analog inputs plus ten single-ended inputs. Two analog inputs are used to monitor reference inputs for diagnostic test.

A single D/A converter drives four sample and hold circuits. Three circuits provide rock angle commands to the three actuators and provides an analog output for instrumentation monitoring.



GPT9-0256-103

FIGURE 137
PROCESSOR FUNCTIONAL DIAGRAM

An accurate RPM measurement is needed. The time base for RPM measurement is a 240 kHz frequency derived from the microprocessor's 1.92 MHz crystal-controlled frequency. A 16 bit binary counter accumulates the number of time base periods which occur during the time interval required for 128 cycles of the RPM sensor. Each 128th cycle of the RPM sensor transfers the contents of the counter to a holding register and sets a flag which signals the processor to read out the contents of the register.

A sync option module which provides for synchronization to a small utility grid (mini-grid) is designed to be mounted on the control unit logic assembly. Electrical connection to the logic assembly is via two ribbon cables. This module contains a hardware counter which measures line voltage, and generator voltage cycle (labeled LINE AC LV and GEN AC LV in Figure 138), and computes generator voltage to line voltage phase delay. The control unit processor determines the counter mode and evaluates measurement results. When synchronization is completed the generator is connected and the processor monitors the load sensor's output signal. This signal provides data relative to direction and magnitude of power transfer between the generator and utility grid. Section 11.5 describes the electrical connections to implement the grid. For the small utility grid application, it has been assumed that a central load switching center is provided which will not apply load until a sufficient number of generators are on-line to share the load.

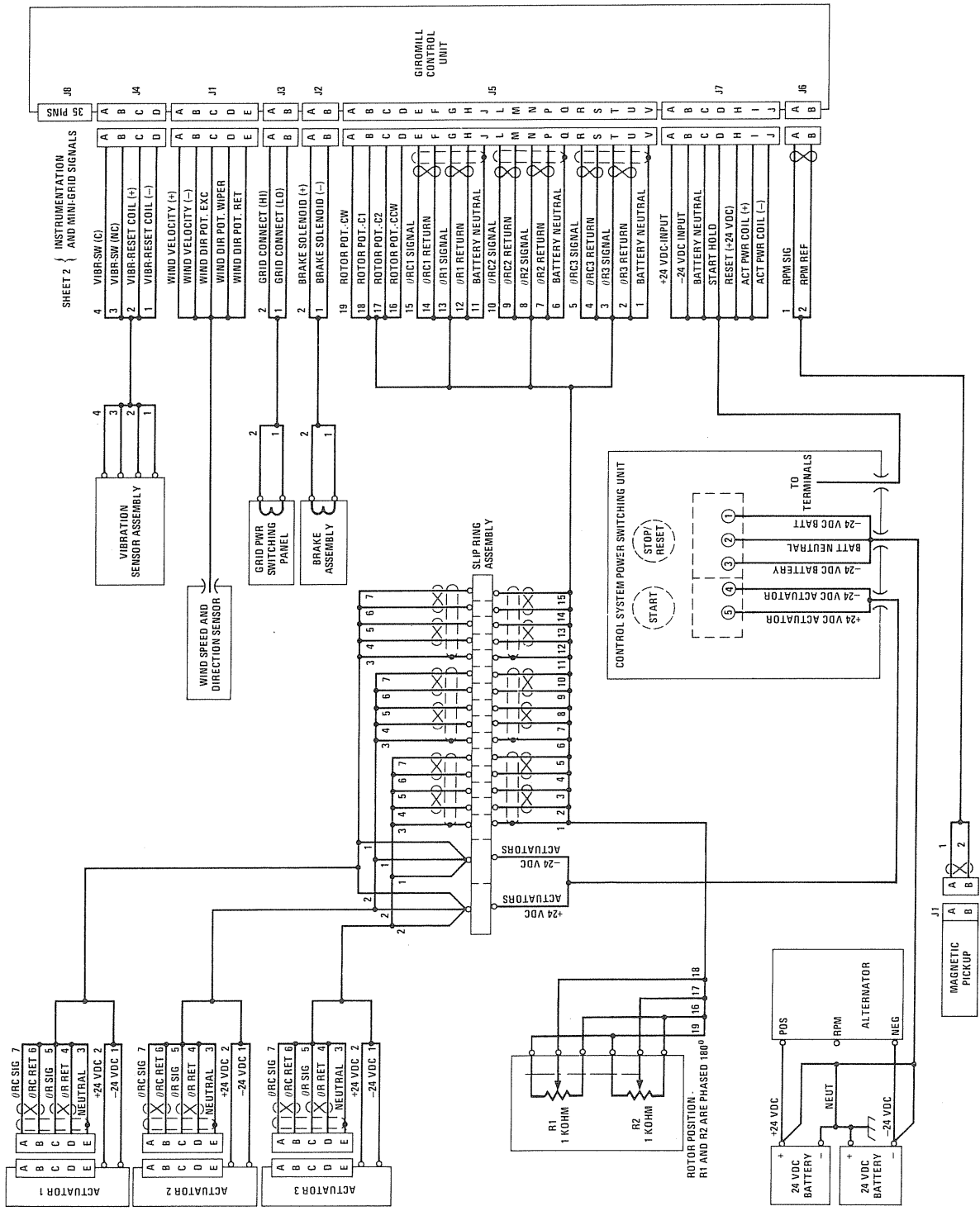
10.2.2 Sensor Interface - The control system interface schematic is shown in Figure 138. Sensor inputs to the control unit are signals from the following sensors:

- o Wind speed and direction sensor
- o Vibration sensor
- o RPM sensor magnetic pick-up
- o Rotor position sensor

The wind speed sensor input is an ac voltage with amplitude proportional to wind speed. The sensor scale is 10 Vac at a wind speed of 100 MPH. The ac voltage is converted to dc voltage in the control unit's standby circuits. The dc voltage, which is proportional to wind speed, is amplified and output to analog comparator circuits. It is also made available to the processor's analog to digital converter input if processor power is on.

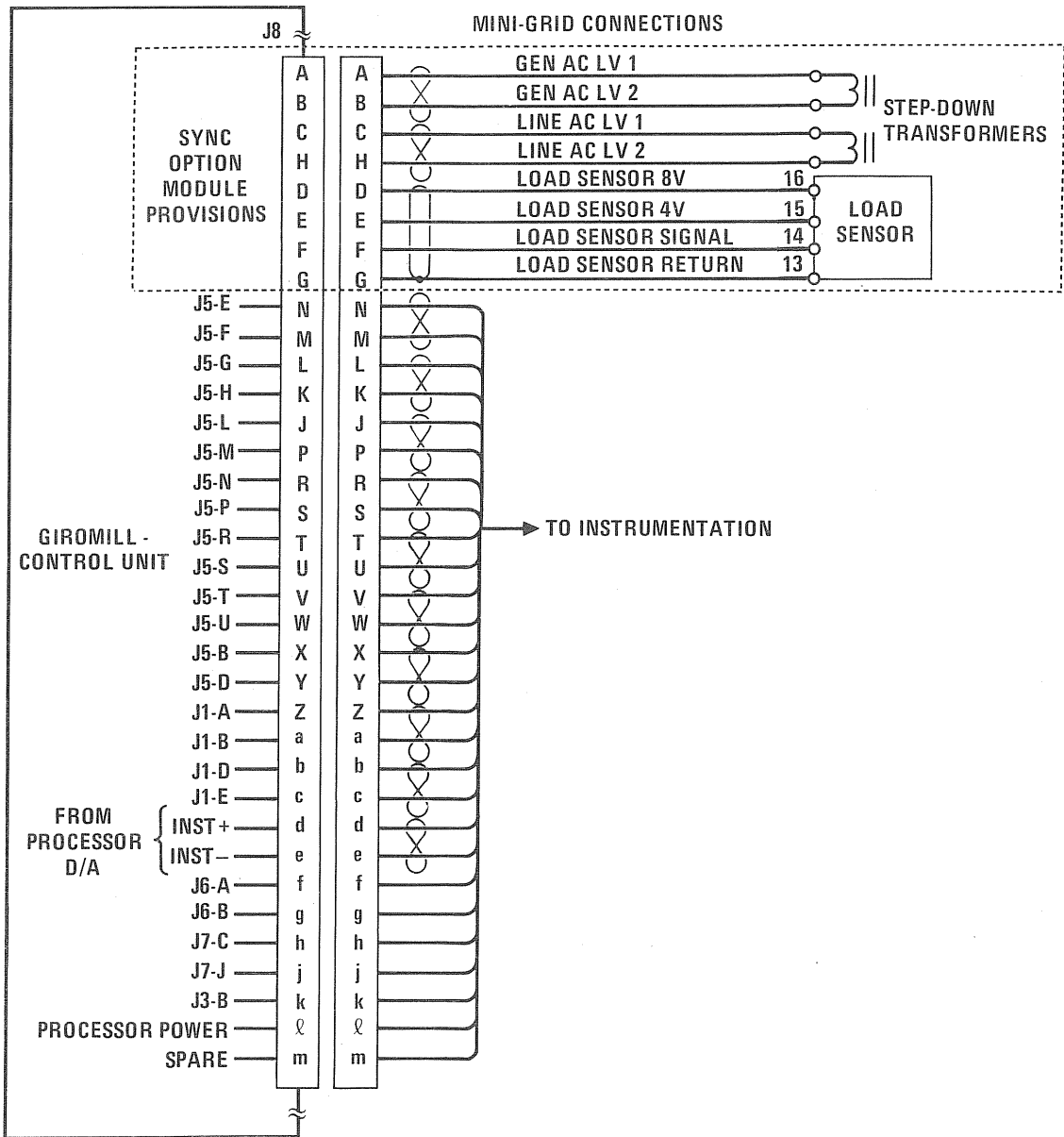
Four analog comparators with adjustable thresholds enable digital filtering of the wind speed input in accordance with the flow diagram shown in Figure 139. The time delay of the digital filter is controlled by the counter sampling frequency, which is potentiometer adjustable. The initial setting provides a time delay of about one minute.

The wind direction sensor input is activated by a potentiometer which is excited by the 10 Vdc reference in the processor's analog-to-digital circuitry. The wiper signal from the potentiometer is converted to digital data via the multiplexer and digital-to-analog converter, and stored in RAM memory for subsequent processing.



0173303101

FIGURE 138
GIROMILL CONTROL SYSTEM DIAGRAM



GP79-0636-102

FIGURE 138 (Continued)
GIROMILL CONTROL SYSTEM DIAGRAM

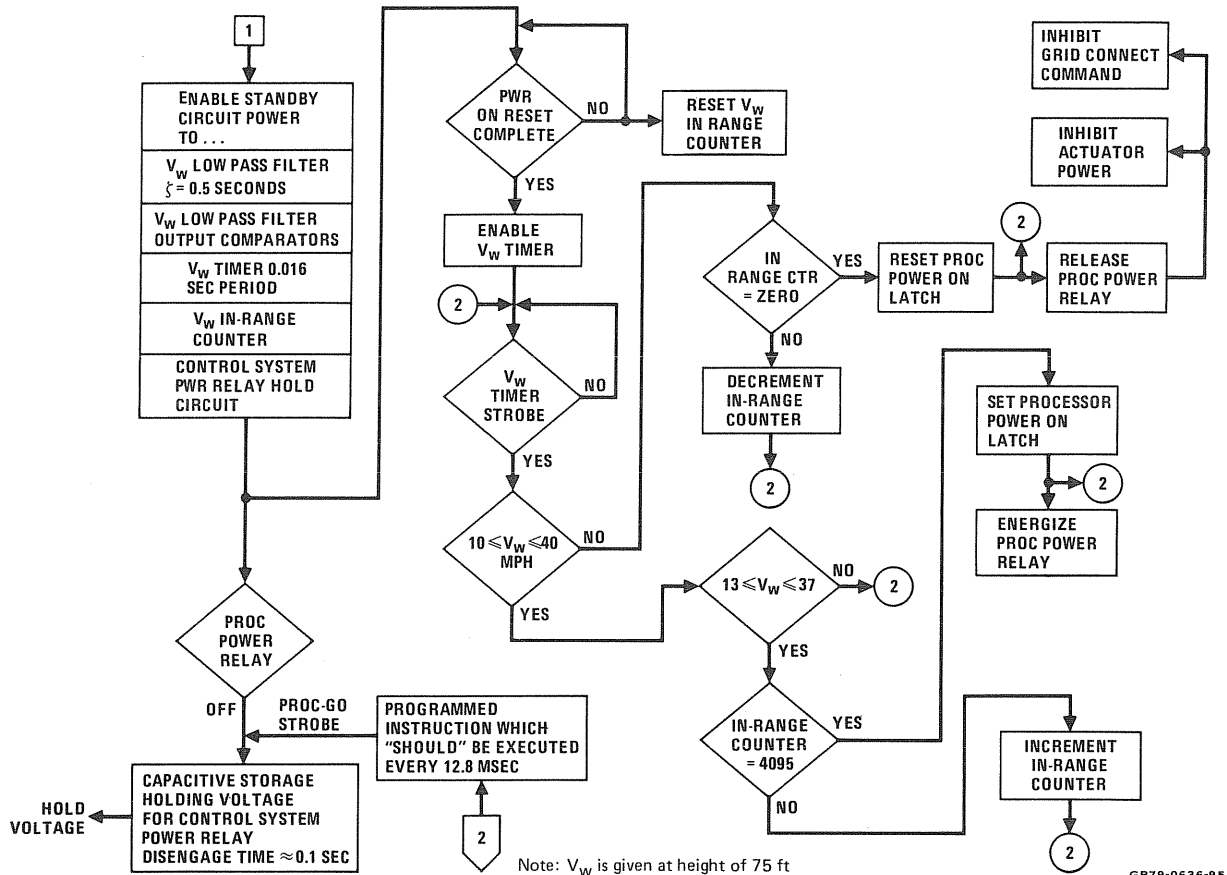


FIGURE 139
WIND SPEED SENSING FLOW DIAGRAM

The vibration sensor contains a set of contacts which open in the presence of excessive vibration. These contacts are in a series with the control unit's dc voltage input line and shut down the system. A reset coil enables remote reset when the operator depresses the STOP/RESET pushbutton on the control system power switching unit.

The RPM speed sensor input is activated by a magnetic pickup element which senses gear teeth and provides an output frequency equal to 3936.6 times rotor frequency. Installation is shown in Figure 158. In the control unit the magnetic pickup signal is terminated by a differential line receiver, which converts low level signals to the logic level signals required by the RPM measurement circuits.

The rotor position sensor input is sourced by dual potentiometers, which rotate on a 1:1 ratio with the rotor. Installation is shown in Figure 155. The potentiometers are excited by the 10 Vdc reference in the control unit. The potentiometer wipers are connected to the A/D input multiplexer, converted to digital, and stored in RAM memory. Dual potentiometers, phased 180° apart, are utilized to avoid deadband ambiguity which occurs at potentiometer endpoints for a span of approximately 10 degrees. The microprocessor's program determines which potentiometer is in the unambiguous region and utilizes that output to determine rotor position.

10.2.3 Actuator Interface - The control unit sends rock angle commands to three actuators and receives rock angle position feedback signals. The rock angle command is a dc voltage with a range of +10 Vdc, which corresponds to a rock angle range of $\pm 63.5^\circ$. The rock angle command signal and its return is transmitted via twisted pair cable and is terminated differentially with a 1000 ohm load inside the actuator.

The rock angle position signal from the actuator is a dc voltage with a range corresponding to a rock angle position of $\pm 63.5^\circ$. This signal is received via twisted pair cable and is also terminated differentially with a 1000 ohm load in the control unit. A composite shielded cable connects each actuator to the control unit. The shield not only eliminates noise, but also establishes a low current power supply return between the control unit and actuators. High current actuator power is controlled by a power relay inside the control system power switching unit.

10.2.4 Software - The control unit's microprocessor program is resident in Programmable Read Only Memories (PROMs). Referring again to Figure 137, three PROM are provided for program and fixed data tables. The PROMs are Intel 2716's, and each PROM has a capacity of 2048 eight bit words. These PROMs are field reprogrammable but require a knowledge of the microprocessor's machine language coding.

The microprocessor program was initially written in COSMAC assembly language, Level I, and the program assembled using the COSMAC Software Development Package (CSDP). This package includes software checking plus program simulation.

The software program for the control system consists of a main program plus subroutines and look-up tables. The main program and subroutines reside in memory locations 0 through Hex 07FF. The look-up tables reside in memory locations Hex 1000 thru Hex 17FF.

Look-up tables primarily consist of computer-generated rock angle profiles, as shown in Figure 140. Each profile is stored in memory as a function of blade phase angle. Successive profiles are stored as a function of blade speed ratio. Memory storage is thus analogous to a three-dimensional cam. Figure 141 is a memory map of the look-up table PROM which contains the rock angle profiles plus additional tables.

The main program is sequenced by operating phase, which is related to rotor RPM. This sequencing is shown in Figure 142. The main program is shown in Figures 143. Circled numbers on the flow diagrams correspond to phase sequence numbers. Software symbols are defined in Figure 144.

Subroutines called by the main program are as follows:

- o ADC routine - This routine controls the conversion of all analog inputs to digital data. Each analog input conversion consists of setting up the input multiplexer followed by a processor-controlled "start convert" command. After each conversion the A/D

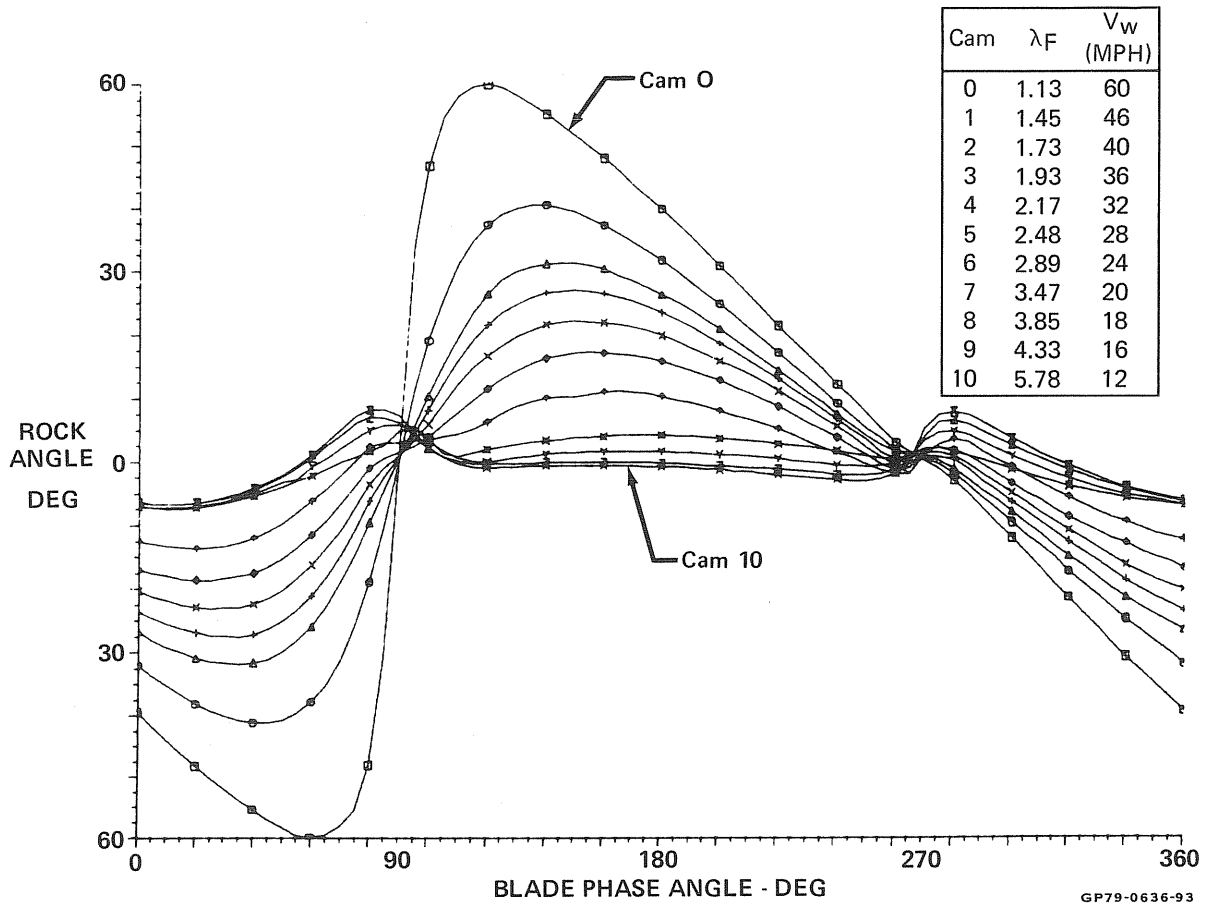


FIGURE 140
PROGRAMMED ROCK ANGLE PROFILES

PROM ADDR SPAN	NO. OF WORDS	LABEL	DESCRIPTION
0-127	128	CAM0:	ROCK ANGLE vs ψ_1 $\lambda \leq 1.13$
128-255	128	CAM1:	ROCK ANGLE vs ψ_1 $\lambda \leq 1.45$
256-383	128	CAM2:	ROCK ANGLE vs ψ_1 $\lambda \leq 1.73$
384-511	128	CAM3:	ROCK ANGLE vs ψ_1 $\lambda \leq 1.93$
512-639	128	CAM4:	ROCK ANGLE vs ψ_1 $\lambda \leq 2.17$
640-767	128	CAM5:	ROCK ANGLE vs ψ_1 $\lambda \leq 2.48$
768-895	128	CAM6:	ROCK ANGLE vs ψ_1 $\lambda \leq 2.89$
896-1023	128	CAM7:	ROCK ANGLE vs ψ_1 $\lambda \leq 3.47$
1024-1151	128	CAM8:	ROCK ANGLE vs ψ_1 $\lambda \leq 3.85$
1152-1279	128	CAM9:	ROCK ANGLE vs ψ_1 $\lambda \leq 4.33$
1280-1407	128	CAM10:	ROCK ANGLE vs ψ_1 $\lambda \leq 5.78$
1408-1535	128	CAM11:	ROCK ANGLE vs ψ TEST (SAW TOOTH)
1536-1663	128	CAM12:	ROCK ANGLE vs ψ TEST (SINE WAVE)
1664-1711	48	TBLMK:	GAIN CONSTANTS vs RPM
1712-1727	16	TBLBS:	λ_F LIMIT vs WIND VELOCITY
1728-1791	64	TBLUN:	λ_{cm} vs RPM AND WIND VELOCITY
1792-2047	256	CAMLU:	CAM AND FRACTION vs λ_F

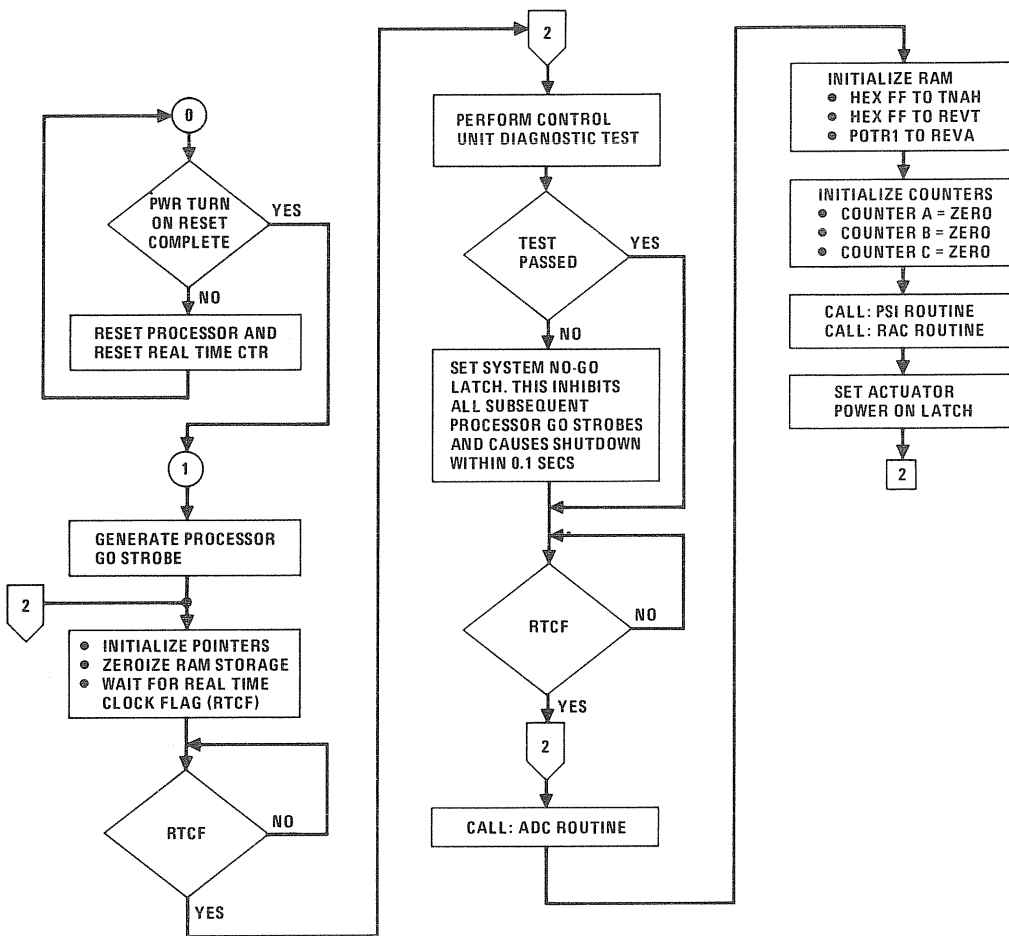
GP79-0573-37

FIGURE 141
MEMORY MAP OF LOOK-UP TABLE PROM

PHASE	RPM RANGE	ACTUATOR POWER	GRID CONNECT	NEXT PHASE	CONDITIONS FOR GOING TO NEXT PHASE	TIME LIMIT	SHUTDOWN CONDITIONS
0	—	OFF	NO	1	PROCESSOR POWER TURN ON	—	—
1	—	OFF	NO	2	INITIALIZE COMPLETE AND SELF-TEST GO	—	SELF TEST FAILURE
2	$\omega < 7$ RPM	ON	NO	2A	ROTOR HAS FORWARD ROTATION	120 SEC ↓	TIME LIMIT
2A	$\omega < 7$ RPM	ON	NO	3	FIRST RPM SENSOR FLAG		TIME LIMIT
3	$\omega < 32.92$ RPM	ON	NO	6 4	TIME LIMIT $\omega \geq 32.92$ RPM		RPM FROM RPM SENSOR \neq RPM FROM ROTOR ANGLE POT
4	$32.92 \leq \omega \leq 33.83$	ON	YES	3 5	$\omega < 32.92$ RPM $\omega > 33.83$ RPM	NO LIMIT	RPM SENSOR FLAG PERIOD > 64 MILLISECONDS
5	$33.83 \geq \omega \geq 32.92$	OFF	YES	6	$\omega < 32.92$ RPM	60 SEC	TIME LIMIT
6	$32.92 > \omega \geq 15$ RPM	OFF	NO	3	$\omega < 15$ RPM	↓	TIME LIMIT OR PHASE 6 → PHASE 3 LOOP COUNT > 5

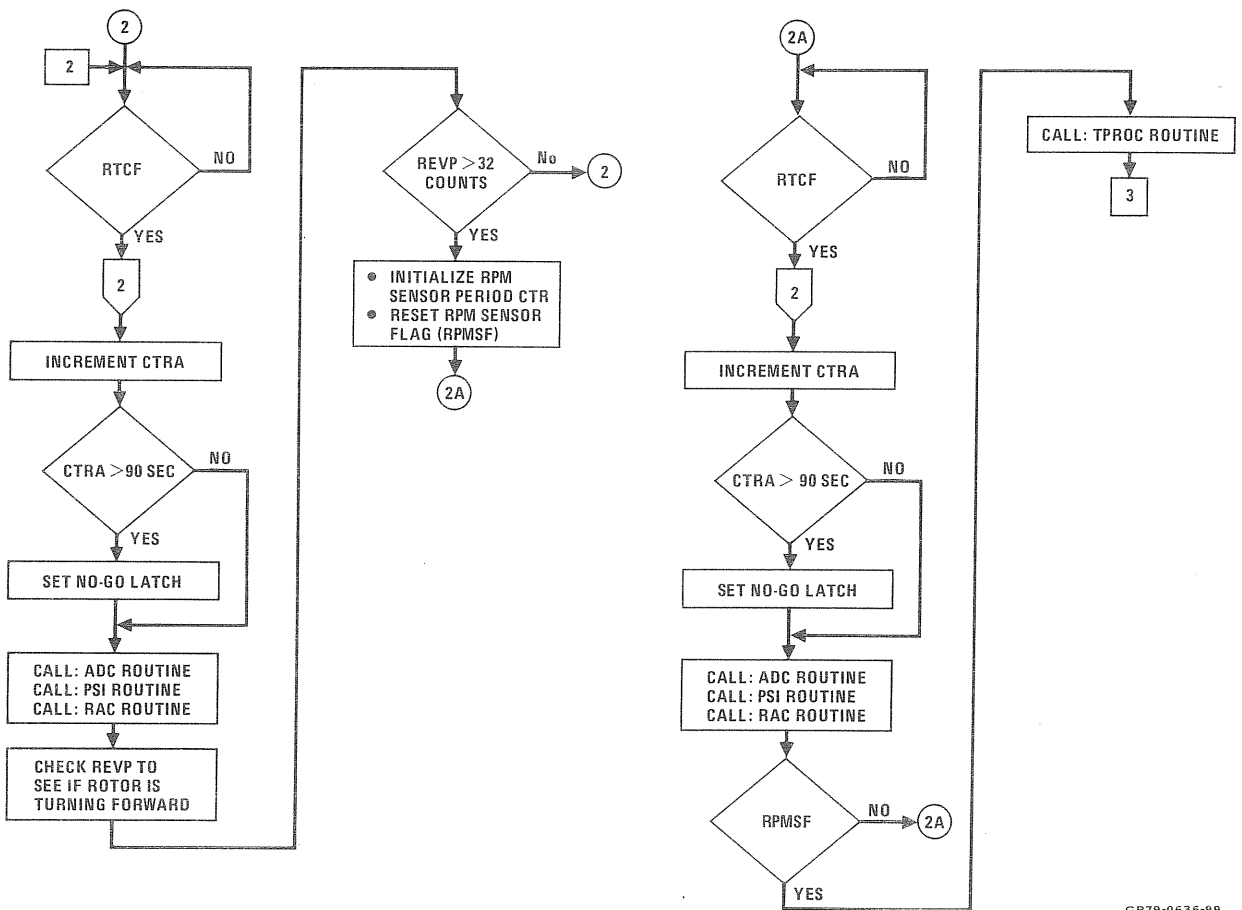
GP79-0573-1

FIGURE 142
GIROMILL CONTROL SYSTEM - PROCESSOR PHASE SEQUENCE



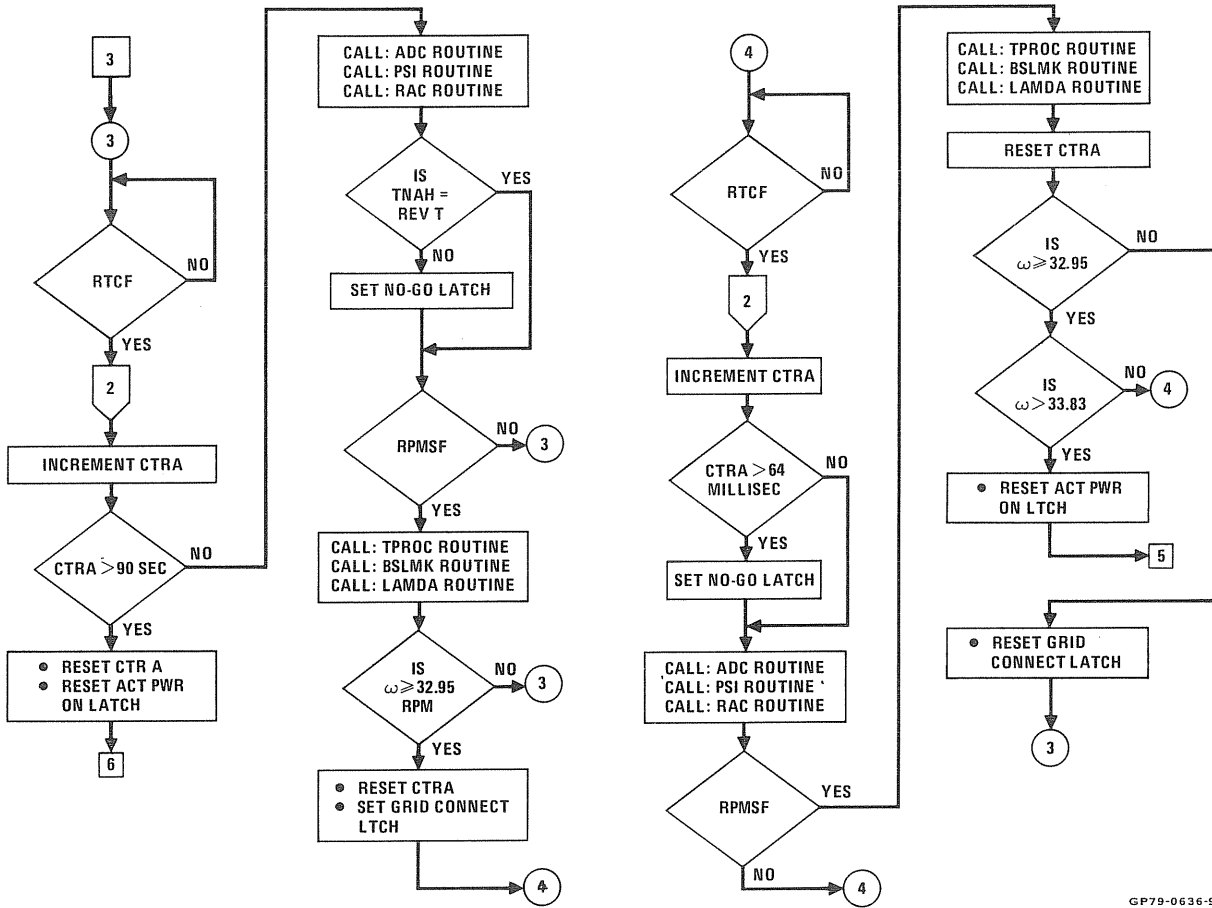
GP79-0636-98

**FIGURE 143
PROCESSOR FLOW DIAGRAM**



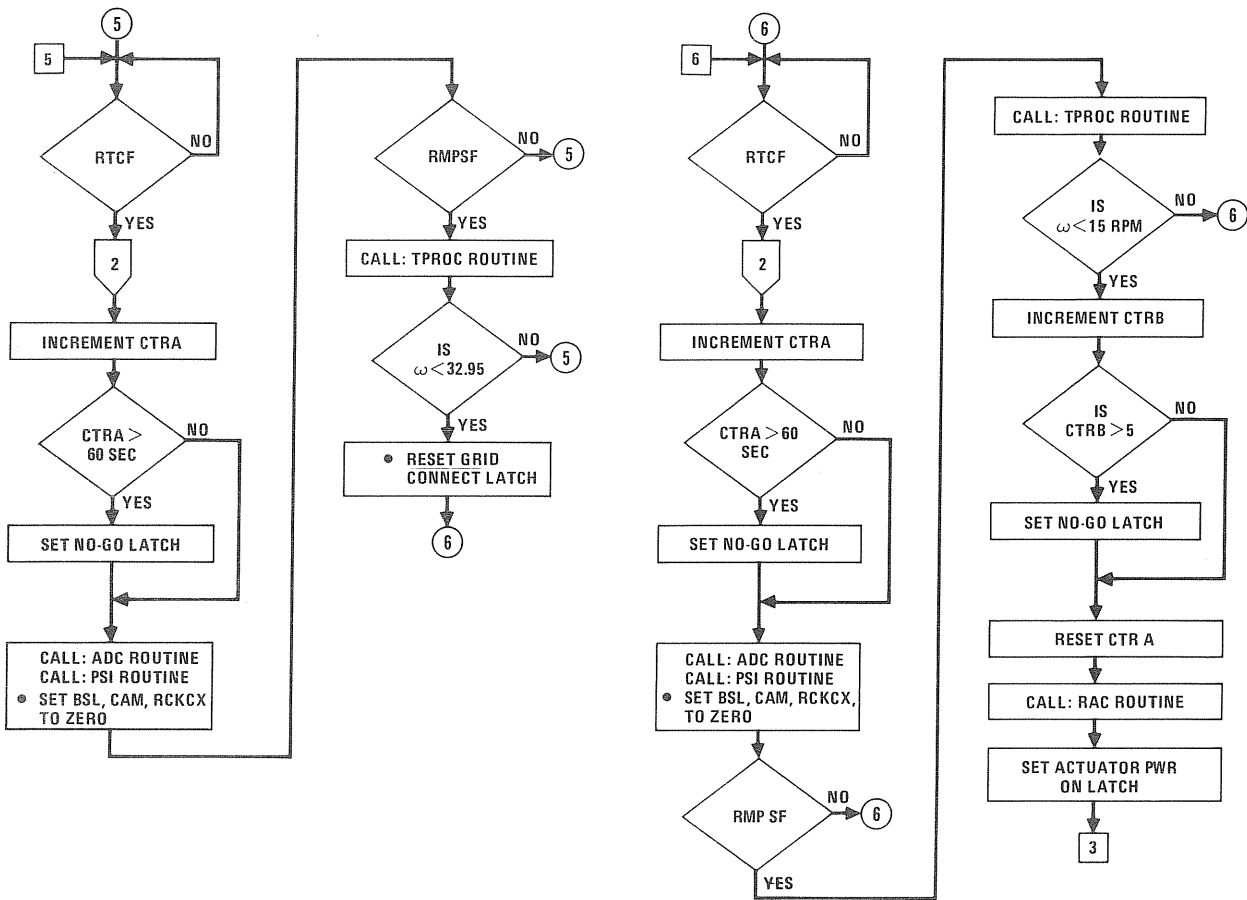
GP79-0636-99

FIGURE 143 (Continued)
PROCESSOR FLOW DIAGRAM



GP79-0636-96

FIGURE 143 (Continued)
PROCESSOR FLOW DIAGRAM



GP79-0636-97

FIGURE 143 (Concluded)
PROCESSOR FLOW DIAGRAM

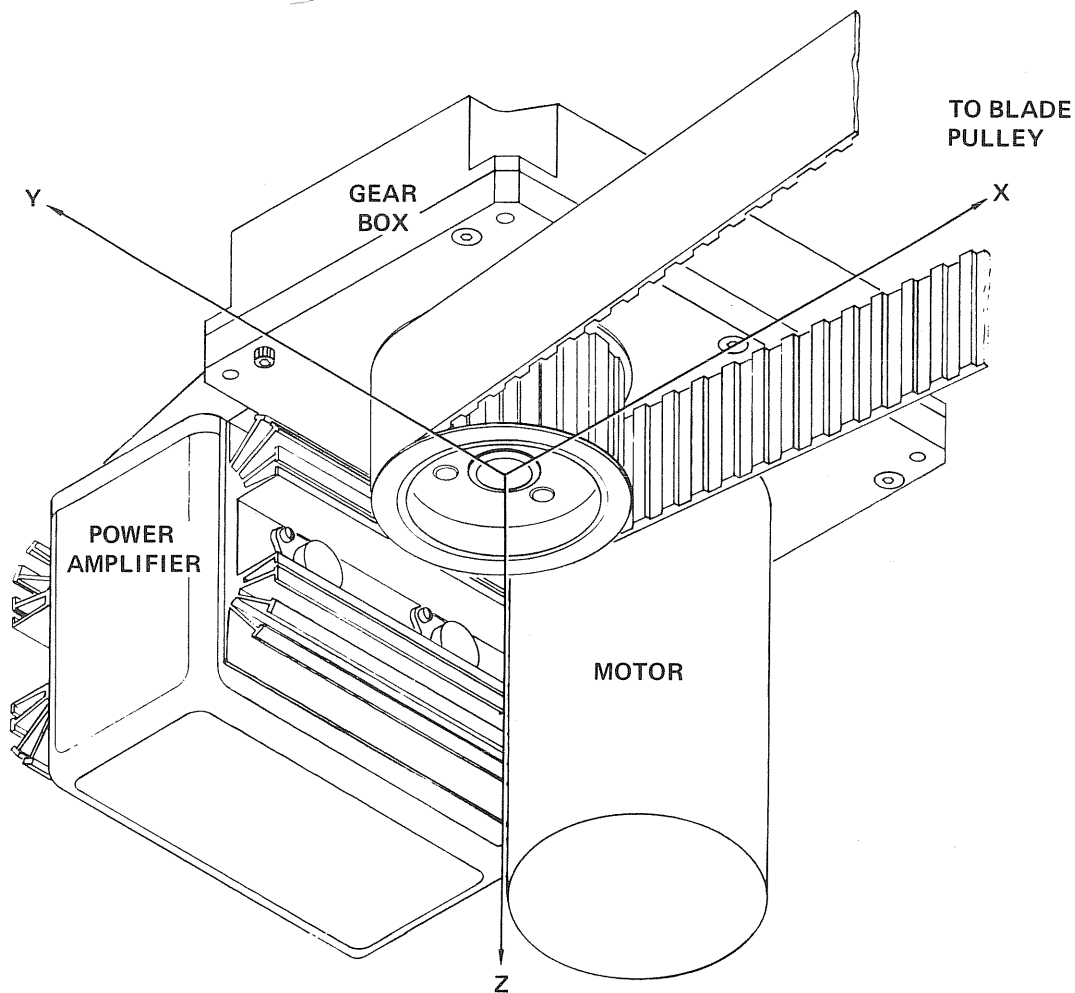
output is stored in fixed locations of RAM memory to be utilized by the main program or other subroutines. Digitized analog inputs are stored in RAM locations #16 thru #22. Refer to symbol definitions in Figure 144.

- o PSI Routine - This routine calculates the rotor angle relative to wind direction and stores the difference in RAM as PSIN. Prior to storing the PSI angle, a lead angle which is proportional to RPM is added to the PSI angle. This routine additionally calculates RPM based on delta values of rotor position potentiometer inputs. This RPM value is stored in RAM as REVT and is utilized by the main program for error check comparison with RPM sensor values.
- o RAC Routine - This routine is the rock angle command routine. Input variables CAM and PSIN are utilized to generate RCKC1, RCKC2, and RCKC3. The routine also loads the rock angle output converters.
- o TPROC Routine - This routine inputs data from the RPM measurement circuitry and generates RAM variables TERR, TDEL, and TNAH, by the Lambda Processing Routine.
- o BSLMK Routine - This routine is the Blade Speed Limit and Multiply Constant routine. It utilizes look-up tables to generate KMPR, KMTD, KMTE, and LEAD as a function of RPM and to also store BSLH and BSLL as a function of wind speed.
- o LAMBDA Routine - This routine calculates delta lambda by the following equation $BSD = KMPR ((KMTE) (TERR) + (KMTD) (TDEL))$ The routine calculates (WVEL) (TNAH) and utilizes the resulting product to look up BSCM. RAM variables stored by the routine are BSDL, BSDH, BSL, BSH, CAM, BSCM, BSFL, and BSFH.

10.3 ACTUATOR - The Giromill rock angle actuator is a self contained servo mechanism which controls the angular position of the output shaft in response to an input position signal. This servo mechanism consists of an electronic control amplifier and a dc motor powered, direct drive actuator. An isometric view of the actuator is shown in Figure 145.

10.3.1 Motor - The prime mover for the rock angle control actuator is a conventional dc motor, operating from the 48 volt supply. This permanent magnet motor is mechanically commutated through four brushes on a 42 bar commutator. This is a modification of a motor manufactured by Electro-Craft Corporation. The driving electronics of a conventional brushed DC motor are more simple than those of a brushless motor.

The motor is fully enclosed and non-ventilated. During steady-state operation the armature windings are expected to reach a maximum of only 140° C. The motor armature is built with a 220° C class insulation system, and should not suffer performance degradation through the short excursions to the maximum temperature.

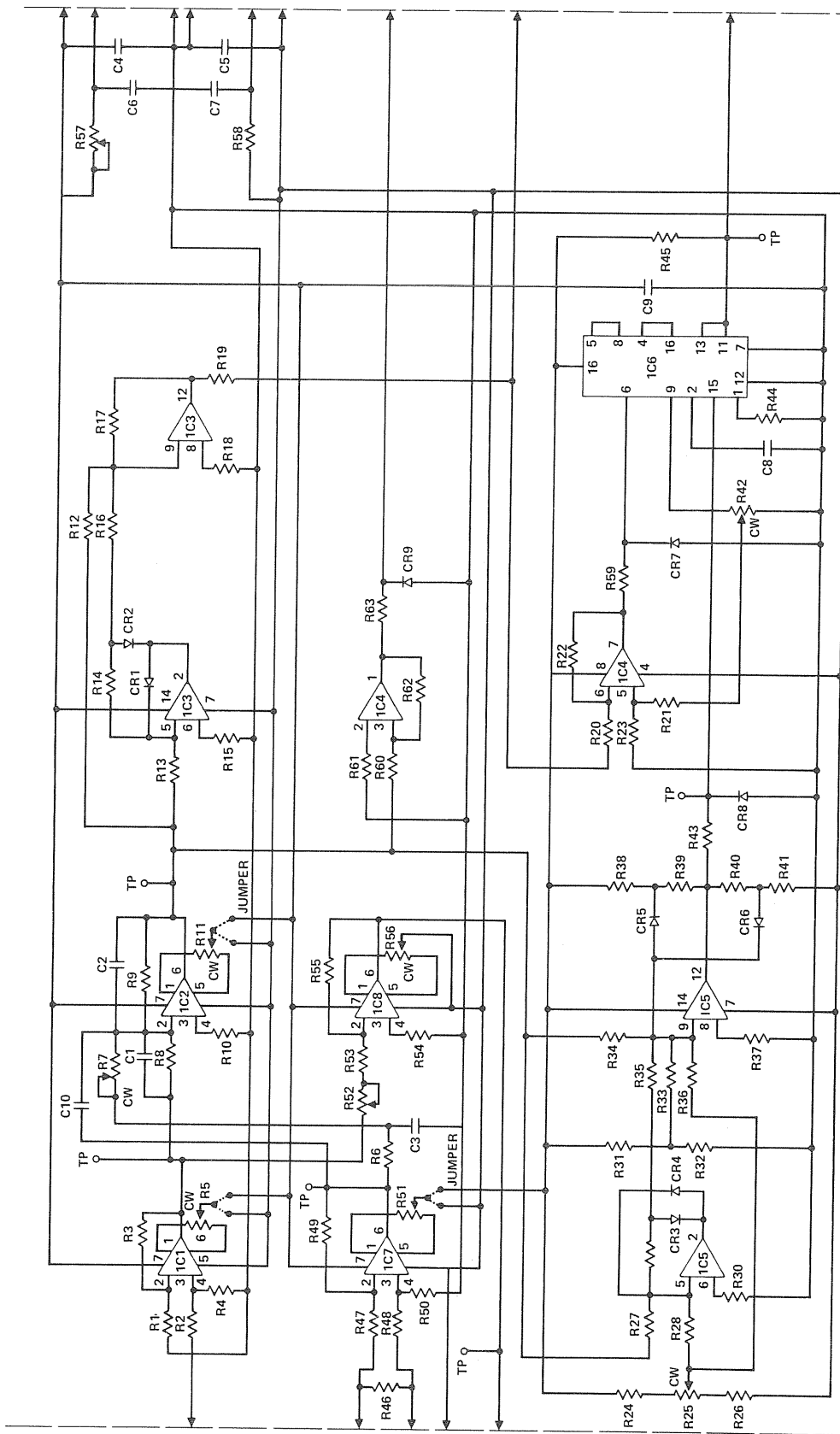


GP79-0636-19

**FIGURE 145
BLADE ACTUATOR ASSEMBLY**

Motor performance as installed in the actuator is rated at 40 volts. This is the minimum voltage the motor should see in operation, excluding start up. At maximum load, with the motor drawing 40 amps, there will be a 2 volt drop in voltage through the power wiring and a 2.5 to 3 volt drop across the amplifier power transistors.

10.3.2 Amplifier - The power amplifier consists of a servo amplifier board and a servo driver board which are connected together by an interconnect board. The output power transistors are mounted on two heat sinks. The electronics, exclusive of the heat sinks and transistors are enclosed. The electronic board schematics are shown in Figures 146 and 147.



CPT9-0638-66

FIGURE 146
SCHEMATIC SERVO AMPLIFIER BOARD

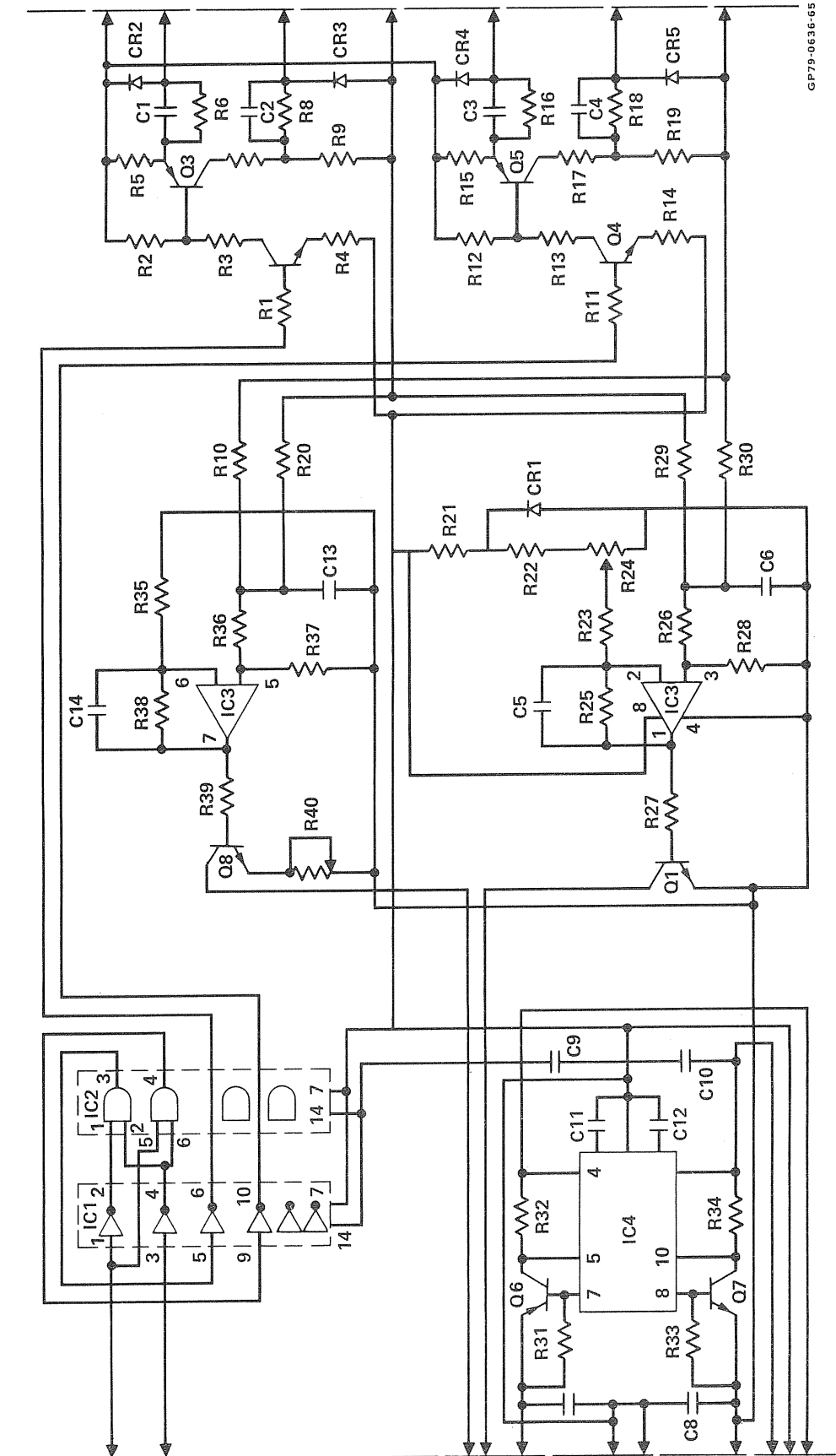


FIGURE 147
SCHEMATIC SERVO DRIVER BOARD

The input from the controller is brought into a differential input of an amplifier. The amplifier has a shaft position output for use by the controller. The amplifier uses pulse width modulation techniques for power control and has both current feedback and current limiting. It operates from a 48 volt supply.

The input from the control unit is fed into a differential amplifier, where it is amplified and summed with a buffered signal from the shaft position servo potentiometer. The summing amplifier also amplifies the error signal and contains the unit stabilization components. The error signal output of the summing amplifier is fed into a absolute value circuit, a polarity checker and a crossover detector.

The output of the absolute value circuit is a positive signal, whose amplitude is proportional to the absolute value of the error signal. The output signal is fed into a pulse width modulator, which provides a digital output whose pulse width is proportional to the input signal.

The polarity checker circuit provides a digital output signal which corresponds to the polarity of the input signal. The signal is used in conjunction with the pulse width modulator signal to drive the appropriate pair of output transistors.

The crossover detector provides an inhibit pulse to the pulse width modulator whenever the input signal passes through zero. This signal turns off the pulse width modulator momentarily to allow one pair of transistors to turn off before the second pair turns on.

The power output consists of two pairs of power darlington transistors plus the driver circuits. Each pair is dedicated to one rotation of the motor.

The amplifier contains a current limit circuit which limits the output current and a current feedback circuit which linearizes the amplifier.

The buffered output of the servo potentiometer is fed into a amplifier which serves as a line driver. The output signal is provided to indicate output shaft position for use by the controller.

10.3.3 Gearbox - The rock angle actuator has a two stage, spur gear reduction gearbox. Under normal operating conditions, the lubricant in the gearbox is centrifuged to the outermost side (+ x direction in Figure 145) where the gearing will be constantly lubricated by running partially submerged in oil. The highest calculated stress level was found to be in the intermediate pinion gear. The motor shaft alone has a shaft seal to prohibit oil seepage into the motor. The output shaft is unsealed because there is an oil dam around the output bearing bore. This should prevent oil seepage during shut down, but allow some lubricant to be thrown off the intermediate stage and find its way to the output needle bearing.

The calculated loads on bearings and the highest calculated fatigue stresses are summarized in Figure 148. Fatigue limits and bearings are chosen to perform as designed for 72,000 hours.

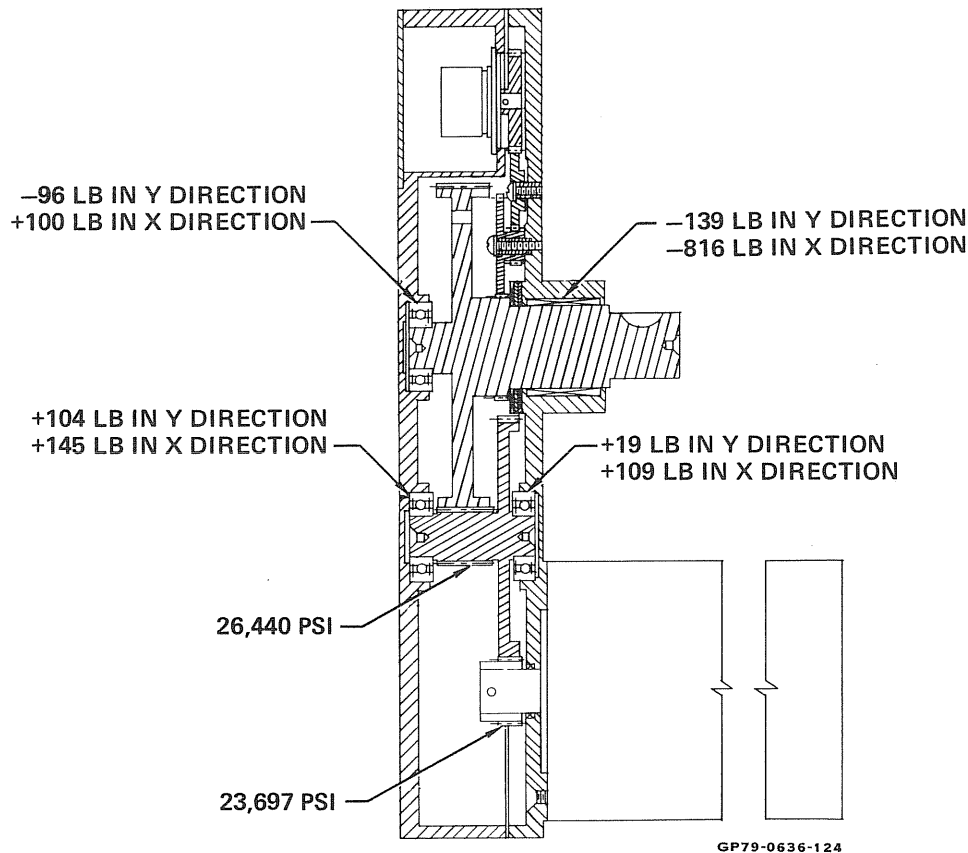


**FIGURE 148
GEAR BOX LOADS**

The output potentiometer is driven by anti-backlash gearing from the output shaft through a 3 to 1 ratio. The potentiometer position then corresponds to the blade rock angle, and not shaft position directly.

10.4 POWER DISTRIBUTION

10.4.1 Power System - Power for the control system is generated by a 48 Vdc alternator which is driven by a toothed belt from the main gearbox at the bottom of the rotating tower. Natural Power, Inc., manufactures the alternator which produces 1200 watts at 2000 RPM. The alternator is mounted to the gearbox as shown in Figures 149 and 150. Four 12 volt storage batteries are used. The batteries are sized to provide 5 false starts during 5 days at -20° C and meet the requirements of Design Criteria Section 3.6.4. These batteries are mounted on the panel which holds the electrical enclosures, as shown in Figure 151.

10.4.2 Power Switching - The control system power switching unit is shown in Figure 152 and the schematic in Figure 153. Pushbuttons are used for startup and shutdown. K1, the power control relay, can be activated only by depressing the START pushbutton. Once activated, it can be released manually by depressing the STOP/RESET pushbutton or automatically by removal of the "START HOLD" signal, which originates in the control

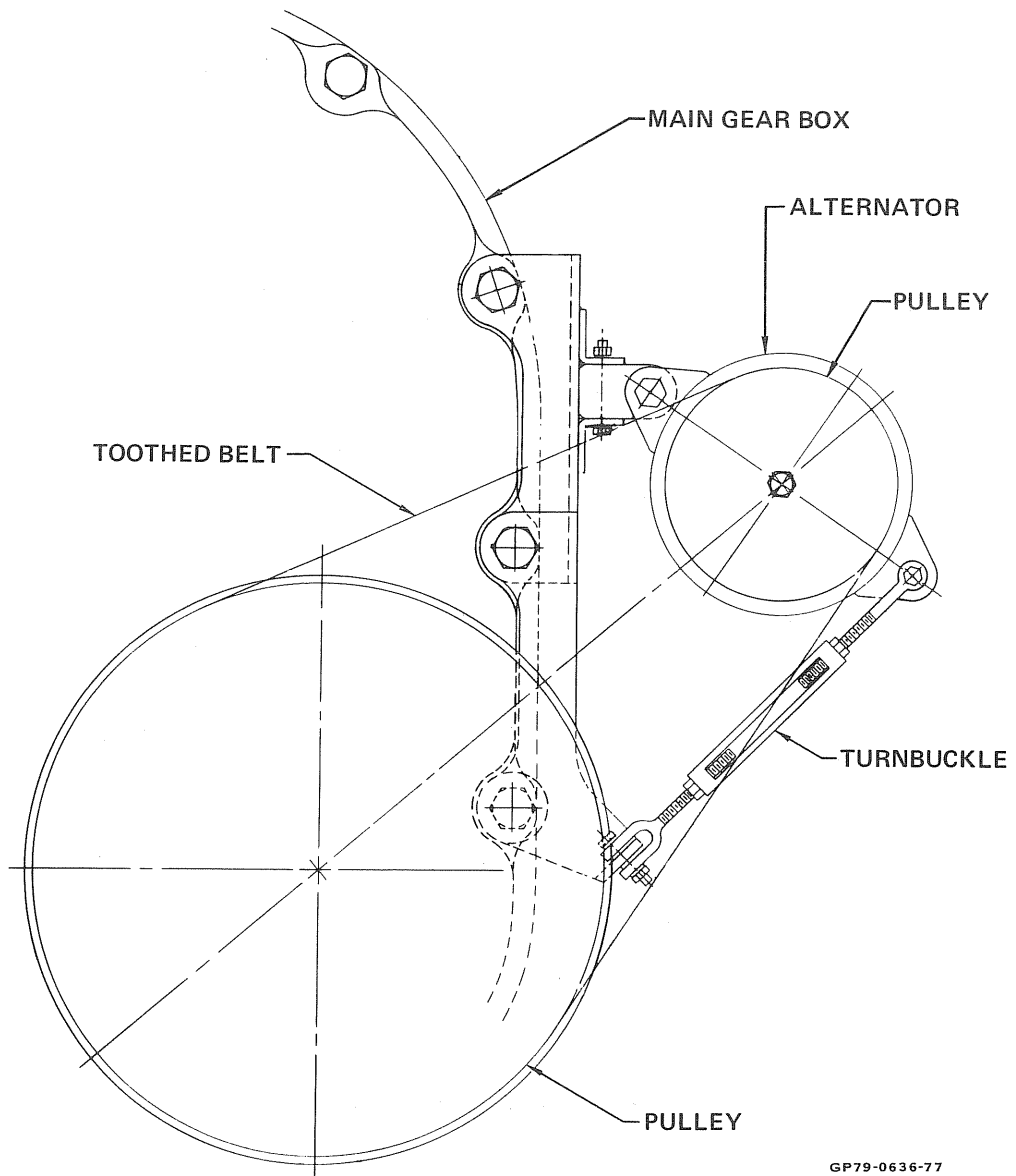
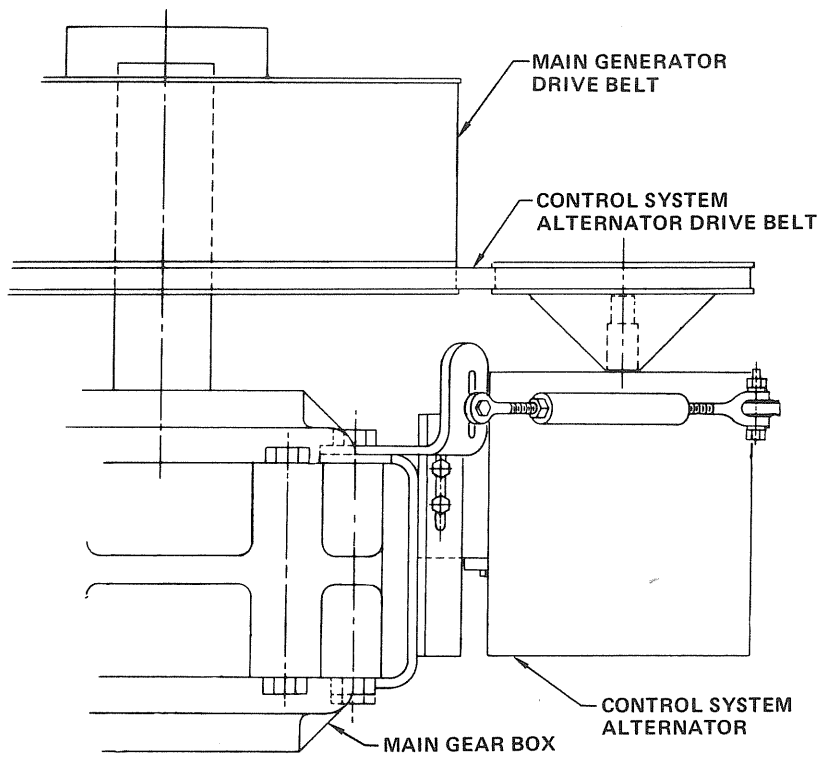


FIGURE 149
CONTROL SYSTEM ALTERNATOR
 Plan View



GP79-0636-78

FIGURE 150
CONTROL SYSTEM ALTERNATOR
 Side View

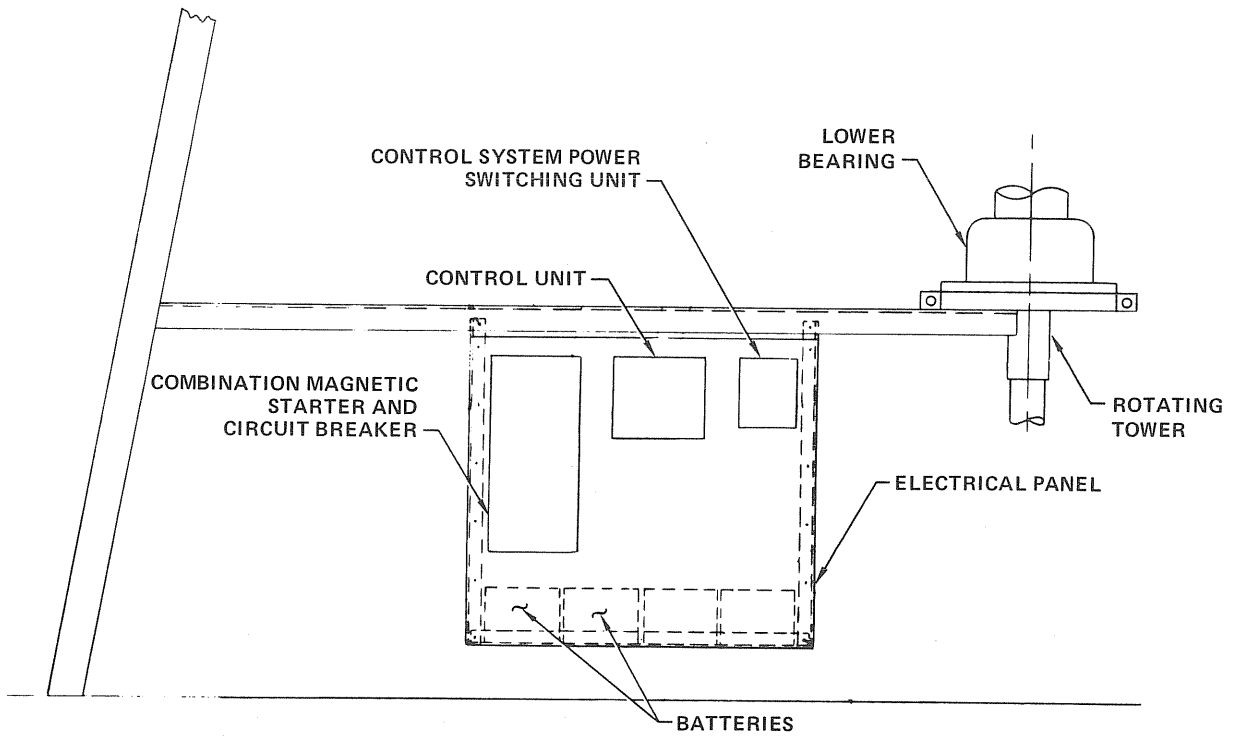
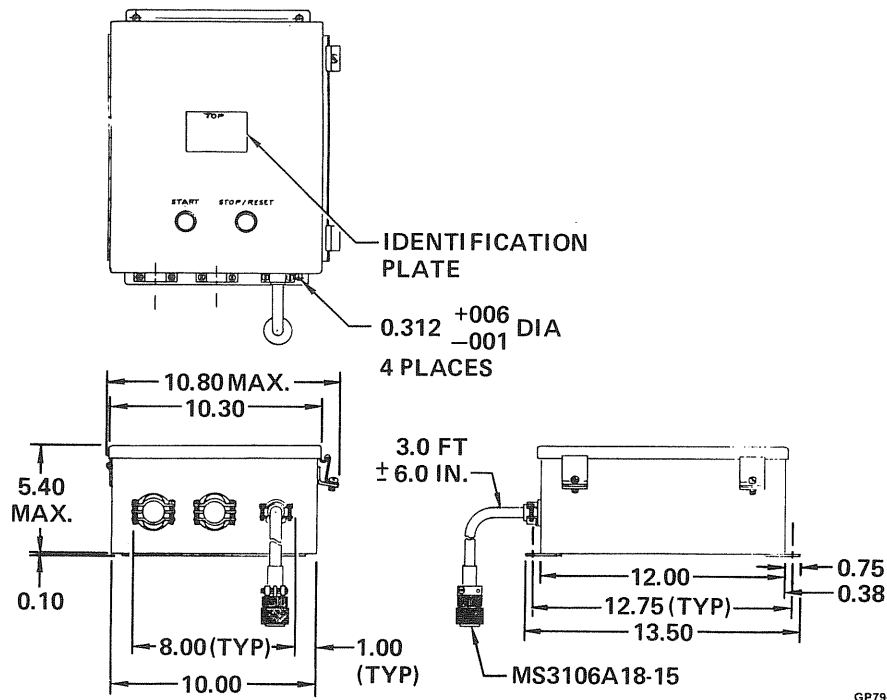


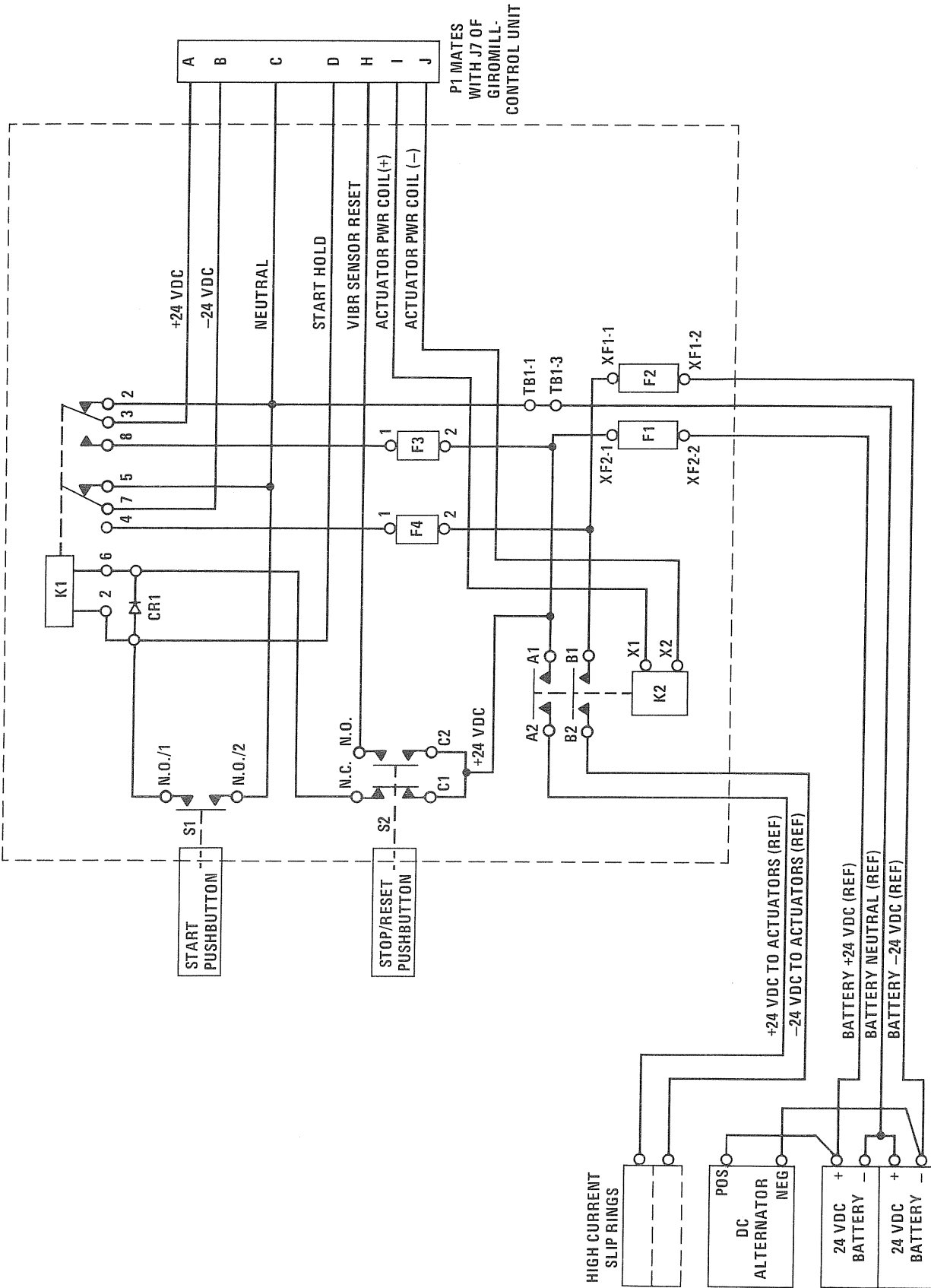
FIGURE 151
ELECTRICAL PANEL

GP79-0636-79



GP79-0573-39

FIGURE 152
ENVELOPE DRAWING GIROMILL CPSU



GP79-0636-100

FIGURE 153
GIROMILL CPSU SCHEMATIC DIAGRAM

unit. The "START HOLD" signal is normally present as soon as relay K1 is activated, and is removed via the control unit if (1) the vibration sensor is tripped, (2) the processor fails, or (3) the processor detects a system failure. F1 and F2 are 100 amp fuses and F3 and F4 are low current 3 amp fuses. A power control flow diagram is shown in Figure 154.

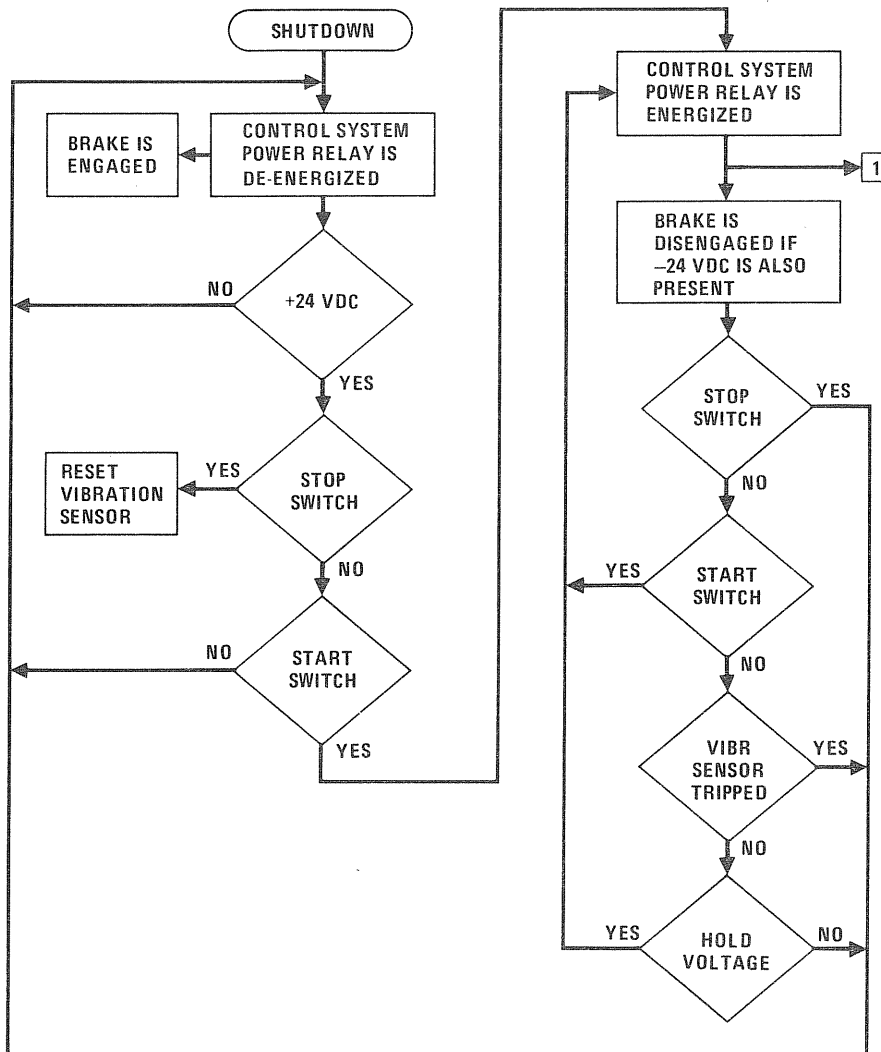


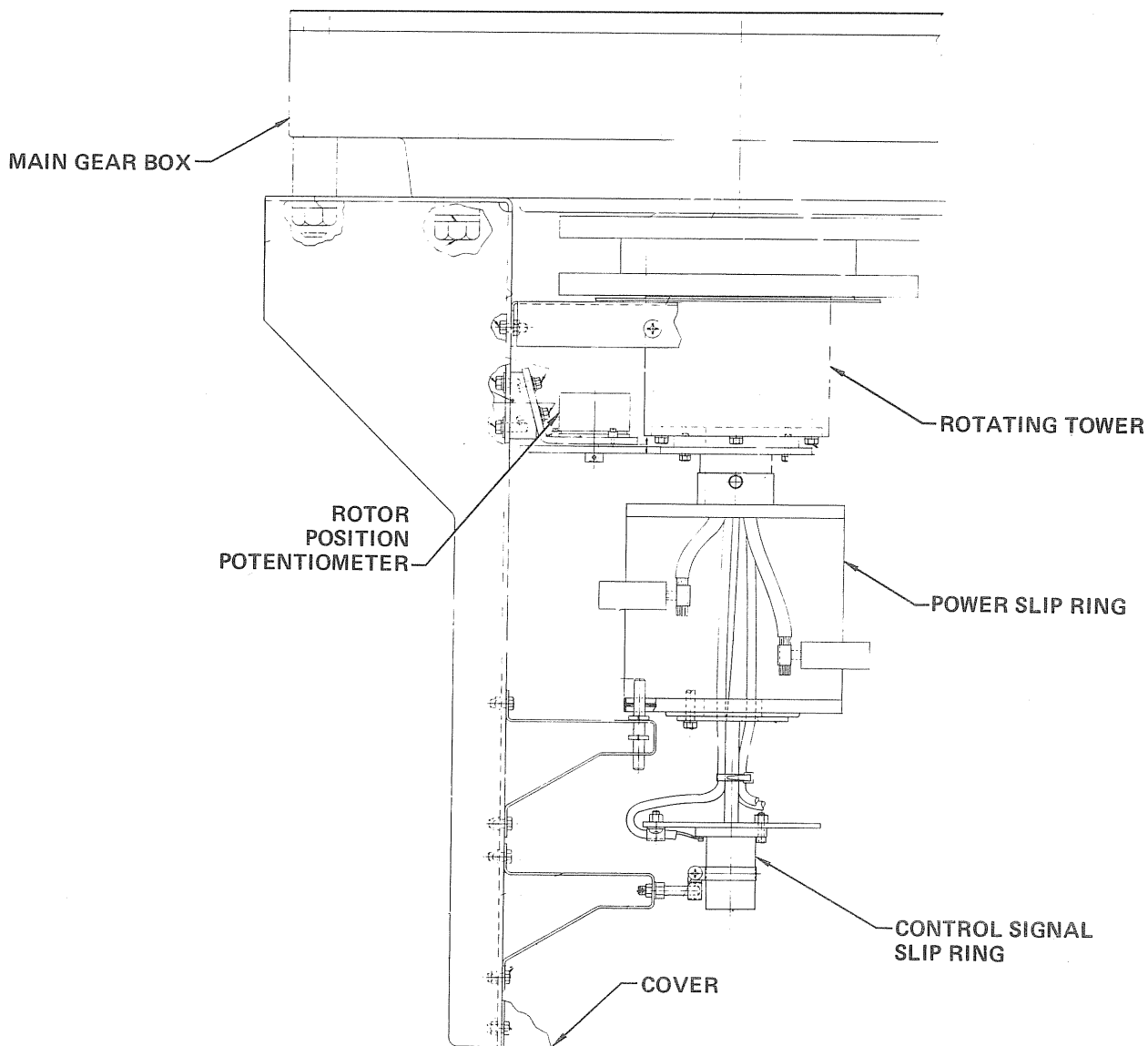
**FIGURE 154
POWER CONTROL FLOW DIAGRAM**

10.5 INTERCONNECT WIRING - Electrical power to the actuators is conducted through the power slip rings, manufactured by Aero-Motive, at the lower end of the rotating tower. Control signals are conducted through the control signal slip rings mounted below the power slip rings. Figure 155 shown the slip ring assembly.

The control signal slip rings have 20 channels and are manufactured by Michigan Scientific Corporation. 15 signal channels are required for the control system leaving 5 channels available for instrumentation. In

event more instrument channels are required a 36 channel slip ring assembly can be used in place of the 20. Two #6 AWG 48 Vdc power wires and a shielded cable containing two twisted pairs of signal wires are routed up the rotating tower and through the lower support arm to each blade actuator, as shown in Figure 156.

Figure 155 shows the location of the position potentiometer which is driven by a gear at the lower end of the rotating tower.



GP79-0636-80

FIGURE 155
SLIP RING ASSEMBLY

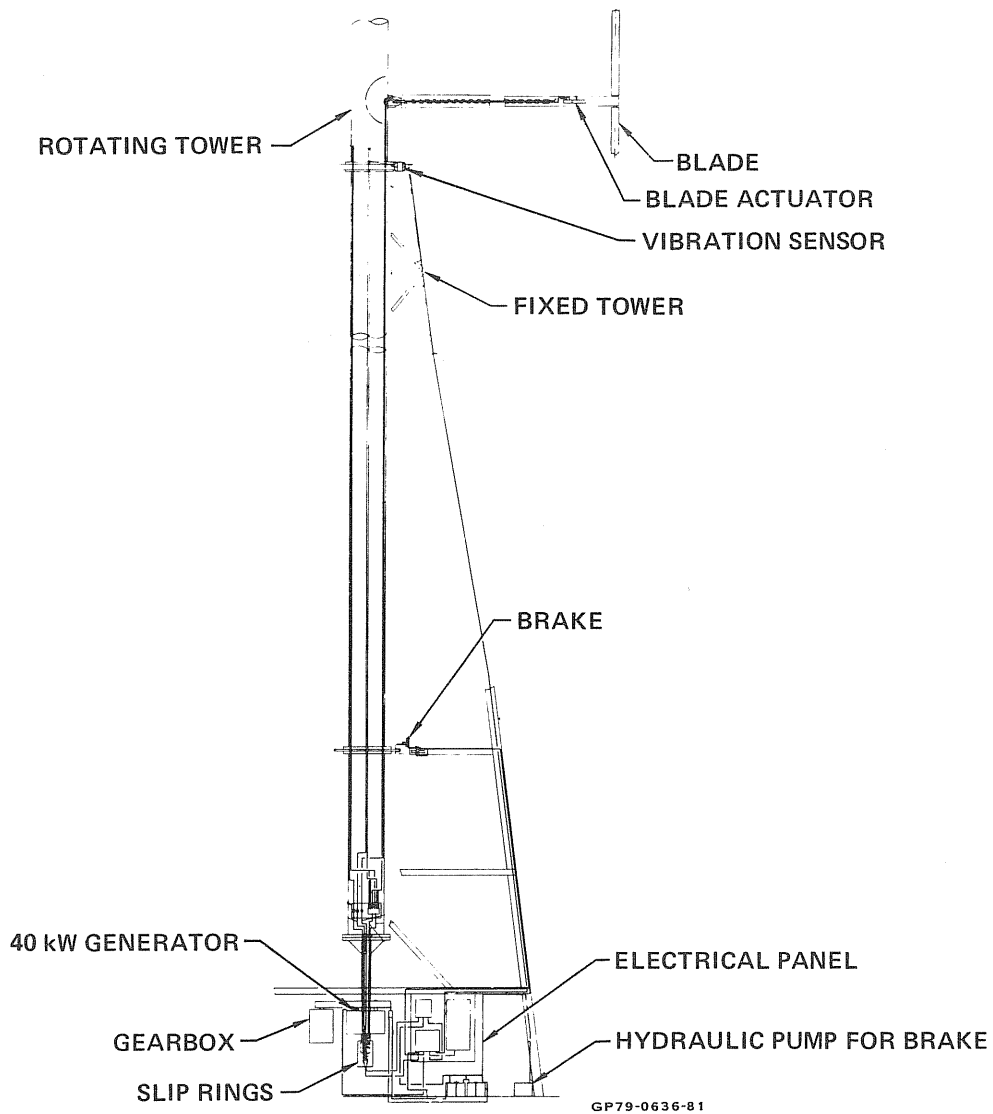


FIGURE 156
WIRE ROUTING

11. MECHANICAL AND ELECTRICAL OUTPUT POWER SYSTEM

11.1 RPM INCREASER - A shaft mounted helical gearbox, manufactured by Reliance Electric Company, (Figure 157) is mounted on the lower end of the rotating tower. It has a gear ratio of 24.3 to 1. The output shaft then drives the generator through a toothed belt stage of 2.25 to 1 for an overall increase in RPM of 54.675 to 1. The toothed belt, manufactured by Goodyear Tire and Rubber Company, is used to give a positive drive to the generator for RPM control. For the electrical output design 1 described in 11.2, the generator speed is 1830 RPM. Figures 158 and 159 show the electrical drive system assembly.

The torque of the gearbox is resisted with tubular member, extended to one of the fixed tower legs. A shear pin is designed into one of the pulleys to protect the drive train from excessive torque (see Figure 159).

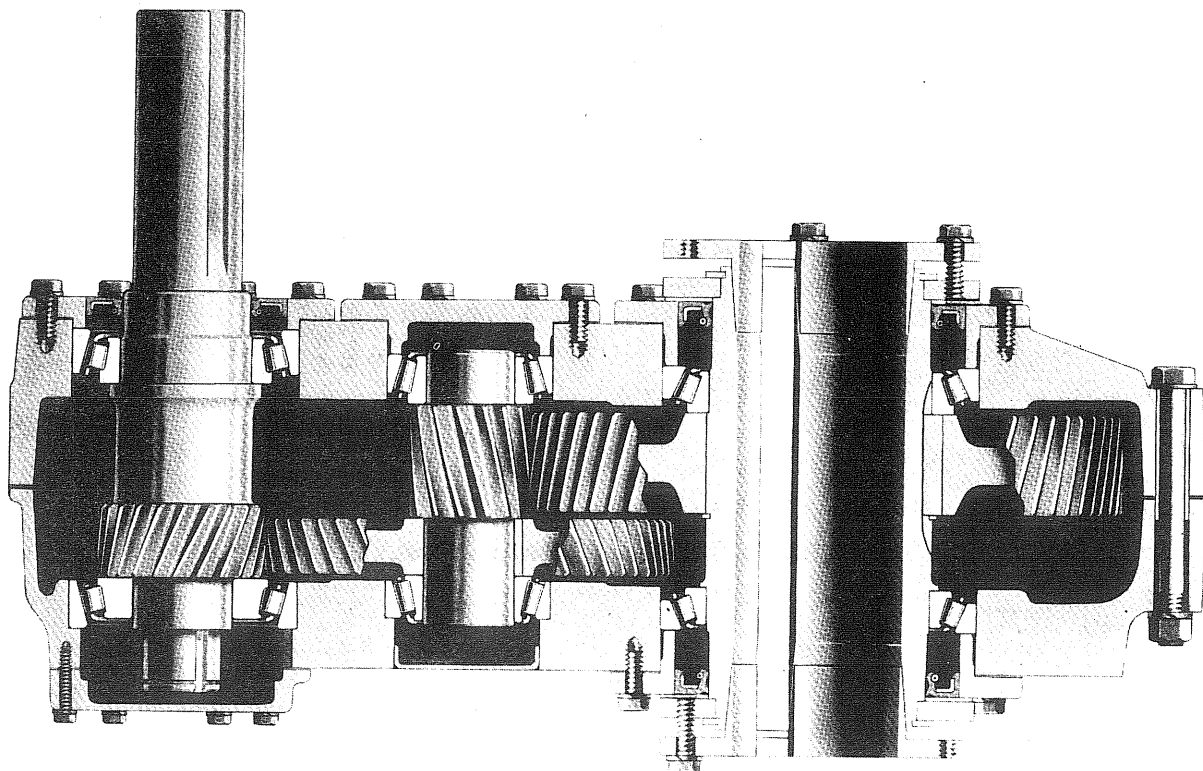
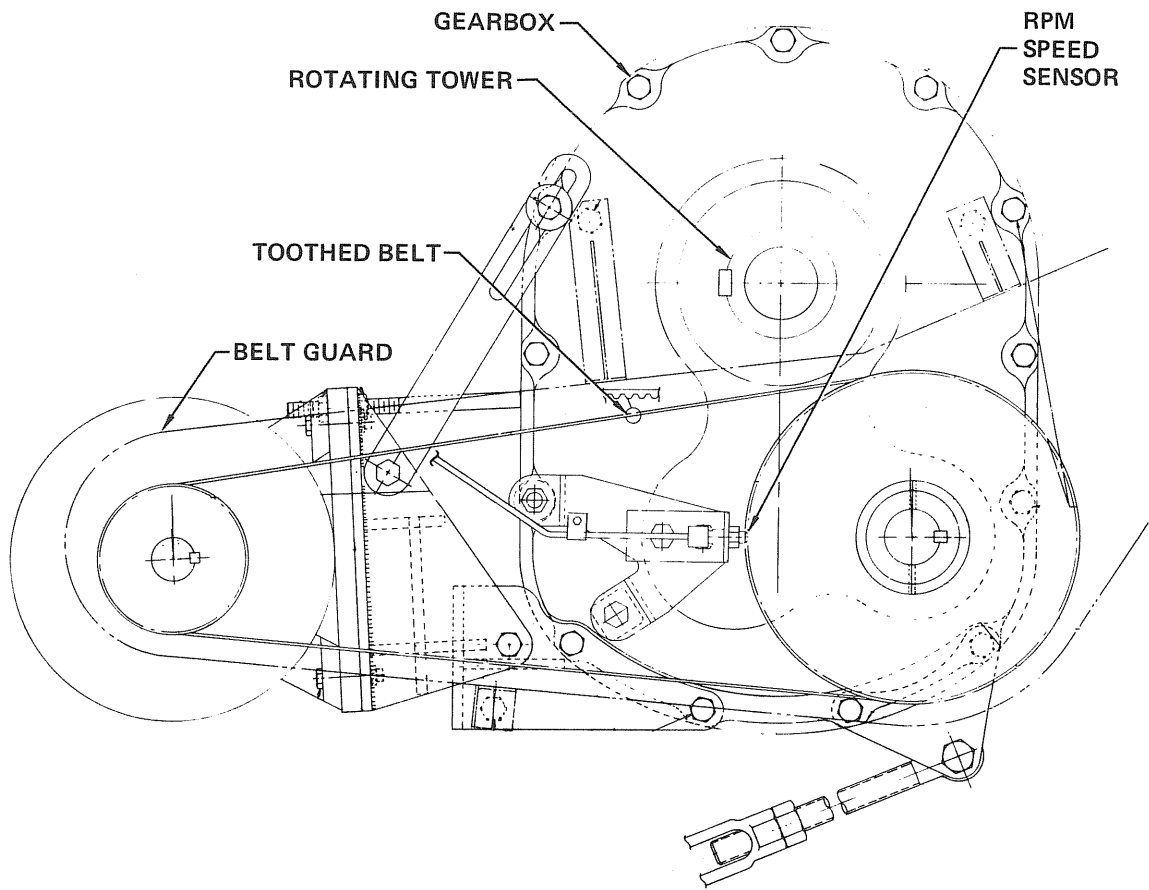


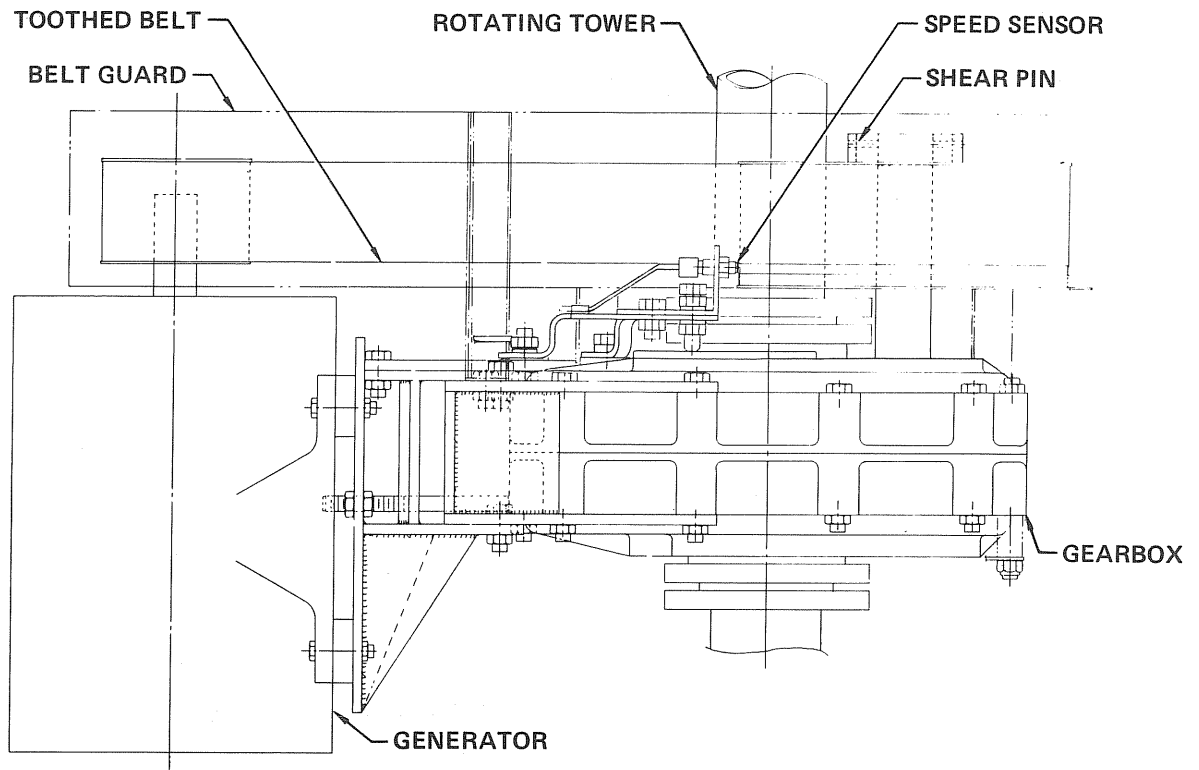
FIGURE 157
SPEED INCREASER

GP79-0349-03



GP79-0636-69

FIGURE 158
ELECTRICAL DRIVE SYSTEM ASSEMBLY
Plan View

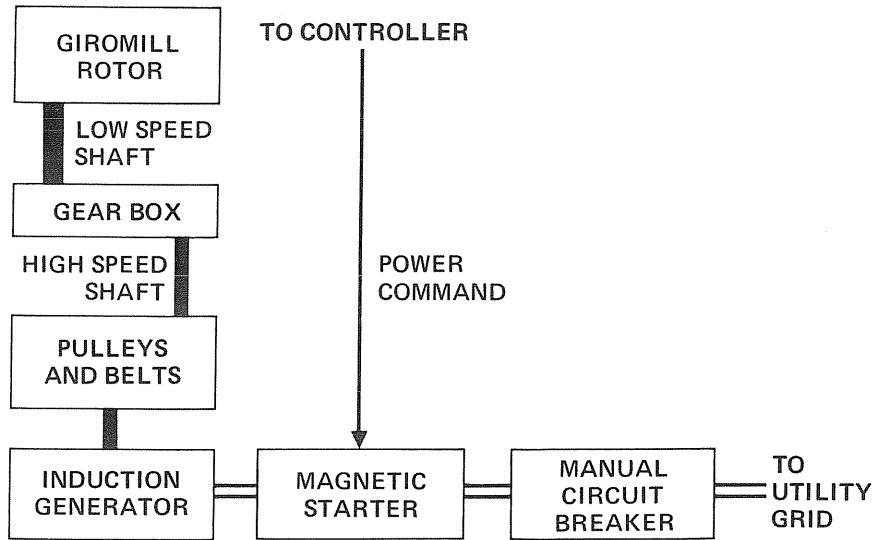


GP79-0636-70

FIGURE 159
ELECTRICAL DRIVE SYSTEM ASSEMBLY
 Side View

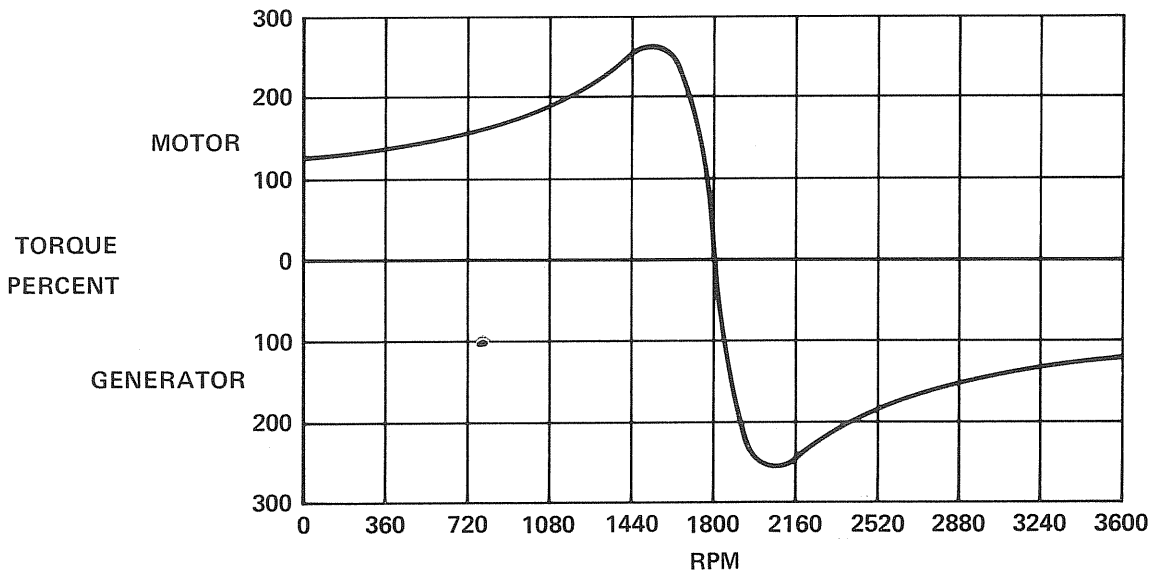
11.2 ELECTRICAL OUTPUT DESIGN 1 - An induction generator, manufactured by Gould, Inc., is used to feed three phase 480 volt, 60 Hz power into a large utility grid. A magnetic starter is controlled by signals from the control system to connect or disconnect the Giromill to or from the utility grid (reference connector J3 on Figure 138). A manual circuit breaker is provided to disconnect the Giromill from the utility grid. Figure 160 is a block diagram of Design 1. Figure 161 shows the characteristic torque curve of the generator.

11.3 ELECTRICAL OUTPUT DESIGN 2 - Design 2 is a three phase 480 volt, 60 Hz stand-alone system. A synchronous generator, with voltage regulator and exciter, is used to produce electrical power. The generator is run at 1800 RPM. Power is fed to the load through a magnetic starter and manual circuit breaker. The starter is controlled by the Giromill control system (connector J3). Figure 162 is a block diagram for Designs 2 and 3.



GP79-0349-103

FIGURE 160
BLOCK DIAGRAM OF GIROMILL ELECTRICAL OUTPUT POWER FOR OPERATION WITH A LARGE UTILITY GRID - DESIGN 1



GP79-0636-129

FIGURE 161
TORQUE vs RPM

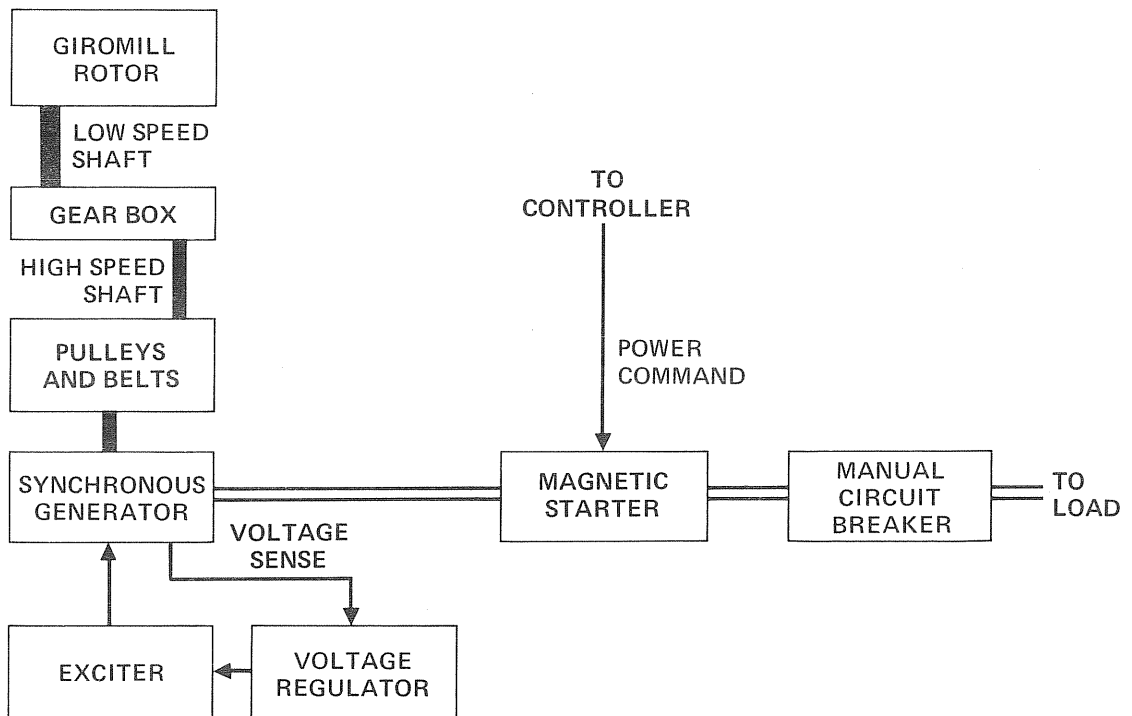


FIGURE 162
BLOCK DIAGRAM OF GIROMILL ELECTRICAL
OUTPUT POWER SYSTEM FOR OPERATION
AS A SINGLE UNIT
 Designs 2 and 3

11.4 ELECTRICAL OUTPUT DESIGN 3 - Electrical Output Design 3 is identical to Design 2, except that the voltage is 240 volts.

11.5 ELECTRICAL OUTPUT DESIGN 4 - Design 4 is a three phase 480 volt 60 Hz Giromill suitable for tie-in with one or more other small generators as part of a small utility grid. A synchronous generator, with voltage regulator and exciter, is used to produce electrical power. The generator is run at 1800 RPM.

A load sensor is provided to feed information to the Giromill controller so the machine will pick up the load properly. The power is fed to the load through a magnetic starter and a manual circuit breaker. A voltage sense from each side of the magnetic starter through step-down transformers is sent to the Giromill controller so it can synchronize the generator to the grid before the magnetic starter is closed. Figure 138 shows the control unit connections to perform these functions. The magnetic starter is closed by the Giromill control unit using the existing grid connect wiring (connector J3). See Figure 163 for the block diagram of Design 4.

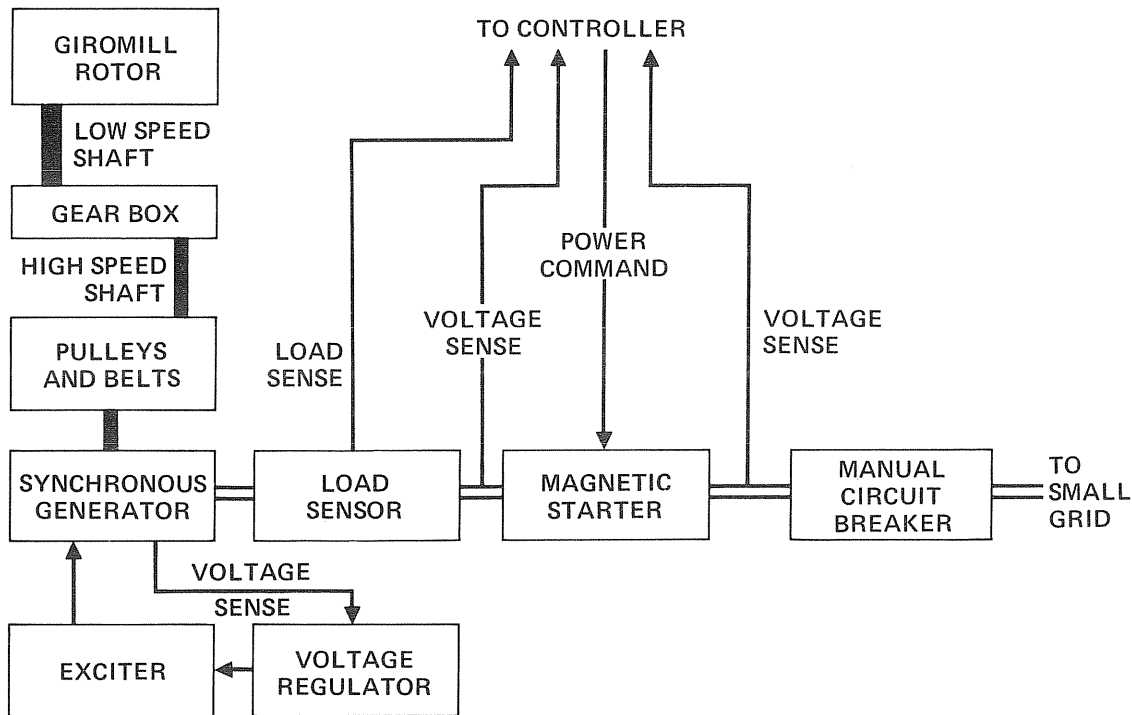


FIGURE 163
BLOCK DIAGRAM OF GIROMILL ELECTRICAL OUTPUT
POWER SYSTEM FOR OPERATION WITH TWO OR MORE
MACHINES TO FORM AN INDEPENDENT SMALL UTILITY GRID
 Design 4

11.6 MECHANICAL OUTPUT KIT - The Mechanical Output Kit converts the Giromill from electrical output to a 1760 RPM horizontal mechanical shaft output. A right angle gearbox and mounting bracket replaces the electrical generator (see Figures 164 and 165). A slightly larger pulley is used, changing the ratio of the toothed belt stage to 2.16 to 1 and the overall ratio of the RPM increaser to 52.488 to 1. This ratio provides 1760 RPM at the horizontal output shaft.

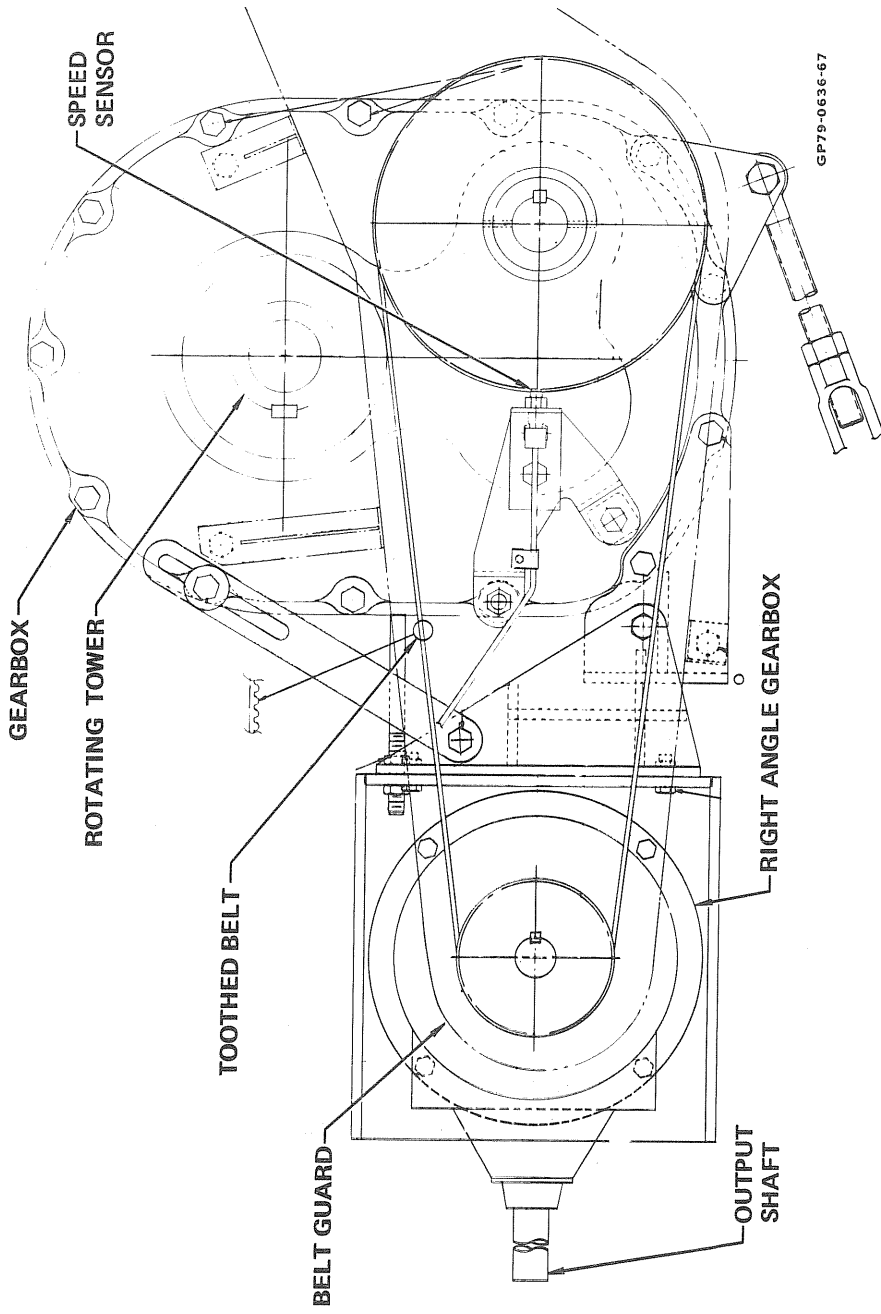


FIGURE 164
MECHANICAL DRIVE SYSTEM ASSEMBLY
 Plan View

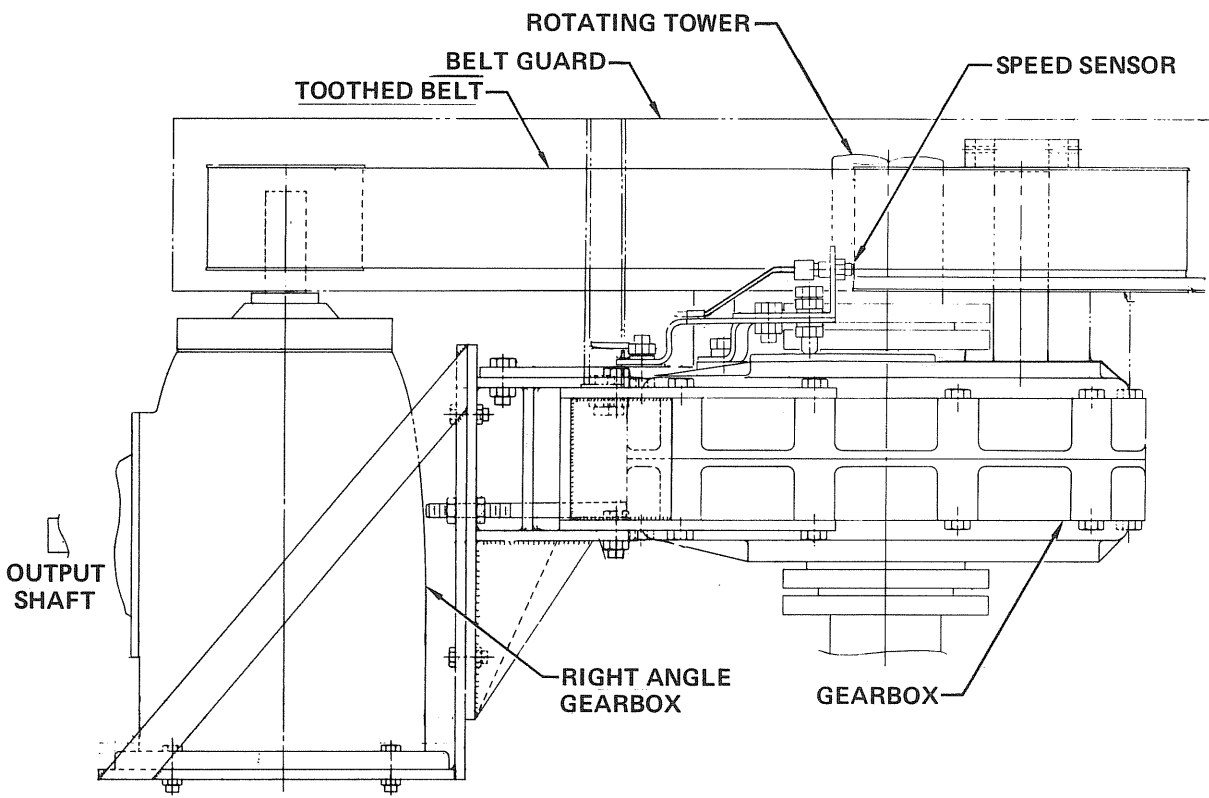


FIGURE 165
MECHANICAL DRIVE SYSTEM ASSEMBLY
 Side View

12. FAILURE MODE AND EFFECTS ANALYSIS

An analysis was conducted to determine the possible modes of failure and their effects on system reliability and safety. The critical sub-systems and components considered and their effects in event of failure are shown in Figure 166.

From this analysis, two failures were considered to be somewhat critical. One was if the wind speed sensor operates slower than the actual wind (second item on first page of Figure 166). This could cause the Giromill to be operating at a wind velocity greater than 40 MPH. The only critical thing about that is that the blade actuators may not be able to follow the specified rock angle schedule, making them work too hard. This could cause an actuator to burn out, creating a controller shutdown.

The other item is where the line magnetic contactor fails closed and, for some reason, shutdown is commanded by the controller (second item on last page of Figure 166). Then, if the RPM is below rated speed, the generator will drive the Giromill. Commanding a shutdown under these conditions means that the brake would be applied, but the generator would be trying to keep up the RPM. The probable result would be an overloading of the generator circuit breakers, opening the line.

All other failures are non-critical. There are several, though where the Giromill could be driven by the generator. If this is not identified by the operator, a substantial amount of power could be lost.

FAILURE MODE	EFFECTS ANALYSIS
● CONTROL UNIT PROCESSOR	TIMEOUT CIRCUIT IS NOT RETRIGGERED AND RELEASES START RELAY'S HOLDING VOLTAGE WITHIN ≈ 100 MILLI-SECONDS.
● WIND SPEED SENSOR – STOP OR WIRE BREAK – SLOWER THAN SPECIFIED	SYSTEM GOES TO STANDBY MODE. GIROMILL COULD BE OPERATING AT $V_w > 40$ MPH.
● WIND DIRECTION SENSOR	PROCESSOR DETECTS ABSENCE OF CHANGE IN WIND DIRECTION AND COMMANDS SHUTDOWN.
● RPM SENSOR	PROCESSOR CONTROLLED SHUTDOWN.
● ROTOR POSITION SENSOR	PROCESSOR CONTROLLED SHUTDOWN.
● VIBRATION SENSOR – WIRE BREAK – CONTACT SHORT	EMERGENCY SHUTDOWN EXCESSIVE VIBRATION - NO DETECTION
● EXCESSIVE TOWER VIBRATION	VIBRATION SENSOR CONTACTS OPEN AND RELEASE START RELAY - EMERGENCY SHUTDOWN.
● DC POWER ELECTRICAL SHORT	FUSE OPENS IN CONTROL SYSTEM POWER SWITCHING UNIT (CSPSU) – EMERGENCY SHUTDOWN

**FIGURE 166
FAILURE MODE EFFECTS ANALYSIS**

FAILURE MODE	EFFECT ANALYSIS
<ul style="list-style-type: none"> ● DC POWER WIRE BREAKS BETWEEN BATTERY AND CSPSU OR C PSPU AND CONTROL UNIT. 	<p>EMERGENCY SHUTDOWN - POWER SWITCHING RELAYS DEPEND ON BOTH +24 VDC AND -24 VDC.</p>
<ul style="list-style-type: none"> ● DC POWER WIRE BREAKS BETWEEN C PSPU AND ACTUATOR. 	<p>PROCESSOR CONTROLLED SHUTDOWN.</p>
<ul style="list-style-type: none"> ● OVERSPEED - WIND GUST 	<p>PROCESSOR RELEASES POWER TO ACTUATORS, DISCONNECTS GRID POWER, AND RECYCLES THROUGH STARTUP WHEN $\omega < \text{RPM}_{\text{MIN}}$.</p>
<ul style="list-style-type: none"> ● BLADE BEARING 	<p>PROCESSOR CONTROLLED SHUTDOWN OR VIBRATION SENSOR EMERGENCY SHUTDOWN.</p>
<ul style="list-style-type: none"> ● BELT BREAKS <ul style="list-style-type: none"> - BLADE-ACTUATOR - GENERATOR - ALTERNATOR 	<p>PROCESSOR CONTROLLED SHUTDOWN IF RPM CANNOT BE MAINTAINED.</p> <p>GENERATOR IS DRIVEN BY POWER LINE-GIROMILL CONTINUES TO OPERATE.</p> <p>BATTERIES DISCHARGE UNTIL PROCESSOR DETECTS AND CONTROLS SHUTDOWN.</p>

**FIGURE 166 (Continued)
FAILURE MODE EFFECT ANALYSIS**

FAILURE MODE	EFFECT ANALYSIS
● ACTUATOR POWER AMPLIFIER	PROCESSOR CONTROLLED SHUTDOWN
● ACTUATOR CONTROL ELECTRONICS	PROCESSOR CONTROLLED SHUTDOWN
● SHEAR PIN BREAKS	PROCESSOR DETECTS DIFFERENCE BETWEEN RPM SENSOR AND ROTOR POSITION SENSOR – PROCESSOR CONTROLLED SHUTDOWN
● MAIN BEARING	PROCESSOR CONTROLLED SHUTDOWN IF RPM CANNOT BE MAINTAINED OR VIBRATION SENSOR EMERGENCY SHUTDOWN
● BRAKE ENGAGES INADVERTANTLY	PROCESSOR CONTROLLED SHUTDOWN IF RPM CANNOT BE ATTAINED OR MAINTAINED
● STRUCTURAL FAILURE	PROCESSOR CONTROLLED SHUTDOWN OR VIBRATION SENSOR EMERGENCY SHUTDOWN

**FIGURE 166 (Continued)
FAILURE MODE EFFECT ANALYSIS**

FAILURE MODE	EFFECT ANALYSIS
<ul style="list-style-type: none"> ● POWER UTILITY WIRE BREAKS 	<p>INDUCTION GEN LOSES EXCITATION. CONTACTOR OPENS. GIROMILL CONTINUES TO ROTATE UNLOADED.</p>
<ul style="list-style-type: none"> ● MAGNETIC CONTACTOR <ul style="list-style-type: none"> – FAILS CLOSED – FAILS OPEN 	<p>NO EFFECT WHILE GIROMILL IS AT RATED SPEED. GENERATOR DRIVES GIROMILL IF BELOW RATED SPEED. MANUAL STOP REQUIRED. IF BRAKE APPLIED, CIRCUIT BREAKER OVERLOADS AND OPENS. INDUCTION GENERATOR LOSES EXCITATION. GIROMILL OPERATES UNLOADED.</p>
<ul style="list-style-type: none"> ● GENERATOR FAILURE <ul style="list-style-type: none"> – OPEN WINDING – GROUNDED WINDING 	<p>GENERATOR WILL NOT PRODUCE POWER. GIROMILL OPERATES UNLOADED. CIRCUIT BREAKERS OVERLOAD AND OPEN. GIROMILL OPERATES UNLOADED.</p>
<ul style="list-style-type: none"> ● GENERATOR MECHANICAL FAILURE (EXCESSIVE DRAG) 	<p>PROCESSOR CONTROLLED SHUTDOWN BECAUSE GIROMILL CANNOT REACH RATED RPM.</p>

**FIGURE 166 (Concluded)
FAILURE MODE EFFECT ANALYSIS**

13. TEST INSTRUMENTATION

Desired quantities to be measured by installed instrumentation during the test phase include structural loads, structural vibration frequencies and mode shapes, control system performance parameters, and overall Giromill performance. Instrumentation to acquire these data during the test has been defined. Figures 167 and 168 present the structural instrumentation required. Figure 169 shows other sensors or measurements needed. Data specified as coming from the controller is available from an instrumentation plug on the control unit enclosure mounted on the control/electrical system panel.

Discussion with Rocky Flats test personnel revealed that all these quantities could not be handled at this time, by the available test site equipment. Consequently a partial instrumentation approach was defined. This approach made provisions for the extracting of all the data. However, at this time only the bare minimum of instrumentation would be hooked up. This partial instrumentation approach is shown in Figure 170.

One blade will have the instruments installed during assembly with the wires routed to a terminal connector and tied off. Provisions will be made in the same blade for mounting a signal conditioner and multiplexer. Also a series of slip rings will be manufactured and installed between the blade and support arm to transfer multiplexed conditioned data from the blade to the rotor.

Three thermocouples will be mounted in an actuator and the wires taped and tied down. To gain a qualitative insight of actuator temperatures, several temperature sensitive indicators will be put on an actuator. Provisions will be made to install signal conditioning and multiplexing equipment on the rotor. Also, a larger control signal slip ring that can accommodate the instrumentation data can be easily installed.

The fixed tower will have the strain gauges and accelerometers installed after assembly of the Giromill. The wires for these instruments will be run down to a terminal connector on the control/electrical panel. These instruments can be hooked up and data taken depending on the number of recorders available.

Control system parameters, such as rock angles, rotor position, and wind velocity, are available from the instrumentation plug on the controller box. Again, depending on the ground equipment available, these can be hooked up and data taken.

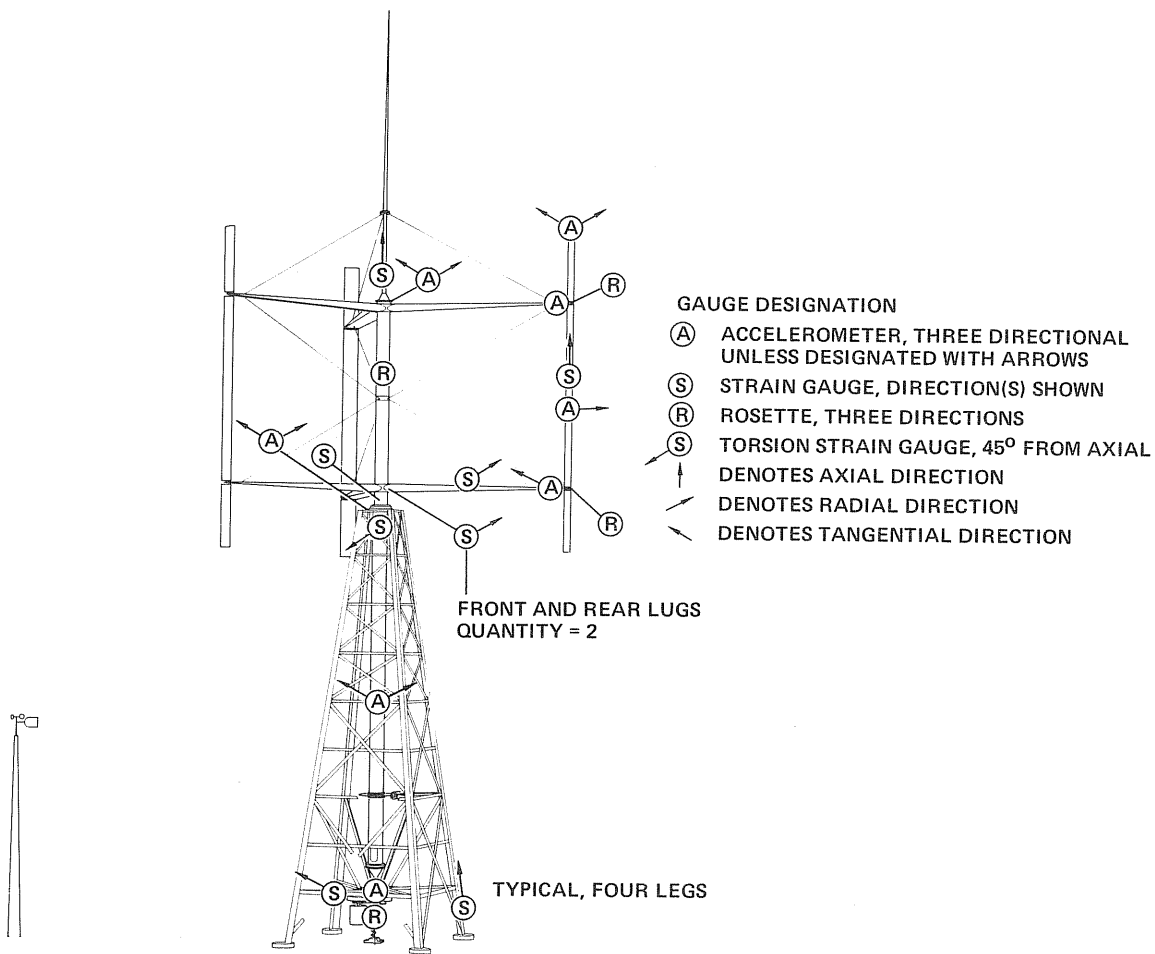


**FIGURE 167
GIROMILL SCHEMATIC WITH INSTRUMENTATION LOCATION**

INSTRUMENTATION TYPE AND LOCATION						
COMPONENT	ACCELEROMETERS		STRAIN GAUGES		ROSETTES	
	NO.	LOCATION	NO.	LOCATION	NO.	LOCATION
BLADES UPPER CENTER LOWER	2 1	END RIB (RADIAL AND TANGENTIAL) MID-SPAN (RADIAL)	1	MID-SPAN (AXIAL)	1 1	STEEL TUBE NEAR OUTBOARD RIB STEEL TUBE NEAR LOWER OUTBOARD RIB
SUPPORT ARMS UPPER LOWER	3 1	OUTER END OF UPPER SURFACE (3-AXIS) OUTER END OF UPPER SURFACE (TANGENTIAL)	1 2	UPPER SURFACE NEAR MID-AXIS (RADIAL) FORE AND AFT AT ARM ROOT LUGS		
ROTATING	2 2	BOTTOM OF SMALL TUBE (RADIAL AND TANGENTIAL) BETWEEN UPPER AND LOWER BEARINGS (RADIAL AND TANGENTIAL)	1 1 1	BOTTOM OF SMALL TUBE (AXIAL) ABOVE UPPER BEARING (AXIAL) TORSION BELOW UPPER BEARING	1 1	MID-SPAN BETWEEN SUPPORT ARMS BETWEEN LOWER BEARING AND SPEED INCREASER
FIXED TOWER AND TRANSMISSION	2	TOP OF FIXED TOWER (RADIAL AND TANGENTIAL)	4 1	BOTTOM OF EACH LEG (AXIAL) TRANSMISSION TORQUE ARM		
TOTAL	16		12		4	

(1) Intensive testing data collection gauges

**FIGURE 168
STRUCTURAL INSTRUMENTATION**

	MEASURED PARAMETER	SENSOR	COMMENT
SUPPORT ARMS LOWER	3 TEMPERATURES 2 ACTUATOR MOTOR 1 MOTOR AMPLIFIER	THERMOCOUPLE	INTENSIVE TESTING
ROTOR	1 POSITION OF ARM 1 1 ROTOR RPM 1 WIND DIRECTION 1 WIND SPEED 1 WIND DIRECTION 1 WIND SPEED 3 ROCK ANGLE COMMANDS θ_{RC1} , θ_{RC2} AND θ_{RC3} 3 ROCK ANGLE POSITION θ_{R1} , θ_{R2} AND θ_{R3}	FROM CONTROLLER FROM CONTROLLER FROM CONTROLLER WIND DIRECTION SENSOR WIND SPEED SENSOR FROM CONTROLLER FROM CONTROLLER	INTENSIVE AND LONG TERM TESTING ROCKWELL SUPPLIED FOR DATA REDUCTION ALL THREE FOR INTENSIVE TESTING ONE FOR LONG TERM
ELECTRICAL SYSTEM ONLY	3 VOLTAGE (EACH PHASE) 3 CURRENT (EACH PHASE) 1 POWER 1 POWER FACTOR 1 GENERATOR WINDING TEMPERATURE	VOLTIMETER AMMETER WATTMETER COMPUTED OHMMETER (WHEATSTONE BRIDGE)	ROCKWELL SUPPLIED INTENSIVE AND LONG TERM TESTING GROUND MEASUREMENT
MECHANICAL SYSTEM ONLY	1 OUTPUT TORQUE 1 OUTPUT RPM	TORQUEMETER RPM SENSOR	ROCKWELL SUPPLIED ROCKWELL SUPPLIED

GP79-0573-14

**FIGURE 169
ADDITIONAL SENSORS OR CONTROLLER SUPPLIED MEASUREMENTS**

- **BLADE**
 - INSTALL STRAIN GAUGES AND ACCELEROMETERS-
3 ACCELEROMETERS, 1 STRAIN GAUGE AND 2 ROSETTES
 - RUN WIRES TO JUNCTION TERMINAL
 - MAKE MOUNTING PROVISIONS FOR SIGNAL CONDITIONER
AND MULTIPLEXER
 - INSTALL SLIP RINGS BETWEEN BLADE AND SUPPORT ARM
- **SUPPORT ARM**
 - INSTALL TEMPERATURE PROBES IN ACTUATORS -
3 THERMOCOUPLES
 - USE TEMPERATURE SENSITIVE INDICATORS ON
ACTUATOR MOTORS
- **FIXED TOWER**
 - INSTALL STRAIN GAUGES AND ACCELEROMETERS-
2 ACCELEROMETERS AND 5 STRAIN GAUGES
 - HOOK UP AND USE AS NEEDED
- **CONTROL PARAMETERS AVAILABLE**

FIGURE 170
PARTIAL INSTRUMENTATION APPROACH

14. TEST PLAN

Preliminary testing will be performed with the electrical system configuration at Valley Industries Plant at Tallulah, La. Tests will include pre-start inspections, functional instrumentation checks and limited functional testing. These tests will be repeated at Rocky Flats along with the conduct of data collection phases categorized as long term and intensive. Long term data collection at Rocky Flats will include the continuous measurement of machine performance and measurement of the input wind characteristics. Intensive testing data collection is characterized by short periods of data collection during continuous Giromill operation, as well as during specific operational conditions critical to structural and dynamic performance characteristics of the machine.

The overall plan is to proceed through the following test phases at Rocky Flats with the electrical system configuration.

- Pre-start up checkout
- First start up checks
- Dynamic tests
- Performance tests
- Special tests

Upon satisfactory completion of electrical system tests, the unit will be converted to the mechanical system for final operational testing.

14.1 PRE-START UP CHECKOUT - This checkout consists of a visual inspection of the entire system, and a functional check of selected systems. It will be performed by contractor personnel (MDC and Valley) at Tallulah, and by Rockwell personnel at Rocky Flats, before the unit is started for the first time.

Pre-start up checkout can be accomplished without a wind blowing. However, a visual verification of the blade weathervaning shall have been made.

14.1.1 Visual Checkout - A visual inspection of the entire Giromill assembly shall be conducted to assure all parts are properly installed and serviced. A check list of the critical areas requiring a visual inspection and the servicing checks has been completed to facilitate this visual inspection, Figure 171. Parts of this inspection will be accomplished as the Giromill is being assembled, with the inspector verifying correct assembly per the drawings.

14.1.2 Functional Checks - The control system, brake system, and vibration sensor will have one final functional check performed before the Giromill is certified ready for operation. These checks will be performed as outlined in Figure 172.

14.2 FIRST START UP CHECKS - ELECTRICAL CONFIGURATION - Start up checks will be performed at Tallulah, by contractor personnel at Rocky Flats by Rockwell personnel, with contractor personnel present.

1. MAIN ROTOR BEARINGS CORRECTLY ADJUSTED. WITH ROTOR TURNING SLOWLY, EITHER MANUALLY OR BY ITSELF, LISTEN AT THE BEARINGS AND FEEL THE BEARINGS TO ASSURE SMOOTH OPERATION.
2. DISK BRAKE CORRECTLY ADJUSTED AND NOT RUBBING. PERFORM THIS CHECK AT THE SAME TIME THE MAIN BEARINGS ARE CHECKED.
3. BLADE BEARINGS CHECKED. TURN BLADES BY HAND AND LISTEN AND FEEL FOR SMOOTH BEARING OPERATION. DO PRIOR TO INSTALLING ACTUATOR BELT.
4. BLADE SEALS ADJUSTED FOR SMOOTH AND EASY BLADE OPERATION.
5. SUPPORT ARMS ALIGNED, CABLES TENSIONED, AND COTTER PINS INSTALLED CORRECTLY. VERIFY DURING INSTALLATION.
6. BLADE ACTUATORS CORRECTLY INSTALLED AND ALIGNED WITH BLADE. SHAFT TURNS FREELY. ACTUATOR BELT TENSION CORRECT. NOTE: CHECK ALL BELT TENSIONS AS PER GOODYEAR POSITIVE DRIVE BELT PROCEDURES.
7. ROTOR POSITION POTENTIOMETER ALIGNED WITH THE WIND DIRECTION SENSOR. CHECK THIS DURING INSTALLATION. CHECK FOR SMOOTH OPERATION OF POTENTIOMETER GEARING WHEN GIROMILL TURNED SLOWLY FOR BEARING CHECK.
8. SPEED INCREASER OPERATES SMOOTHLY. CHECK THIS WHEN GIROMILL TURNED SLOWLY FOR BEARING CHECK.
9. SLIP RINGS WIRING NOT RUBBING.
10. ALL BELTS CORRECTLY TENSIONED.
11. WIRING ALL HOOKED UP. NO LOOSE WIRES OR FRAYED INSULATION. WIRING CONNECTORS TIGHT. STRAIN RELIEF CLAMPS PROPERLY INSTALLED.
12. ALL BOLTS, SCREWS, AND NUTS ARE TIGHT. ALL INSPECTION AND ACCESS COVERS INSTALLED. SAFETY COVERS INSTALLED. ASSEMBLY JIGS, ALIGNMENT PINS, AND OTHER FIXTURES REMOVED.
13. ALL COMPONENTS SERVICED:
 - BATTERIES – FLUID SPECIFIC GRAVITY CHECKED.
 - MAIN BEARINGS GREASED.
 - BLADE BEARINGS GREASED.
 - BRAKE SYSTEM HYDRAULIC FLUID AND ACCUMULATOR PRESSURE.
 - SPEED INCREASER OIL LEVEL.
 - BLADE ACTUATOR OIL LEVEL.

FIGURE 171
VISUAL INSPECTION CHECKOUT LIST

1. CONTROL SYSTEM
USE BUILT IN SINE WAVE BLADE ROCK ANGLE MODULATION PROFILE. CONNECT UP RECORDING INSTRUMENTS (θ_R , θ_C , T_A). WITH ROTOR LOCKED ACTUATE BLADES. VISUAL CHECK OF SINE WAVE BLADE MODULATION.
2. BRAKE SYSTEM
MANUALLY CONNECT 48V ACROSS BRAKE SOLENOIDS TO CHECK OPERATION. CHECK PUMP AND PRESSURE SWITCH OPERATION BY LEAKING FLUID OUT OF A LINE.
3. VIBRATION SENSOR
CONNECT METER TO VIBRATION SENSOR CIRCUIT. LOOSEN SENSOR MOUNTING. MANUALLY SHAKE TO OPEN CIRCUIT.

GP79-0636-118

FIGURE 172 FUNCTIONAL CHECK OF SELECTED SYSTEMS

First start up will not be attempted in any wind greater than 25 MPH. The controller will be configured to give a blade modulation for the $\lambda_F = 1.13$ cam profile. This will limit rotor RPM to about 15. When this limit has been reached, the stop button will be depressed to simulate an emergency stop.

The $\lambda_F = 1.13$ cam profile will also be used in the next check. When the RPM is again stabilized, the wind speed sensor will be disconnected. This will simulate that the wind is below 10 MPH, and the controller will begin decrementing the wind in-range counter. After about one minute, the controller will signal for the blades to be released. The Giromill will stabilize on RPM (or stop) with the blades released, and then the stop button will be pushed to engage the brake.

The Giromill will then be run up using the normal control scheme of varying the cam profiles. RPM will be limited to 15, and if everything is all right, speed will be increased to 20, 25, and finally 33.5 RPM. At each of these RPM points the blades will be released by disconnecting the wind speed sensor.

Operating RPM will first be had without engaging the generator. Also, an emergency stop check where the brake is engaged will be made at operating RPM. Normal operation including the generator connected to the line can then be completed.

14.3 DYNAMICS TEST - Because of the lack of instrumentation, no specific dynamics tests are to be conducted.

14.4 PERFORMANCE (LONG TERM) TESTING - This testing will all be done at Rocky Flats under the cognizance of Rockwell personnel. The primary purpose is to verify predicted performance. Testing takes place 24 hrs per day whenever the wind is within range.

Prior to certifying unmonitored running of the Giromill, at least two weeks of satisfactory operation must have occurred, covering the entire wind range spectrum. Also, all emergency simulations, Section 14.5.1, must have been completed.

14.5 SPECIAL TESTS (INTENSIVE TESTING) - This testing will also be done at Rocky Flats. Primary cognizance of the tests will lie with Rockwell, but contractor (MDC and Valley) personnel will participate, as requested by Rockwell. The tests are described below.

14.5.1 Emergency Simulations - These simulations must be completed prior to letting the Giromill operate unmonitored. They are summarized in Figure 173. These tests are to be conducted under carefully controlled conditions. All instrumentation, including real time recorders, will be available.

EMERGENCY	HOW IMPLEMENTED	OPERATING CONDITIONS	NORMAL REACTION
RPM SENSOR FAILURE	DISCONNECT RPM SENSOR	MODERATE WIND NORMAL OPERATING	CONTROLLER SHOULD SHUT DOWN GIROMILL
GENERATOR DROPS OFF LINE	MANUAL OPENING OF GENERATOR CONTACTORS	NORMAL WITH FULL POWER ON GENERATOR	OVERSPEED AND BLADES FEATHER OR CONTROLLER CORRECTS - GIROMILL OPERATES UNLOADED
GENERATOR CONTACTOR FAILS CLOSED	DISCONNECT GRID CONNECT FROM CONTROLLER. USE BATTERY (24V) DIRECTLY ACROSS GRID CONNECT RELAY.	LOW WIND THAT WOULD OCCASIONALLY DROP BELOW GENERATOR CUT-IN SPEED	GENERATOR SHOULD DRIVE THE GIROMILL WHEN WIND BELOW CUT-IN
VIBRATION SENSOR OPENS	DISCONNECT VIBRATION SENSOR	NORMAL	CONTROLLER SHOULD SHUT DOWN GIROMILL
BRAKE FAILURE	DISCONNECT BRAKE SOLENOID	LOW WIND	BRAKE STOPS GIROMILL AND/OR CONTROLLER SHUT DOWN AFTER 90 SECONDS
LARGE FLUCTUATING GENERATOR LOAD	AFTER SEVERE GUST CONDITION, MEASURE THE GENERATOR TEMPERATURE RISE	NORMAL	TEST TO BE IN ACCORDANCE WITH IEEE PUB NO. 112-A (1964) TEMPERATURE RISE MEETS SPEC NEMA PUB MG-1, BUT 20°C LESS

GP79-0573-15

**FIGURE 173
EMERGENCY SIMULATIONS**

14.5.2 Development Tests - These tests are used to verify changes made to correct any operating deficiencies uncovered during the other tests. For the control system, these may involve changing control gain constants, putting in different rock angle profiles, changing control laws, or even adding other electronic circuits. Correction of structural or mechanical deficiencies could involve beefing up the structure to replacing or changing mechanical components.

These tests will be conducted only as required.

14.5.3 System Improvement Tests - It is recommended that tests be made to provide data that will allow improvements in the system and increase the cost effectiveness. Two areas where tests should be made include: (1) control system simplification and (2) structural arrangement simplification. The tests recommended are listed in Figure 174.

1. CONTROL SYSTEM SIMPLIFICATION

- (a) REDUCE NUMBER OF CAM PROFILES STORED IN PROCESSOR
 - ELIMINATE LOW WIND (HIGH λ) CAMS
 - SIMULATE MIXING OF A LOW WIND AND HIGH WIND CAM (STEPHENSONS LINKAGE)
- (b) SMOOTH ROCK ANGLE PROFILES TO A SERIES OF SINE WAVES

2. STRUCTURAL SIMPLIFICATION

- (a) SIMPLIFY SUPPORT ARM MEMBERS
- (b) ELIMINATE BLADE SEALING WIPERS
- (c) BLADE C.G. TOLERANCE INCREASED

GP79-0573-18

FIGURE 174
RECOMMENDED SYSTEM IMPROVEMENT TESTS
Contractor Support Not Completely Covered

These tests could be done after operational data has been obtained on the basic design.

14.6 MECHANICAL SYSTEM TESTING - It is recommended that the electrical system be thoroughly tested prior to changing to the mechanical system. It is also recommended that the driven unit for the mechanical system be configured so that variable amounts of power can be extracted from the Giromill. This is necessary to allow definition of the entire Giromill performance envelope. The variable mechanical load could be provided by a dynamometer, water twister, pony brake, etc.

With an electrical system tied to a grid, the Giromill is always putting out maximum power. Operating RPM could be reduced slightly to get intermediate power levels from the generator. This is not recommended due to low generator efficiency and the probability of cutting the generator in and out because of wind gusts.

The mechanical system should explore the reduced power envelope at both above and below rated wind speeds. It is recommended that the 3/4, 1/2, and 1/4 power envelope points be determined. This would define the power envelope as shown in Figure 175.

14.7 MAINTENANCE PROCEDURES - Maintenance procedures have been defined for the Rocky Flats test center to follow during the various phases of Giromill testing. A preliminary estimate of the inspection and servicing frequency for various critical components is included. The actual testing will, however, assist in developing a more realistic estimate of maintenance frequencies and an overall maintenance plan for production units.

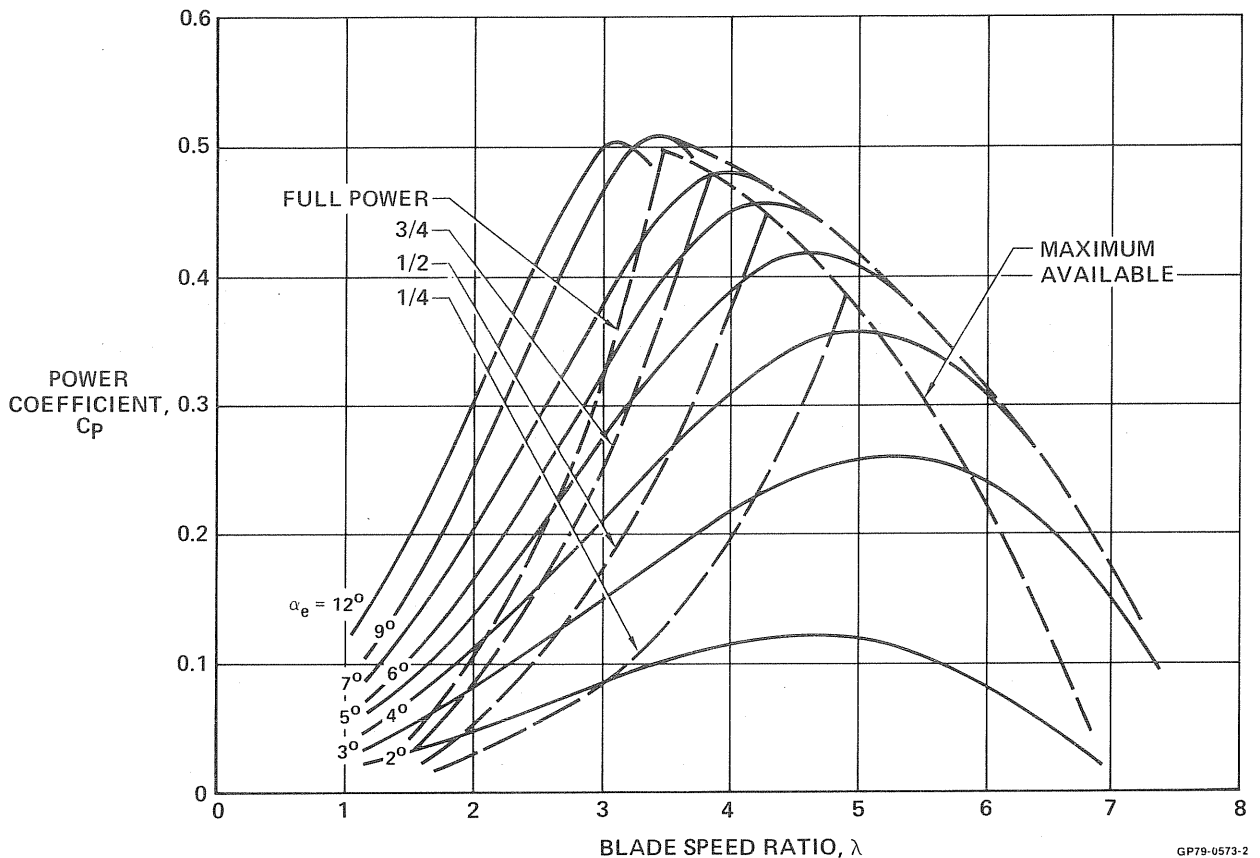


FIGURE 175
GIROMILL ESTIMATED PERFORMANCE

The routine maintenance and checking procedures recommended by the component manufacturer will be adhered to during the test. In addition, periodic inspections of the components listed in Figure 176 will be performed. When necessary, oil or other lubricants will be added and mechanical parts replaced or reworked.

A record of maintenance and servicing, should be maintained which contains: (1) the parts/components affected, (2) what went wrong, (3) corrective action taken, (4) redesign suggestions, (5) any other pertinent remarks. These records will be used to set up production system maintenance procedures and provide a first estimate of the spares inventory that should be established.

COMPONENT	INSPECTION INTERVAL	COMMENTS
MAIN BEARINGS	EVERY MONTH AND AFTER ANY LIGHTNING STRIKE.	CHECK GREASE RETENTION AND SEAL CONDITION.
BLADE BEARINGS	AFTER FIRST MONTH AND THEN EVERY 6 MONTHS. ALSO AFTER ANY LIGHTNING STRIKE.	CHECK FOR GREASE RETENTION UNDER g LOAD.
DRIVE BELTS	AFTER FIRST MONTH AND THEN EVERY 6 MONTHS.	CHECK TENSION AS PER GOODYEAR PROCEDURES.
TENSION CABLES	AFTER FIRST MONTH AND THEN EVERY 6 MONTHS.	CHECK CLEVIS PIN COTTER PIN INSTALLED AND CABLES NOT LOOSE.
BRAKE SYSTEM	AFTER FIRST MONTH AND THEN EVERY 6 MONTHS.	RUN PUMP TO CHECK PRESSURE. CHECK HYD. FLUID LEVEL, ACCUMULATOR PRESSURE, AND BRAKE PADS THICKNESS.
RPM SPEED INCREASER	EVERY MONTH.	CHECK OIL LEVEL.
BLADE ACTUATOR	MONTHLY FOR THE FIRST 3 MONTHS AND THEN EVERY 3 MONTHS.	CHECK OIL LEVEL AND MOTOR BRUSHES. ALSO CHECK FOR ANY EVIDENCE OF OVERHEATING.
POWER SLIP RING CONTACTORS	AFTER FIRST MONTH AND THEN EVERY 6 MONTHS.	

These are in addition to the component manufactures suggested maintenance

GP79-0636-116

FIGURE 176
TEST MAINTENANCE PROCEDURE

15. PRELIMINARY BUDGETARY PRODUCTION COSTS

One of the required tasks is to make a preliminary budgeting estimate of the production cost for the 1000th unit. Since there was not time in the program to try to optimize the Giromill for large scale production, the cost of a true productionized Giromill should be lower than the costs presented herein.

The basic ground rules followed for this task are listed in Figure 177. These ground rules were formulated by MCAIR and Valley Industries and approved by Rockwell prior to Final Design Review.

- 1977 DOLLARS WILL BE USED
- THE COST WILL INCLUDE G AND A AND PROFIT
- SELLING EXPENSE AND TRANSPORTATION WILL NOT BE INCLUDED
- FOUNDATION AND ERECTION COSTS WILL NOT BE INCLUDED
- VALLEY INDUSTRIES WILL BUILD THE ENTIRE UNIT
- RDT&E AND TOOLING COSTS WILL NOT BE INCLUDED
- ROTOR CENTERLINE WILL BE PLACED TO PROVIDE A 30 FT GROUND CLEARANCE
- CUT OUT SPEED SHALL BE AT A WIND SPEED OF 40 MPH
- ALL OTHER REQUIREMENTS SHALL BE AS SPECIFIED IN TABLE I OF THE SOW
- AN APPROPRIATE LEARNING CURVE WILL BE DETERMINED AND APPLIED FOR EACH COMPONENT PART OF THE GIROMILL

GP79-0349-124

FIGURE 177 GROUND RULES FOR COSTING 1000th UNIT

For all parts which might be produced by MCAIR, Valley, or MDEC, the preliminary production cost was obtained through normal production estimating channels in each company. In each case, the cost was broken down into direct labor man hours and material costs. It was then assumed that by the time production reached 1000 units, Valley Industries would be manufacturing all the parts. Material costs were assumed to be the same no matter which company did the buying.

Procured components were estimated in two different ways. First, potential vendors were contacted and asked to quote prices for 1, 10, 100, and 1000 units, to try to establish a learning curve. In some cases, vendors would make the effort to quote what might be a fairly realistic number even though they were well aware that orders for such quantities would be some time off. In many cases though, the standard catalog price quote was given which does not represent a reasonable learning curve. In these cases, a second estimate was made, using first a 95% learning curve, for purchased items and then a 90% learning curve. The results are shown in Figure 178.

	1st UNIT	1000th UNIT		
		①	②	③
FIXED TOWER	\$ 5,961	\$ 3,636		
ROTATING TOWER	11,686	4,006		
SUPPORT ARMS	6,862	2,076		
STREAMLINE RODS	1,556	724		467
BLADES	13,693	4,944		
UPPER BEARING	878	583	488	263
LOWER BEARING	1,624	1,446	902	487
CONTROL SYSTEM	7,039	4,084		
SPEED INCREASER	3,810	3,026	2,118	1,143
MAIN DRIVE PULLEY	559	167		
MAIN GENERATOR PULLEY	194	58		
MAIN DRIVE BELT	89	67	49	27
INDUCTION GENERATOR	1,060	622	589	318
ELECTRIC COMPONENTS	369	301	205	111
TOTAL MATERIAL, LABOR, OVERHEAD	\$55,380	\$25,740	\$24,046	\$21,787
G&A (7%)	3,877	1,802	1,683	1,525
PROFIT (10%)	5,926	2,754	2,573	2,331
TOTAL	\$65,183	\$30,296	\$28,302	\$25,643
DOLLARS/KILOWATT (41.7 kW)	\$ 1,563	\$ 727	\$ 679	\$ 615

① Based on vendor quotations

② Based on 95% learning curve on vendor items

③ Based on 90% learning curve on vendor items

GP79-0573-82

FIGURE 178
GIROMILL BUDGETARY COST ESTIMATE
 Design 1 - 1977 Dollars

The specific cost estimate for each of the major elements is shown in Figures 179 through 183. An explanation of each is included below.

Figure 179 is the budgetary cost estimate for the fixed tower, showing direct labor hours for the tower and for the brackets to mount the upper bearing, lower bearing, electrical panels, and the electrical output system and the ladder. A 95% learning curve was used for the direct labor hours for the tower. For the brackets and ladder, an 85% learning curve was used. The material cost for the 1000th unit was based on quantity discounts.

Figure 180 summarizes the budgetary cost estimate for the rotating tower. An 85% learning curve was used for the direct labor hours. The material cost for the 1000th unit was based on quantity discounts.

The support arm estimate is summarized in Figure 181. An 85% learning curve was used for direct labor hours. The material cost for the 1000th unit was based on quantity discounts.

		1st UNIT	1000th UNIT
DIRECT LABOR HOURS (TOWER = 95% LC, BRACKETS = 85% LC)	(HR)	126	39
DIRECT LABOR COST (\$6.05/HR)	(\$/HR)	762	236
OVERHEAD COST (220%)	(\$)	1677	519
MATERIAL	(\$)	2408	2140
GALVANIZING	(\$)	1114	741
TOTAL MATERIAL, LABOR AND OVERHEAD	(\$)	5961	3636
\$/LB		0.64	0.39

Total weight: 9280 lb

GP79-0573-01

FIGURE 179
FIXED TOWER BUDGETARY COST ESTIMATE
 Includes Fabricated Parts for Bearing, Electrical
 Output and Control System - 1977 Dollars

		1st UNIT	1000th UNIT
DIRECT LABOR HOURS (85% LC)	(HR)	414	63
DIRECT LABOR COST (\$6.05/HR)	(\$/HR)	2,505	381
OVERHEAD COST (220%)	(\$)	5,510	839
MATERIAL	(\$)	3,671	2,786
TOTAL MATERIAL, LABOR AND OVERHEAD	(\$)	11,686	4,006
\$/LB		1.40	0.48

Total weight: 8,350 lb

FIGURE 180
ROTATING TOWER BUDGETARY COST ESTIMATE
 1977 Dollars

		1st UNIT	1000th UNIT
DIRECT LABOR HOURS (85% OF LC)	(HR)	283	43
DIRECT LABOR COST (\$6.05/HR)	(\$/HR)	1712	260
OVERHEAD COST (220%)	(\$)	3767	572
MATERIAL	(\$)	1383	1244
TOTAL MATERIAL, LABOR AND OVERHEAD	(\$)	6862	2076
\$/LB		1.54	0.47

Total weight: 4430 lb

FIGURE 181
SUPPORT ARM BUDGETARY COST ESTIMATE
 1977 Dollars

	1st UNIT	1000th UNIT
FABRICATION		
– SHEET METAL (LC = 0.90)	217	75
– CONVENTIONAL MACHINING (LC = 0.90)	191	66
ASSEMBLY(1)	98	24
TOTAL MANHOURS	506	165
– LABOR AND OVERHEAD	\$ 9,796	\$3,194
– STRUCTURAL MATERIAL (LC = 0.93)	3,201	1,506
– BLADE BEARINGS (LC = 0.90)	696	244
MATERIAL, LABOR AND OVERHEAD	\$13,693	\$4,944

(1) LC based on MCAIR aircraft assembly experience

(2) Total weight: 1,308 lb

GP79-0636-82

FIGURE 182
BLADE BUDGETARY COST ESTIMATE
1977 Dollars

	1st UNIT	1000th UNIT
CONTROLLER	\$2544	\$1363
ACTUATORS	2836	1683
ALTERNATOR 	331	116
BELTS 	107	81
BATTERIES 	225	135
POWER SLIP RING 	155	98
CONTROL SLIP RING 	558	331
PULLEY	118	41
WIRING	165	132
(MATERIAL, LABOR AND OVERHEAD)	\$7039	\$4084

 Quotes

GP79-0573-73

FIGURE 183
CONTROL SYSTEM BUDGETARY COST ESTIMATE
1977 DOLLARS

The blade estimate is summarized in Figure 182. A 90% learning curve was used for conventional machining and sheet metal fabrication. The learning curve used for blade assembly was based on MCAIR aircraft assembly experience. A learning curve of 93% was used for blade material, to account for material scrappage and the possibility of switching to lower cost materials during production. The bearing vendor was not willing to quote on the 1000th unit cost, so we used a 90% learning curve. This should be fairly accurate since the bearings require a lot of machining.

The control system estimate is summarized in Figure 183. The 1000th unit costs of the controller and actuator were based on a learning curve previously established by MDEC. A 90% learning curve was used for the pulley, since this is a machining. It was assumed that for large quantity buying for the wiring, that it would cost 80% of the first unit.

The cost for all the remaining items in the control system was based on quotes (Figure 183).

As Figure 178 shows, the design goal of \$500/kW in 1977 dollars would not be met even with the more optimistic 90% learning curve applied to the purchased items. In order to meet that goal, it will be necessary to find ways to lower the cost of major items of structure and the control system. It is believed that an engineering cost value study and a weight reduction program could aid in reducing the cost.

16. CONCLUSIONS AND RECOMMENDATIONS

The Design Phase determined that the Giromill was feasible and a strong candidate for further development in certain areas as follows:

The cost of structural components could be considerably reduced by having a shorter fixed tower. This would also make the blade actuators more accessible for inspection and maintenance. Cost effectiveness of this modification should be explored.

The present rock angle profiles employ the concept of maintaining a constant effective angle of attack. This is good at low wind speeds but requires high blade rates and accelerations at the higher wind speeds. Since maximum efficiency is not required at high speeds a method could be developed to modify the rock angle profiles to reduce the actuator requirements in higher winds. The ramifications of this modification are not well understood, and a research effort to define modified rock angles and to evaluate implementation methods, should be undertaken.

A mechanical type of controller is potentially feasible. This would eliminate the electronic circuitry and possibly improve reliability and reduce cost. Further analysis effort in this area is warranted.

The feasibility analyses of the Giromill have shown that both capital cost per kW and operating costs are reduced as the size of the Giromill is increased. For irrigation purposes 40 kW output is just barely sufficient. Studies to uprate the present 40 kW prototype machine and develop cost information for rural units to 500 kW should be undertaken.

During the trade studies it was determined that a two bladed rotor showed a definite cost advantage over a three-bladed rotor. Possible problem areas precluded selection of a two bladed rotor for the prototype. Detailed analysis of a two-bladed rotor should be undertaken to get solutions to the possible problem areas.

The induced flow effects of a Giromill are much more complex than for a conventional horizontal axis windmill. Also, the induced effects of a Giromill occur over a large volume while those of a conventional windmill can almost be considered a disc. The downwind blades of a Giromill must operate in a high level of induced environment. A means of experimentally investigating the induced effects should be developed. This would require developing a suitable means for measuring blade angle of attack. Instrumentation to do this under the high g loads at the blade is not available. The means of performing this measurement and then evaluating the effects should be undertaken. Knowing the downstream flowfield could lead to a blade modulation scheme that would increase the efficiency of the Giromill and decrease the operating costs.

REFERENCES

1. Brulle, R. V., "Feasibility Investigation of the Giromill for Generation of Electrical Power", Vol I - Executive Summary, Vol II - Technical Discussion, ERDA Report C00-2617-76/1, April 1976.
2. Moran, W. A., "Giromill Wind Tunnel Test and Analysis", Vol I - Executive Summary, Vol II - Technical Discussion, ERDA Report C00/2617-4, October 1977.
3. Kaufman, J. W., "Terrestrial Environment (Climatic) Criteria Guidelines for Use in Aerospace Vehicle Development, 1977 Revision", NASA Technical Memorandum 78118, November 1977.
4. Frost, W., et al, "Engineering Handbook on the Atmospheric Environmental Guidelines for Use in Wind Turbine Generator Development", NASA TP 1359, December 1978.
5. Press, H., Steiner, R., "An Approach to the Problem of Estimating Severe and Repeated Gust Loads for Missile Operations", NACA TN 4332, September 1958.
6. "Design Fabrication and Testing of up to Three Low-Cost 100-200kW Mod-4 Wind Turbines", U.S. Department of Energy RFP ET-78-R-01-3028, 2 May 1978.
7. "Military Standard Climatic Extremes for Military Equipment", MIL-STD-210B, 15 December 1973.
8. Abbott, I. H., Doenhoff, A. E., Stivers, L. S., "Summary of Airfoil Data", NACA Report No. 824, 1945.
9. Brulle, R. V., et al, "Feasibility Investigation of the Giromill for Generation of Electrical Power, Mid Term Report", ERDA Report C00-2617-1, November 1975.
10. "Airplane Strength and Rigidity Flight Loads" Military Specification, MIL-A-8861 (ASG), 18 May 1962.
11. "Fatigue Manual", North American Aviation Report NA-55-866, Revision dated October, 1964.
12. "Continuous System Modeling Program", International Business Machines (IBM) (Program No. 5734-XS9).
13. Cliff, W. C., Fichtl, G. H., "Wind Velocity Change (Gust Rise) Criteria for Wind Turbine Design", Battelle Memorial Institute - Pacific Northwest Laboratory Report PNL-2526, July 1978.

14. Macklis, S. L., "System Dynamics of Multi-Unit Wind Energy Conversion Systems Application", Proceedings of the Third Wind Energy Workshop, Washington D.C., September 1977, pp 697-711.
15. MacNeal, R. H., "The NASTRAN Theoretical Manual", (Level 15.5), MSR-40, The MacNeal-Schwindler Company, May 1974.
16. "Metallic Materials and Elements for Aerospace Vehicle Structures", Military Standardization Handbook, MIL-HDBK-5C, 15 September 1976.
17. "Manual of Steel Construction", American Institute of Steel Construction, Inc., Seventh Edition, 1970.
18. "Subsurface Investigation Wind Generating Towers North of Rocky Flats Plant", Prepared for Rockwell International by R. V. Lord and Associates, Inc., December 1, 1976.
19. "Structures Handbook", Report 339, McDonnell Aircraft Company, McDonnell Douglas Corporation, Revised June 1973.

APPENDIX A

DETAILED STRENGTH ANALYSIS

A-1 SUPPORT ARM

Cover Skin - The maximum bending moment on the support arm, 36,600 in.-lb, is due to the ice condition, and occurs at 106 in. from the root rib. A cross-section through this area is shown in Figure A-1. The structural arrangement is described in Section 6.2.1.

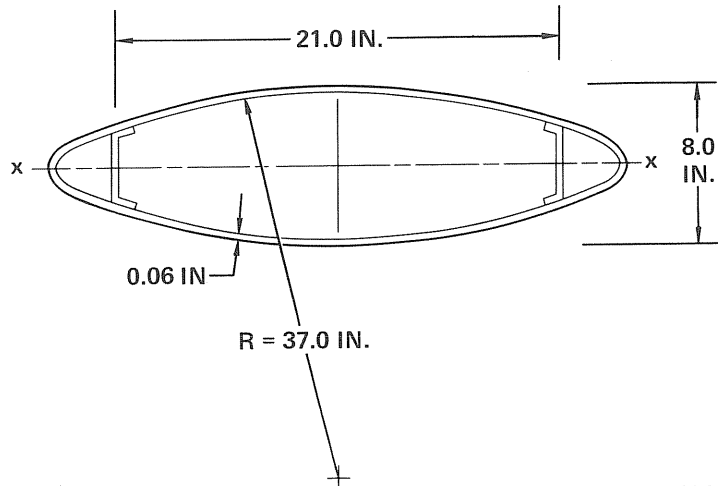


FIGURE A-1
SUPPORT ARM CROSS SECTION

The curved upper skin panel is 21 in. wide, with an unsupported length of 144 in. Based on the methods of analysis outlined in Reference 19, the allowable compressive stress at the onset of buckling is 9753 psi. For the maximum bending stress condition, this results in a positive margin of safety as shown below.

$$M_{xx} = 36,600 \text{ in.-lbs}$$

$$I_{xx} = 28.0 \text{ in.}^4$$

$$f_b = \frac{Mc}{I} = \frac{36614 (4.0)}{28.0} = 5230 \text{ psi}$$

$$\text{M.S.} = \frac{9753}{5230} - 1 = +0.86$$

Strut - The Maximum load on a support strut is 7537 lb (Condition 3A). The support strut is a 5/8 inch diameter stainless steel rod, forged

Allowable Stresses for A-36 Steel: (Reference 15)

$$F_b = 0.66 F_y = 0.66(36,000) = 23,760 \text{ psi}$$

$$F_a = 0.6 F_y = 0.66(36,000) = 21,600 \text{ psi}$$

Stresses at Section A-A:

$$f_a = V_z/A = \frac{16841}{1.5(1.0)} = 11,227 \text{ psi (limit)}, \frac{f_a}{F_a} = \frac{11227}{21600} = 0.520$$

$$f_{bx} = \frac{M_x c_y}{I_{xx}} = \frac{826(1.5)}{(1.5)(0.94)} = 878 \text{ psi (limit)}, \frac{f_{bx}}{F_b} = \frac{878}{23760} = 0.037$$

Margin of Safety for Combined Stresses:

$$\text{M.S.} = \frac{1}{R} - 1$$

$$R = \frac{f_a}{F_a} + \frac{f_{bx}}{F_b} + \frac{f_{by}}{F_b} = (0.520 + 0.037 + 0) = 0.557$$

$$\text{M.S.} = \frac{1}{0.522} - 1 = +0.80$$

The attach yoke lug was checked according to the methods outlined in Reference 19.

Lug Check:

$$R = 2.625$$

$$D = 1.516$$

$$R/D = \frac{2.625}{1.516} = 1.73$$

$$\frac{F_{BR}}{F_{TU}} = 1.52$$

$$P_{ALL} = \frac{F_{BR}}{F_{TU}} (D \times T) (F_{TU})$$

$$= 1.52 (1.516) (0.5) (55000) = 63,369 \text{ lbs}$$

$$P = 16844 \text{ lb}$$

$$\text{M.S.} = \frac{63369}{16844} - 1 = +2.76$$

Lug Hole Bearing Check:

$$f_{\text{brg}} = \frac{1684}{(1.516)(0.50)(1.5)} = 14812 \text{ psi (limit)}$$

$$F_{\text{BRG}} = 0.9 F_y = 0.9 (36000) = 32,400 \text{ psi (Reference 17)}$$

$$\text{M.S.} = \frac{F_{\text{BRG}}}{f_{\text{brg}}} - 1 = \frac{32400}{14812} - 1 = +1.18$$

A-2 ROTATING TOWER - UPPER BEARING SUPPORT AREA

A cross-section through the upper bearing support area of the rotating tower is shown in Figure A-3. The rotating tower is a 3/16 in. thick A-36 steel pipe.

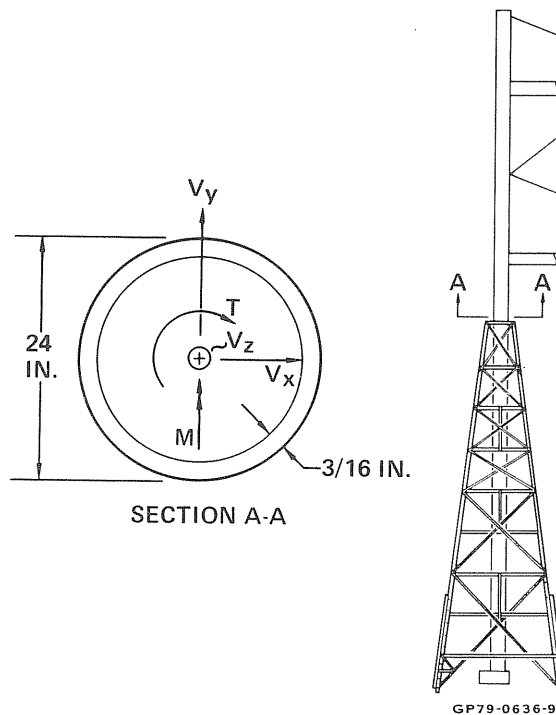


**FIGURE A-3
UPPER BEARING SUPPORT AREA**

This pipe was analyzed as a cylinder in combined bending, compression, and torsion according to the methods outlined in Reference 16. The formula for the margin of safety is;

$$M.S. = \frac{1}{R_c + \sqrt{(R_b)^2 + (R_s)^2}} - 1$$

$$\text{where } R_c = \frac{f_c}{F_c}, R_b = \frac{f_b}{F_b}, \text{ and } R_s = \frac{f_s}{F_s}$$

$$F_b = F_c = 0.6 (F_y) = 21,600 \text{ psi (Reference 17)}$$

where $F_y = 36,000$ psi, for A-36 steel pipe

$$F_s = 0.4 F_y = 14,400 \text{ psi (Reference 17)}$$

For the maximum bending, Condition 1A; (See Figure 72)

$$f_c = \frac{V_z}{A} = \frac{13333}{1.5 (\pi) (24) (0.189)} = 624 \text{ psi (limit)}$$

$$R_c = \frac{624}{21,600} = 0.029$$

$$f_b = \frac{Mr}{I} = \frac{2.49 \times 10^6 (12)}{\pi (12)^3 (0.189) (1.5)} = 19,415 \text{ psi (limit)}$$

$$R_b = \frac{19,415}{21,600} = 0.899$$

$$f_s = \frac{Tr}{J (1.5)} + \frac{\sqrt{(V_x)^2 + (V_y)^2}}{A (1.5)} = \frac{232000 (12)}{2 \pi (12)^3 (0.189)} + \frac{\sqrt{(11304)^2 + (2020)^2}}{\pi (24) (0.189)}$$

$$= 1006 \text{ psi (limit)}$$

$$R_s = \frac{1006}{14400} = 0.07$$

$$\text{M.S.} = \frac{1}{0.029 + \sqrt{(0.899)^2 + (0.070)^2}} - 1 = +0.074$$

For the maximum torsion condition, Condition 2; (See Figure 72)

$$f_c = \frac{V_z}{A} = \frac{13333}{1.5 (\pi) (24) (0.189)} = 624 \text{ psi (limit)}$$

$$R_c = \frac{624}{21600} = 0.029$$

$$f_b = \frac{MR}{I} = \frac{1.27 \times 10^6 (12)}{\pi (12)^3 (0.189) (1.5)} = 9902 \text{ psi (limit)}$$

$$R_b = \frac{9902}{21600} = 0.458$$

$$f_s = \frac{TR}{J (1.5)} + \frac{\sqrt{(v_x)^2 + (v_y)^2}}{A (1.5)} = \frac{1.547 \times 10^6 (12)}{2 (\pi) (12)^3 (0.189) (1.5)} + \frac{\sqrt{(12,863)^2 + (174)^2}}{1.5 \pi (24) (0.189)}$$

$$= 6632 \text{ psi (limit)}$$

$$R_s = \frac{6632}{14400} = 0.461$$

$$\text{M.S.} = \frac{1}{0.029 + \sqrt{(0.461)^2 + (0.458)^2}} - 1 = +0.47$$

A-3 FIXED TOWER

Shown in Figure A-4 is a front view of the fixed tower and a free-body of the critical leg. This section, identified as column No. 144, was analyzed as a beam column according to the methods outlined in Reference 17. The loads shown are for Condition 1B which produced the minimum margin of safety. A cross-section through the leg and accompanying material properties are shown in Figure A-5.

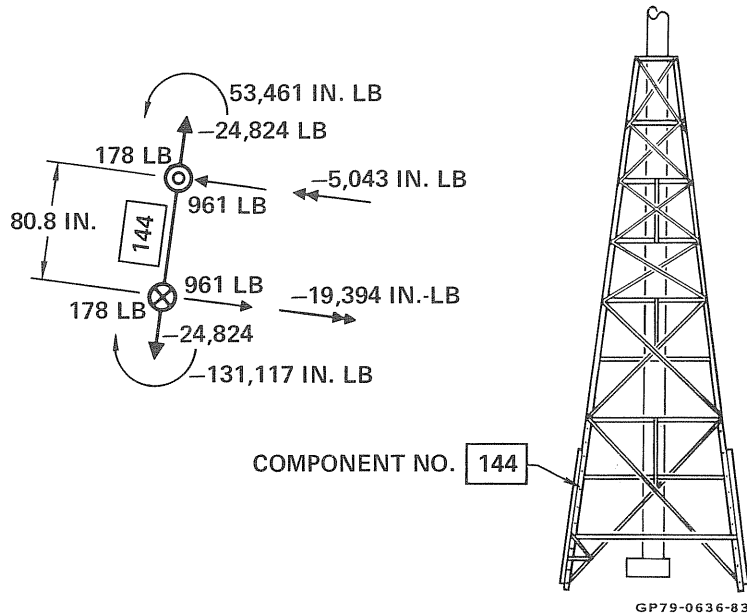
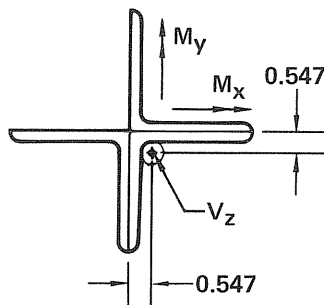


FIGURE A-4
CRITICAL LEG COMPONENT IDENTIFICATION AND FREE-BODY



COLUMN NO. 144

$A = 13.08 \text{ IN.}^2$ $I_x = I_y = 77.47 \text{ IN.}^4$

$C = 6.547 \text{ IN.}$ $r = 2.434 \text{ IN.}$

ULTIMATE LOADS FOR CONDITION 1B

$M_x = 131,117 \text{ IN. LB}$

$M_y = 19,394 \text{ IN. LB}$

$V_z = 24,824 \text{ LB COMP.}$

GP79-0636-138

**FIGURE A-5
FIXED TOWER COLUMN CROSS-SECTION**

The margin of safety is defined by the formula:

$$M.S. = \frac{1}{R} - 1$$

$$\text{where } R = \frac{f_a}{F_a} + \frac{C_{mx} f_{bx}}{\left(1 - \frac{f_a}{F'_{ex}}\right) F_{bx}} + \frac{C_{my} f_{by}}{\left(1 - \frac{f_a}{F'_{ey}}\right) F_{by}}$$

$$C_{mx} = C_{my} = 0.85 \text{ (Reference 17)}$$

$$F_a = 19740 \text{ psi (Reference 17, Table 1-36 for } \frac{Kl}{r} = 32.87)$$

where $K = 1.0$, $l = 80.8 \text{ in.}$, and $r = 2.434$

$$F'_{ex} = F'_{ey} = 19740 \text{ psi}$$

$$f_a = \frac{Vz}{A} = \frac{24824}{13.08} = 1898 \text{ psi}$$

$$F_{bx} = \frac{M_x c}{I_x} = \frac{131,117 (6.547)}{77.471} = 11,081 \text{ psi}$$

$$f_{by} = \frac{M_y c}{I_y} = \frac{19394 (6.547)}{77.471} = 1639 \text{ psi}$$

$$F_y = 0.66 F_y = 23760 \text{ psi (Reference 17)}$$

$$R = \frac{f_a}{F_a} + \frac{c_{mx} f_{bx}}{\left(1 - \frac{f_a}{F'_{ex}}\right) F_{bx}} + \frac{C_{my} f_{by}}{\left(1 - \frac{f_a}{F'_{ey}}\right) F_{by}} = \frac{1898}{19740} + \frac{0.85 (11,081)}{\left(1 - \frac{1898}{19740}\right) 23760} + \frac{0.85 (1639)}{\left(1 - \frac{1898}{19740}\right) 23760}$$

$$R = .600$$

$$M.S. = \frac{1}{.600} - 1 = + \underline{\underline{0.67}}$$